ฤทธิ์ต้านการอักเสบของลิโมนอยด์จาก *Xylocarpus* spp. และอนุพันธ์

นายชนินทร์ สาริกภูติ

วิทยานิพนธ์นี้เป็นส่วนหนึ่งของการศึกษาตามหลักสูตรปริญญาวิทยาศาสตรดุษฎีบัณฑิต
สาขาวิชาเทคโนโลยีชีวภาพ
คณะวิทยาศาสตร์ จุฬาลงกรณ์มหาวิทยาลัย
ปีการศึกษา 2557

ANTI-INFLAMMATORY ACTIVITY OF LIMONOIDS FROM *Xylocarpus* spp. AND THEIR DERIVATIVES

Mr. Chanin Sarigaputi

A Dissertation Submitted in Partial Fulfillment of the Requirements
for the Degree of Doctor of Philosophy Program in Biotechnology
Faculty of Science
Chulalongkorn University
Academic Year 2014

Thesis Title	ANTI-INFLAMMATORY ACTIVITY OF LIMONOIDS FROM *Xylocarpus* spp. AND THEIR DERIVATIVES
By	Mr. Chanin Sarigaputi
Field of Study	Biotechnology
Thesis Advisor	Assistant Professor Khanitha Pudhom, Ph.D.
Thesis Co-Advisor	Damrong Sommit, Ph.D.

Accepted by the Faculty of Science, Chulalongkorn University in Partial Fulfillment of the Requirements for the Doctoral Degree

.....Dean of the Faculty of Science
(Professor Supot Hannongbua, Dr.rer.nat.)

THESIS COMMITTEE

.....Chairman
(Associate Professor Vudhichai Parasuk, Ph.D.)

.....Thesis Advisor
(Assistant Professor Khanitha Pudhom, Ph.D.)

.....Thesis Co-Advisor
(Damrong Sommit, Ph.D.)

.....Examiner
(Associate Professor Chanpen Chanchao, Ph.D.)

.....Examiner
(Assistant Professor Preecha Phuwapraisirisan, Ph.D.)

.....External Examiner
(Professor Apichart Suksamrarn, Ph.D.)

ชนินทร์ สาริกภูติ : ฤทธิ์ต้านการอักเสบของลิโมนอยด์จาก *Xylocarpus* spp. และอนุพันธ์ (ANTI-INFLAMMATORY ACTIVITY OF LIMONOIDS FROM *Xylocarpus* spp. AND THEIR DERIVATIVES) อ.ที่ปรึกษาวิทยานิพนธ์หลัก: ผศ. ดร.ขนิษฐา พุดหอม, อ.ที่ปรึกษาวิทยานิพนธ์ร่วม: ดร.ดำรงค์ สมมิตร์, 205 หน้า.

การศึกษาสารออกฤทธิ์ต้านการอักเสบจากพืชสกุล *Xylocarpus* สามารถแยกสารลิโมนอยด์จากเมล็ดของตะบัน *Xylocarpus rumphii* (Kostel.) Mabb. ได้ 10 ชนิด เป็นสารใหม่ 7 ชนิด คือ xylorumphiins E-J (42-43 และ 45–48) และ 2-hydroxyxylorumphiin F (44) กับสารที่มีการรายงานมาก่อนอีก 3 ชนิด คือ xyloccensin X (49), xyloccensin E (50) และ xyloccensin K (51) นอกจากนี้ลิโมนอยด์จาก *X. rumphii* และที่ได้จาก *X. granatum* และ *X. moluccensis* รวมทั้งหมด 38 ชนิด ได้ถูกนำมาทดสอบฤทธิ์ต้านการอักเสบโดยวิธีการตรวจวัดการยับยั้งการผลิตไนตริกออกไซด์ใน macrophage RAW264.7 ที่ถูกเหนี่ยวนำให้เกิดการอักเสบด้วย LPS และ IFN-**γ** ผลการทดสอบ พบว่า 7-deacetylgedunin (54) ซึ่งเป็นลิโมนอยด์ประเภท gedunin แสดงฤทธิ์ในการยับยั้งได้ดีที่สุด โดยมีค่า IC_{50} เท่ากับ 4.85 μM และสารนี้ยังสามารถยับยั้งการแสดงออกของ mRNA gene และโปรตีนของ inducible NO synthase (iNOS) ในเซลล์ RAW264.7 ที่ถูกกระตุ้นด้วย LPS และ IFN-**γ** ยิ่งไปกว่านั้น transcriptional activity ของ NF-**K**B และการเกิดฟอสโฟรีเลชัน ของ MAPKs (p38, ERK1/2, SAPK/JNK) ที่ถูกเหนี่ยวนำให้เกิดการอักเสบด้วย LPS และ IFN-**γ** ยังถูกยับยั้งด้วย 54 อีกด้วย ซึ่งมีความเชื่อมโยงกับการป้องกันการสลายตัวของ I**K**B**α** รวมถึงการลดระดับของการเกิดฟอสโฟรีเลชันของ p65 นอกจากนี้ ในการศึกษาความสัมพันธ์ของโครงสร้างต่อการออกฤทธิ์ต้านการอักเสบของ dysobinin (80) และ andrographolide (81) สามารถสังเคราะห์อนุพันธ์ของ dysobinin ได้ 7 ชนิด (139-145) และอนุพันธ์ของ andrographolide 25 ชนิด (146-170) เมื่อนำอนุพันธ์ที่ได้ทั้งหมดมาทดสอบฤทธิ์ต้านการอักเสบ พบว่า อนุพันธ์ C-6, C-7 diol 139 แสดงฤทธิ์ได้ดีที่สุด ในขณะที่การรีดักชันหมู่ **α**, *β*-unsaturated ketone พบว่าทำให้สูญเสียการออกฤทธิ์ไป ดังนั้น หมู่ฟังก์ชั่นทั้งสองนี้จึงมีบทบาทสำคัญต่อการออกฤทธิ์ต้านการอักเสบของ dysobinin ในกรณีของสารประกอบในกลุ่มของ andrographolide พบว่าอนุพันธ์ acetyl 147 แสดงฤทธิ์ได้ดีที่สุด ซึ่งชี้ให้เห็นว่าหมู่ **α**-alkylidene-**γ**-butyrolactone, $\Delta^{8,17}$ exomethylene และ $\Delta^{12,13}$ double bond ที่พบในสารตั้งต้นนั้นมีบทบาทสำคัญต่อการออกฤทธิ์ต้านการอักเสบ

สาขาวิชา เทคโนโลยีชีวภาพ ลายมือชื่อนิสิต .....

ปีการศึกษา 2557 ลายมือชื่อ อ.ที่ปรึกษาหลัก .....

ลายมือชื่อ อ.ที่ปรึกษาร่วม .....

5373902823 : MAJOR BIOTECHNOLOGY
KEYWORDS: LIMONOIDS / XYLOCARPUS SPP. / ANTI-INFLAMMATORY ACTIVITY / ANDROGRAPHOLIDE / DYSOBININ

CHANIN SARIGAPUTI: ANTI-INFLAMMATORY ACTIVITY OF LIMONOIDS FROM *Xylocarpus* spp. AND THEIR DERIVATIVES. ADVISOR: ASST. PROF. KHANITHA PUDHOM, Ph.D., CO-ADVISOR: DAMRONG SOMMIT, Ph.D., 205 pp.

In a phytochemical investigation of anti-inflammatory compounds from *Xylocarpus* spp., seven new limonoid, xylorumphiins E–J (42-43 and 45–48) and 2-hydroxyxylorumphiin F (44), together with three known derivatives, xyloccensin X (49), xyloccensin E (50) and xyloccensin K (51) were isolated from the seeds of *Xylocarpus rumphii* (Kostel.) Mabb. In addition to limonoids from *X. rumphii*, the ones from *X. granatum* and *X. moluccensis*, totally thirty-eight compounds, were further evaluated for their *in vitro* anti-inflammatory activities by monitoring the inhibition of nitric oxide (NO) production in LPS and IFN-γ-induced RAW264.7 murine macrophages. Only 7-deacetylgedunin (54), a gedunin-type limonoid, exhibited the most potent activity with an IC_{50} value of 4.85 μM along with the suppression of mRNA gene and protein expression of inducible NO synthase (iNOS) in LPS and IFN-γ-stimulated RAW264.7 cells. Furthermore, transcriptional activity of NF-κB as well as the phosphorylations of MAPKs (p38, ERK1/2, SAPK/JNK), induced by LPS and IFN-γ, was suppressed by 54, which was associated with the protection of IκBα degradation and subsequently decreased the phosphorylation level of p65. Additionally, the structure-activity relationships of dysobinin (80) and andrographolide (81) derivatives were studied. Seven derivatives of dysobinin (139-145) and twenty five analogues of andrographolide (146-170) were thus synthesized and examined for their anti-inflammatory activities. Among dysobinin derivatives, it was found that C-6, C-7 diol 139 provided the most promising activity, while the reduction of α, β-unsaturated ketone moiety led to the loss of activity. Thus these two functionalities play crucial role for anti-inflammatory activity of dysobinin-type compound. In the case of compounds in andrographolide series, the acetylated derivatives provided the most potent activity. It could thus be concluded that α-alkylidene-γ-butyrolactone, $\Delta^{8,17}$ exomethylene and $\Delta^{12,13}$ double bond originally in parent compound played important role for anti-inflammatory activity.

Field of Study: Biotechnology
Academic Year: 2014

Student's Signature .....
Advisor's Signature .....
Co-Advisor's Signature .....

ACKNOWLEDGEMENTS

I would like to express his sincere appreciation to my advisor, Assistant Professor Dr. Khanitha Pudhom, Department of Chemistry, Faculty of Science, Chulalongkorn University, and co-advisor, Dr. Damrong Sommit, Department of Chemistry, Faculty of Science, Mahanakorn University of Technology, for excellent instruction, great valuable advice, kind guidance and support throughout the course of this research.

In addition, many thanks to the Chairperson: Associate Professor Dr. Vudhichai Parasuk, Department of Chemistry, Faculty of Science, Chulalongkorn University; the thesis examiners: Associate Professor Dr. Chanpen Chanchao, Department of Biology, Faculty of Science, Chulalongkorn University, Assistant Professor Dr. Preecha Phuwapraisirisan, Department of Chemistry, Faculty of Science, Chulalongkorn University, and Professor Dr. Apichart Suksamrarn, Department of Chemistry, Faculty of Science, Ramkhamhaeng University, for their invaluable discussion and suggestion.

I am grateful to Associate Professor Dr. Tanapat Palaga, Department of Microbiology, Faculty of Science, Chulalongkorn University and Miss Naunpun Sangphech, Medical Microbiology Interdisciplinary Program, Graduate School, Chulalongkorn University for anti-inflammatory assays and kind guidance. I would like to express my gratitude to Associate Professor Dr. Surat Laphookhieo, School of Science, Mae Fah Luang University, for his kind gifts of bioactive compound from plant which I used for my research. I would like to special thank Associate Professor Dr. Roger G Linington, Department of Chemistry and Biochemistry, University of California Santa Cruz, USA, for their helpful in providing facilities and materials in the part of synthesis of dysobinin derivatives and kindness. The author also thanks Dr. Thapong Teerawatananond, Department of Chemistry, Faculty of Science, Chulalongkorn University, who kindly performed Single-Crystal X-ray crystallographic analysis. Furthermore, I would like to thanks Miss. Siwattra Choodej for her assistance about NMR spectra and kindness.

Moreover, special thanks to member in the laboratory (MHMK 1532), Department of Chemistry, Faculty of Science, Chulalongkorn University for their generousity, help and good friendship.

I wish to thank Thailand Research Fund and Chulalongkorn University through The Royal Golden Jubilee Ph.D. Program (PHD/0009/2553) and The 90th Anniversary of Chulalongkorn University Fund (Ratchadaphiseksomphot Endowment Fund) for financial support to conduct this research.

CONTENTS

Page

Page

Page

Page

Page

LIST OF TABLES

LIST OF FIGURES

Figure Page

Figure Page

Figure Page

Figure Page

LIST OF SCHEMES

LIST OF ABBREVIATIONS

J	Coupling constant
δ	Chemical shift
δ_H	Chemical shift of proton
δ_C	Chemical shift of carbon
s	Singlet (for NMR spectra)
d	Doublet (for NMR spectra)
dd	Doublet of doublet (for NMR spectra)
ddd	Doublet of doublet of doublet (for NMR spectra)
dddd	Doublet of doublet of doublet of doublet (for NMR spectra)
t	Triplet (for NMR spectra)
m	Multiplet (for NMR spectra)
q	Quartet (for NMR spectra)
brs	Broad singlet (for NMR spectra)
brd	Broad doublet (for NMR spectra)
qC	Quaternary carbon
calcd.	Calculated
^{1}H NMR	Proton nuclear magnetic resonance
^{13}C NMR	Carbon-13 nuclear magnetic resonance
2D NMR	Two dimensional nuclear magnetic resonance

^{1}H-^{1}H COSY	Homonuclear (proton-proton) correlation spectroscopy
NOESY	Nuclear overhauser effect spectroscopy
HSQC	Heteronuclear single quantum coherence
HMBC	Heteronuclear multiple bond correlation
ORTEP	Oak ridge thermal ellipsoid plot
HRESIMS	High resolution electrospray ionization mass spectrometry
ESIMS	Electrospray ionization mass spectrometry
CC	Column chromatography
TLC	Thin layer chromatography
MIC	Minimum inhibitory concentration
IC_{50}	Half maximal inhibitory concentration
$CDCl_3$	Deuterated chloroform
CD_3OD	Deuterated methanol
$(CD_3)_2SO$	Deuterated dimethyl sulfoxide
MeOH	Methanol
EtOH	Ethanol
$CHCl_3$	Chloroform
CH_2Cl_2	Dichloromethane
EtOAc	Ethyl acetate
DMSO	Dimethylsulfoxide

KBr	Potassium bromide
$(NH_4)_6Mo_7O_{24}$	Ammonium molybdate
H_2SO_4	Sulfuric acid
SiO_2	Silicon dioxide
g	Gram (s)
mg	Milligram (s)
mL	Milliliter (s)
μg	Microgram (s)
μL	Microliter (s)
μM	Micromolar
mM	Millimolar
L	Liter (s)
M	Molar
min	Minute
h	Hour
rpm	Round per minute
m	Meter (s)
mm	Millimeter (s)
cm	Centimeter (s)
nm	Nanometer

Hz	Hertz
MHz	Megahertz
cm^{-1}	Reciprocal centimeter (unit of wave number)
ppm	part per million
NMR	Nuclear magnetic resonance
MS	Mass spectrometry
IR	Infared
UV	Ultraviolet
m.p.	Melting point
α	Alpha
β	Beta
γ	Gamma
Δ	Delta
m/z	Mass to charge ratio
$[M+H]^+$	Protonated molecule
$[M+Na]^+$	Pseudomolecular ion
$[\alpha]_D^{20}$	Specific rotation at 20 $^{\circ}C$ and sodium D line (589 nm)
λ_{max}	Wavelength of maximum absorption
c	Concentration
ε	Molar extinction coefficient

Å	Angstrom
°C	Degree celcius
deg.	Degree
spp.	Species
No.	Number
ATCC	American type culture collection
NO	Nitric oxide
iNOS	Inducible nitric oxide synthase
LPS	Lipopolysaccharide
IFN-γ	Interferon-gamma
NF-κB	Nuclear Factor Kappa B
MAPK	Mitogen-activated protein kinase
SARs	Structure activity relationships

CHAPTER I

INTRODUCTION

Inflammatory diseases are one of the major health problems worldwide. It is an adaptable response which is incited harmful stimuli and conditions, such as infection and tissue damage. Considerable progress has been invented in perception the cellular and molecular occurrences that are related in the acute inflammatory response to infection and, to tissue damage. Additionally, the occurrences that conduce to localized chronic inflammation, especially in chronic infections and autoimmune afflictions, are partially realized. Nevertheless, about the causes and mechanism of systematic chronic inflammation, which arise in an extensive variety of diseases, include atherosclerosis, rheumatoid arthritis [1] and cancer [2].

Non-steroidal anti-inflammatory drugs (NSAIDs) are the most commonly designated drugs for cure of inflammatory diseases. These drugs achieve their therapeutic effects by suppressing the activity of COX-1 and COX-2 enzymes to inhibit the production of inflammatory mediators. COX-1 inhibitors exhibit several side effects, including gastrointestinal irritation and renal toxicity [3]. Therefore, searching for novel anti-inflammatory therapeutic agents candidates in the treatment of chronic inflammation has remained critically importance.

Medicinal plants have long been utilized in traditional medicine for curative purposes and their healing affects have well been acquainted since ancient times. Furthermore, a notable number of modern medicines have been derived originally from herbal sources. These have improved to produce the conventional medicine that uses both synthetic drugs and isolated natural compounds. Herbal medicines are popular among the public and developments in their construction resulted in a novel generation of phytomedicines which are more efficacious than before. Common examples of Asian herbs traditionally used to heal inflammation are *Curcuma longa* L. (tumeric) and *Zingiber officinale* Rosc. (Zingiberaceae) [4]. A naturally-occurring yellow of *Curcuma longa* L. is a yellow pigment, curcumin. Curcumin has been extensively used in the administration of detachable

inflammation and wound curing. In addition, the anti-inflammatory action of curcumin, including suppression of macrophage activation, and interception of lipooxygenase (LO) and cyclooxygenase 2 (COX-2), metabolite creation through arachidonic acid pathways [5]. *Zingiber officinale* L. (ginger) has contained arylalkalones, which inhibit the enzymatic activity of COX with capability for medicament the symptom of inflammation [6].

Since time antique, numerous herbs and their derived compounds have been used in medicament of inflammation and involved disorders like rheumatism [7]. Relief pain, inflammation and fever with salicylate-containing plant extracts can be trailed throughout written people history. One hundred and fifty years ago, Felix Hoffman acetylated salicylic acid and provided aspirin. The discovery of aspirin from the bark of the Willow tree, *Salix alba* (Salicaceae), is another evidence of the achievement in natural product drug discovery. Aspirin suppresses the cyclooxygenase (COX) enzymes COX-1 and COX-2, which produce inflammatory mediators call as prostaglandins and thromboxanes accounts for aspirin being the world's most used therapeutic drug [8]. The active ingredient in aspirin, acetyl salicylic acid, is a synthetic derivative of a compound, salicin, the glycoside of salicylic acid, occurring naturally and highly level in the bark of this plant [9]. Aspirin has been one of the most extensively used drugs for the anti-inflammatory, analgesic and antipyretic in the world since its discovery more than a century ago. Nevertheless, it has several side effects including gastrointestinal toxicity (peptic ulcer formation, bleeding) and renal activity disorder [10].

Obviously, the enormous majority of the inflammatory diseases arises after medical intervention with anti-inflammatory therapy, both conventional non-steroidal anti-inflammatory drug (NSAIDs) and novel targeted therapy. It seems that these patients might be have a risk of adverse effects in medication. Especially, conventional non-steroidal anti-inflammatory drugs (NSAIDs) cause an expand variety of side-effects. The most clinically important side-effects are upper gastrointestinal tract dyspepsia, peptic ulceration, hemorrhage, and perforation because of inhibition of cyclooxygenase (COX)-1, leading to death in some patients. Generally, activation

of the expression of inducible isoforms of nitric oxide synthase (iNOS) and cyclooxygenase (COX) and prostaglandin E_2 (PGE_2), which play key roles in the inflammation process [11]. A growing number of research have demonstrated that signaling pathways underlying the development of anti-inflammatory drugs. Actually, the major signaling pathway that controls inflammation-associated gene expression is the one leading to activation of transcription factor nuclear factor-κB (NF-κB) and mitogen-activated protein kinase (MAPK) [12, 13]. Thus, the study on inhibitors of the NF-κB and MAPK, are expected to provide alternatively anti-inflammatory agents which are endowed with potent anti-inflammatory activity in clinical setting.

For these reasons, the finding of novel anti-inflammatory agents from medicinal plants might be one of the ways to obtain efficient candidates for healing a variety of inflammatory diseases.

The Meliaceae family has been shown to contain a huge number of compounds with the competence to be developed for medicinal purposes and also justified to produce a variety of chemically unique antifeedant limonoids, such as azadirachtin from the neem tree *Azadiracha indica* and harrisonin from *Harrisonnia abyssinica* [14]. A subgroup of natural compounds known as limonoids, are modified triterpenoid derivatives from a precursor with a 4,4,8-trimethyl-17-furanylsteroid skeleton, have been observed mainly in plants of the order Sapindales, especially in plant of the families Meliaceae, Rutaceae, and Simaroubaceae [15]. They are categorized by the type of four usually highly oxidized rings (defined as A, B, C, and D) in the intact triterpene [16]. Limonoid research from the Meliaceae family is of growing attention because of their various structural patterns and variety of biological activities, such as insect antifeedants and growth regulators, antibacterial, antifungal, antimalarial, anticancer, antiviral, anti-inflammatory agents and other pharmacological activities on humans [17]. Recently, they have been the focus of fervent exploration as a source of innovative drugs against cancer and infectious diseases. The genus *Xylocarpus* is only one type of mangrove plants belonging to the family Meliaceae which comprises only three species, *Xylocarpus granatum*, *Xylocarpus moluccensis* and *Xylocarpus rumphii*. Particulary, *X. granatum* and *X.*

moluccensis are the most popular plants for previous study. *Xylocarpus* plants are vastly distributed along the seacoast of southeastern Asia, Australia, and East Africa [18]. Furthermore, these plants have also established to be a prosperous source of an array of structurally various limonoids, consisting of gedunin, andirobin, mexicanolide and phragmalin type limonoids, with an extensive range of biological properties [19, 20]. *X. granatum* is used as folk medicines in Southeast Asia for the treatment of diarrhea, cholera, viral diseases such as influenza, and malaria [21]. Recent reports indicated that Thaixylomolin B, a limonoid from the seeds of a Thai mangrove, *X. moluccensis* exhibited inhibitory activity against nitric oxide production in lipopolysaccharide (LPS) and IFN-γ-induced RAW264.7 murine macrophages [22]. Although limonoid derivatives have been found in the *Xylocarpus* spp. studied, but their distribution and content varies between different species and between parts, or geocultivars, of the same species. These unique characteristics aroused to explore the anti-inflammatory effects of isolated limonoids from plant in this genus.

Based on the structural diversity and biological properties of limonoids in the genus *Xylocarpus* led to study the other plant in this family, the *Chisocheton* genus is one of the Meliaceae family, a subtropical and tropical plant family vastly acquainted for its insecticidal limonoid (tetranortriterpenoid) constituents. They are contains approximately 50 species that are distributed mainly in India and Malaysia. *Chisocheton* spp. is traditionally used for treatment stomach grievances, backache, fever, kidney complaints, rheumatism and malaria [23, 24]. Prior phytochemical research on *Chisocheton* spp. has given a number of interesting compounds, such as limonoids, antifungal meliacin-type compounds, dammarane triterpenoids, with an inhibitory effect on Epstein-Barr virus activation and spermidine alkaloids [25]. Recently, chisomicine A, a limonoid isolated from the bark of *C. ceramicus* has been reported with marked anti-inflammatory activities by inhibiting NO production in J774.1 cells [26]. Particularly, dysobinin, a limonoids isolated from the seeds of *C. siamensis* has been found to exhibit the antimalarial and cytotoxic activities [27].

Andrographis paniculata (Burm. f) Nees (family Acanthaceae) commonly known as Kalmegh is used both in Ayurvedic and Unani system of medicines for a

number of ailments related to digestion, hepatoprotection, hypoglycaemic and as anti-bacterial, analgesic, vermicidal, antipyretic and other related inflammatory diseases. The therapeutic activity of the herb has been attributed to andrographolide, a bicyclic diterpenoid lactone present in the whole herb [28]. Moreover, andrographolide is currently prescribed for treatment of inflammation related diseases, such as laryngitis, upper respiratory tract infection and rheumatoid arthritis [29, 30]. Recent studies suggested that andrographolide possesses anticancer, anti-inflammatory and hepatoprotective activities [31, 32]. Previous investigation on anti-inflammatory activity of this plant indicated that andrographolide suppresses the secretion of cytokines, chemokines and inflammatory enzymes (iNOS and COX) from macrophages [33, 34]. It has also displayed varying degree of anti-inflammatory and anticancer activities in both *in vitro* and *in vivo* experimental examples of inflammation and cancer. Wide libraries of andrographolide analogues have been synthesized mainly by modification the α,β-unsaturated γ-butyrolactone moiety, the two double bones $\Delta^{8,(17)}$ and $\Delta^{12,(13)}$ and the three hydroxyls at C-3 (secondary), C-14 (allylic) and C-19 (primary). Various of these semi-synthetic derivatives showed superior anti-cancer activity over the naturally existing andrographolide [35].

Most importantly, there are no reports about examination of the anti-inflammatory activity and the structure-activity relationship (SAR) of dysobinin. Moreover, there are few studied on investigation of inhibitory activity on nitric oxide production of andrographolide. Thus, we are interested in the semi-synthesis of the analogues of dysobinin and andrographolide, then study on their anti-inflammatory effects and structure-activity relationships.

Therefore, the objectives of this research are summarized as follow;

1. To extract, isolate and purify limonoids from the seeds of *Xylocarpus rumphii*.

2. To elucidate structures of the isolated limonoids by spectroscopic techniques.

3. To evaluate anti-inflammatory activity of isolated limonoids from *X. granatum*, *X. moluccensis* and *X. rumphii*.

4. To study the action mechanism of selected compounds on anti-inflammatory activity.

5. To synthesize the analogues of dysobinin and andrographolide and study on their structure-activity relationships for anti-inflammatory effects.

CHAPTER II

LIMONOIDS FROM *XYLOCARPUS RUMPHII*

2.1 Introduction

The *Xylocarpus* spp. belongs to the order Geraniales of the family Meliaceae. The family Meliaceae composes of the 50 genera including *Xylocarpus* and 1400 another species distributed all around the world [36]. Normally, *Xylocarpus* genus is spread extensively in the coastal areas of Southeastern Asia, Australia, East Africa and Indian ocean [37]. The *Xylocarpus* genus has been found only three species, *X. granatum* Koenig, *X. moluccensis* (Lam.) M. Roem. and *X. rumphii* (Kostel.) Mabb. All of them are found in mangrove forests, marsh or coastal scrub of the world, including in Thailand [38]. Especially, *X. granatum* and *X. moluccensis* are the most popular ones for empirical investigation [39]. Major constituents of plants in the genus *Xylocarpus* are limonoids, the bitter substances [40]. *X. granatum* is widely used as a traditional medicine in Southeast Asia and Indian for the medicament of diarrhea, cholera, and fever diseases such as malaria, and also as an antifeedant [41], while fruits of *X. moluccensis* are applied as a heal for elephantiasis and swelling of the breast. A balm made from seed ash of *X. moluccensis*, sulfur, and coconut oil is used for treatment of itch. The bark of this plant is utilized as an astringent and a febrifuge, and has been applied in traditional medicine for cure the symptom of dysentery, diarrhea, and other abdominal diseases [42]. Recently, much interest has been focused on *Xylocarpus* genus due to their limonoids with unique of characteristic feature of C-skeletons and their tumor cytotoxic activities [43]. Although *X. granatum* and *X. moluccensis* have mainly distributed in the tropics including mangrove habitat such as Africa, Australia, Malaysia, India and China. However, *X. rumphii* is only found in some mangrove areas in Thailand. To date, there are a few reports on detailed structural diversity and biological activity in this plant [44]. Hence, there is considerable interest to investigate the structural characteristics and biological properties of this mangrove species, *X. rumphii* (Kostel.) Mabb. (Meliaceae).

2.1.1 Taxonomical Characteristic of *Xylocarpus rumphii* (Kostel.) Mabb.

Taxonomy of *Xylocarpus rumphii* (Kostel.) Mabb. is classified as

Kingdom : Plantae

Division : Tracheophyta

Class : Magnoliopsida

Order : Rutales

Family : Meliaceae

Genus : Xylocarpus

Species : *Xylocarpus rumphii* (Kostel.) Mabb.

2.1.1.1 Botanical Characteristics of Xylocarpus rumphii (Kostel.) Mabb.

X. rumphii is a tree up to 4-12 m tall with neither obvious buttresses nor pneumatophores; trunk customarily solitary, to 50 cm diameters, regularly of poor form. Bark is lenticellate to delicately fissured, grayish; internal bark bright pink to red. Leaf is rachis and petiole to 22 cm with apex spike to 1 mm. Leaflets in 2-4 pairs, 5-10 by 3-5 cm, elliptical to heart-shaped, sometimes bent, base widely cuneal or rounded to truncate or heart-shaped, asymmetric, terminal acute to acuminate; venation protuberant on both surfaces in sicco, apparent in vivo; petiolule 1-3 mm. Thyrses 10-18 cm long, lax, pendent, main axis distinct; lateral branches to 8 cm; bracts and bracteoles 0.5 mm, narrowly triangular, long-lasting; pedicles 3-8 mm, not flagrantly swollen near calyx. Calyx lobes 1-1.5 mm long. Petals 3.5-6 by 2-2.5 mm, elliptic-oblong, creamy white. Staminal tube 2-2.5 mm diameters, lobes apiculate or bifid to retuse. Fruit 6-8 cm diameters, globose. Seeds 8-16, 3.6-7 cm long. Genrally, *X. rumphii* is abundantly found in South-Eastern part of Thailand as follow Krabi, Chon Buri, Ranong and Rayong province that extended along rocky seaboards and forelands. Moreover, it also found in East Africa to Tonga; throughout Malaysia but so far unrecorded from the Bornean (or New Caledonian)

mainland and infrequent in Sumatra. Additionally, the dialectal names of this plant are “Niri” or “Nyireh” and local name in Thailand is “Ta Ban” [45].

The pictures of *X. rumphii* are shown in Figure 2.1.

Figure 2.1 *Xylocarpus rumphii* (Kostel.) Mabb.

2.1.2 Limonoids

2.1.2.1 Chemistry and biosynthesis of limonoids

Limonoids, triterpene derivatives from a precursor with a 4,4,8-trimethyl-17-furanyl-substituted steroid skeleton, have mainly been found in plants of the order Rutales (Meliaceae, Rutaceae, and Simaroubaceae). They are classified by the four (usually highly oxidized) rings (designated as A, B, C, and D) of the intact triterpene backbone as illustrated in Figure 2.2 [46]. Their structures can be usually classified based on the ring systems such as phragmalin, mexicanolide, obacunol and andirobin types. All naturally occurring limonoids contain a furan ring

attached to the D-ring, at C-17, as well as oxygen-containing functional groups at C-3, C-4, C-7, C-16 and C-17 [47].

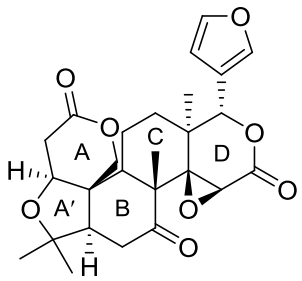

Figure 2.2 Chemical structure of the prototypical limonoid (limonin)

These substances are moderately polar, insoluble in water but soluble well in alcohols and ketones [48]. They are mostly bitter in taste and account for the scent of fresh peels of citrus fruits. Limonoids are occurence in neutral (noncarboxylated/aglycone) as well as acidic (carboxylated/glucoside) forms, the former are insoluble and bitter while latter are soluble and tasteless. Chemically they are highly oxygenated triterpenes which are the side chain has become a furan ring by the deficiency of four carbon, classified as tetranorterpenoids [49].

The biosynthesis pathway of limonoids suggests that limonoids are synthesized through terpenoid biosynthetic pathway, starting with cyclization of squalene (Figure 2.3), which results in a tetracyclic ion, euphane and tirucallane (Figure 2.4), two chemically analogous compounds may be the ultimate biogenetic precursors. Oxidative degradation at the C-17 side chain of either of these nucleus results in loss of four carbon atoms and formation of β-substituted furan, further oxidations and skeletal rearrangements in one or more of the four rings, which are assigned as A, B, C and D (Scheme 2.1), originate to different groups of limonoids shown in Scheme 2.2 [18]. However, the oxidations are either epoxidations of double bonds or Baeyer Villiger of ketones and all of the types to be anticipated from a biological peracid equivalent, reasonable a peroxidase [49].

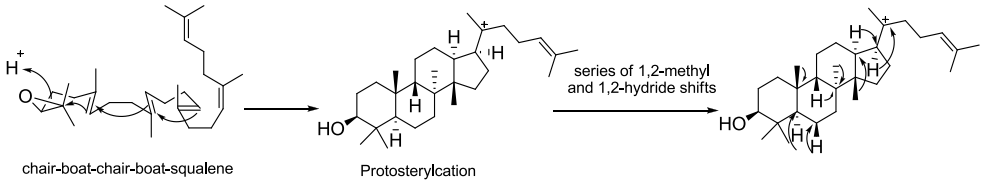

Figure 2.3 Squalene epoxide leading to different intermediate triterpene cations.

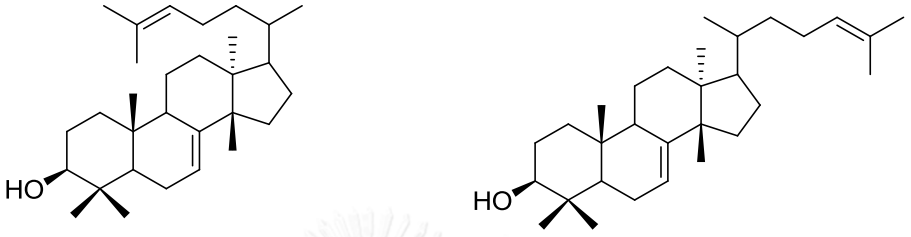

Euphane Tirucallane

Figure 2.4 Precursors of limonoids.

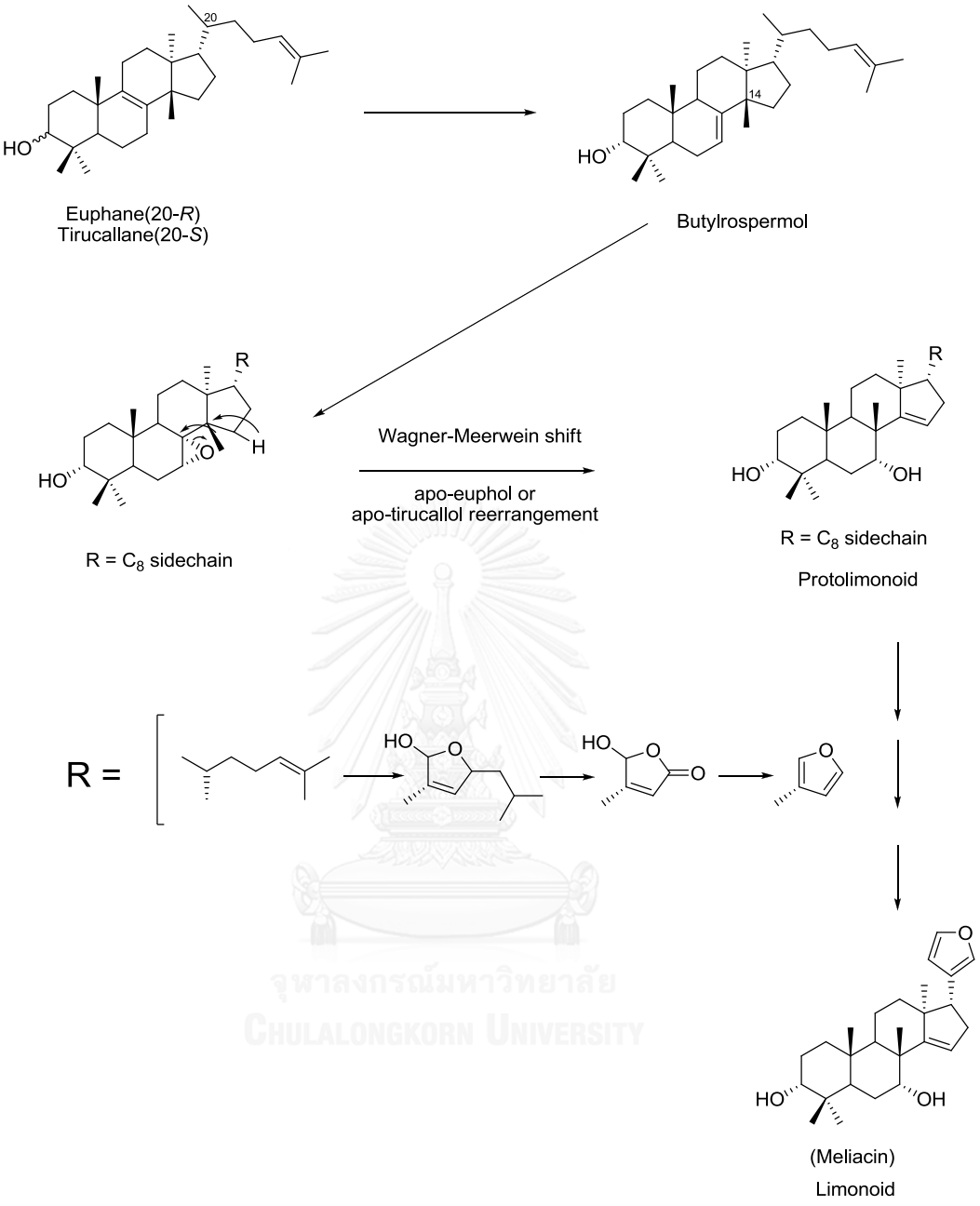

Scheme 2.1 Biosynthetic pathway leading to the formation of a simple limonoid [18].

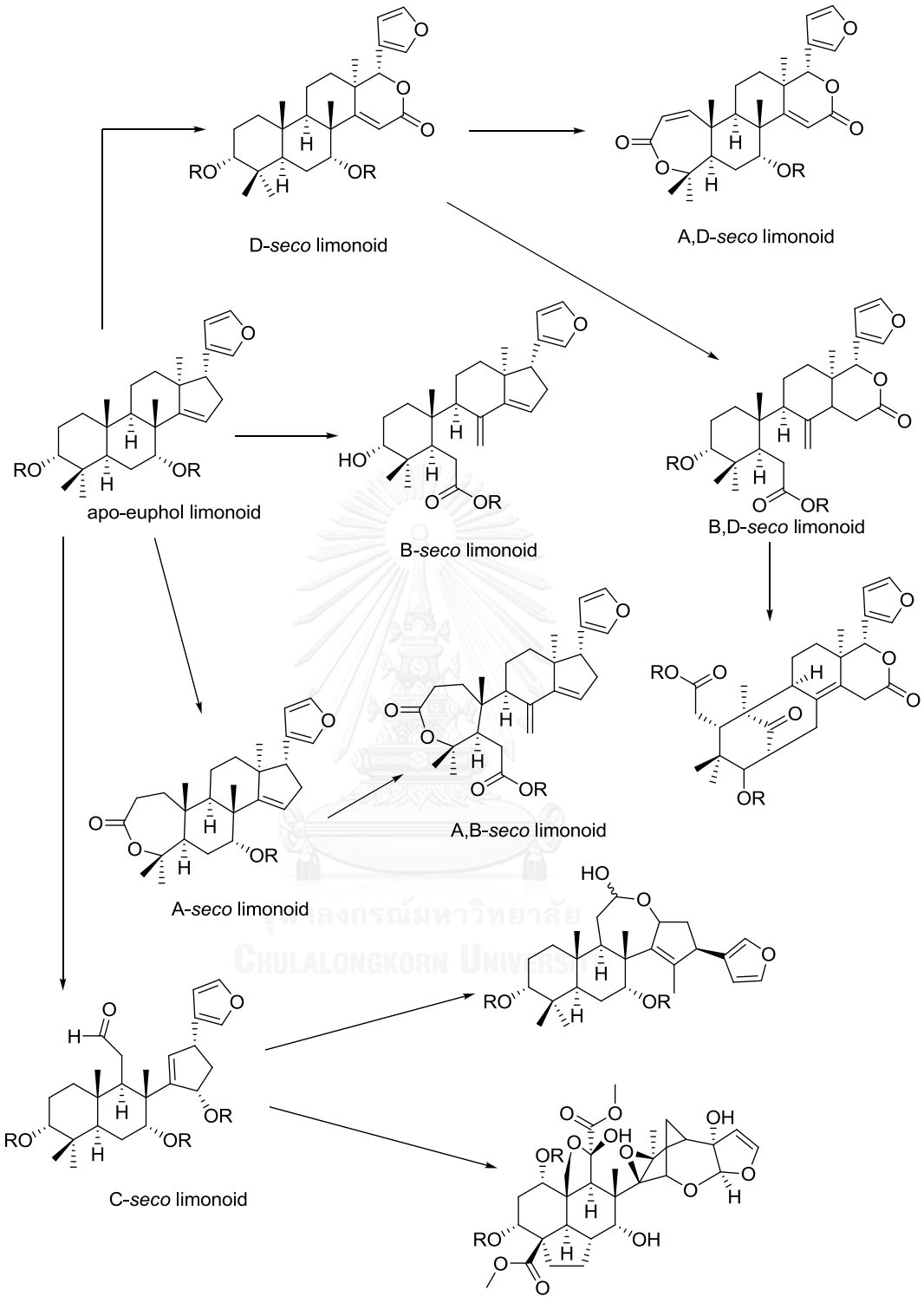

Scheme 2.2 Major biosynthetic routes of limonoids [18].

2.1.2.2 Classes of limonoids

The tetranortriterpenoids or limonoids are classified following by the oxygenation of ring A to D and cyclization to modified skeleton [40].

Normally, the limonoids from only Meliaceae family plants can be divided into 12 groups as follows;

1. Protolimonoids and related compounds triterpenoids
2. Havanensin group (all rings intact)
3. Gedunin group (Ring D opened)
4. Limonoids with ring B and D opened
5. Mexicanolide group (modified ring B opened and recyclised)
6. Phragmalin group (modified, ring B opened and recyclised)
7. Methyl ivorensate group (Rings A, B and D opened)
8. Obacunol group (rings A and D opened)
9. Nimbin group (ring C opened)
10. Toonafolin group (ring B opened)
11. Evodulone group (ring A opened)
12. Prieurianin group (ring A and B opened)

In the case of the *Xylocarpus* plants it has been found only some of the above-mentioned groups of limonoids including gedunin, andirobin, mexicanolide, phragmalin, obacunol and protolimonoid. However, mexicanolide and phragmalin type limonoids are major components. The fruits mainly contain mexicanolides, and some minor components, obacunol and andirobins. The stem and bark are rich in phragmalin orthoesters, accompanied by a few unusual polyhydroxyphragmalins [50].

To date, 88 mexicanolides and 53 phragmalins have been isolated from the timber, fruits, and seeds of mangrove plants of the genus *Xylocarpus* as well as they are natural products with numerous structural diversity

and display a board range of bioactivities [51]. Although the limonoid metabolites have been found in all *Xylocarpus* plants studied, but their distribution and content vary in different plant parts, or geocultivars, of the same species.

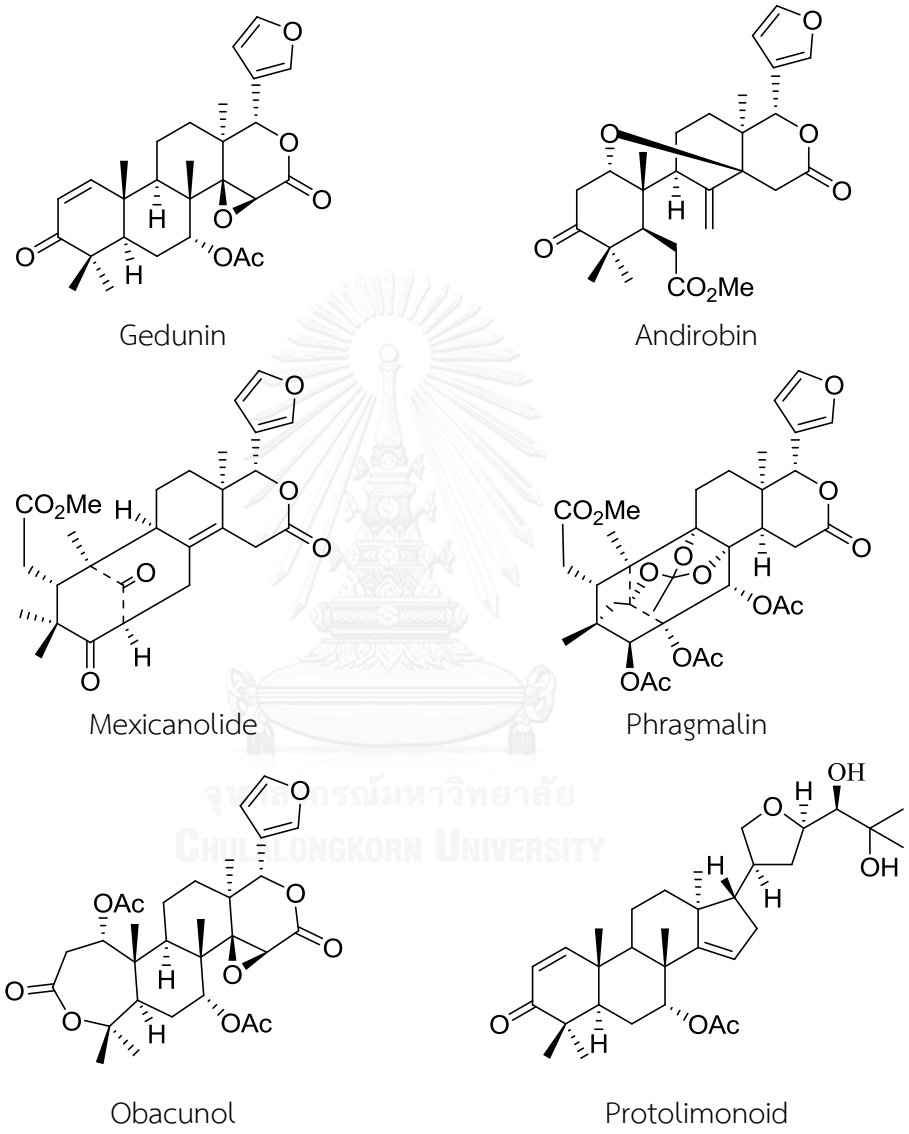

Figure 2.5 Representative limonoids found in the genus *Xylocarpus*.

2.2 Biolgical activities of limonoids from *Xylocarpus* genus

2.2.1 Cytotoxic activities

In 2007, Yin and co-workers reported that five new limonoids, granaxylocarpins A-E (**1-5**), isolated from the seeds of the Chinese marine mangrove *X. granatum*. Granaxylocarpins A and B showed weak cytotoxic activities against the P-388 cell line with IC_{50} values of 9.3 and 4.9 μM, respectively [52].

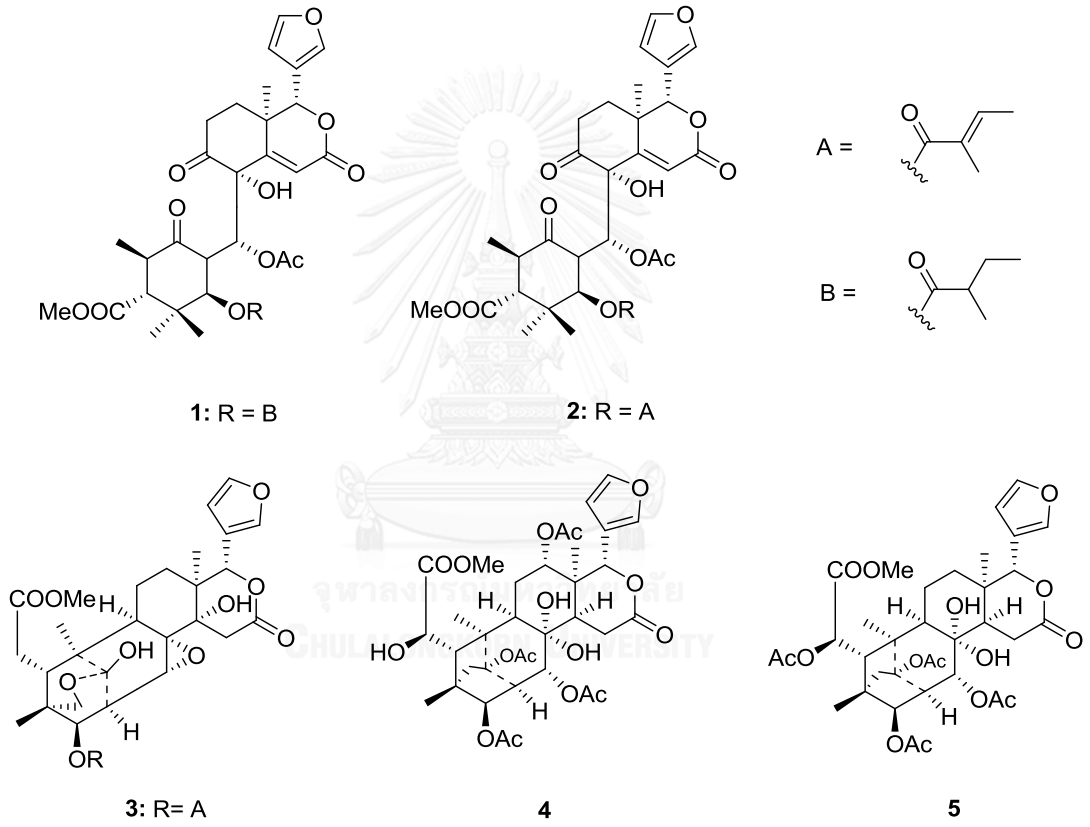

Figure 2.6 The structures of limonoids from *X. granatum*.

In 2007, Uddin and co-workers studied the anti-colon cancer activity of gedunin (**6**) and 1α-hydroxy-1,2-dihydrogedunin (**7**) which were isolated from the bark of *X. granatum*. Only gedunin showed moderate levels of cytotoxic activity against CaCo-2 colon cancer cell lines with IC_{50} value of 16.83 μM [53].

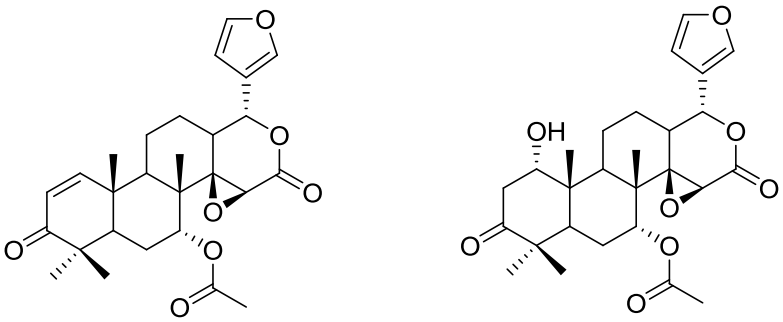

6 **7**

Figure 2.7 The structures of limonoids from *X. granatum*.

In 2009, Cui and co-workers determined the chemical constituents of fruits of a Chinese mangrove plant *X. granatum*. Five new protolimonoids, protoxylocarpins A-E (**8-12**), and two new limonoids, xylocarpins J and K (**13** and **14**), together with xyloccensins M and Y (**15** and **16**) have been isolated. These compounds exhibited moderate to weak activity against HCT-8, Bel-7402, BGC-823 and A2780 tumor cell lines [50].

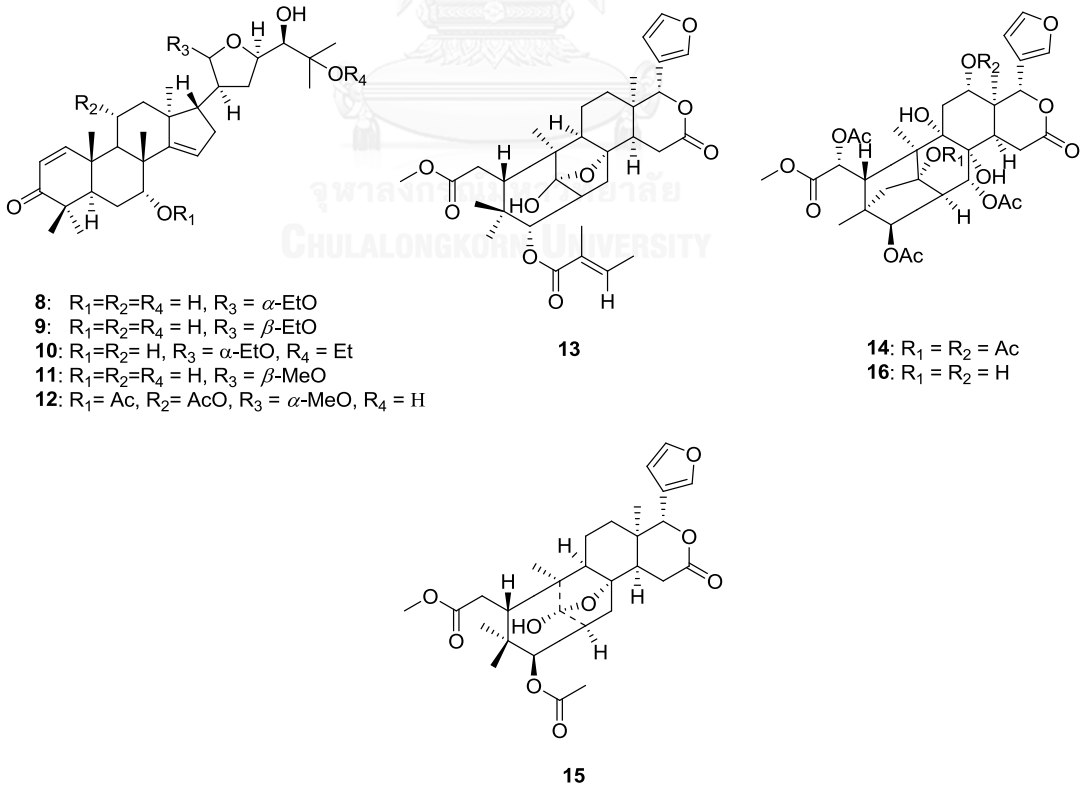

8: R_1=R_2=R_4 = H, R_3 = α-EtO
9: R_1=R_2=R_4 = H, R_3 = β-EtO
10: R_1=R_2= H, R_3 = α-EtO, R_4 = Et
11: R_1=R_2=R_4 = H, R_3 = β-MeO
12: R_1= Ac, R_2= AcO, R_3 = α-MeO, R_4 = H

13

14: R_1 = R_2 = Ac
16: R_1 = R_2 = H

15

Figure 2.8 The structures of limonoids from *X. granatum*.

In 2013, Toume and co-workers reported that xylogranin B (**17**) was isolated from *X. granatum* leaves, by use of a cell-based luciferase screening system targeting a Wnt signaling pathway. This compound inhibited TCF/β-catenin transcriptional activity (IC_{50} 48.9 nM) and exhibited strong cytotoxicity against colon cancer cell lines. Moreover, xylogranin B significantly decreased β-catenin protein levels in nuclei but not in the cytosol. These results indicated that a decrease in β-catenin levels in nuclei resulted in the Wnt signal inhibitory effects of this limonoid [54].

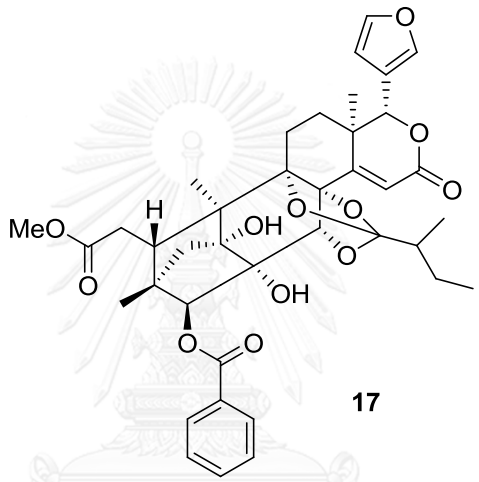

Figure 2.9 The structure of xylogranin B (**17**).

In 2013, Wu and co-workers found two new limonoids, named xylomexicanins C and D (**18** and **19**), from a dichloromethane extract of the seeds of *X. granatum*, cultivated in Hainan, China. Xylomexicanin C (**18**) exhibited antiproliferative activity against human breast carcinoma cell (KT) with an IC_{50} value of 4.60 μM [55].

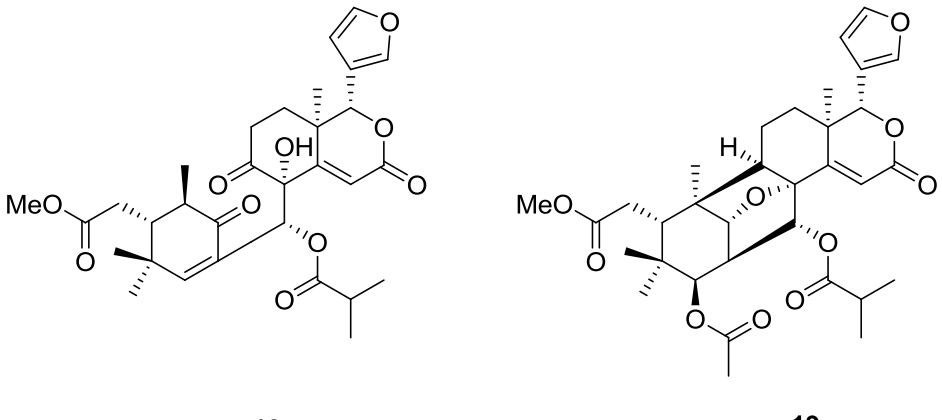

Figure 2.10 The structures of limonoids from *X. granatum*.

2.2.2 Antimicrobial activities

In 2010, Pudhom and co-workers found three new phragmalin limonoids, moluccensins H-J (**20-22**), which were isolated from seed kernels of the cedar mangrove, *X. moluccensis*. Only moluccensin I (**21**) displayed weak antibacterial activity against *Staphylococcus hominis* ATCC 27844 and *Enterococcus faecalis* ATCC 29212, with a MIC at 256 μg/mL [56].

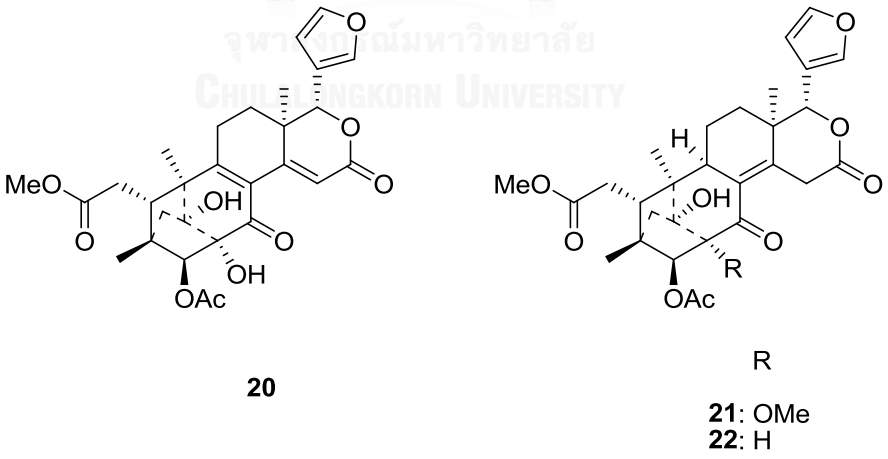

Figure 2.11 The structures of limonoids from *X. moluccensis*.

2.2.3 Anti-osteoclastogenic activities

In 2011, Wisutsitthiwong and co-workers reported 7-oxo-7-deacetoxygedunin (**23**), a gedunin type limonoid from seeds of the mangrove *X. moluccensis*, as a potent inhibitor of osteoclastogenesis. In addition, This compound showed strong anti-osteoclastogenic activity with low cytotoxicity against the monocyte/macrophage progenitor cell line, RAW264.7. The IC_{50} for anti-osteoclastogenic activity was 4.14 μM [57].

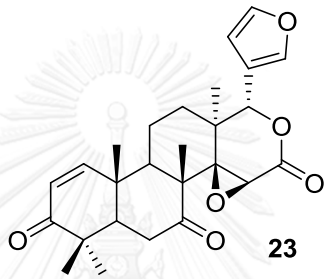

Figure 2.12 The structure of 7-oxo-7-deacetoxygedunin (**23**).

2.2.4 Anti-inflammatory activities

In 2010, Ravangpai and co-workers found a new andirobin, thaimoluccensin A (**24**), and two new phragmalin-type limonoids, thaimoluccensins B (**25**) and C (**26**), from seeds of a Thai *X. moluccensis*, together with eight known compounds (**27-34**). Only 7-deacetylgedunin (**30**), a gedunin-type limonoid, exhibited significant inhibitory activity against nitric oxide production from activated macrophages with IC_{50} value less than 10 μM, suggesting that the compound has anti-inflammatory activity [58].

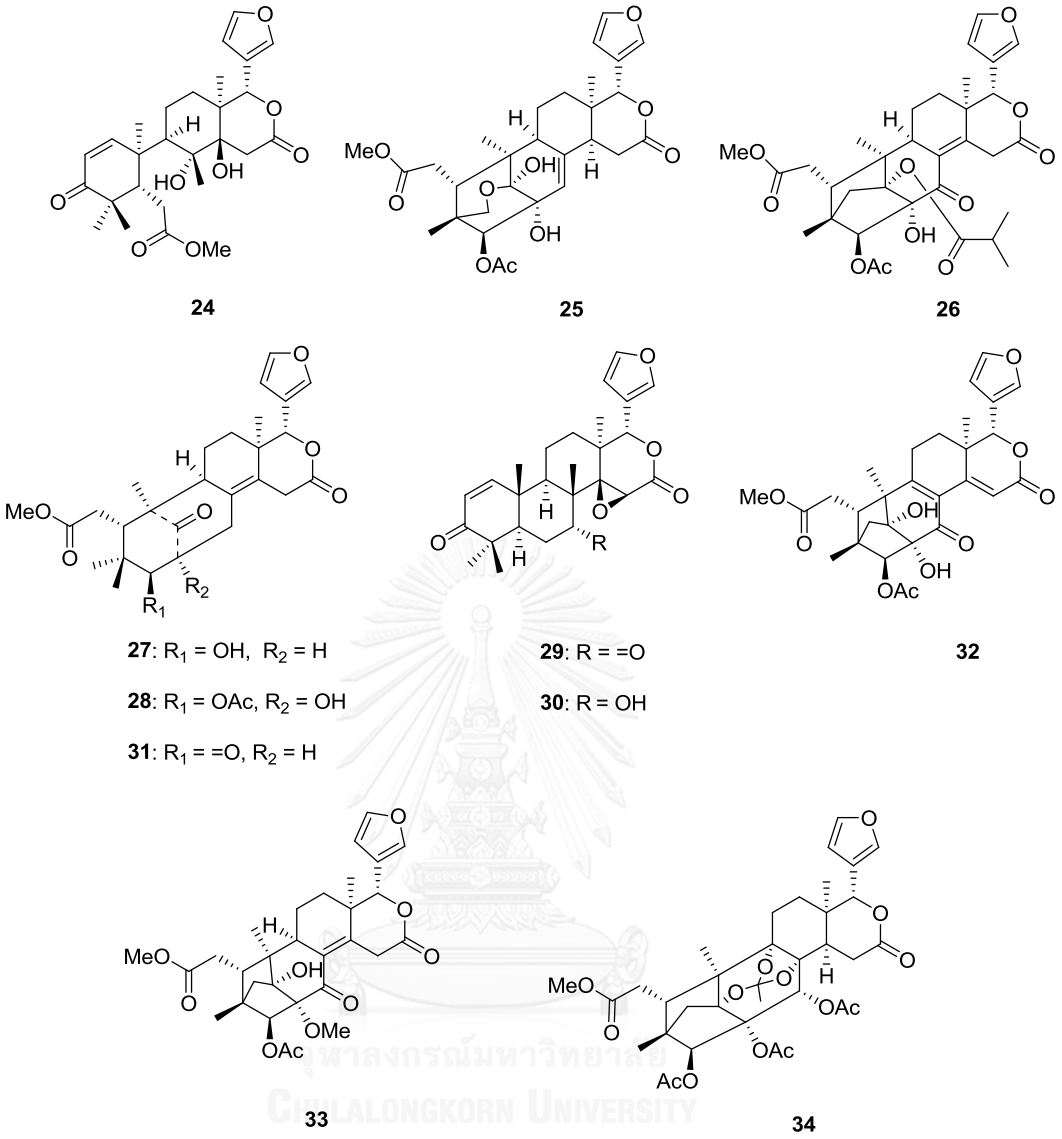

Figure 2.13 The structures of limonoids from *X. moluccensis*.

In 2013, Li and co-workers found three limonoids named thaixylomolins A-C (**35-37**), featuring two new motifs, isolated from the seeds of a Thai mangrove, *X. moluccensis*. Thaixylomolin B (**36**) exhibited inhibitory activity against nitric oxide production in lipopolysaccharide and IFN-γ-induced RAW264.7 murine macrophages with an IC_{50} value of 84.3 μM [22].

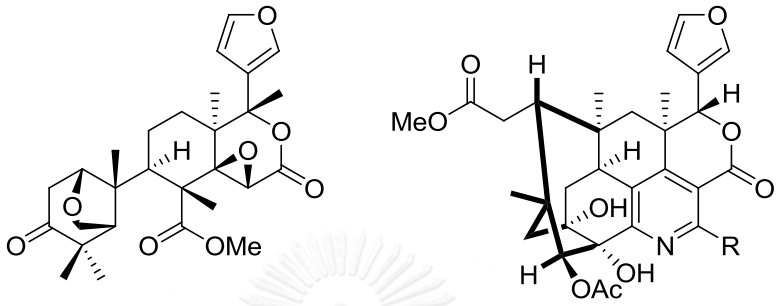

Figure 2.14 The structure of limonoids from *X. moluccensis*.

2.3 Chemical constituents of *X. rumphii*

Normally, The *Xylocarpus* plants could be found in mangrove forest both eastern and southern part of Thailand. More recently, we reported the isolation and identification of four new mexicanolide limonoids, named xylorumphiins A-D (**38-41**) from the seed kernels of *X. rumphii* which collected from Rayong Province, Thailand [44]. However, the different of ecological system in each area and the period of harvesting have exceedingly effect on characteristic feature of limonoids. This prompted us to explore limonoids from another mangrove area in Thailand because there are very few reports of limonoids and its biological activity from this species. Particularly, anti-inflammatory effect of isolated limonoids would be evaluated.

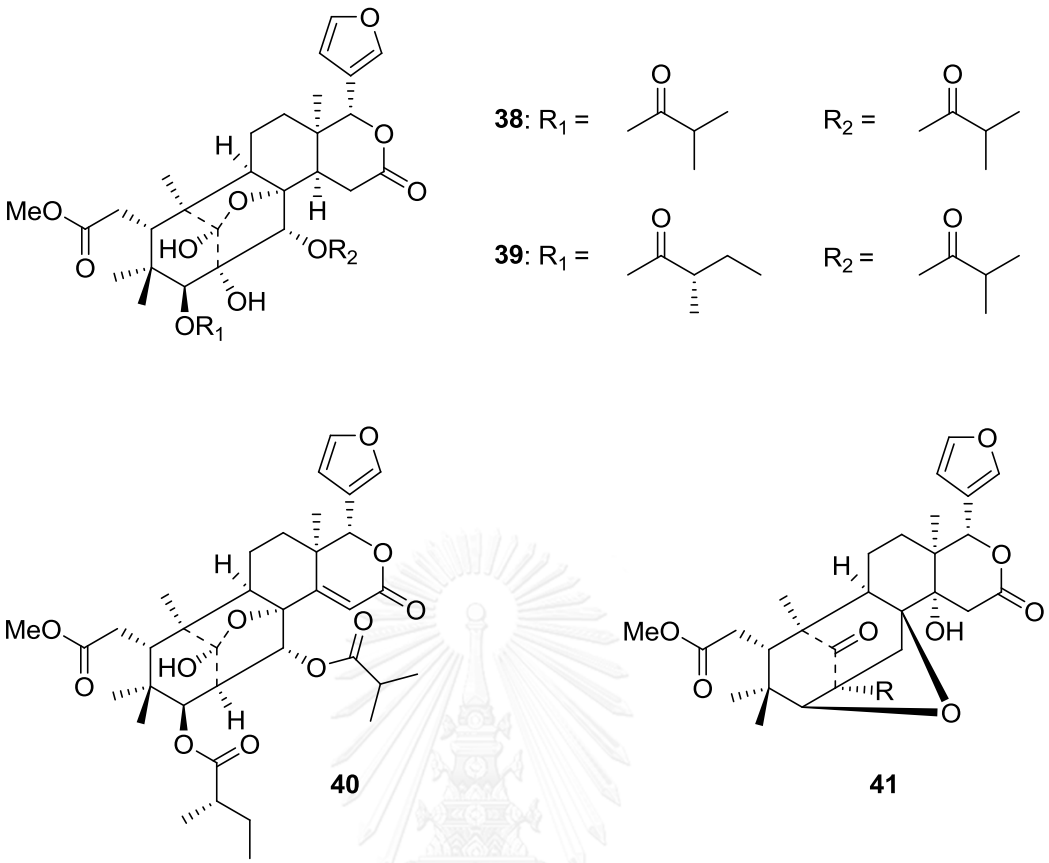

Figure 2.15 The structures of limonoids from *X. rumphii*.

2.4 Experiments

2.4.1 Plant materials

The fruits of *X. rumphii* were collected in February 2011 from Kudee island, Thailand, and authenticated by the Royal Forest Department, Bangkok, Thailand. A voucher specimen (BKF No. 1638) was deposited at the Forest Herbarium, Royal Forest Department, Bangkok, Thailand.

2.4.2 General Experimental Procedures

2.4.2.1 Nuclear magnetic resonance spectrometer (NMR)

The NMR spectra were recorded in $CDCl_3$ using a Bruker AV400 and Varian Mecury 400 plus spectrometer at 400 MHz for ^{1}H NMR and at 100 MHz for ^{13}C NMR using TMS (tetramethylsilane) as internal standard.

2.4.2.2 Mass spectrometer (MS)

HRESIMS spectra were obtained with a Bruker micrOTOF.

2.4.2.3 Ultraviolet-visible spectrophotometer (UV-vis)

UV data were recorded on a CARY 50 Probe UV-visible spectrophotometer.

2.4.2.4 Fourier transforms infrared spectrophotometer (FT-IR)

FT-IR spectra were recorded on a Perkin-Elmer Model 1760X Fourier Transform Infrared Spectrophotometer. Solid samples were formally examined by incorporating the sample with potassium bromide (KBr) to form a pellet.

2.4.2.5 Optical rotation

Optical rotations were measured on a Perkin-Elmer 341 polarimeter at 589 nm.

2.4.2.6 Melting point

Melting points were recorded on a Fisher-Johns melting point apparatus.

2.4.2.7 X-ray crystallography

The crystal structure was performed at 296 K on a Bruker APEX-II CCD diffractometer with Mo Kα radiation (λ = 0.710 73 Å) by using SHELXS97 program. Crystallographic data, excluding structure factors, have been deposited at the Cambridge Crystallographic Data Centre.

2.4.3 Chemicals

2.4.3.1 Solvents

All commercial grade solvents, used in this research such as hexane, dichloromethane (CH_2Cl_2), ethyl acetate (EtOAc), acetone and methanol (MeOH), were purified by distillation prior to use. In addition, the deuterated solvent for NMR emperiments was $CDCl_3$

2.4.3.2 Other chemicals

Merck's silica gel 60 No. 7734 and No. 9385 were used as adsorbents for open column chromatography. Merck's thin layer chromatography (TLC) aluminum sheets, silica gel 60 F_{254} precoated, 20 x 20 cm, layer thickness 0.2 mm were used for TLC analysis. Detection was visualized under ultraviolet light at wavelengths of 254 nm and dipped with $(NH_4)_6Mo_7O_{24}$ in 5% H_2SO_4 solution then heating for 1-2 min at 105–120°C on a hot plate.

2.4.4 Extraction and Isolation

The air-dried, powdered seeds of *X. rumphii* (5 kg) were extracted three times with MeOH (10 L, each for 3 days) at room temperature. The extract was concentrated under reduced pressure. The combined MeOH extract was partitioned between EtOAc and H_2O to obtain the EtOAc crude extract (107 g). The EtOAc extract was fractionated over a column of silica gel with a gradient of EtOAc–*n*-hexane (from 1:9 to 1:0) to give 14 fractions, A–N. Fraction G (7.84 g) was subjected to passage over a column of Sephadex LH-20 (MeOH) to afford four fractions (G1–G4), and fraction G2 (376.31 mg) was rechromatographed over silica gel eluting with an EtOAc–*n*-hexane gradient (from 3:7 to 1:1) to yield seven subfractions (G2a–G2g). Fraction G2a (47.9 mg) was purified by silica gel CC (EtOAc–n-hexane, from 2:3 to 1:1) to give **45** (4.3 mg). Fraction G2e (74.6 mg) was chromatographed over a silica gel column with MeOH–CH_2Cl_2 (2:98), and the major fraction G2e.4 (45.2 mg) was rechromatographed with EtOAc–*n*-hexane (from 3:7 to 1:1) to obtain compounds **47** (7.7 mg) and **49** (19.3 mg). Fraction G2f (22.0 mg) was purified by CC over silica gel with EtOAc–*n*-hexane (2:3) to give compounds **42** (2.9 mg) and **44** (11.3 mg). Using the same procedure, fraction G2g (19.7 mg) yielded compound **43** (11.2 mg). Fraction J (256.9 mg) was recrystallized from MeOH to give xyloccensin E (**50**, 178.8 mg). Fraction K (3.44 g) was subjected to a column of Sephadex LH-20 with MeOH to afford six fractions, K1–K6. Fraction K2 (115.6 mg) was further purified by silica gel CC eluted with MeOH–CH_2Cl_2 (4:96) to yield compounds **46** (7.6 mg) and **48** (9.9 mg). Fraction K4 (157.8 mg) was recrystallized from MeOH to afford xyloccensin K (**51**, 85.3 mg).

2.4.5 Absolute configuration of C-2 of the 2-methylbutyryl group of xylorumphiins F, G, and I (43, 45 and 47) and 2-hydroxyxylorumphiin F (44)

Each compound (3 mg) was dissolved in EtOH (0.5 mL) and treated with 10% aqueous KOH solution (1 mL). After stirring overnight, the mixture was concentrated and washed with EtOAc (×3), and the aqueous layer was acidified with HCl to pH 3.0 and extracted with CH_2Cl_2 (×3). The combined organic layer was subjected to Sephadex LH-20 CC (CH_2Cl_2–MeOH, 1:1) to yield 2*S*-methylbutanoic acid, $[\alpha]^{20}_D$ +10, +12, +15, and +18, for compounds **43**-**45** and **47**, respectively, lit. $[\alpha]^{25}_D$ +19.2 [59].

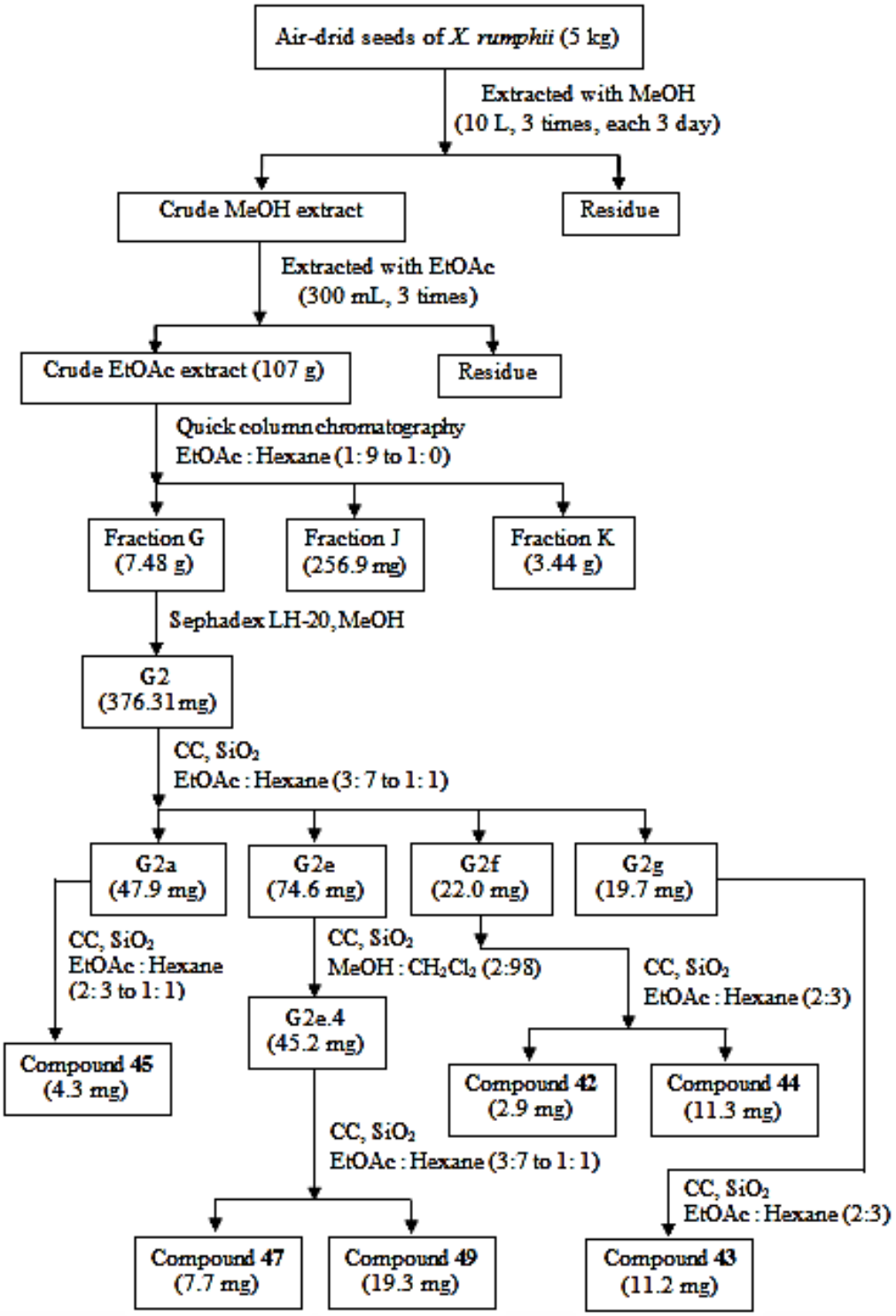

Scheme 2.3 The extraction and isolation procedure of *X. rumphii* seeds.

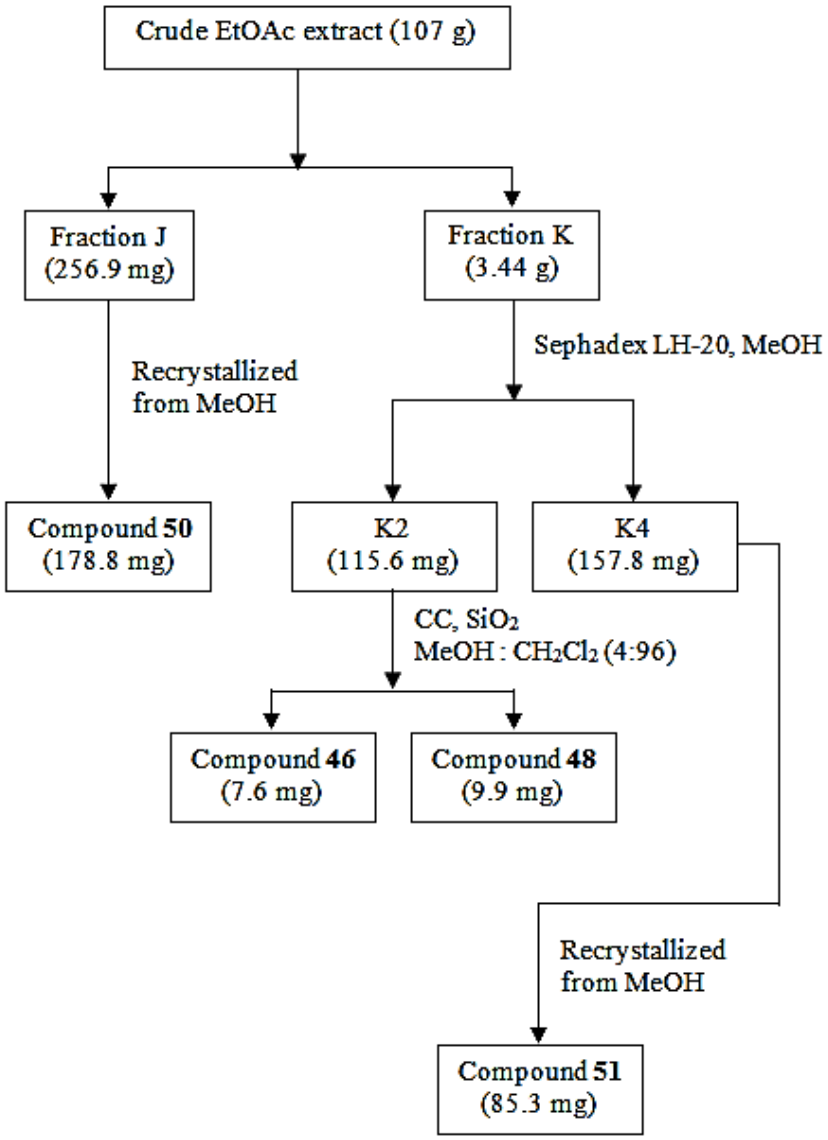

Scheme 2.3 The extraction and isolation procedure of *X. rumphii* seeds (Continued)

2.5 Results and Discussion

2.5.1 The isolated compounds from *Xylocarpus rumphii* (Kostel.) Mabb.

The EtOAc crude extract of the seeds of *X. rumphii* was purified by chromatographic techniques to obtain ten limonoids including six new mexicanolides, xylorumphiins E-F (**42-43**), 2-Hydroxyxylorumphiin F (**44**), xylorumphiins G-I (**45-47**) and a new phragmalin, xylorumphiin J (**48**) together with

three known derivatives namely xyloccensins X, E and K (**49-51**). Their structures are shown in Figure 2.16.

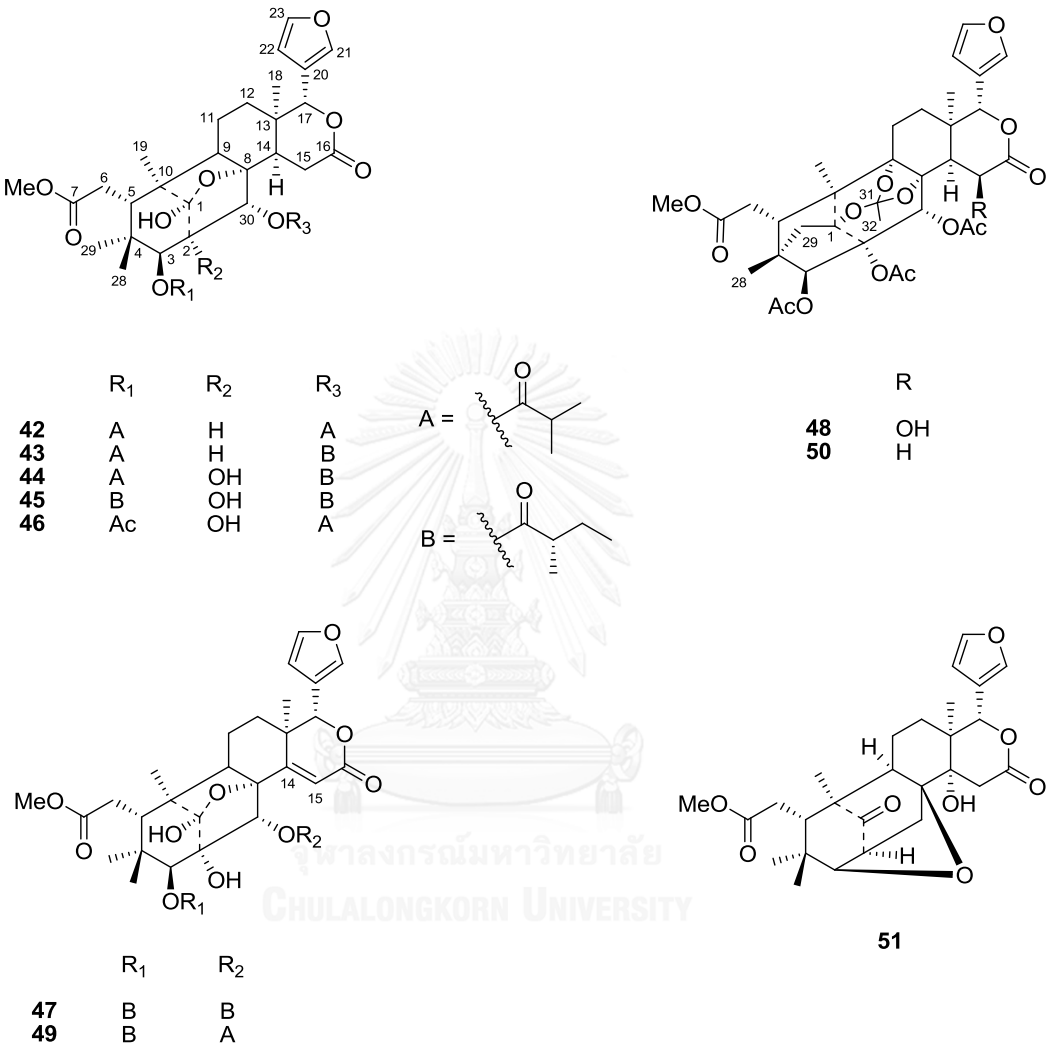

	R_1	R_2	R_3
42	A	H	A
43	A	H	B
44	A	OH	B
45	B	OH	B
46	Ac	OH	A

	R
48	OH
50	H

	R_1	R_2
47	B	B
49	B	A

Figure 2.16 Isolated compounds from the seeds of *X. rumphii*.

Xylorumphiin E (**42**) was obtained as white amorphous powder, $[\alpha]_D^{20}$ -13.0 (*c* 0.03, MeOH), UV (MeOH) λ_{max} (log ε) 209 (3.24) nm, had the molecular formula $C_{35}H_{48}O_{11}$, as established by ^{13}C NMR data and HRESIMS based on *m/z* 667.2996 $[M + Na]^+$ ion (calcd 667.3089), corresponding to 12 indices of hydrogen deficiency. From the ^1H and ^{13}C NMR spectroscopic data (Table 1.1), it was clear that six of the 12 indices of hydrogen deficiency came from two carbon–carbon double bonds (furan ring) and four esters carbonyls. Therefore, it required six additional rings in the structure of **42**. The NMR data of **42** (Table 1.1) and its 2D correlations (Figure 2.17) indicated the presence of four tertiary methyls (δ_H 0.75 s, 1.04 (×2) s, and 1.19 s; δ_C 21.0, 22.1, 22.2 and 24.6), a typical β-substituted furan moiety (δ_H 6.39 s, 7.39 s, and 7.54 s; δ_C 110.0, 121.0, 141.5 and 142.9), a methoxycarbonyl (δ_H 3.70 s; δ_C 51.9 and 173.9), and two isobutyryl groups (δ_H 1.04 br s, 6H, 1.10 d (*J* = 6.8 Hz), 1.21 d (*J* = 6.8 Hz), 2.53 m, and 2.66 m; δ_C 17.5, 18.3, 19.1, 20.0, 33.3, 33.9, 174.9 and 177.0). The aforementioned data strongly suggested that **42** was a mexicanolide-type limonoid. The NMR data of **42** were very similar to those of xylorumphiin A (**38**) (Figure 2.15) [44], except for the presence of an additional methine (δ_H 2.61 m; δ_C 57.1) in place of an oxygenated carbon in xylorumphiin A (**38**). The methine functionality was assigned to C-2 by the ^1H–^1H COSY correlations from its proton at δ_H 2.61 to H-3 and H-30 and by its HMBC correlations to C-1, C-3 and C-30 (Figure 2.17). The quaternary carbon resonance at δ_C 106.7 was assigned to C-1, a hemiacetal carbon, by its HMBC correlation with a proton resonance at δ_H 3.57 (1-OH) that did not show correlation with any carbon in the HSQC spectrum. The HMBC correlations from H-3 (δ_H 5.09, d (*J* = 9.2 Hz) and H-30 (δ_H 6.17, br s) to the carbonyl carbons (C-1' and C-1'') of the isobutyryl groups confirmed their location at C-3 and C-30, respectively. The relative configuration of **42** was established by NOE interactions (Figure 2.17). The NOESY spectrum showed close similarity with reported NOE data of xylorumphiin A (**38**) [44]. The NOE cross-peaks observed from H-3 to H-2 and H_3-29 indicated δ-orientation of these protons and the corresponding 3β-isobutyryl group, whereas the lack of an interaction from H-3 to H-5 indicated a β-orientation of H-5. The δ-orientation of the 30-isobutyryl group was deduced by the NOE cross-peaks between H-3/H-30 and/or

H-2/H-30. On the basis of the above results, the structure of **42** was elucidated as shown in Figure 2.17.

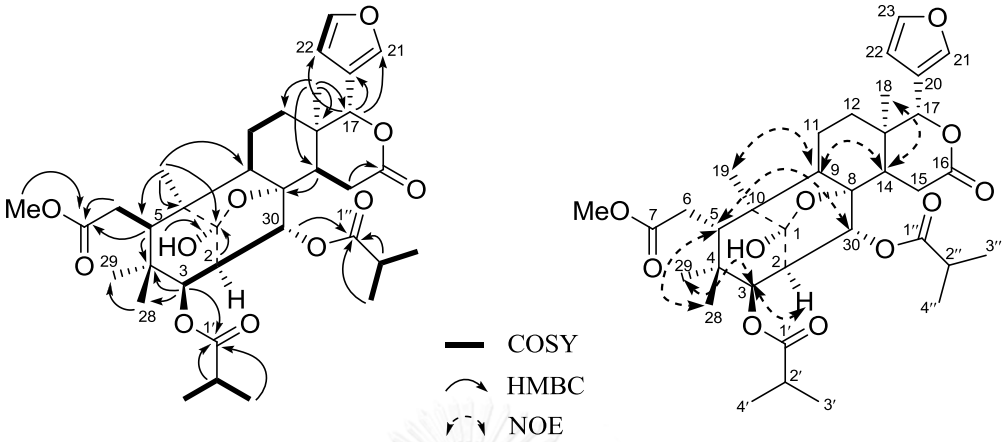

Figure 2.17 Key HMBC, COSY and NOE correlations of compound **42**.

Table 2.1 The NMR data of compound **42** in $CDCl_3$.

Position	^{1}H, mult. (*J* in Hz)	^{13}C	HMBC
1		106.7	
2	2.61, m	57.1	C- 1, C-3, C-30
3	5.09, d (9.2)	73.4	C-2,C-4, C-1′
4		38.1	
5	2.59, m	40.5	C-4, C-6, C-7, C-10
6	2.32, d (10.0)	32.5	C-5, C-7
	2.28, br s		
7		173.9	
8		82.4	
9	1.44, d (12.4)	64.4	C-8, C-10, C-12
10		43.7	
11	1.92, d (14.0)	19.6	C-9, C-13
	1.67, m		
12	1.83, d (16.4)	35.9	C-13, C-17
	1.33, m		
13		36.3	
14	2.19, d (10.0)	46.6	C-8, C-13, C-15, C-17
15	3.25, d (20.0)	29.0	C-13, C-14, C-16
	2.73, dd (10.0, 20.0)		
16		169.9	
17	5.26, s	77.1	C-13, C-14, C-20, C-21, C-22
18	1.04, br s	21.0	C-12, C-13, C-14, C-17
19	1.04, br s	22.2	C-1, C-5, C-9, C-10
20		121.0	
21	7.54, s	141.5	C-17, C-20, C-22
22	6.39, s	110.0	C-20,C-23
23	7.39, s	142.9	C-20,C-22
28	0.75, s	24.6	C-3, C-4, C-5, C-29
29	1.19, s	22.1	C-3, C-4, C-5, C-28
30	6.17, br s	75.9	C-2, C-8, C-1"
7-OMe	3.70, s	51.9	
1'		177.0	
2'	2.53, m	33.3	C-1′, C-3′, C-4′
3'	1.10, d (6.8)	18.3	C-1′, C-2′, C-4′
4'	1.21, d (6.8)	20.0	C-1′, C-2′, C-3′
1"		174.9	
2"	2.66, m	33.9	C-1′′, C-3′′,C-4′′
3"	1.04, br s	19.1	C-1′′, C-2′′,C-4′′
4"	1.04, br s	17.5	C-1′′, C-2′′,C-3′′

Xylorumphiin F (**43**) was obtained as a white amophous powder, $[\alpha]^{20}_{D}$ +18.0 (*c* 0.11, MeOH), UV (MeOH) λ_{max} (log ε) 208 (3.50) nm, gave a molecular formula $C_{36}H_{50}O_{11}$ as determined by ^{13}C NMR and a HRESIMS ion at *m/z* 657.3270 [M – H]$^-$ (calcd 657.3269). The MS and NMR data suggested the presence of an additional –CH_2– unit in **43** compared to xylorumphiin E (**42**). The NMR spectroscopic data of **43** (Table 1.2) were similar to those of **42** except for the replacement of an isobutyryl group in **42** by a 2-methylbutyryl group at C-30. The existence of the 2-methylbutyryl group was confirmed by ^{1}H–^{1}H COSY correlations between H_3-5"/H-2", H-2"/H_2-3", and H_2-3"/H_3-4". The HMBC correlation from H-30 (δ_H 6.17, br s) to the carbonyl carbon (δ_C 174.9) of the 2-methylbutyryl group defined its location at C-30. The absolute configuration at C-2″ in the 2-methylbutyryl group could be determined according to the specific rotation of the corresponding acid derived from the alkaline hydrolysis of **43** $[\alpha]^{20}_{D}$ -14.3 for (*R*)-2-methylbutyric acid and $[\alpha]^{20}_{D}$ +19.2 for (*S*)-2-methylbutyric acid) [60]. Although a 1:1 mixture with isobutanoic acid was obtained from the hydrolysis, 2-methylbutanoic acid is optically active. Therefore, the absolute configuration at C-2″ in the 2-methylbutyryl group was assigned as *S* from the $[\alpha]^{20}_{D}$ value of +10 (*c* 0.05, MeOH) of this mixture. Both compounds **42** and **43** shared the same relative configuration, as confirmed by similar NOE correlations as shown in Figure 2.18.

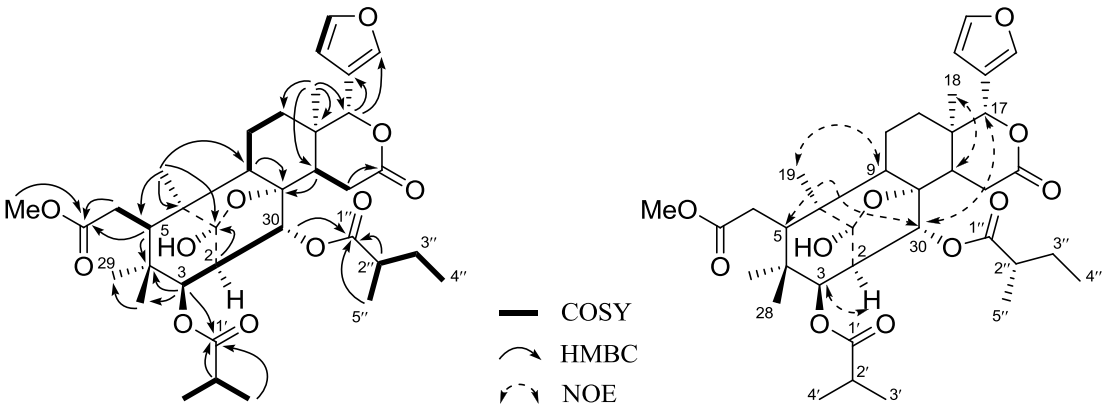

Figure 2.18 Key HMBC, COSY and NOE correlations of compound **43**.

Table 2.2 The NMR data of compound **43** in $CDCl_3$.

Position	^{1}H, mult. (*J* in Hz)	^{13}C	HMBC
1		106.6	
2	2.59, m	57.1	C- 1, C-3, C-30
3	5.11, d (9.6)	73.5	C-2,C-4, C-1′
4		38.0	
5	2.61, m	40.4	C-4, C-6, C-7, C-10
6	2.33, d (9.6)	32.5	C-5, C-7
	2.25, d (16.4)		
7		173.9	
8		82.3	
9	1.42, m	63.4	C-8, C-10, C-12
10		43.7	
11	1.92, dd (3.6, 13.2)	19.6	C-9, C-13
	1.66, m		
12	1.83, d (16.4)	35.9	C-13, C-17
	1.31, m		
13		36.3	
14	2.19, d (9.6)	46.6	C-8, C-13, C-15, C-17
15	3.26, d (20.0)	29.0	C-13, C-14, C-16
	2.73, dd (9.6, 20.0)		
16		170.0	
17	5.25, s	77.1	C-13, C-14, C-20, C-21, C-22
18	1.05, s	22.0	C-12, C-13, C-14, C-17
19	1.04, s	21.0	C-1, C-5, C-9, C-10
20		121.0	
21	7.53, s	141.5	C-17, C-20, C-22
22	6.39, s	110.0	C-20,C-23
23	7.39, s	143.0	C-20,C-22
28	0.75, s	22.1	C-3, C-4, C-5, C-29
29	1.19, s	24.6	C-3, C-4, C-5, C-28
30	6.17, br s	75.8	C-2, C-8, C-1″
7-OMe	3.70, s	51.9	
1′		177.2	
2′	2.65, m	33.9	C-1′, C-3′, C-4′
3′	1.11, d (6.8)	18.3	C-1′, C-2′, C-4′
4′	1.21, d (6.8)	20.0	C-1′, C-2′, C-3′
1″		174.9	
2″	2.41, m	40.6	C-1″, C-3″,C-4″
3″	1.66, m	25.3	C-1″, C-2″,C-4″
	1.42, m		
4″	0.90, t (7.6)	11.2	C-1″, C-2″,C-3″
5″	1.20, d (7.2)	16.4	

2-Hydroxyxylorumphiin F (**44**), a white amorphous powder, $[\alpha]^{20}_{D}$ -19.0 (*c* 0.10, MeOH), UV (MeOH) λ_{max} (log ε) 209 (3.61) nm, was assigned a molecular formula of $C_{36}H_{50}O_{12}$ by ^{13}C NMR data and an HRESIMS *m/z* 697.3169 [M + Na]+ ion (calcd 697.3194). Its ^{1}H and ^{13}C NMR data (Table 1.3) closely resembled those of **43**, except for the presence of an oxygenated tertiary carbon (δ_C 82.1) instead of a methine group in **43**. This carbon was assigned to C-2 due to its HMBC correlation with H-3 (δ_H 4.89 s). A proton resonance at δ_H 3.21 that did not show correlation with any carbon in the HSQC spectrum was assigned to 2-OH by its HMBC correlations to C-1, C-2, C-3, and C-30 (Figure 2.19). Similar NOE correlations suggested that compound **44** possessed the same relative configuration as those of **42** and **43**. The key NOE cross-peak observed in **44** from 2-OH to H-3, along with the lack of correlation from 2-OH to H-30, confirmed the α-orientation of 2-OH (Figure 2.19). The absolute configuration at C-2″ in the 2-methylbutyryl group was determined as *S*, the same as that in **43**, from the $[\alpha]^{20}_{D}$ value of +12 (*c* 0.05, MeOH) of the corresponding acid.

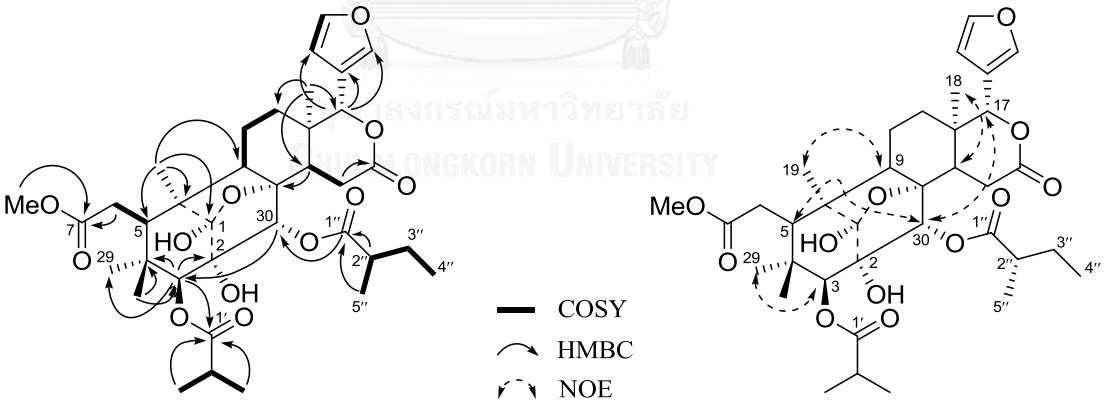

Figure 2.19 Key HMBC, COSY and NOE correlations of compound **44**.

Table 2.3 The NMR data of compound **44** in $CDCl_3$.

Position	^{1}H, mult. (*J* in Hz)	^{13}C	HMBC
1		107.2	
2		82.1	
3	4.89, s	80.3	C-2, C-4, C-29, C-30, C-1′
4		38.9	
5	2.64, m	40.3	
6	2.37, dd (9.6,16.4)	32.3	C-7
	2.27, br s		
7		173.9	
8		81.1	
9	1.51, m	63.3	
10		42.6	
11	1.89, m	19.7	
	1.69, m		
12	1.83, m	35.8	
	1.35, m		
13		36.3	
14	2.75, dd (9.2, 19.6)	46.5	C-8, C-13, C-16, C-17
15	2.22, d (9.2)	29.0	C-8,C-13, C-16
	3.13, d (19.6)		
16		169.6	
17	5.18, s	77.2	C-12, C-13, C-20, C-21, C-22
18	1.03, s	22.2	C-12, C-13, C-14, C-17
19	1.12, s	21.0	C-1, C-5, C-9, C-10
20		120.8	
21	7.55, s	141.6	C-17, C-20, C-22
22	6.40, s	109.9	C-17, C-20, C-23
23	7.40, s	143.1	C-20, C-21
28	0.73, s	24.2	C-3, C-4, C-5, C-29
29	1.25, s	22.0	C-3, C-4, C-5, C-28
30	6.23, s	76.7	C-1′′
7-OMe	3.71, s	52.0	C-7
1-OH	4.21, s		
2-OH	3.21, s		
1'		177.6	
2'	2.61, m	33.9	
3'	1.09, d (6.8)	18.2	C-1', C-2', C-4'
4'	1.21, d (6.8)	20.2	C-1', C-2', C-3'
1''		174.3	
2''	2.43, m	40.7	
3''	1.67, m	27.2	
	1.28, m		
4''	0.91, t (7.6)	12.0	C-2'', C-3''
5''	1.08, d (6.4)	14.9	C-1′′, C-2'', C-3''

Xylorumphiin G (**45**) was obtained as a colorless crystals, $[\alpha]^{20}_{D}$ -68.0 (*c* 0.09, MeOH), UV (MeOH) λ_{max} (log ε) 208 (3.51) nm. The molecular formula $C_{37}H_{52}O_{12}$ was assigned by ^{13}C NMR and an HRESIMS ion at *m/z* 687.3390 $[M - H]^-$ (calcd 687.3381). The NMR data (Tables 1.3 and 1.5) indicated that **45** was similar to **44**, except for the presence of a 2-methylbutyryl group in place of the isobutyryl group in **44**. The HMBC correlations from H-3 and H-30 to the respective carbonyl carbon of the 2-methylbutyryl groups placed these acyl groups at C-3 and C-30. A proton at δ_H 4.25, which did not display correlation with a carbon in the HSQC spectrum, was assigned to 1-OH; the second 2-methylbutyryl group was thus assumed to be attached at C-3. Thus, the 2-methylbutyryl groups at C-3 and C-30 were α-oriented (Figure 2.20). The absolute configurations at C-2′ and C-2″ in the respective 2-methylbutyryl groups were determined as *S* due to the $[\alpha]^{20}_{D}$ value of +15 (*c* 0.03, MeOH) of the corresponding acid obtained from alkaline hydrolysis.

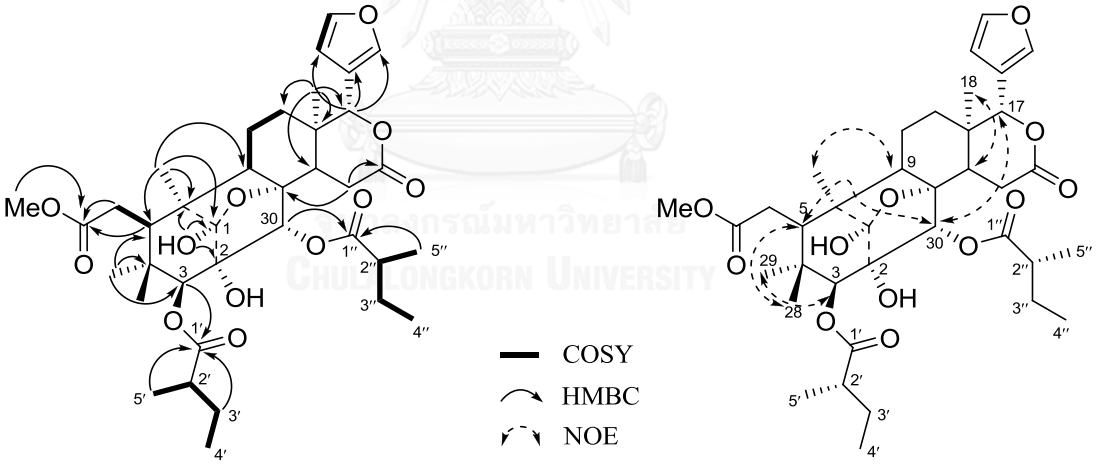

Figure 2.20 Key HMBC, COSY and NOE correlations of compound **45**.

In order to clarify the full structure and establish the relative configuration of **45**, single-crystal X-ray diffraction analysis was utilized.

X-ray Crystallographic Analysis of 45. The single-crystal X-ray diffraction data were collected at 296 K on a Bruker APEX-II CCD diffractometer with Mo Kα radiation (λ = 0.71073 Å). The crystal structure was solved by direct methods using SHELXS-97 and refined with full-matrix least-squares on all F^2 data using SHELXS-97 to final *R* values. All non-hydrogen atoms were anisotropically refined, except for the oxygen C-3A atom, which was refined isotropically. The C-3A atom is disordered over two positions with site occupancies of 0.52 and 0.48. All hydrogen atoms were added at calculated positions and refined using a rigid model, with C–H = 0.93 Å (aromatic), 0.97 Å (CH_2), and 0.98 Å (CH_3) and O–H = 0.82 Å. Crystallographic data for **45** have been deposited with the Cambridge Crystallographic Data Centre under the deposition number CCDC 998571.

Crystal data of **45**: colorless crystal; $C_{37}H_{52}O_{12}$, M_r = 688.80, prism, a = 12.1699(10) Å, b = 12.3165(16) Å, c = 24.075(3) Å, space group $P2_12_12_1$, Z = 4, V = 3608.6(7) Å^3, μ(Mo Kα) = 0.07 mm^{-1}, and F(000) = 1200. Crystal dimensions: 0.38 × 0.22 × 0.20 mm^3. Independent reflections: 3394 (R_{int} = 0.035).

Table 2.4 Crystal data and structure refinement for compound **45**

Identification code	Xylorumphiin G
Empirical formula	$C_{37}H_{52}O_{12}$
Formula weight	688.80
Temperature	296 K
Wavelength	0.71073 Å
Crystal system, space group	Orthorhombic, $P2_12_12_1$
Unit cell dimensions	a = 12.1699(10) Å alpha = 90 deg.
	b = 12.3165(16) Å beta = 90 deg.
	c = 24.075(3) Å gamma = 90 deg.
Volume	3608.6(7) $Å^3$
Z, Calculated density	4, 1.268 mg/m^3
Absorption coefficient	0.07 mm^{-1}
F(000)	1200
Crystal size	0.38 × 0.22 × 0.20 mm^3
Theta range for data collection	0.923 to 20.83 deg.
Limiting indices	-11<=h<=10, -8<=k<=12,-23<=l<=21
Reflections collected / unique	3394 (R_{int} = 0.035)
Completeness to theta = 23.83	?
Refinement method	Full-matrix least-squares on F^2
Data / restraints / parameters	3394 / 478 / 445
Goodness-of-fit on F^2	0.774
Final R indices [I>2sigma(I)]	R_1 = 0.0750, *wR2* = 0.1888
R indices (all data)	R_1 = 0.0540, *wR2* = 0.1545
Absolute structure parameter	0(2)
Largest diff. peak and hole	0.923 and -0.402 $e.Å^3$

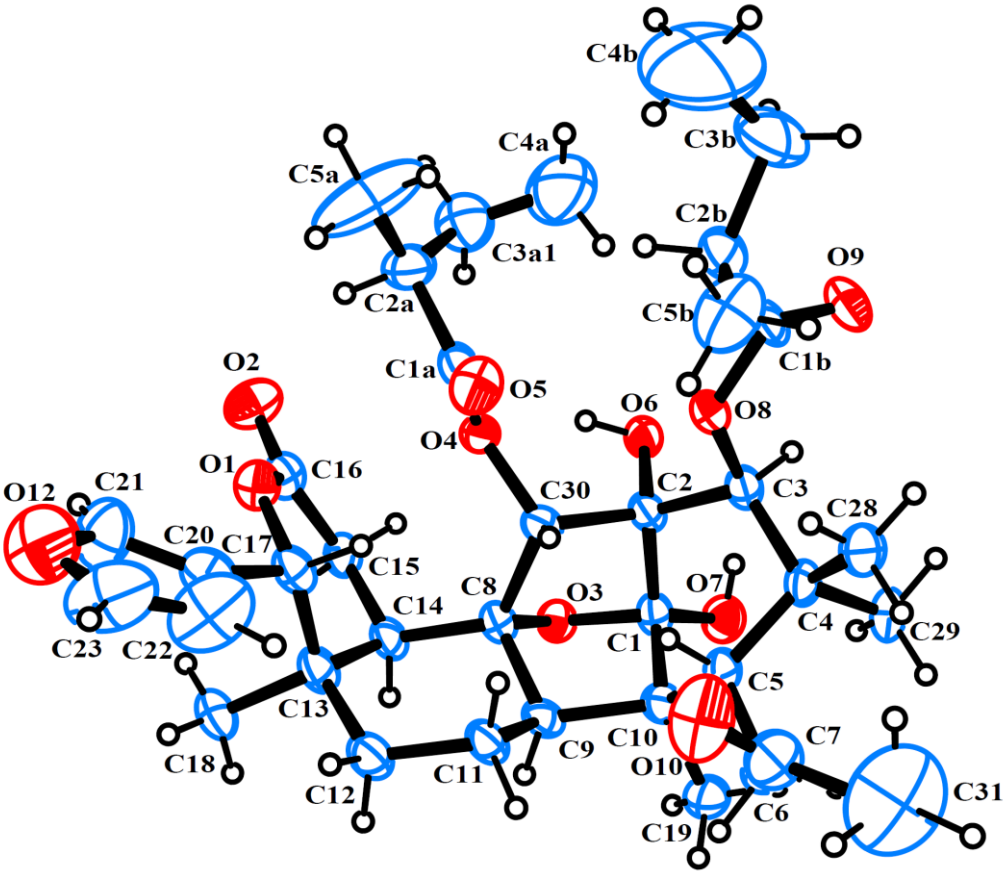

Figure 2.21 Perspective drawing of the X-ray structure of **45**.

Table 2.5 The NMR data of compound **45** in $CDCl_3$.

Position	^{1}H, mult. (*J* in Hz)	^{13}C	HMBC
1		107.2	
2		82.1	
3	4.89, s	80.3	C-1′
4		38.9	
5	2.64, m	40.4	C-7
6	2.35, m	32.3	C-7
	2.24, m		
7		173.8	
8		81.1	
9	1.48, dd (2.8, 12.8)	63.3	
10		42.6	
11	1.89, m	19.7	
	1.69, m		
12	1.85, m	35.9	
	1.33, m		
13		36.3	
14	2.22, d (9.6)	46.5	
15	3.15, d (20.0)	29.1	C-8, C-16
	2.74, dd (9.6, 20.0)		
16		169.5	
17	5.18, s	77.0	C-20, C-21, C-22
18	1.05, s	22.1	C-12, C-13, C-14, C-17
19	1.12, s	21.0	C-1, C-5, C-9, C-10
20		120.9	
21	7.53, s	141.5	
22	6.39, s	109.3	
23	7.40, s	143.1	
28	0.73, s	24.2	C-3, C-4, C-5
29	1.25, s	22.0	
30	6.24, d (5.2)	75.6	C-1″
7-OMe	3.69, s	51.9	C-7
1-OH	4.25, s		
1′		177.1	
2′	2.35, m	40.5	
3′	1.41, m	16.8	
	1.65, m		
4′	0.90, t (7.6)	25.3	C-2′
5′	1.21, d (7.2)	11.2	C-1′, C-2′, C-4′
1″		174.1	
2″	2.45, m	40.6	
3″	1.28, m	27.0	
	1.67, m		
4″	0.91, t (7.6)	11.9	C-2″, C-3″
5″	1.08, d (7.2)	14.8	C-1″, C-2″, C-3″

Xylorumphiin H (**46**), a white amorphous powder, $[\alpha]^{20}_{D}$ +11.5 (*c* 0.10, MeOH), UV (MeOH) λ_{max} (log ε) 210 (3.64) nm, had molecular formula of $C_{33}H_{44}O_{12}$ as determined by ^{13}C NMR HRESIMS based on the molecular ion *m/z* 631.2781 $[M - H]^-$ (calcd 631.2749). The NMR spectroscopic data of **46** (Table 1.6) were similar to those of xylorumphiin A (**38**) [44], with the only difference being the appearance of an acetyl rather than an isobutyryl group at C-3. This deduction was validated by the HMBC correlation from H-3 to acetyl carbonyl (δ_C 171.3). The relative configuration of **46** was assigned to be identical to that of xylorumphiin A (**38**) by analysis of the NOESY data (Figure 2.22).

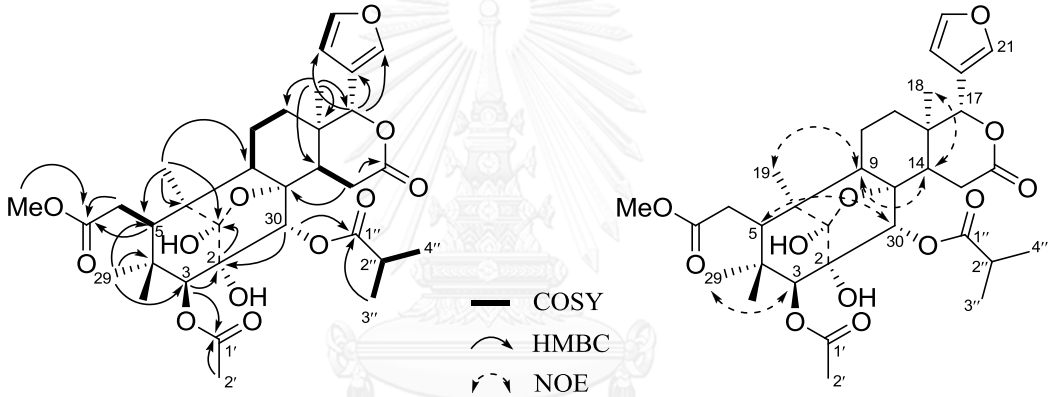

Figure 2.22 Key HMBC, COSY and NOE correlations of compound **46**.

Table 2.6 The NMR data of compound **46** in $CDCl_3$.

Position	^{1}H, mult. (*J* in Hz)	^{13}C	HMBC
1		107.1	
2		82.2	
3	4.85, s	80.5	C-1′, C-2, C-30
4		38.7	
5	2.61, m	40.3	C-6, C-7
6	2.36, dd (9.2, 16.4)	32.3	C-7
	2.25, d (16.4)		
7		173.9	
8		81.0	
9	1.48, dd (2.4, 12.8)	63.3	
10		42.6	
11	1.90, dd (3.2, 13.2)	19.7	
	1.69, m		
12	1.83, m	35.9	
	1.33, m		
13		36.2	
14	2.21, d (9.2)	46.4	
15	3.11, d (19.6)	29.0	C-8, C-14, C-16
	2.74, dd (9.2, 19.6)		
16		169.5	
17	5.21, s	77.1	C-20, C-21, C-22
18	1.05, s	22.2	C-12, C-13, C-14, C-17
19	1.12, s	21.0	C-1, C-5, C-9, C-10
20		120.8	
21	7.55, s	141.6	
22	6.39, s	110.0	
23	7.40, s	143.0	
28	0.72, s	23.8	C-3, C-4, C-5
29	1.24, s	21.9	
30	6.19, s	75.6	C-1, C-2, C-3, C-8 C-1″
7-OMe	3.70, s	51.9	C-7
1-OH	4.25, s		C-1, C-2, C-10
2-OH	3.27, s		C-2, C-3, C-30
1′		171.3	
2′	2.07, s	21.3	C-1′
1″		174.5	
2″	2.65, m	34.0	
3″	1.09, d (6.4)	17.9	C-1″, C-2″
4″	1.11, d (6.4)	19.5	

Xylorumphiin I (**47**) was obtained as a white amorphous powder, $[\alpha]^{20}_{D}$ +4.0 (*c* 0.10, MeOH), UV (MeOH) λ_{max} (log ε) 209 (4.16) nm. It gave a molecular formula of $C_{37}H_{50}O_{12}$ as established by ^{13}C NMR and an HRESIMS ion at *m/z* 685.3266 $[M - H]^-$ (calcd 685.3219). The NMR spectroscopic data of **47** (Table 1.7) were similar to those of **45**, except for the presence of a $\delta^{14,15}$ double bond (δ_H 6.01 s; δ_C 118.3 and 158.6). The location of the $\delta^{14,15}$ double bond was corroborated by HMBC correlations from H-15 to C-8 and C-16 (Figure 2.23). The presence of two 2-methylbutyryl groups was confirmed by ^{1}H–^{1}H COSY correlations. Their positions at C-3 and C-30 were validated by the HMBC correlations from H-3 and H-30 to the respective 2-methylbutyryl carbonyls, C-1′ and C-1″. The absolute configurations at C-2′ and C-2″ in the respective 2-methylbutyryl groups were assigned as *S* from the $[\alpha]^{20}_{D}$ value of +18 (*c* 0.05, MeOH) of the corresponding acid. The similar NOE correlations suggested that compound **47** possessed the same relative configuration as those of **44–46**.

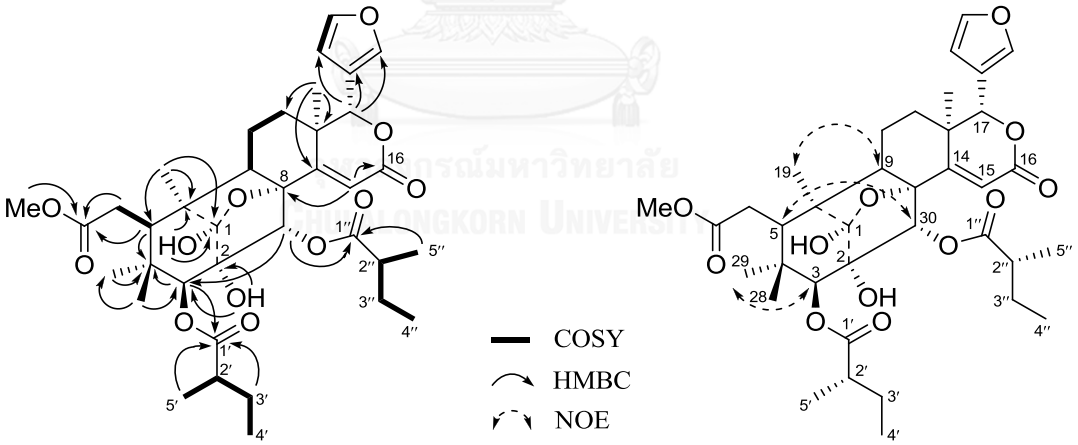

Figure 2.23 Key HMBC, COSY and NOE correlations of compound **47**.

Table 2.7 The NMR data of compound **47** in $CDCl_3$.

Position	^{1}H, mult. (*J* in Hz)	^{13}C	HMBC
1		108.4	
2		80.9	
3	4.83, s	82.4	C-2, C-30, C-1′
4		38.7	
5	2.66, d (8.8)	40.3	C-4, C-7, C-10
6	2.18, m	31.9	C-7
	2.35, m		
7		173.7	
8		80.4	
9	2.20, m	51.5	C-8, C-10
10		42.2	
11	2.35, m	15.1	C-12
	1.81, m		
12	2.04, m	25.1	C-11
	1.40, m		
13		38.9	
14		158.6	
15	6.01, s	118.3	C-8, C-16
16		163.1	
17	4.92, s	81.2	C-20, C-21, C-22
18	1.22, s	19.6	C-12, C-13, C-14
19	1.14, s	20.6	C-1, C-5, C-9, C-10
20		119.9	
21	7.48, s	141.3	
22	6.41, s	109.9	
23	7.41, s	142.9	
28	0.78, s	24.5	C-3
29	1.30, s	21.7	C-3, C-4, C-5
30	5.61, s	75.4	C-1, C-2, C-1″
7-OMe	3.69, s	51.9	C-7
1-OH	4.52, s		C-1, C-2, C-10
2-OH	3.90, s		C-2, C-3, C-30
1′		176.7	
2′	2.30, m	40.9	
3′	1.66, m	26.1	
	1.40, m		
4′	0.90, t (7.2)	11.4	C-2′
5′	1.15, d (7.2)	16.2	C-1′, C-2′
1″		174.7	
2″	2.30, m	40.9	
3″	1.66, m	26.4	
	1.40, m		
4″	0.92, t (7.6)	11.6	C-2″, C-3″
5″	1.10, d (7.2)	15.7	C-1″, C-2″

Xylorumphiin J (**48**), a white amorphous solid, $[\alpha]^{20}_{D}$ -6.7 (*c* 0.11, MeOH), UV (MeOH) λ_{max} (log ε) 210 (3.64) nm, had the molecular formula $C_{35}H_{42}O_{15}$ as established by ^{13}C NMR HRESIMS (*m/z* 701.2471 [M – H]$^-$, calcd 701.2440). Analysis of 1D and 2D NMR spectroscopic data revealed that **48** was a phragmalin *ortho* ester. The existence of an *ortho* acetate group was characterized by a methyl singlet at δ_H 1.73, showing a HMBC correlation with a quaternary carbon at δ_C 119.4. This was further supported by the presence of three oxygenated tertiary carbons at δ_C 85.4, 85.1 and 86.8, assigned as C-1, C-8 and C-9, respectively, by HMBC correlations of H-14/C-8, -30/C-8, H_3-19/C-1, H_3-19/C-9 and H_2-29/C-1 (Figure 2.24). These data suggested that **48** was a phragmalin 1,8,9-*ortho* acetate. The NMR data of **48** (Table 1.8) were similar to those of xyloccensin E [61], except for the presence of an oxygenated methine (δ_H 5.06 br s; δ_C 64.2) instead of the C-15 methylene group in xyloccensin E. HMBC cross-peaks from a hydroxyl proton at δ_H 3.12, which was not correlated with any carbon in the HSQC spectrum, to C-14, C-15 and C-16 confirmed the location of this hydroxyl group at C-15. Similar NOE correlations suggested that compound **48** possessed the same relative configuration as those of xyloccensin E [61]. The α-orientation of H-15 was established by its NOE correlations with H-14 (Figure 2.24).

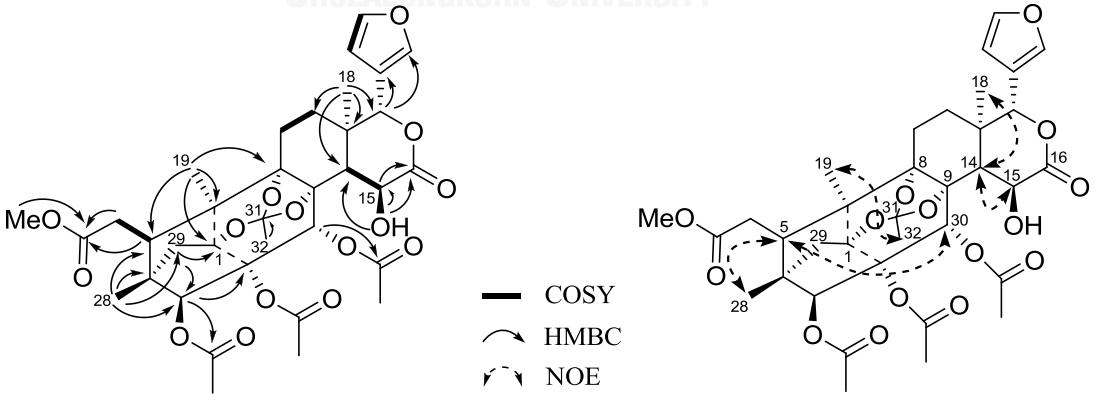

Figure 2.24 Key HMBC, COSY and NOE correlations of compound **48**.

Table 2.8 The NMR data of compound **48** in $CDCl_3$.

Position	^{1}H, mult. (*J* in Hz)	^{13}C	HMBC
1		85.4	
2		86.0	
3	5.11, s	81.1	C-2, C-1′
4		46.2	
5	2.99, d (10.0)	35.5	C-6, C-7
6	2.46, dd (10.0, 16.4)	33.3	C-7
	2.24, m		
7		172.6	
8		85.1	
9		86.8	
10		45.8	
11	2.06, m	25.5	
	1.67, m		C-12
12	1.51, m	28.8	C-11
	1.20, m		
13		36.2	
14	2.09, d (2.4)	53.0	C-8, C-15
15	5.06, br s	64.2	C-14, C-16
16		174.2	
17	5.58, s	78.8	C-20, C-21, C-22
18	1.05, s	19.2	C-12, C-13, C-14, C-17
19	1.16, s	16.7	C-1, C-5, C-9, C-10
20		120.5	
21	7.56, s	141.0	
22	6.48, s	109.6	
23	7.42, s	143.2	
28	0.89, s	14.6	C-3, C-4, C-5, C-29
29	1.98, d (11.2)	40.1	C-1
	1.68, d (11.2)		
30	6.32, s	69.8	C-1″
31		119.4	
32	1.73, s	20.9	C-31
7-OMe	3.68, s	52.0	C-7
15-OH	3.12, br s		C-14, C-15, C-16
1′		170.0	
2′	2.26, s	21.0	C-1′
1″		168.2	
2″	1.94, s	21.0	C-1″
1‴		170.4	
2‴	2.16, s	21.7	C-1‴

Xyloccensin X (**49**) was obtained as colorless crystals, mp 214-216 °C. Compound **49** was first reported in 2006 as a mixture with xyloccensin Y [62]. In the current study, the ^{1}H and ^{13}C NMR data for compound **49** (Table 1.9) were assigned unambiguously.

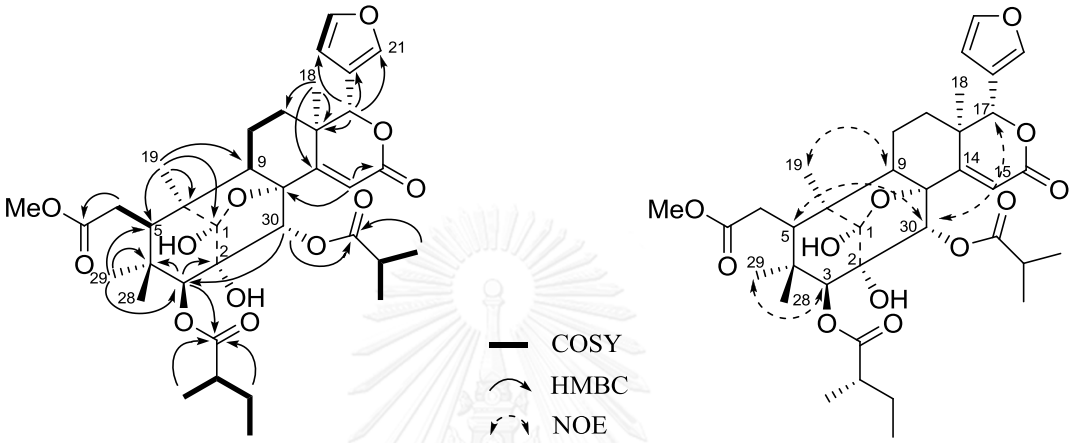

Figure 2.25 Key HMBC, COSY and NOE correlations of compound **49**.

Table 2.9 The NMR data of compound **49** in $CDCl_3$.

Position	^{1}H, mult. (*J* in Hz)	^{13}C	HMBC
1		108.5	
2		81.0	
3	4.80, s	82.6	C-1, C-2, C-4, C-30, C-1′
4		38.7	
5	2.66, br d (9.2)	40.3	
6	2.36, m	31.9	
	2.16, d (15.2)		
7		173.7	
8		80.4	
9	2.21, d (10.0)	51.5	
10		42.3	
11	2.34, m	15.1	
	1.80, m		
12	2.05, m	25.0	
	1.39, m		
13		38.9	
14		158.5	
15	6.07, s	118.4	C-8, C-16
16		163.1	
17	4.91, s	81.3	
18	1.21, s	19.6	
19	1.14, s	42.3	
20		120.0	
21	7.48, s	141.3	
22	6.41, s	109.9	
23	7.41, s	142.9	
28	0.79, s	24.5	
29	1.31, s	21.7	
30	5.58, s	75.4	C-1″
7-OMe	3.68, s	51.9	C-7
1-OH	4.66, s		C-1, C-10
2-OH	4.13, s		C-1, C-3
1′		176.8	
2′	2.29, m	41.0	C-1′
3′	1.65, m	26.1	C-1′
	1.40, m		
4′	0.90, t (7.2)	11.4	C-2′, C-3′
5′	1.14, d (6.8)	16.1	C-1′, C-2′, C-3′
1″		175.2	
2″	2.54, m	34.3	C-1″
3″	1.12, d (7.2)	18.8	C-1″, C-2″
4″	1.15, d (6.8)	19.0	

Xyloccensin E (**50**), colorless crystals, had a molecular formula $C_{35}H_{42}O_{14}$ determined by ESIMS (*m/z* 687.27 $[M+H]^+$, calcd. 687.26). The ^1H, ^{13}C data and 2D NMR data (Table 1.10) of **50** indicated the presence of the following functional groups; a carbomethoxy [δ_H 3.69 s, δ_C 52.1 CH_3, 172.7 qC], three oxygenated methines [δ_H 5.10 s, 6.30 s, 5.54 s; δ_C 81.1 CH, 69.3 CH, 78.6 CH], an orthoacetate [δ_H 1.66 s; δ_C 21.0 CH_3, 119.0 qC], two sp^3 methines [δ_H 2.96 (d, *J* = 8.5 Hz), 2.06 m; δ_C 35.5, 43.1], ten sp^3 methylenes [δ_H 2.47 m, 2.24 m, 2.07 m, 1.65 m, 1.54 m, 1.30 m, 3.28 (d, *J* = 20.3 Hz), 2.70 m, 1.98 m, 1.67 m; δ_C 33.3, 25.4, 29.1, 26.5, 40.2], three methyls [δ_H 1.06 s, 1.14 s, 0.89 s; δ_C 19.9, 16.5, 14.6], three acetyls [δ_H 1.94 s, 2.25 s, 2.15 s; δ_C 21.6 CH_3, 168.6 qC; 21.1 CH_3, 170.2 qC; 21.1 CH_3, 170.2 qC]. The ^1H and ^{13}C NMR data of **50** were characteristic of a phragmalin type limonoid. The quaternary carbon at δ_C 119.0 (C-31) showing a HMBC correlation (Figure 2.26) to H-32 suggested the presence of an orthoacetate group. In addition, the nature of oxygenated carbons assigned for C-1 (δ_C 86.9), C-8 (δ_C 86.0) and C-9 (δ_C 85.3) was comparable to xyloccensin E. This suggested the position of the orthoacetate at C-1, C-8 and C-9. Three acetoxy groups were assigned to C-2, C-3 and C-30 according to HMBC correlations of H-3 and H-30 to both acetyl carbonyls and its molecular formula. From these results, the structure of **50** was identified as xyloccensin E [61].

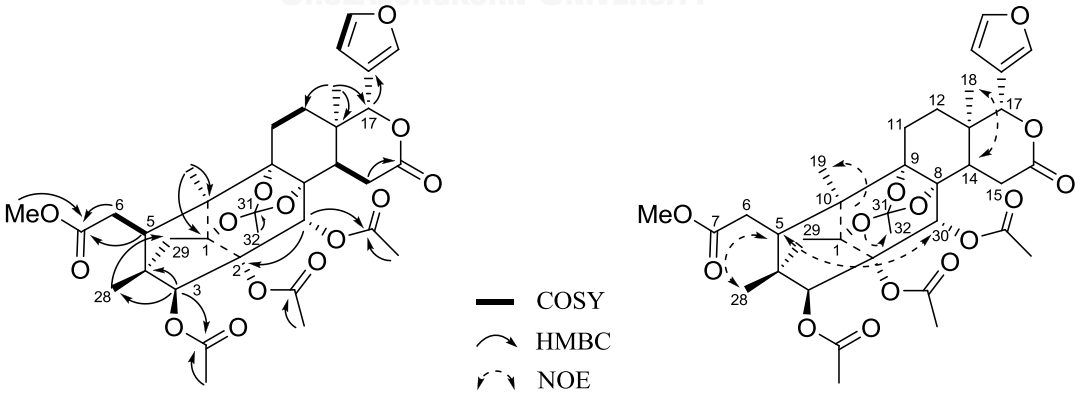

Figure 2.26 Key HMBC, COSY and NOE correlations of compound **50**.

Table 2.10 The ^{1}H and ^{13}C NMR data of xyloccensin E and compound **50**.

Position	Xyloccensin E		Compound 50	
	^{1}H, mult. (*J* in Hz)	^{13}C	^{1}H, mult. (*J* in Hz)	^{13}C
1		86.9		86.8
2		85.3		85.2
3	5.09	81.1	5.10, s	81.1
4		46.2		46.2
5		35.5	2.96, d (8.5)	35.5
6		33.3	2.47, m	33.3
			2.24, m	
7		172.9		172.7
8		86.0		85.9
9		85.3		85.3
10		45.8		45.7
11		25.4	2.07, m	25.4
			1.66, m	
12		29.2	1.54, m	29.1
			1.30, m	
13		34.4		34.3
14		43.2	2.06, m	43.1
15		26.2	3.28, d (20.3)	26.5
			2.70, m	
16		170.3		170.4
17	5.53	78.6	5.54, s	78.6
18		19.6	1.06, s	19.9
19		16.6	1.14, s	16.5
20		121.2		121.1
21	7.50	140.8	7.51, s	140.8
22	6.42	109.8	6.44, s	109.7
23	7.38	143.0	7.40, s	143.0
28		14.6	0.89, s	14.6
29		40.2	1.98, m	40.2
			1.67, m	
30	6.29	69.3	6.30, s	69.3
31		119.1		119.0
32		21.1	1.66, s	21.0
2-OAc		21.1	2.25, s	21.1
		170.3		170.2
3-OAc		21.7	2.15, s	21.7
		170.3		170.2
30-OAc		21.7	1.94, s	21.6
		168.6		168.6
7-OMe		52.1	3.69, s	52.1

Xyloccensin K (**51**) was isolated as a white amorphous solid and its molecular formula was determined as $C_{27}H_{34}O_8$ on the basis of ESIMS (*m/z* 487.23 $[M+H]^+$, calcd. 487.22) and NMR data (Table 1.11). The ^{1}H NMR data of **51** exhibited typical signals for four methyls [δ_H 0.66s, 0.94 s, 1.09 s, 0.99 s], two oxymethines [δ_H 6.28 s, 4.22 (d, *J* = 5.6 Hz)], a methoxy [δ_H 3.69 s], together with a β-furyl ring [δ_H 7.45 br s, 6.49 s, 7.57 (d, *J* = 0.5 Hz)]. The ^{13}C NMR and HSQC experiment revealed the presence of a ketone carbonyl [δ_C 215.1], two ester carbonyls [δ_C 175.0, 170.3], a β-furyl ring [δ_C 121.0 qC, 141.3 CH, 110.3 CH, 143.3 CH], two oxymethine carbons [δ_C 76.8, 91.7] and two oxygenated quaternary carbons [δ_C 85.8, 74.8]. The above NMR studies suggested that **51** was a mexicanolide type limonoid. On the basis of HMBC correlations (Figure 2.27), oxymethine proton at δ_H 4.22 (d, *J* = 5.6 Hz) showing correlations with C-8, C-5 and C-29, was attributed to H-3. The oxygen bridge between C-3 and C-8 was corroborated by the HMBC cross-peak from H-3 to H-8. On the basis of the above results, compound **51** was identified as xyloccensin K. The structure of this compound was finally confirmed by comparing its NMR data with those previously reported as shown in Table 1.11 [63]. Additionally, its relative stereochemistry was confirmed by NOE analysis (Figure 2.27) and found to be identical to that of xyloccensin K as reported.

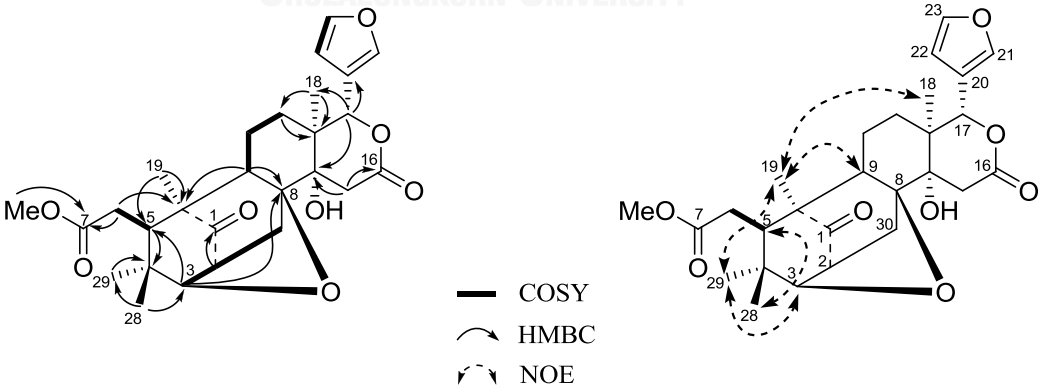

Figure 2.27 Key HMBC, COSY and NOE correlations of compound **51.**

Table 2.11 The ^{1}H and ^{13}C NMR data of xyloccensin K and compound **51**.

Position	Xyloccensin K		Compound 51	
	^{1}H, mult. (*J* in Hz)	^{13}C	^{1}H, mult. (*J* in Hz)	^{13}C
1		215.2		215.1
2	2.96, d (6.0)	48.9	2.97, t (6.0)	49.3
3	4.22, d (6.0)	91.3	4.22, d (5.6)	91.7
4		37.5		37.3
5	3.08, dd (2.0, 11.0)	42.9	3.07, m	43.3
6	2.14, dd (2.0, 17.0)	32.6	2.11, m	32.9
	2.24, dd (11.0, 17.0)		2.23 m	
7		174.2		175.0
8		85.4		85.8
9	1.97, dd (5.0, 12.5)	52.0	1.95, dd (4.0, 12.6)	52.4
10		51.0		51.5
11	1.46, m	17.8	1.47, m	18.0
	2.10, m		2.11, m	
12	1.50, dd (1.5, 14.0)	28.6	1.53 ,m	29.1
	1.70, dd (1.5, 14.0)		1.69, m	
13		40.0		40.4
14		74.1		74.8
15	2.54, d (17.0)	36.8	2.52, m	37.4
	3.13, d (17.0)		3.15, d (17.7)	
16		170.7		170.3
17	6.28, br s	76.7	6.28, s	76.8
18	0.67, s	16.0	0.66, s	16.4
19	0.94, s	16.8	0.94. s	17.2
20		120.6		121.0
21	7.45, d (2.0)	142.9	7.45, br s	141.3
22	6.49, br d (2.0)	109.9	6.49, s	110.3
23	7.56, br s	140.7	7.55, d (0.5)	143.3
28	1.03, s	20.0	1.09, s	20.4
29	0.98, s	27.9	0.99, s	28.4
30	2.04, d (12.0)	42.4	2.05, m	42.8
	2.52, dd (7.0, 12.0)			
7-OMe	3.70, s	51.8	3.69 ,s	52.2

2.6 Conclusion

Chemical examination of the seeds of *X. rumphii* collected from Kudee Island led to the isolation of seven new limonoids, namely, xylorumphiins E–J (**42-43** and **45–47**) and 2-hydroxyxylorumphiin F (**44**), along with three known derivatives namely xyloccensins X, E and K (**49-51**). Among of these limonoids, compounds (**42-47**, 49 and 51) were identified as limonoids Their structures were characterized on the basis of spectroscopic methods (1D and 2D NMR, HREIMS and single-crystal X-ray diffraction analysis). Furthermore, the structures of known compounds were confirmed by comparing their spectral data with those previously reported in literature. Among of these limonoids, compounds **42-47**, **49** and **51** were classified as mexicanolide type limonoids, while xylorumphiin G (**48**) and xyloccensin E (**50**) were categorized as phragmalin type limonoids.

CHAPTER III

ANTI-INFLAMMATORY EFFECT OF LIMONOIDS FROM *XYLOCARPUS SPP.* THROUGH SUPPRESSION OF iNOS SIGNALING PATHWAY

3.1 Introduction

Inflammation is the body's immediate response to damage to its tissues and cells by pathogens, pernicious stimuli such as chemicals or physical injury. This process is causes of the cardinal signs of inflammation such as rubor (redness), calor (heat), tumor (swelling), and dolor (pain) and loss of function. The primary physical effect of the inflammatory response is for blood circulation to increase around the infected area. Particularly, the blood vessels around the site of inflammation enlarge, permitting increased blood flow to the area. Gaps appear in the cell walls surrounding the infected area, allowing the larger cells of the blood such as immune cells (white blood cell) and chemical mediators to pass for protection cells and tissues from injury which are the results of inflammation [64]. Inflammation can be measured by gene expression in innate immune cells such as inducible nitric oxide synthase (iNOS) and pro-inflammatory cytokines, i.e. interleukin-1 (IL-1), interleukin-6 (IL-6) and tumor necrosis factor alpha (TNF-α). These genes are induced by pathogen associated molecular patterns (PAMP) such as lipopolysaccharide (LPS), the major component of the outer membrane of gram-negative bacteria in combination with certain cytokines such as interferon gamma (IFN-γ). NO (Nitric Oxide), a cytotoxic weapon generated by macrophages. In eukaryotic cells, NO is metabolically produced by NOS (Nitric oxide Synthase) from L-Arginine, O_2 (Molecular Oxygen), and NADPH (Nicotinamide Adenine Dinucleotide, reduced). In macrophages, an inducible NO synthase (iNOS or NOS2) is produced after activation by endotoxins or cytokines and generates large amounts of NO presumably to help remove or inhibit the growth of invading microorganisms or neoplastic tissue conduced to the inflammation. Inflammation can be classified as acute inflammation and chronic inflammation. Acute inflammation occurs as an immediate response to an injury and usually only sustains in a short duration. When inflammation becomes chronic, it may cause

result in serious or even life threatening clinical condition. Mainly, chronic inflammation leads to progressive destruction of the host tissue, which is a major cause of diseases such as atherosclerosis, rheumatoid arthritis [1] and cancer [2]. These damages may cause a wide variety of other pathological processes.

At present, anti-inflammatory drugs used to treat symptoms of chronic inflammation, are non-steroidal anti-inflammatory drugs (NSAIDs) exerting their effects by inhibition of prostaglandin production. The pharmacological target of NSAIDs is cyclooxygenase (COX), which catalyses the first committed step in arachidonic acid metabolism. Two isoforms of the membrane protein COX are composed of COX-1, which is constitutively expressed in most tissues that responsible for the physiological production of prostaglandins and COX-2, induced by cytokines, mitogens and endotoxins in inflammatory cells reliable for the increased production of prostaglandins during inflammation. NSAIDs act at the COX active site, and most inhibit both COX-1 and COX-2 with the little specificity, leading to serious side effect such as gastric lesions and renal toxicity. COX-2 selective inhibitors have been identified that show potent anti-inflammatory activity *in vivo* with minimal gastric side effects. Although inhibition of COX may underlie the advantageous anti-inflammatory, analgesic and antipyretic effect of NSAIDs, simultaneous COX inhibition in the gastrointestinal mucosa often results in gastric and intestinal ulcers, which may have serious consequences. Therefore, the finding and development of new effective anti-inflammatory agents are still require.

In ongoing program to search for anti-inflammatory agents from Thai natural products and based on the activity of the extracts of the *Xylocarpus* plants, the present study was to evaluate the effects of isolated limonoids on inflammatory responses and to investigate molecular mechanism of action of selected limonoid.

3.2 Literature Review

3.2.1 Inflammation

Inflammation is a critical process in the host defense system response to stimuli such as pathogens or irritants. Clinically, acute inflammation is characterized by 5 cardinal signs such as redness, heat, swelling, pain and loss of function of the host tissue in the inflammatory area. The response consists of changes in blood flow, an increasing in permeability of blood vessels and the migration of fluid, proteins and white blood cells (leukocytes) from the circulation to the site of tissue damage. An inflammatory response that lasts only a few days is called acute inflammation, while a response of longer duration is referred to as chronic inflammation. However, long-lasting chronic inflammation is known to directly or indirectly contribute to various diseases, including cancer, rheumatoid arthritis, atherosclerosis, asthma, Alzheimer's and Parkinson's diseases [65]. Upon inflammatory stimulation, macrophages play an important role and produce inflammatory mediators, such as nitric oxide (NO), and pro-inflammatory cytokines including tumor necrosis factor-α (TNF-α), interferon-γ (IFN-γ), interleukins [66, 67]. The high-output of NO sustainably produced by inducible nitric oxide synthase (iNOS) in activated macrophages has been found to play a major role in many inflammatory diseases [68]. Inflammatory stimuli, lipopolysaccharide (LPS) or a combination with IFN-γ, trigger NO production and up-regulate iNOS expression in stimulated macrophages via NF-κB and MAPKs signaling pathways. Therefore the effective blockade of NO production might be an essential approach for the development of therapeutic agents.

3.2.1.1 Chemical mediator

Tissue macrophages, mast cells, and endothelial cells at the site of inflammation, as well as leukocytes that are recruited to the site from the blood, are all capable of producing different mediators of inflammation. Generally,

the mediators of acute inflammation are classified into systems based on their source and/or chemical composition as follow;

3.2.1.1.1 Vasoactive amines

The two vasoactive amines, histamine and serotonin are stored as preformed molecules in mast cells and other cells and are among the first mediators to be released in acute inflammatory reactions. Histamine is produced by many cell types, particularly mast cells adjacent to vessels, as well as circulating basophils and platelets. In humans, histamine causes arteriolar dilation and rapidly increases vascular permeability by inducing venular endothelial contraction and formation of interendothelial gaps. Serotonin (5-hydroxytryptamine) is a preformed vasoactive mediator found within platelet granules that is released during platelet aggregation. It induces vasoconstriction during clotting [69].

3.2.1.1.2 Cytokines (Polypeptide products)

Cytokines are polypeptide products of many cell types that function as mediators of inflammation and immune responses. They are elaborated by a variety of cells including lymphocytes, monocytes and endothelial cells. Interleukin 1 (IL-1), interleukin 6 (IL-6) and tumor necrosis factor-α (TNF-α) are three major cytokines implicated to be important inflammatory mediators. The principal role of these cytokines in inflammation is in endothelial activation. Both TNF-α and IL-1 stimulate the expression of adhesion molecules on endothelial cells, resulting in increased leukocyte binding and recruitment, and enhance the production of additional cytokines (notably chemokines) and eicosanoids. TNF-α also increases the thrombogenicity of endothelium and induces priming and aggregation of neutrophils while IL-1 activates tissue fibroblasts, resulting in increased proliferation and production of ECM. In addition, Interferon-gamma (IFN-γ), another potent stimulus for macrophage activation and cytokine production, is produced by a subset of T lymphocytes as part of the immune response. It is also synthesized by natural killer (NK) cells in the primary host response to intracellular pathogens and certain viral infections [70]. Cellular effects of IFN-γ including up-regulation of

pathogen recognition, antigen processing and presentation, the antiviral state, inhibition of cellular proliferation and effects on apoptosis, activation of microbicidal effector functions, immunomodulation and leukocyte trafficking.

3.2.1.1.3 Eicosinoids and their derivatives

The immediate precursor of the eicosinoids is arachidonic acid, present in the beta position of phospholipids in cell membranes and membranes of subcellular particles. Eicosinoids are synthesized via two major enzymatic pathways (1) cyclooxygenase stimulates the synthesis of prostaglandins and thromboxanes and (2) lipoxygenase is responsible for production of leukotrienes and lipoxins. Prostaglandins and thromboxanes are included prostaglandin E_2 (PGE_2), PGD_2, $PGF_{2\alpha}$, PGI_2 (prostacyclin), and thromboxane A_2 (TXA_2), each derived by the action of a specific enzyme on an intermediate. Some of these enzymes have a restricted tissue distribution. For example, platelets contain the enzyme thromboxane synthase, and hence TXA_2, a potent platelet-aggregating agent and vasoconstrictor, is the major prostaglandin produced in these cells. Endothelial cells, on the other hand, lack thromboxane synthase but contain prostacyclin synthase, which is responsible for the formation of PGI_2, a vasodilator and a potent inhibitor of platelet aggregation. PGD_2 is the major metabolite of the cyclooxygenase pathway in mast cells along with PGE_2 and $PGF_{2\alpha}$ which are more widely distributed. it causes vasodilation and potentiates edema formation. The prostaglandins also contribute to the pain and fever that accompany inflammation. Especially, PGE_2 augments pain sensitivity to a variety of other stimuli and interacts with cytokines to cause fever. Leukotrienes are produced by the action of 5-lipoxygenase, the major arachidonic acid metabolizing enzyme in neutrophils type leads to synthesis of 5-hydroperoxyeicosatetraenoic acid (5-HpETE) and leukotriene A_4 (LTA_4) which are a precursor for other leukotrienes (LTB_4, LTC_4, LTD_4 and LTE_4). These three cysteinyl-leukotrienes are stimulated smooth muscle contraction and also enhanced vascular permeability.

3.2.1.1.4 Nitric oxide (NO)

NO is a short-lived, soluble, free radical gas generated by many cell types and capable of mediating a category of functions. In the central nervous system it regulates neurotransmitter release as well as blood flow. Macrophages use it as a cytotoxic agent for killing microbes and tumor cells. When produced by endothelial cells it alleviates vascular smooth muscle and causes vasodilation. NO is synthesized de novo from L-arginine, molecular oxygen, and NADPH by the enzyme nitric oxide synthase (NOS) [71]. There are three isoforms of NOS with different tissue distributions, Type I, neuronal NOS (nNOS), is constitutively expressed in neurons, and does not play an important role in inflammation. Type II, inducible NOS (iNOS), is induced in macrophages and endothelial cells by a number of inflammatory cytokines and mediators, most noticeably by IL-1, TNF-α, and IFN-γ, and by bacterial endotoxin, and is reliable for production of NO in inflammatory reactions. This inducible form is also appear in many other cell types, including hepatocytes, cardiac myocytes, and respiratory epithelial cells. Type III, endothelial NOS, (eNOS), is constitutively synthesized primarily (but not exclusively) in endothelium. An important function of NO is as a microbicidal (cytotoxic) agent in activated macrophages. NO plays other roles in inflammation, including vasodilation, antagonism of all stages of platelet activation (adhesion, aggregation, and degranulation), and reduction of leukocyte recruitment at inflammatory sites[72].

3.2.1.1.5 Plasma Protein–Derived Mediators

Circulating proteins of three interrelated systems, the complement, kinin, and coagulation systems are associated in various aspects of the inflammatory reaction. Complement components, numbered C1 to C9, are present in plasma in inactive forms, and many of them are activated by proteolysis to obtain their own proteolytic activity, thus setting up an enzymatic cascade. C3a and C5a increase vascular permeability and cause vasodilation by inducing mast cells to release histamine [73]. C3b and its inactive proteolytic product iC3b act as opsonins, increasing phagocytosis by neutrophils and macrophages, which express receptors for these complement products. Kinin system activation leads eventually

to the formation of bradykinin which is causes increased vascular permeability, arteriolar dilation, and bronchial smooth muscle contraction [74]. In the clotting system, the proteolytic cascade leads to activation of thrombin, which then cleaves circulating soluble fibrinogen to generate an insoluble fibrin clot. Thrombin participates in inflammation by binding to protease-activated receptors that are expressed on platelets, endothelial cells, and many other cell types. Binding of thrombin to these receptors on endothelial cells leads to their activation and enhanced leukocyte adhesion. In addition, thrombin generates fibrinopeptides (during fibrinogen cleavage) that increase vascular permeability and are chemotactic for leukocytes [75].

3.2.1.2 Anti-inflammatory drugs

Nonsteroidal anti-inflammatory drugs (NSAIDs), such as aspirin and ibuprofen, suppress cyclooxygenase activity, therefore blocking all prostaglandin synthesis hence their potency in healing pain and fever [76]. There are two isoforms of the cyclooxygenase enzyme, COX-1 and COX-2. COX-1 is produced in response to inflammatory stimuli and also is constitutively expressed in most tissues, where it stimulates the production of prostaglandins that sustain a homeostatic function (e.g., fluid and electrolyte balance in the kidneys, cytoprotection in the gastrointestinal tract). In contrast, COX-2 is induced by inflammatory stimuli but it is absent from most normal tissues. Consequently, COX-2 inhibitors have been developed with the expectation that they will inhibit harmful inflammation but will not block the protective effects of constitutively produced prostaglandins. These differences between the roles of the two cyclooxygenases are unclear. However, COX-2 inhibitors may enlarge the risk for cardiovascular and cerebrovascular events, possibly because they debilitate endothelial cell production of prostacyclin (PGI_2), an inhibitor of platelet aggregation, but leave intact the COX-1-mediated production by platelets of TXA_2, a mediator of platelet aggregation.

There are two main types of NSAIDs, nonselective and selective. The terms nonselective and selective refer to different NSAIDs' ability to inhibit specific types of cyclooxygenase (COX) enzymes.

3.2.1.2.1 Non-selective NSAIDs

Non-selective NSAIDs are drugs that inhibit both COX-1 and COX-2 enzymes and they are associated with an increased risk of gastric ulceration, supposed to be both through the reduction in gastric protection that is provided by prostaglandins, as well as direct irritation of the gastric lining. Examples of non-selective NSAIDs included aspirin, ibuprofen, diclofenac, piroxicam and naproxen.

3.2.1.2.2 Selective NSAIDs

Selective NSAIDs (also called COX-2 inhibitors) inhibit only the COX-2 enzyme, allowing for the production of the prostaglandins that protect the stomach, while still relieving fever, pain and inflammation. They do not have the anti-platelet effects associated with nonselective NSAIDs and so do not alter clotting. The selective NSAID such as celebrex and mobic.

However, there are some anxious side effects can occur. The most common side effects including cardiovascular disorder, gastrointestinal disease, hepatic and renal toxicity were reported.

3.2.1.3 Toll-like receptor signaling (TLR signaling)

3.2.1.3.1 Macrophage

Macrophages are a major component of the mononuclear phagocyte system which compose of closely related cells of bone marrow origin, including blood monocytes, and tissue macrophages. From the blood, monocytes emigrate into several tissues and transform macrophages. In inflammation, macrophages have three major function; antigen presentation, phagocytosis, and immunomodulation through production of various cytokines and growth factors. Macrophages display a crucial role in the initiation, conservation, and resolution of inflammation. They are activated and deactivated in the inflammatory process. Activation signals include nitric oxide (NO), cytokines (IL-1, IL-6, IFN-γ, TNF-α and granulocyte-monocyte colony stimulating factor), bacterial lipopolysaccharide (LPS), extracellular matrix proteins, and other chemical mediators. Inhibition of

inflammation by removal or deactivation of mediators and inflammatory effector cells permits the host to repair damages tissues. Activated macrophages are deactivated by anti-inflammatory cytokines (IL-10 and transforming growth factor-β) and cytokine antagonists that are mainly produced by macrophages. Macrophages participate in the autoregulatory loop in the inflammatory process. Because macrophages produce a wide range of biologically active molecules concerned in both beneficial and injurious outcomes in inflammation, therapeutic interventions targeted macrophages and their products may open new ways for controlling inflammatory diseases.

3.2.1.3.2 Toll-like receptor 4 (TLR4 signaling)

Toll-like receptors (TLRs) perceive distinct pathogen-associated molecular patterns (PAMPs) and play an important role in innate immune responses. They concern in the first line of defense against attacking pathogens and play a significant role in inflammation, immune cell regulation, survival and proliferation. This crucial information is transmitted through the cell membrane, and resulting signal is ultimately transmitted into the nucleus so that specific gene sets can be activated to originate an appropriate response. To date, 11 members of the TLR family have been identified, of which TLR1, TLR2, TLR4, TLR5, TLR6, and TLR11 are located on the cell surface and TLR3, TLR7, TLR8, and TLR9 are localized to the endosomal/lysosomal compartment. The activation of the TLR signaling pathway originates from the cytoplasmic Toll/IL-1 receptor (TIR) domain that associates with a TIR domain-containing adaptor, MyD88. Upon stimulation with ligands, MyD88 recruits IL-1 receptor-associated kinase-4 (IRAK-4) to TLRs through interaction of the death domains of both molecules. IRAK-1 is activated by phosphorylation and associates with TRAF6, thereby activating the IKK complex and leading to activation of MAP kinases (JNK, p38 MAPK) and NF-κB. Tollip and IRAK-M interact with IRAK-1 and negatively regulate the TLR-mediated signaling pathways. Additional modes of regulation for these pathways include TRIF-dependent induction of TRAF6 signaling by RIP1 and negative regulation of TIRAP-mediated downstream signaling by ST2L, TRIAD3A, and SOCS1. Activation of MyD88-independent pathways

occurs via TRIF and TRAF3, leading to recruitment of IKKε/TBK1, phosphorylation of IRF3, and expression of interferon-β. TIR domain containing adaptors such as TIRAP, TRIF, and TRAM regulate TLR-mediated signaling pathways by providing specificity for individual TLR signaling cascades. TRAF3 plays a critical role in the regulation of both MyD88-dependent and TRIF-dependent signaling via TRAF3 degradation, which activates MyD88-dependent signaling and suppresses TRIF-dependent signaling and vice versa [77]. A schematic diagram of the TLRs is shown in Figure 3.1. In addition, TLR4 is the best characterized cell surface TLR. The recognition of LPS by TLR4 requires several other proteins comprising LPS binding protein (LBP), CD14 and MD2. LPS responsiveness is partly regulated by the levels of TLR4 present of the cell surface and this is determined by the amount of TLR4 trafficking from the Golgi complex to the plasma membrane and the amount of TLR4 internalized into endosomes. These are two distinct pathways involving many different regulators, LPS then engages with TLR4, with the help of LBP, CD14 and MD2 at the plasma membrane initiating the binding of Mal and MyD88. This results in the activation of the NF-κB pathway. TLR4 then moves into the endosome in a dynamin and clathrin-dependent manner causing the displacement of Mal and the binding of TRAM and TRIF resulting in the activation of the IRF3 pathway. The binding of TAG to TRAM in the late endosome results in the dissociation of TRIF from TRAM, terminating the signal [78]. TLR4 activates both the MyD88-dependent and MyD88-independent, TRIF-dependent pathways. The MyD88-dependent pathway is reliable for early-phase NF-κB and MAPK activation, which regulate the induction of proinflammatory cytokines. The MyD88-independent, TRIF-dependent pathway activates IRF3, which is required for the induction of IFN-β and IFN-inducible genes. Additionally, this signaling pathway mediates late-phase NF-κB as well as MAPK activation, also involving to inflammatory responses [79] as illustrated in Figure 3.2.

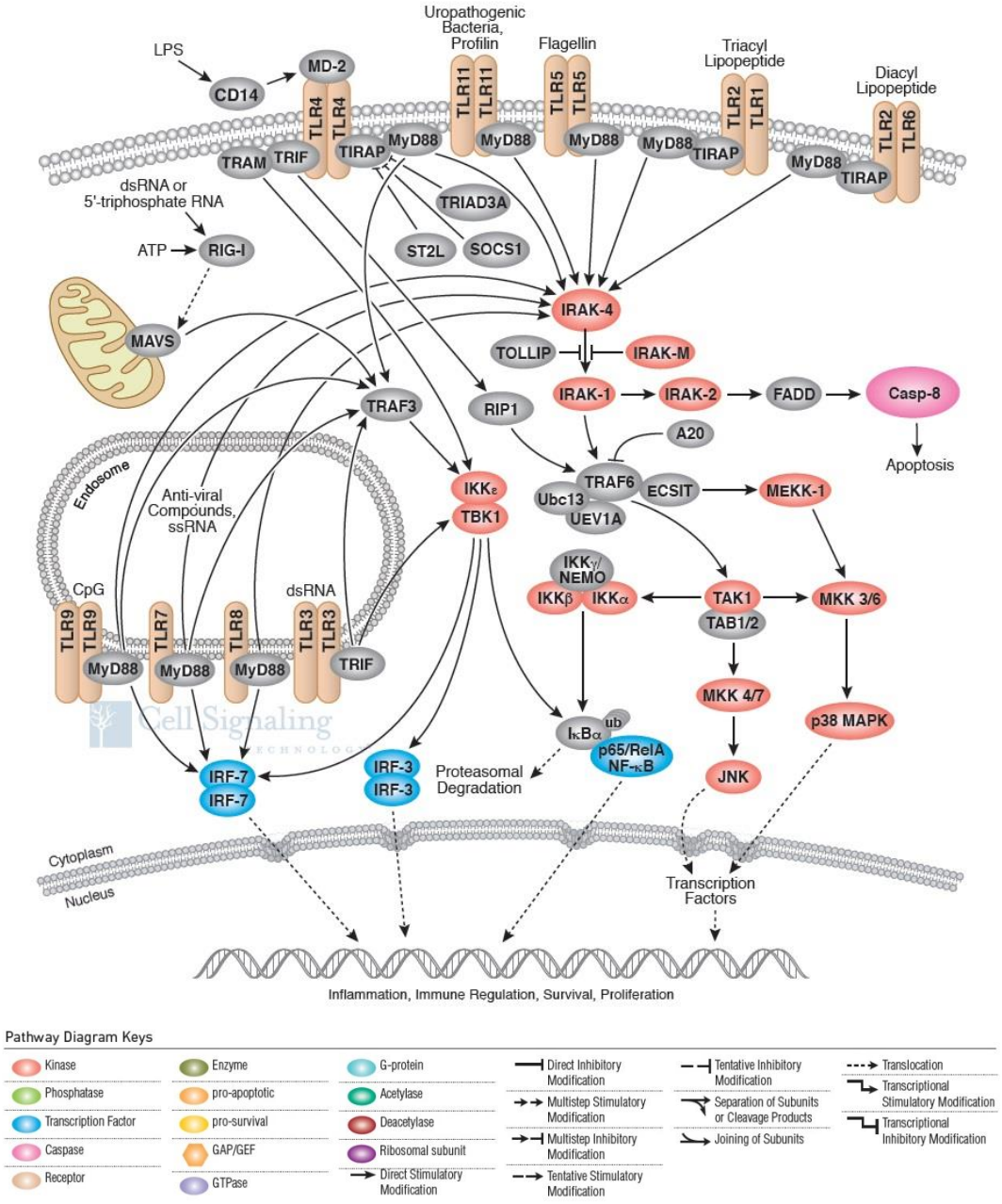

Figure 3.1 Toll-like receptor signal transduction.

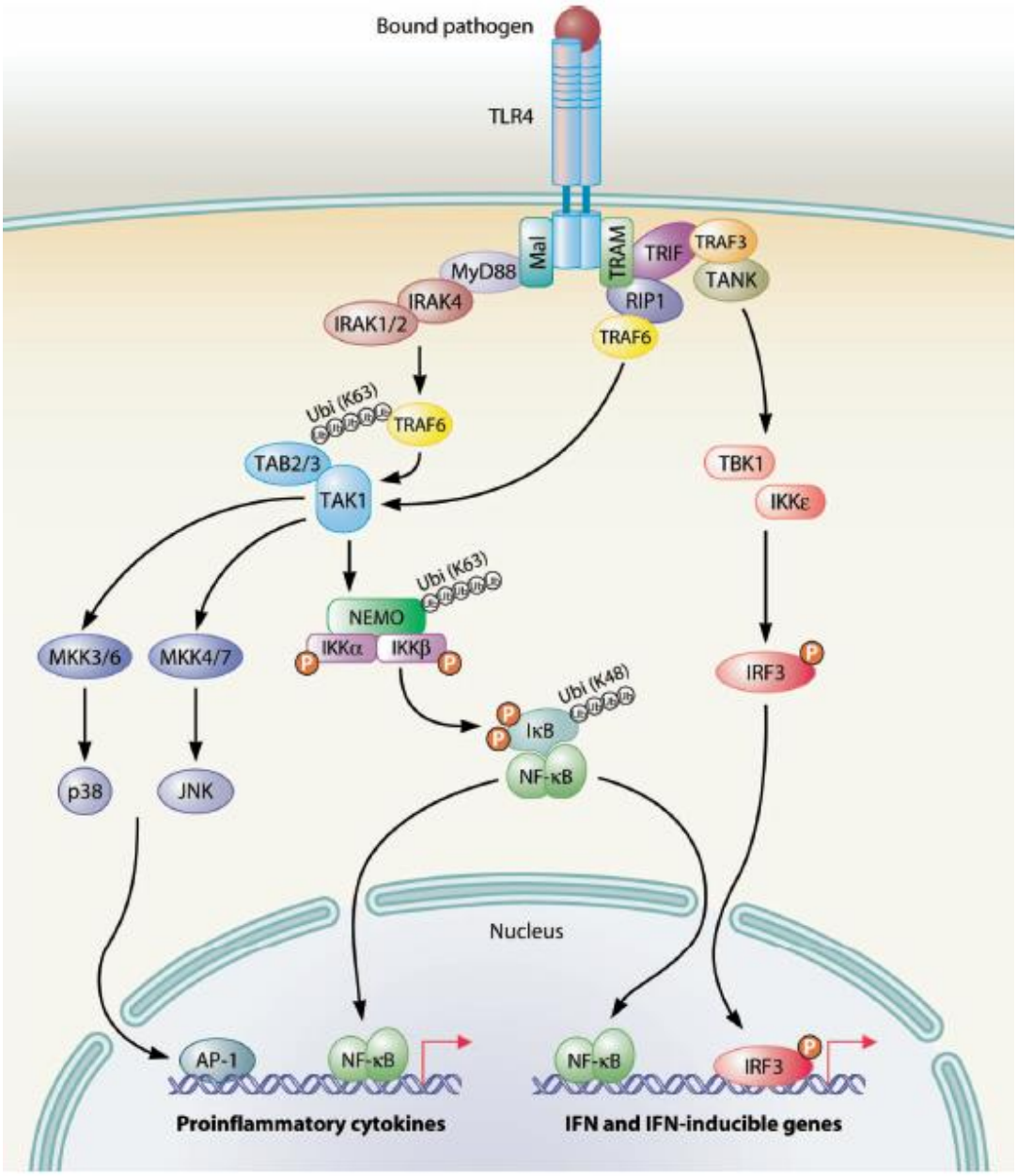

Figure 3.2 Trafficking of TLR4 from the plasma membrane [79].

Upon inflammatory stimulation, macrophages play an important role and produce inflammatory mediators, such as nitric oxide (NO), and pro-inflammatory cytokines including tumor necrosis factor-α (TNF-α), interferon-γ (IFN-γ), interleukins-6 (IL-6). The high-output of NO sustainably produced by inducible nitric oxide synthase (iNOS) in activated macrophages has been found to play a major role in many inflammatory diseases. Inflammatory stimuli, lipopolysaccharide (LPS) or a

combination with IFN-γ, trigger NO production and up-regulate iNOS expression in stimulated macrophages via NF-κB and MAPKs signaling pathways. Therefore the effective blockade of NO production might be an essential approach for the development of therapeutic agents.

3.3 Experiments

3.3.1 Cell Culture

The murine macrophage RAW264.7 cells (ATCC No. TIB-71) were obtained from the American Type Culture Collection. These cells were maintained in Dulbecco's modified Eagle's medium (DMEM) supplemented with 10% (v/v) fetal bovine serum (FBS), 100 mM sodium pyruvate, HEPES free acid (Hyclone), penicillin G and streptomycin at 37 $^{\circ}$C in a humidified incubator with 5% CO_2.

3.3.2 Preparation of stock solution of compounds

The pure compounds were dissolved in dimethyl sulfoxide (DMSO, cell culture grade) to get an initial concentration of 50 mM from which serial dilutions were made using DMSO to get 25, 12.5, 6.25, 3.13 and 1.56 mM.

3.3.3 Nitric oxide inhibitory assay (NO assay)

The amount of NO was determined by measuring the amount of nitrite in the cell culture supernatant, using Greiss reagent (a mixture of 1% sulfanilamide and 0.1% naphthylethylenediamine dihydrochloride in 5% phosphoric acid). RAW264.7 cells (1×10^4 cells/well) were treated by various concentrations of the test compounds and vehicle (DMSO) for 2 h, followed by LPS (100 ng/mL) and IFN-γ (10 ng/mL). Indomethacin was used as a positive control. After an additional 24 h of incubation, the nitrite released in culture medium was reacted with Griess reagent, followed by incubation for 10 min under dark condition at room temperature. The absorbance was measured at 540 nm by using a microplate reader, and the inhibitory activities were calculated from a standard calibration curve obtained from different

concentrations of sodium nitrite. The results were displayed as the percentage of inhibition and the half maximal inhibitory concentration (IC_{50}).

Calculation of the percentage of nitric oxide (NO) inhibition

$$\% \text{ NO inhibition} = 100 - \left(\frac{A_N}{A_C} \times 100 \right)$$

A_N = Absorbance of test - Absorbance of blank

A_C = Absorbance of control - Absorbance of blank

The IC_{50} values were calculated from line graph between the percentage of inhibition (Y axis) and the concentration of compound (X axis).

3.3.4 Cytotoxic assay (MTT assay)

Cell viability was assessed by the mitochondrial-respiration-dependent 3-(4,5-dimethylthiazol-2-yl)-2,5-diphenyl-tetrazolium bromide (MTT) colorimetric method. The succinate dehydrogenase in living cells can reduce the yellow tetrazolium salt MTT to a purple formazan crystals. After the Griess reaction, MTT solution (5 mg/mL) was added to each well and further incubated for 4 h. The medium was discarded, and 0.04 N HCl in isopropanol was added to dissolve the formazan crystals. The absorbance was measured at 540 nm, and percent survival was determined by comparison with a control group. The results were presented as the percentage of inhibition and the half maximal inhibitory concentration (IC_{50}).

Calculation of the percentage of cell viability

$$\% \text{ cell viability} = \frac{\text{Absorbance of tested cells}}{\text{Absorbance of control cells}} \times 100$$

3.3.5 Western blot analysis

Cell treated as indicated in the text were washed with cold PBS and lysed with cell lysis buffer according to the manufacturer's instructions. Cell lysates were centrifuged at 5000 rpm for 5 min, and supernatants were collected as samples. Equal amounts (30 μg) of total protein in each cell lysate were separated in 10% SDS-PAGE and transferred to PVDF membrane. The membranes were blocked

with 3% skim milk in PBS containing 0.05% Tween-20 and incubated overnight at 4 $^{\circ}$C with corresponding primary antibodies in 3% skim milk in PBS containing 0.05% Tween-20, followed by incubation with horseradish peroxidase-conjugated secondary antibodies for 1 h at room temperature. The signals were detected using the chemiluminescence method.

3.3.6 Quantitative Reverse Transcription Polymerase Chain Reaction (qRT-PCR)

Total RNA was isolated from cell culture by using TriZol reagent (Invitrogen), and cDNA was synthesized from 0.2 μg RNA by using RevertAid^{TM} Reverse transcriptase (Fermentas). The quantitative real-time PCR was performed by using Maxima^{TM} SYBR Green qPCR Master Mix (Fermentas). The specific primers used to amplify were as follow: iNOS: 5′-CCCTTCCGAAGTTTCTGGCAGCAGC-3′ (forward) and 5′-GGCTGTCAGAGCCTGCTGGTCTTGG-3′ (reverse); β-actin: 5′-ACCAACTGGGACGACATG GAGAA-3′ (reverse). The PCR was performed with the following conditions: initial denaturation step at 95 $^{\circ}$C for 3 min, repeated cycling (40 times) step of denaturation for 30 s, annealing at 60 $^{\circ}$C (55 $^{\circ}$C for β-actin) for 30 s, and elongation at 72 $^{\circ}$C for 1 min, followed by one cycle of 72 $^{\circ}$C for 10 min for final extension. The relative expression levels were calculated and analyzed by $2^{-\Delta\Delta}$CT method.

3.3.7 Immunofluorescent staining

The NF-κB p65 nuclear localization was detected by immunofluorescence assays using a fluorescence microscope. For this study, Macrophages RAW 264.7 were seeded directly on 8-well glass slide for 12 h, pre-treated for 2 h with tested compound (10 μM). Cells were stimulated with LPS and IFN-γ in the presence of tested sample or DMSO for 0, 15, 30 and 60 min. Cells were washed with PBS, fixed with 4% paraformaldehyde in PBS for 10 min, permeabilized with 0.2% Triton-X 100 for 2 min, and then blocked with 10% anti-FcγR blocker (2.4G2) in 10% FBS for 10 min at room temperature. After blocking, cells were stained with rabbit anti-p65 antibody in 1.5% FBS and incubated for 1 h. After washing with PBS, the secondary antibody, anti-rabbit IgG (H + L, (Fab′)2 fragment) Alexa Fluor®

555 (Cell Signaling Technology, USA), was added and incubated for 1 h in the dark. The position of the cell nuclei was examined with 4′,6-diamidino-2-phenylindole dihydrochloride (DAPI). After washing with PBS, the coverslips were mounted on glass slide with anti-fade medium (Mowiol), and the fluorescence was visualized using inverted fluorescent microscopy and images were recorded.

3.3.8 Statistical Analysis

Unless otherwise indicated, all data were analyzed by an independent t-test using SPSS software. The results were considered to be significant when $p < 0.05$.

3.4 Results and Discussion

3.4.1 Anti-inflammatory effect of limonoids from seeds of *Xylocarpus* spp.

In order to study the anti-inflammatory effect of limonoids from seeds of *Xylocarpus* plants: *X. rumphii*, *X. moluccensis*, and *X. granatum*, thirty-eight limonoids (**42-79**) obtained from their seeds, including phragmalins, mexicanolides, gedunins, andirobins, and protolimonoids, were examined for their anti-inflammatory activities by monitoring their inhibition of NO production in RAW264.7 murine macrophages co-stimulated with LPS and IFN-γ. The structures of all limonoids examined are depicted in Figure 3.3. Cells were pretreated with tested limonoids at doses of 25 and 50 μM for 2 h, then activated with LPS (100 ng/mL) and IFN-γ (10 ng/mL) for an additional 24 h. The results were represented as % NO production and shown in Figures 3.4 and 3.5. In addition, the cell viability was determined by the MTT assay. The results displayed as % cell viability are illustrated in Figures 3.6 and 3.7. Moreover, compounds exhibiting acceptable anti-inflammatory activity with the percentage of NO production lower than 50% and less toxicity (cell viability $>$ 80%) were further examined at various concentrations by subjecting them to the same assay for determination of the IC_{50} values.

According to Figures 3.4-3.7, ten limonoids, **44**-**45**, **47**, **54**, **56**, **58**, **67**, **69**, **74**, and **77**, have been selected to determine their IC_{50} values, since they

provided % NO inhibition and cell viability dropped in the criteria as abovementioned, at least at 25 μM. Based on these results, it could be concluded that, among them, the most potent anti-inflammatory compound was 7-deacetylgedunin (**54**), a gedunin-type limonoid, by inhibiting NO production more than 95%, without any significant toxicity at 25 μM, and its 7-OH might be required for the activity. This was because compounds **55** and **56** bearing –OAc and ketone (-C=O) at C-7 position, respectively, caused significant decrease in their anti-inflammatory activity. In addition, it was found that ring B opening as in **57**, an andirobin-type limonoid, might lead to the big loss of activity (Figure 3.4). Most of mexicanolide- and phragmalin-type limonoids was found to not show any significant activity or to be inactive. Among compounds **74**-**78** which have no C-17 furan ring, **74** and **78** were more active than the ones possessing the alkyl side chain on tetrahydrofuran ring, which might cause the loss of activity.

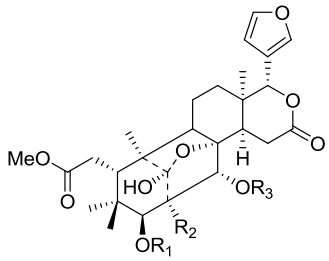

A =

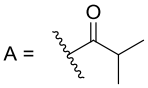

B =

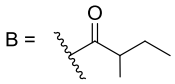

	R_1	R_2	R_3
Xylorumphiin E (**42**)	A	H	A
Xylorumphiin F (**43**)	A	H	B
2-Hydroxyxylorumphiin F (**44**)	A	OH	B
Xylorumphiin H (**45**)	B	OH	B
Xylorumphiin I (**46**)	Ac	OH	A

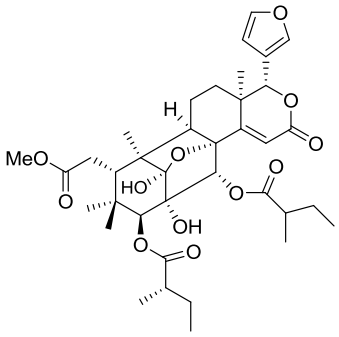

Xylorumphiin I (**47**)

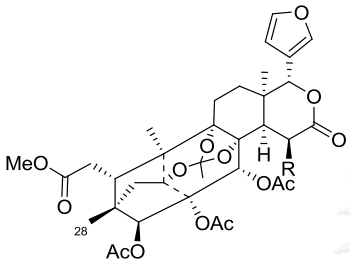

Xylorumphiin J (**48**) R = OH
Xyloccensin E (**50**) R = H

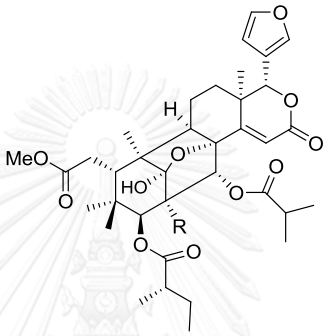

Xyloccensin X (**49**) R = OH
Xylorumphiin C (**53**) R = H

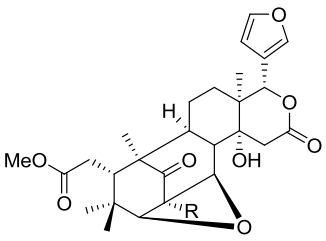

Xyloccensin K (**51**) R = H
Xylorumphiin D (**52**) R= OH

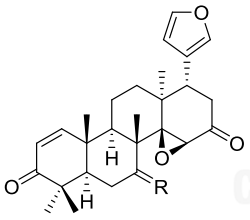

7-deacetylgedunin (**54**) R = α-OH, β-H
Gedunin (**55**) R = α-OAc, β-H
7-oxo-7-deacetoxygedunin (**56**) R = O

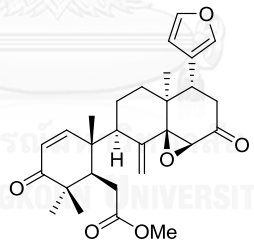

Andirobin (**57**)

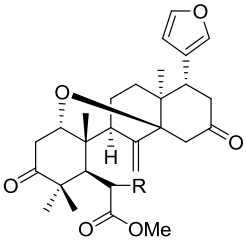

Methyl angolensate (**58**) R = H
Methyl-6-β-hydroxy angolensate (**59**) R = OH

Figure 3.3 Chemical structures of limonoids from *Xylocarpus* spp.

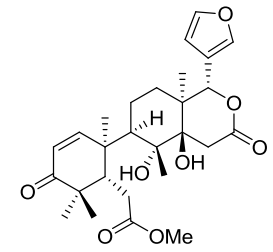

Thaimoluccensin A (**60**)

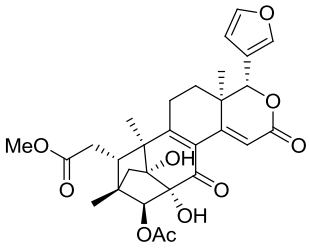

Moluccensin H (**61**)

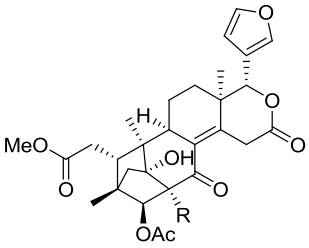

Moluccensin J (**62**)
Moluccensin I (**63**)

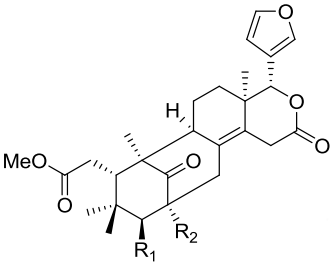

Mexicanolide (**64**) R_1 = =O, R_2 = H
3β-deacetylfissinolide (**65**) R_1 = OH, R_2 = H
2-hydroxyfissinolide (**66**) R_1 = OAc, R_2 = OH
Thaimoluccensin D (**67**) R_1 = OAc, R_2 = H

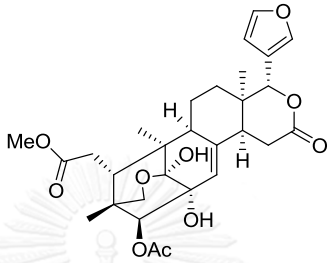

Thaimoluccensin B (**68**)

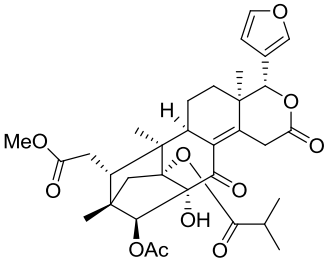

Thaimoluccensin C (**69**)

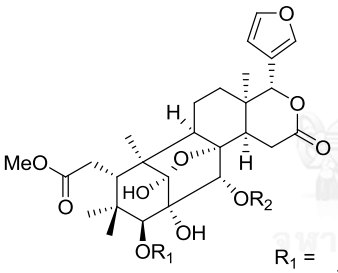

Xylorumphiin A (**70**)
Xylorumphiin B (**71**)

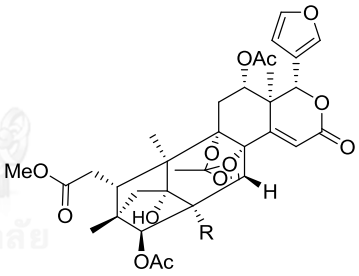

Xyloccensin P (**72**) R = H
Xyloccensin Q (**73**) R = OAc

Figure 3.3 Chemical structures of limonoids from *Xylocarpus* spp. (continued)

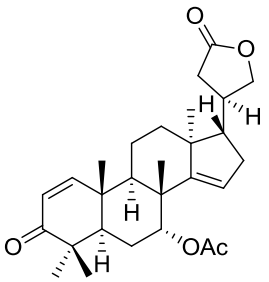

Chisocheton F (**74**)

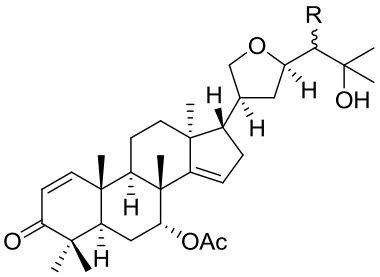

Protoxylocarpin G (**75**) R = α-OH

Protoxylocarpin F (**76**) R = β-OH

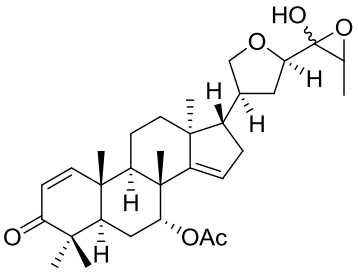

Protoxylocarpin H (**77**)

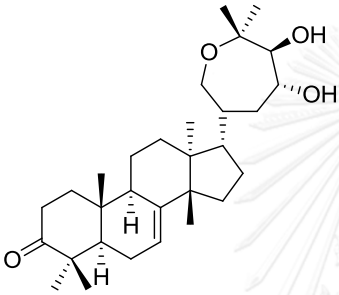

Hispidone (**78**)

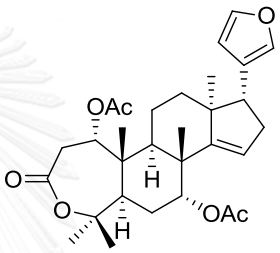

Kihadalactone (**79**)

Figure 3.3 Chemical structures of limonoids from *Xylocarpus* spp. (continued).

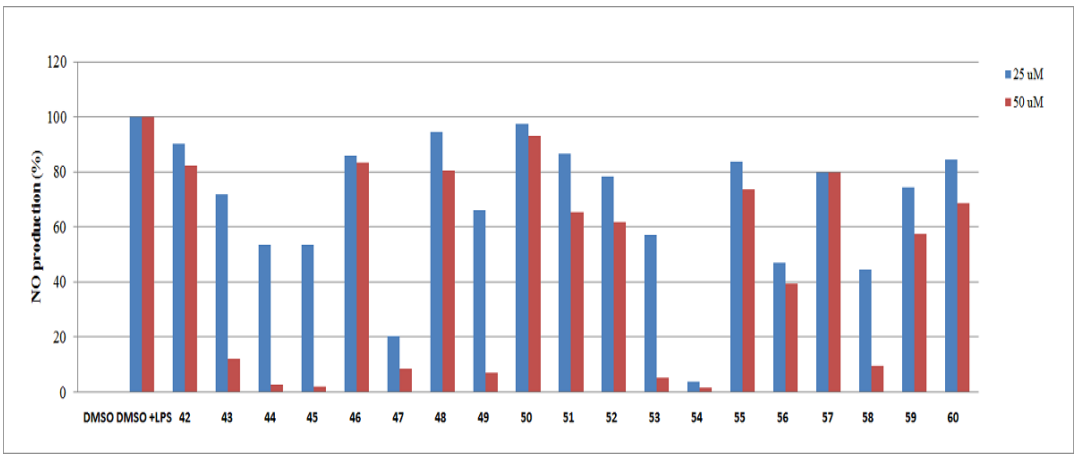

Figure 3.4 Percentage of nitric oxide (NO) production in LPS and IFN-γ stimulated murine macrophages RAW264.7 in the presence of limonoids (**42-60**).

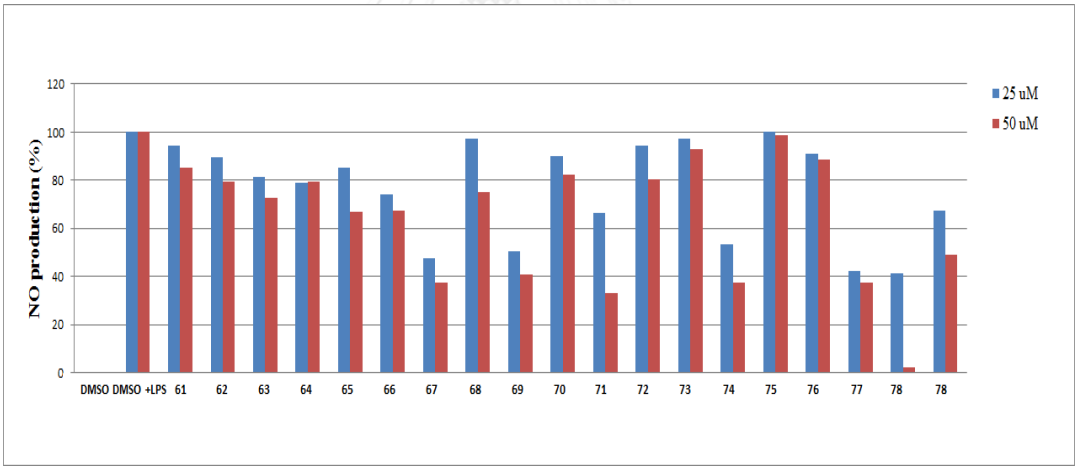

Figure 3.5 Percentage of nitric oxide (NO) production in LPS and IFN-γ stimulated murine macrophages RAW264.7 in the presence of limonoids (**61-79**).

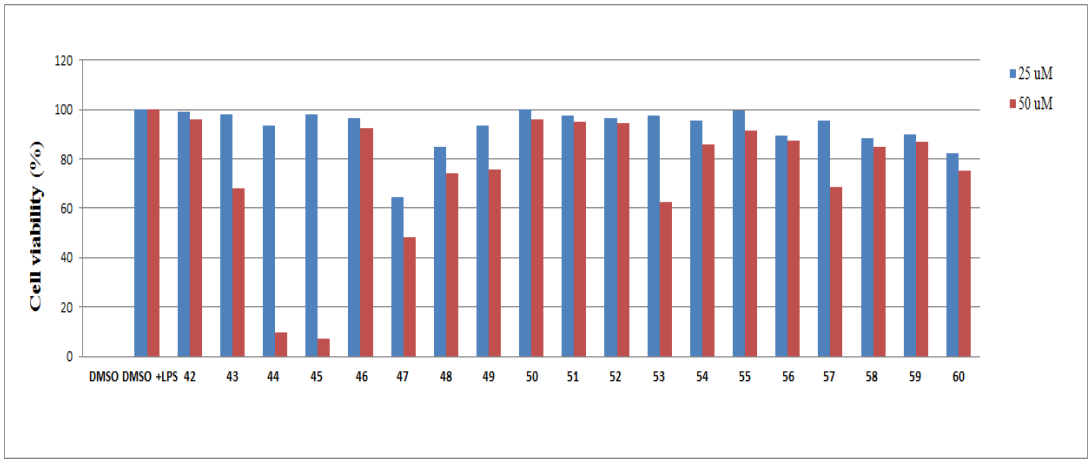

Figure 3.6 Cytotoxicity of limonoids (**42-60**) in LPS and IFN-γ stimulated murine macrophages RAW264.7.

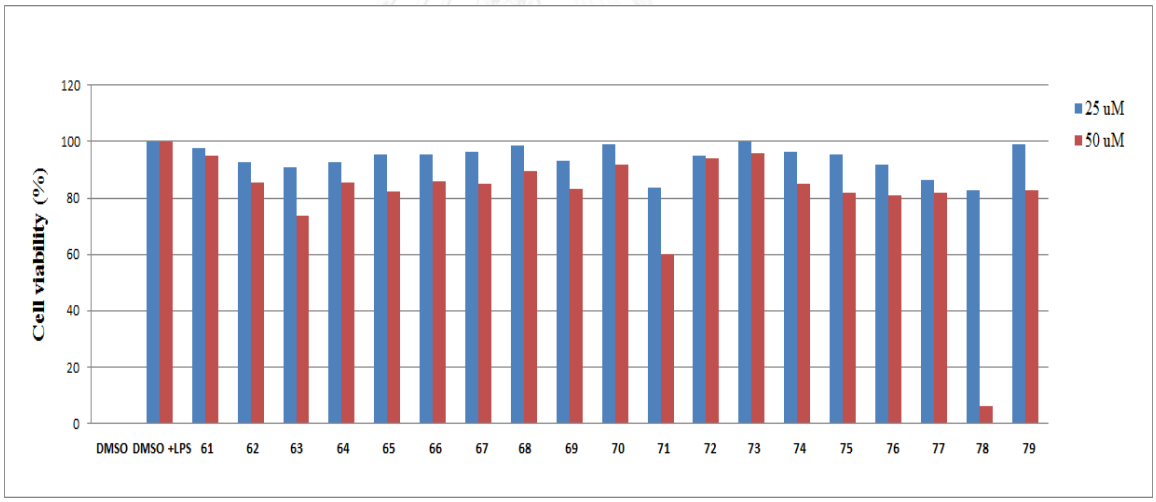

Figure 3.7 Cytotoxicity of limonoids (**61-79**) in LPS and IFN-γ stimulated murine macrophages RAW264.7.

Table 3.1 Inhibitory effect of limonoids on nitric oxide production in stimulated macrophages.

Compounds	IC_{50} (μM)
2-Hydroxyxylorumphiin F (**44**)	24.50
Xylorumphiin H (**45**)	26.61
Xylorumphiin I (**47**)	31.30
7-Deacetylgedunin (**54**)	4.85
7-Oxo-7-deacetoxygedunin (**56**)	22.80
Methyl angolensate (**58**)	20.99
Thaimolucensin D (**67**)	30.18
Thaimoluccensin C (**69**)	32.26
Chisocheton F (**74**)	11.20
Protoxylocarpin H (**77**)	28.56
Indomethacin	28.80

The IC_{50} values of ten selected limonoids are shown in Table 3.1. Base on these results, it could confirm that 7-deacetylgedunin (**54**) displayed the most potent, among limonoids tested and remarkable anti-inflammatory activity by an IC_{50} value of 4.85 μM, compared to indomethacin, a non-steriodal anti-inflammatory agent. Chisocheton F (**74**) also exhibited good activity with IC_{50} value of 11.20 μM, although it was around 2-fold weaker than **54**, whereas the remaining limonoids provides weak activity by IC_{50} values > 20 μM. Therefore, 7-deacetylgedunin (**54**) was selected for further investigation on which signaling pathways are involved to clarify their action mechanism.

3.4.1.1 Cytotoxicity of 7-deacetylgedunin (54) on RAW264.7

To ensure 7-deacetylgedunin less toxicity toward macrophage RAW264.7 cell lines at dose tested, it was subjected to the MTT assay again at various concentrations ranging from 1.56 to 25.0 μM. Results showed compound **54** was not cytotoxic against RAW264.7 cell at any doses (Figure 3.8 B), indicating that the inhibitory effect of **54** on LPS and IFN-γ-induced inflammation

were not as a result of cytotoxicity caused cell viability reduction. Thus, its action mechanism was further studied.

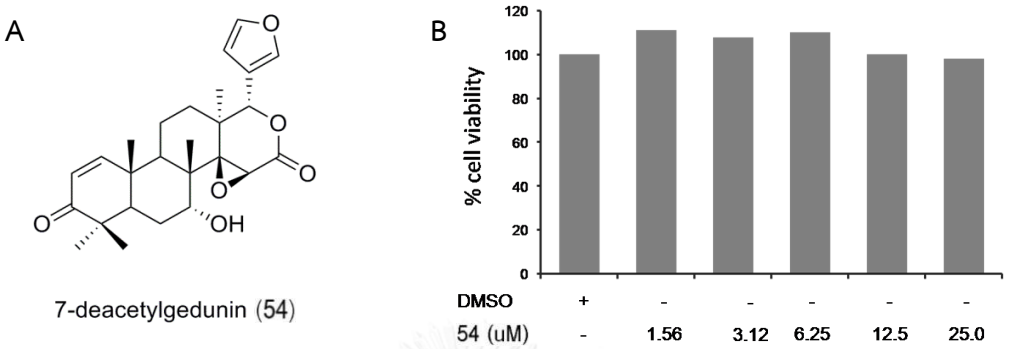

Figure 3.8 Chemical structure of 7-deacetylgedunin (**54**) (**A**). Cytotoxicity of **54** (**B**). Cell were treated with various concentrations of **54** or vehicle control (DMSO) and cell viability was measured by the MTT assay.

3.4.2 Study on action mechanism of 7-deacetylgedunin (54)

Next, 7-deacetylgedunin (**54**) was tested on macrophage cells to examine whether it can reduce iNOS expression, a protein expression of inflammation-associated molecules triggered by LPS and IFN-γ. Herein, RAW 264.7 cells were treated with LPS and IFN-γ with or without the indicated concentrations of **54** to observe the effect on iNOS expression. As shown in Figure 3.9, upon treatment with LPS and IFN-γ, the protein expression level of iNOS were increased markedly, while the expression level was almost undetectable in unstimulated cells. Pretreatment of the cells with different concentrations of **54** led to a decrease in iNOS expression in a dose-dependent manner (Figure 3.10). Additionally, the result obtained suggested that treatment of **54** at a concentration of 10 μM also attenuated LPS and IFN-γ induced iNOS gene expression (Figure 3.11). The reduction in NO concentration in the cell culture supernatant was further found. These data indicated that **54** can down-regulate LPS and IFN-γ induced iNOS expression at the transcriptional level.

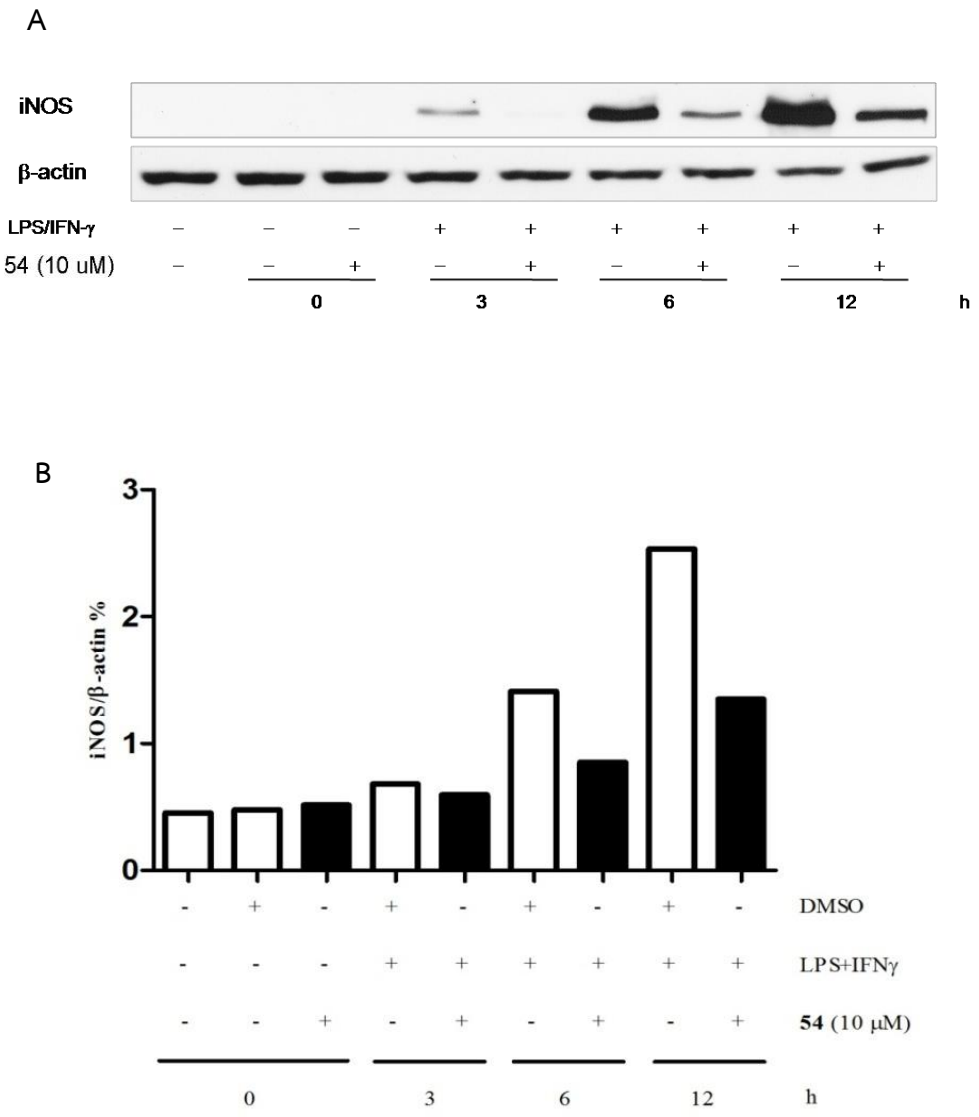

Figure 3.9 Effect of **54** on the expression of iNOS protein. Inhibitory effect of **54** on iNOS expression in RAW 264.7 cells in a time-dependent manner. Cells were pretreated with **54** at 10 μM for 2 h, and then stimulated with LPS (100 ng/mL) and IFN-γ (10 ng/mL) the indicated time (**A**). The levels of iNOS protein were examined by Western blot analysis. The relative iNOS protein levels were measured by densitometry analysis (**B**).

A

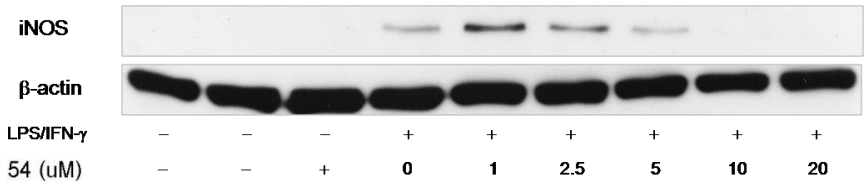

B

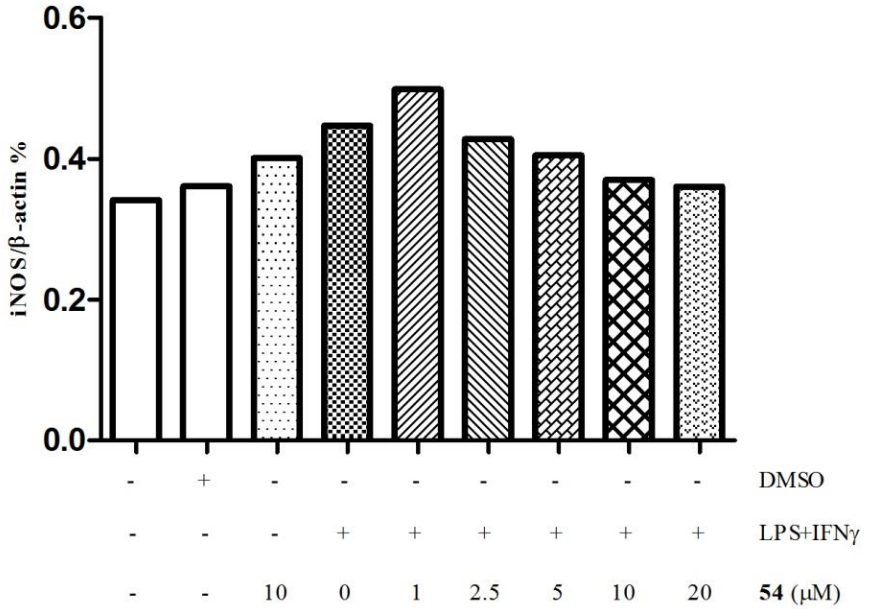

Figure 3.10 Effect of **54** on the expression of iNOS protein. Dose-dependent inhibitory effect of **54** on iNOS expression. Cells were pretreated with the indicated concentrations of **54** for 2 h, and then stimulated with LPS (100 ng/mL) and IFN-γ (10 ng/mL) for further 3 h (**A**). The levels of iNOS protein were examined by Western blot analysis. The relative iNOS protein levels were measured by densitometry analysis (**B**).

A

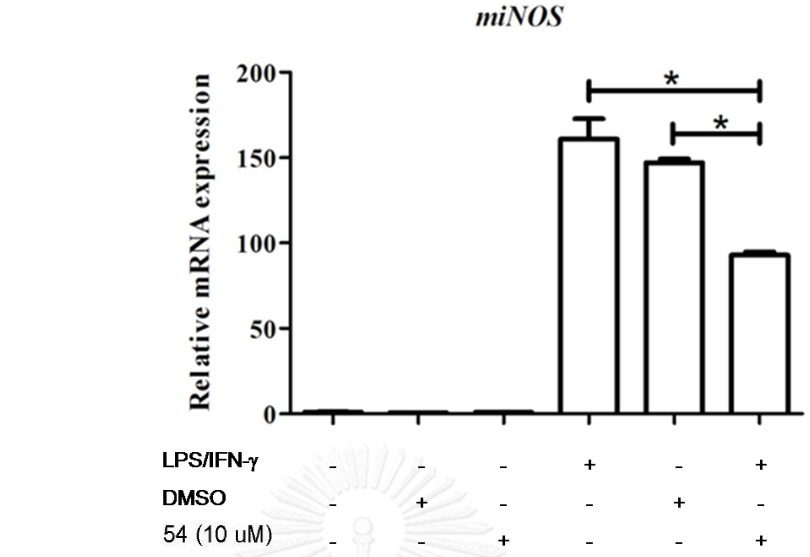

B

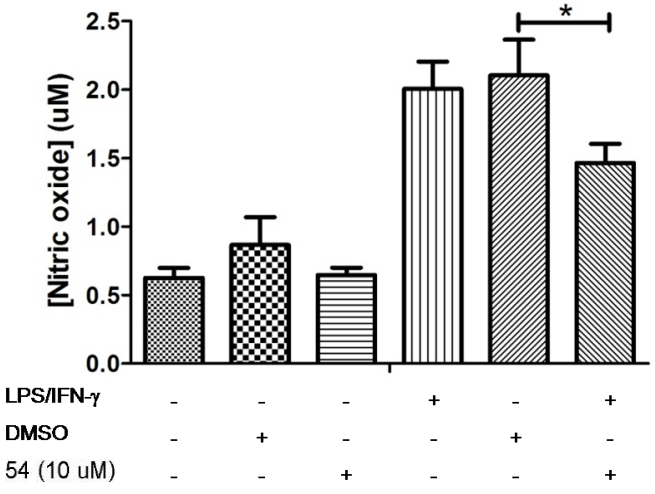

Figure 3.11 Inhibitory effect of **54** on iNOS gene expression in RAW 264.7 (**A**). Cells were pretreated with **54** at 10 μM for 2 h, and then stimulated with LPS (100 ng/mL) and IFN-γ (10 ng/mL) for further 6 h. Expression of iNOS gene was quantified by qRT-PCR. Inhibitory effect of **54** on NO production in RAW 264.7 cells (**B**). Concentration of NO in the cell culture supernatant was determined by Griess reagent.

To elucidate the molecular mechanism of **54** in suppressing LPS and IFN-γ induced iNOS gene expression, the activation of the MAPK and NF-κB signaling pathways were investigated. In this study, three types of MAPKs including p38, ERK1/2 and SAPK/JNK as well as two kinds of NF-κB comprising IκBα and p65 are expressed by using Western blot analysis.

The phosphorylation of MAPK has been proved to be a critical component in the production of NO and pro-inflammatory cytokines in stimulated macrophages. To explore whether the inhibition of NO production by **54** is mediated through the MAPK pathways, the presence of phosphor-p38, phosphor-ERK1/2, and phosphor-SAPK/JNK in compound **54** treated or DMSO-treated cells upon LPS and IFN-γ stimulation was assessed. Interestingly, pretreatment of the cells with **54** markedly suppressed LPS and IFN-γ-induced phosphorylation of p38 and SAPK/JNK after 15 min of stimulation, whereas the level of ERK1/2 phosphorylation was slightly reduced (Figure 3.12). Therefore, it could be concluded that compound **54** has the potent to inhibit NO production by decreasing MAPKs pathway expression.

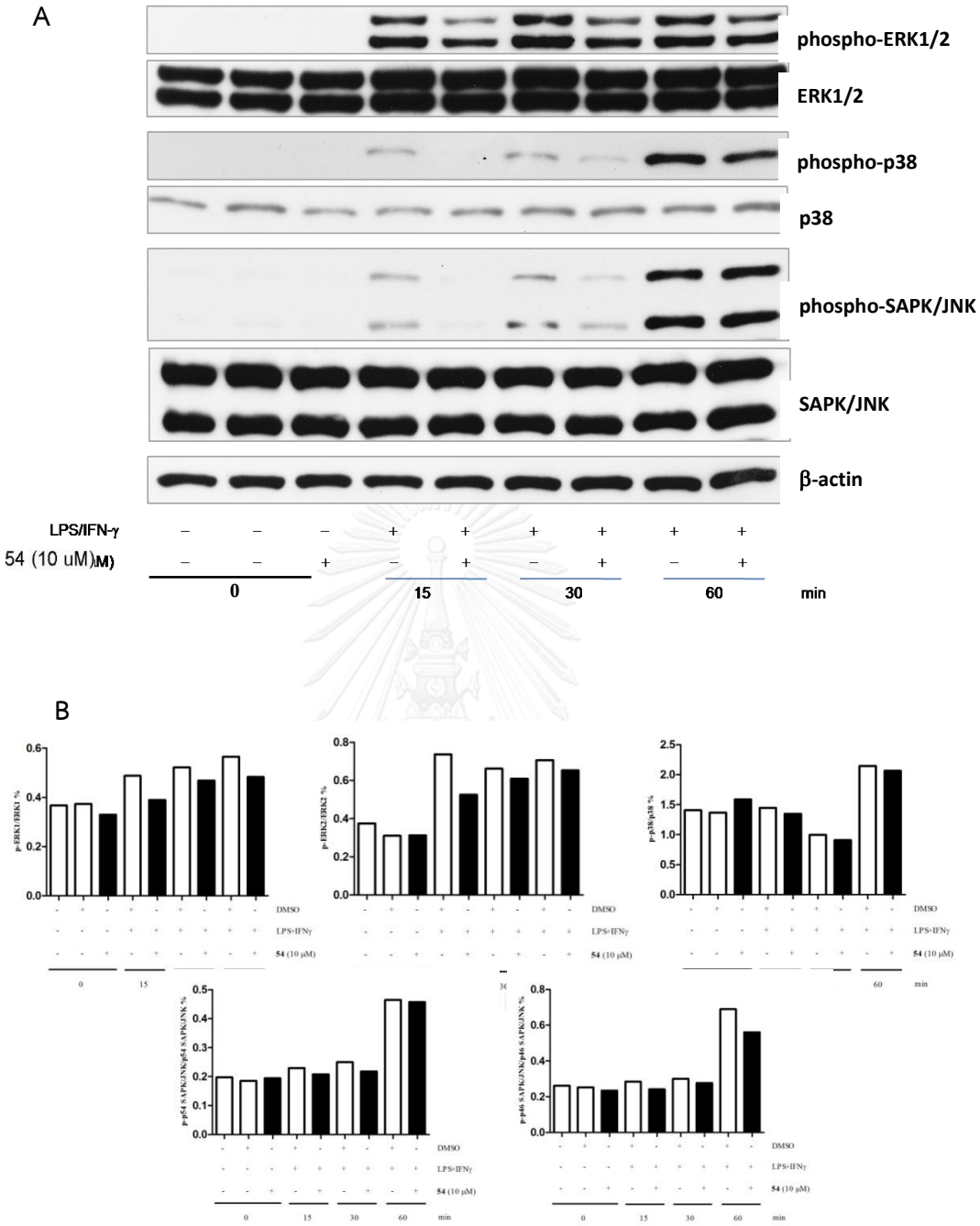

Figure 3.12 Effect of **54** on the activation of the MAPK pathways. RAW264.7 cells were pretreated with **54** at 10 μM for 2 h, and then stimulated with LPS (100 ng/mL) and IFN-γ (10 ng/mL) for the indicated time. Cell lysates were analyzed by Western blots (**A**). The relative MAPKs levels were measured by densitometry analysis (**B**).

The crucial steps in the NF-κB activation are ubiquitination and subsequent degradation of IκBα and nuclear translocation of NF-κB. NF-κB is a heterodimeric complex consisting of p65 and p50 subunits, normally existing in the cytoplasm of the unstimulated cells, due to association with inhibitory proteins, IκBα. However, when the cells are activated by pro-inflammatory stimuli, IκBα are rapidly phosphorylated, degraded, and thereby dissociated from NF-κB. The free active NF-κB complex is then translocated into the nucleus where it regulates gene expression. The degradation of IκBα and the subsequent nuclear translocation of p65 subunit of NF-κB are both important in NF-κB activation by various stimuli. Thus we investigated the effect of **54** on the degradation of IκBα by Western blotting. A time-course experiment showed the level of IκBα obviously decreased at 30 and 60 min after treating with LPS and IFNγ, whereas IκBα degradation was protected by **54** (Figure 3.13). Consistent with this suppression of IκBα degradation, when the level of phosphorylated p65 was examined, pretreatment with **54** clearly suppressed the level of phosphor-p65 compared to cells treated with DMSO, the vehicle control (Figure 3.13).

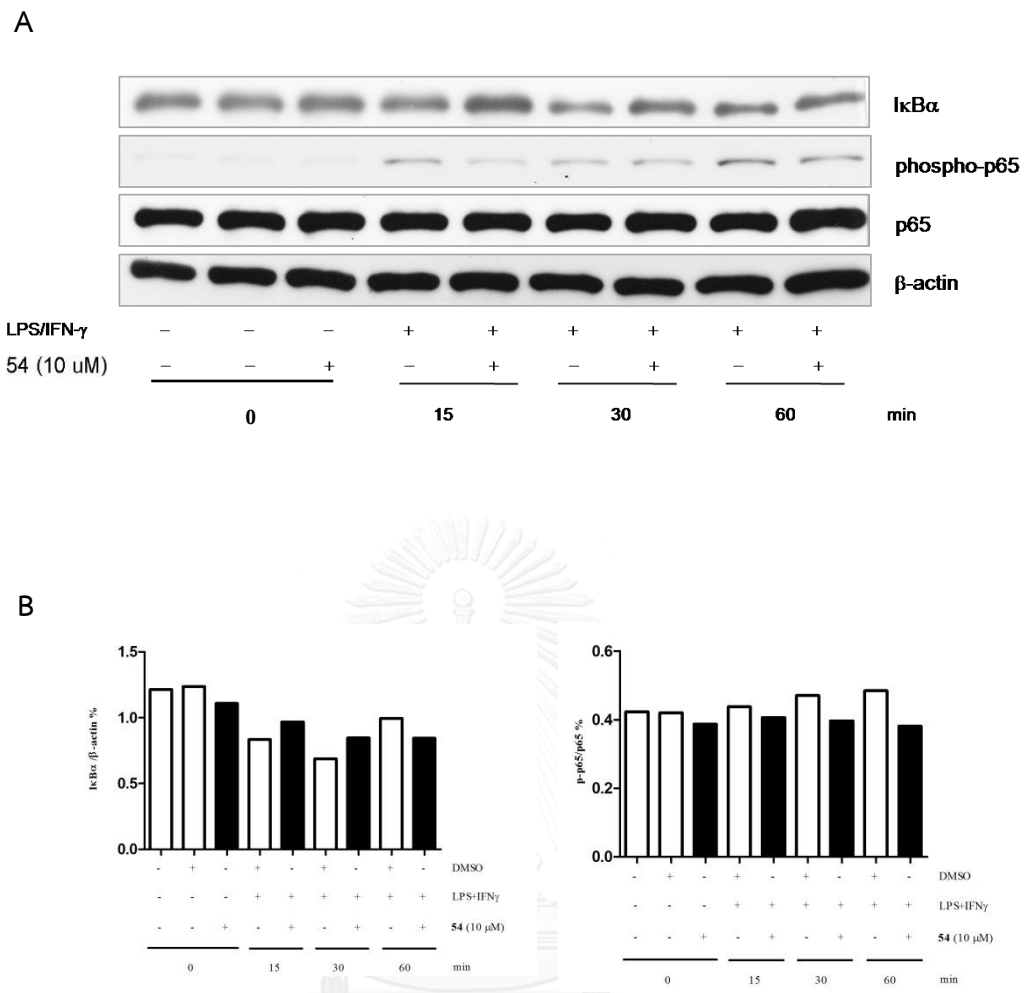

Figure 3.13 Effect of **54** on the activation of the NF-κB pathways. RAW264.7 cells were pretreated with **54** at 10 μM for 2 h, and then stimulated with LPS (100 ng/mL) and IFN-γ (10 ng/mL) for the indicated time. Cell lysates were analyzed by Western blots (**A**). The relative NF-κB levels were measured by densitometry analysis (**B**).

To confirm the suppression of **54** on p65 phosphorylation, the expression of phospho-p65 by **54** was explored again by Western blot analysis. Results showed the expression of phospho-p65 was suppressed in RAW264.7 treated with **54** at every time point, compared to vehicle control DMSO-treated cells (Figure 3.14). Thus, it was assured that compound **54** had an effect on NF-κB activity by inhibiting through phosphorylation of p65.

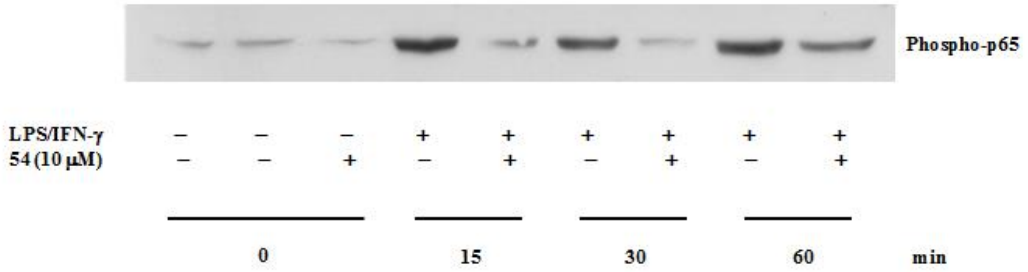

Figure 3.14 Effects of **54** on p65 phosphorylation. RAW 264.7 cells were pretreated with 10 μM of **54** for 2 h and then stimulated with LPS (100 ng/mL) and IFN-γ (10 ng/mL) for the indicated time. Cell lysates were analyzed by Western blots. Data are representative of three independent experiments with similar results.

To further confirm this inhibitory effect of **54** on NF-B activation, we therefore monitored its impact on the nuclear translocation of NF-κB p65 by a localization study using immunofluorescence staining. In LPS and IFN-γ-co-stimulated control cells, p65 was normally sequestered in the cytoplasm at the start of the stimulation (Figure 3.15A), while the nuclear localization of p65 in RAW 264.7 cells was significantly induced within 15 min of the stimulation. Obviously, upon the treatment with **54** for 15 min, the nuclear localization of p65 from cytoplasm into nucleus was inhibited; however, it has been recovered at 30 min (Figure 3.15B). This suggested that compound **54** suppressed NF-κB activation by delaying, not abrogating, the nuclear localization of NF-κB p65.

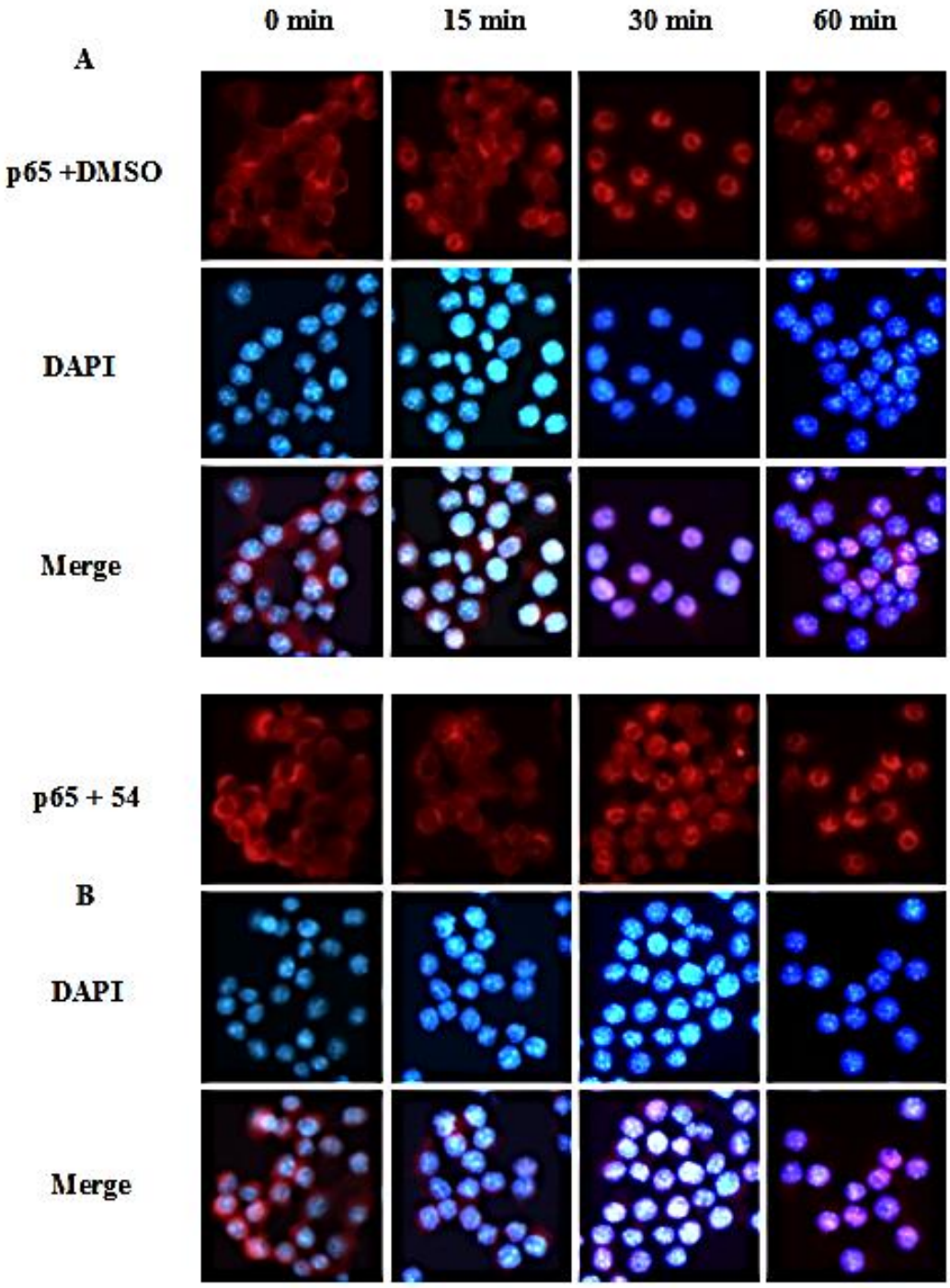

Figure 3.15 Immunofluorescence microscopy analysis of the nuclear translocation of p65 in RAW 264.7 cell. RAW 264.7 cell lines were pretreated with **54** (10 μM) for 2 h, stimulated with LPS and IFN-γ in the presence of vehicle control, DMSO (**A**) or **54** (**B**), for indicated time and then conducted to an immunofluorescence staining. The cells were observed under a fluorescent microscope.

Consequently, the suppression of the MAPKs and NF-κB activation pathways by **54**, upon stimulation with LPS and IFN-γ, cooperatively contributed to its anti-inflammatory activity. Taken together, our finding indicated that a gedunin limonoid, 7-deacetylgedunin (**54**), has a promising anti-inflammatory activity by interfering with iNOS expression, which is mediated mainly by suppressing the MAPK and NF-κB pathways. Hence, this compound might have therapeutic potential for inflammation related diseases.

3.5 Conclusion

Among thirty-eight limonoids isolated from seeds of *Xylocarpus* spp., 7-deacetylgedunin (**54**), a gedunin type limonoid, exhibited the most potent anti-inflammatory activity with the inhibition of NO production in LPS and IFN-γ-stimulated in murine macrophage RAW264.7 cells and provided an IC_{50} value of 4.85 μM. The suppression of NO production by **54** was correlated with the down regulation of mRNA and protein expression of inducible nitric oxide synthase (iNOS). Furthermore, mechanistic studies revealed that the transcriptional activity of NF-κB, the IκBα degradation, and the activation of mitogen-activated protein kinases, stimulated with LPS and IFN-γ, were suppressed by 7-deacetylgedunin (**54**).

CHAPTER IV

STRUCTURE ACTIVITY RELATIONSHIP ON ANTI-INFLAMMATORY ACTIVITY OF DYSOBININ AND ANDROGRAPHOLIDE DERIVATIVES

4.1 Introduction

In the finding for novel bioactive, small chemical molecules for research in chemical biology and medicinal chemistry, one must select a starting point from the huge chemical space. In this aspect, natural products may render as biologically pre-validated leads. In fact, more than 60% of the recently marketed drugs have been isolated from natural products or synthetic compounds based on natural products. With the recent advances in natural products science, comprising the synthesis of complex libraries, biosynthesis, and isolation techniques, the field has a promising future. Particularly, Thai medicinal plants may serve as a source of new bioactive chemical compounds [80].

One of the major fields which pharmaceutical chemists can provide to the development of novel therapeutic agents is the investigation of the structure-activity relationships (SARs) of lead compounds. Derivative synthesis of potential natural products will not only spread the resources from natural metabolites to an almost unlimited degree, but also help characterize functional groups or structure features that are reliable for specific interactions of the bioactive molecules with receptors in target cells in the body, hence allowing the design of derivatives with improved biological properties. Moreover, the bioavailability of synthetic drug derivatives is frequently important in cell molecular biology research, especially with suitable techniques such as radioactive, fluorescent, and photo affinity labeling [81].

Plants belonging to the Meliaceae family have proved to be rich sources of limonoids, which are well known for their antifeedant activity and bitterness. They are especially abundant and structurally diversified in the Meliaceae family. Structurally, they are highly oxygenated and modified nortriterpenoids either containing or derived from a precursor with a 4,4,8-trimethyl-17-furanylsteroid skeleton. Moreover, compounds belonging to this group have been demonstrated to

possess a broad range of biological activities, such as antifeedant, antibacterial, antifungal, antiviral, antimalarial, anticancer and anti-inflammatory activities [47, 82]. In previous chapter, it was found that 7-deacetylgedunin (**54**), a gedunin type limonoid from *Xylocarpus* spp. (Meliaceae), showed the most potent anti-inflammatory effect against nitric oxide (NO) production in macrophages by inhibition of mRNA and protein expression of iNOS gene and also suppressed transcriptional activity through iNOS signaling pathway. Therefore, we have wisely become interested in designing and synthesizing another series of limonoids from dysobinin (**80**) (Figure 4.1), a limonoid isolated from another plant in this family, *Chesocheton siamensis*. Since its structure is similar to that of gedunin, the semi-synthesis of some derivative has been performed and the structure activity relationships (SARs) have subsequently been studied.

Andrographolide (**81**), a diterpenoid lactone isolated from the medicinal plant *Andrographis paniculata*, which has been used as a folk medicine to cure upper respiratory infections, sore throats and many other infectious diseases. Recently, pharmacological chemists have synthesized enormous numbers of andrographolide analogues, which bear considerable biological activities such as anti-inflammatory, antibacterial, antivirus, antitumor, antidiabetic and antifeedant. Hence, corresponding SARs were increasingly apparent. Although there has been extensively examined on the anti-inflammatory effect of andrographolide and its derivatives but details of structure activity relationships on this activity are still lacking. Herein, semi-synthetic analogues of andrographolide were carried out at various parts of the structure, and their anti-inflammatory activity has been explored.

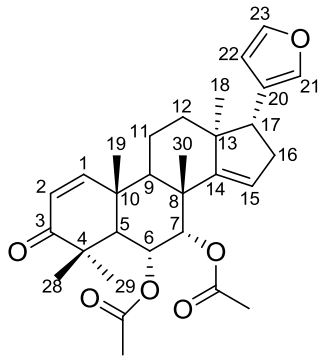

Dysobinin (**80**)

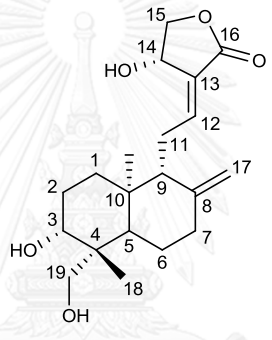

Andrographolide (**81**)

Figure 4.1 Chemical structures of dysobinin (**80**) and andrographolide (**81**).

4.2 Literature Review

In 2010 Das and co-worker studied structure-activity relationship of andrographolide (**81**) isolated from the leaves of *A. paniculata* and its analogues (Figure 4.2). All compounds were evaluated cytotoxicity against human leukemic cell lines (U937, K562 and THP1), together with normal cell lines (NIH3T3 and L132). The results showed that two of the synthesized analogues (**84** and **89**) inhibited the proliferation of U937 and THP1 cells at a concentration less than 6.5 μM, while others displayed the cytotoxic activity at higher concentration. This exploration suggested that activities of the unsaturated (Δ^{12}) compounds (**84-85** and **88-89**) were lost when the double bond between C-12 and C-13 (α-alkylidene) was reduced. The

presence of the α-alkylidene part attached to the γ-butyrolactone ring would be required cytotoxicity [83].

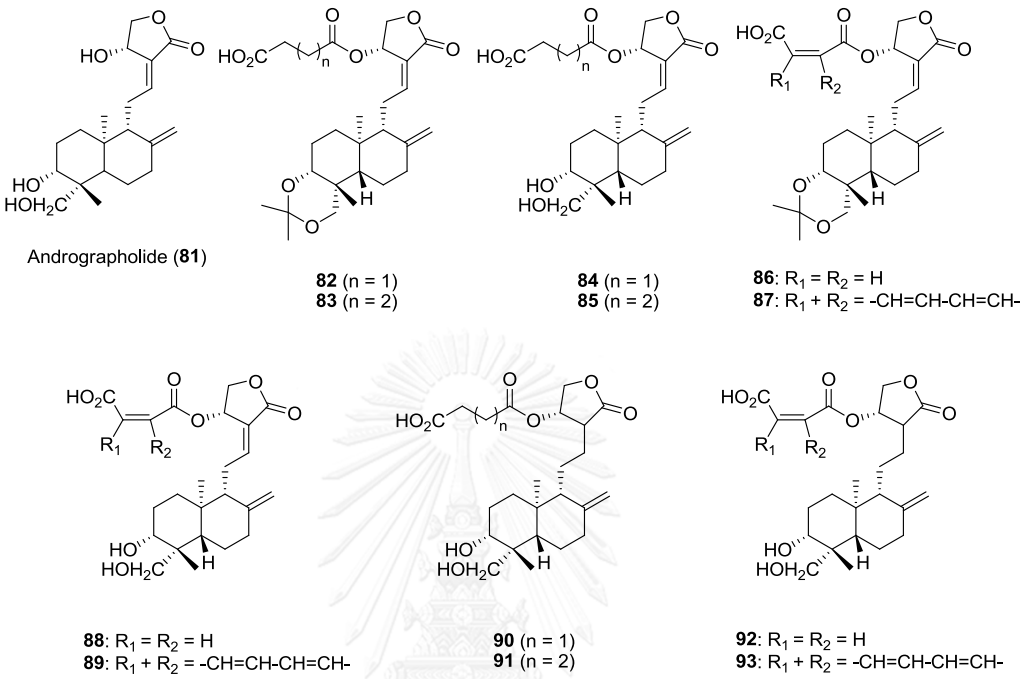

Figure 4.2 Chemical structures of andrographolide (**81**) and its analogues (**82-93**).

In 2011 Dai and co-worker investigated the anti-inflammatory activity of andrographolide (**81**) and its derivatives (**94-98**) through inhibition of NO and PGE_2 production. Results revealed that **97** and **98** significantly inhibited ear edema compared with **81**. Furthermore, compound **98** was also showed the most potent anti-inflammatory effect against ear edema in mice (79.4%; 1.35 mmol/kg, ig) and paw edema in rats (50.4%; 0.90 mmol/kg, ig). Additionally, compound **98** significantly ($p<0.05$) obstructed granuloma formation and reduced the increasing in vascular permeability induced by peritoneal injection of 0.6% acetic acid solution in mice. The analysis of the structure-activity relationship of compounds **94-98** indicated that the introduction of *p*-chlorobenzylidene to C-15 of **94** are greatly responsible for the enhancement in the anti-inflammatory effects of compounds **97** and **98** [84].

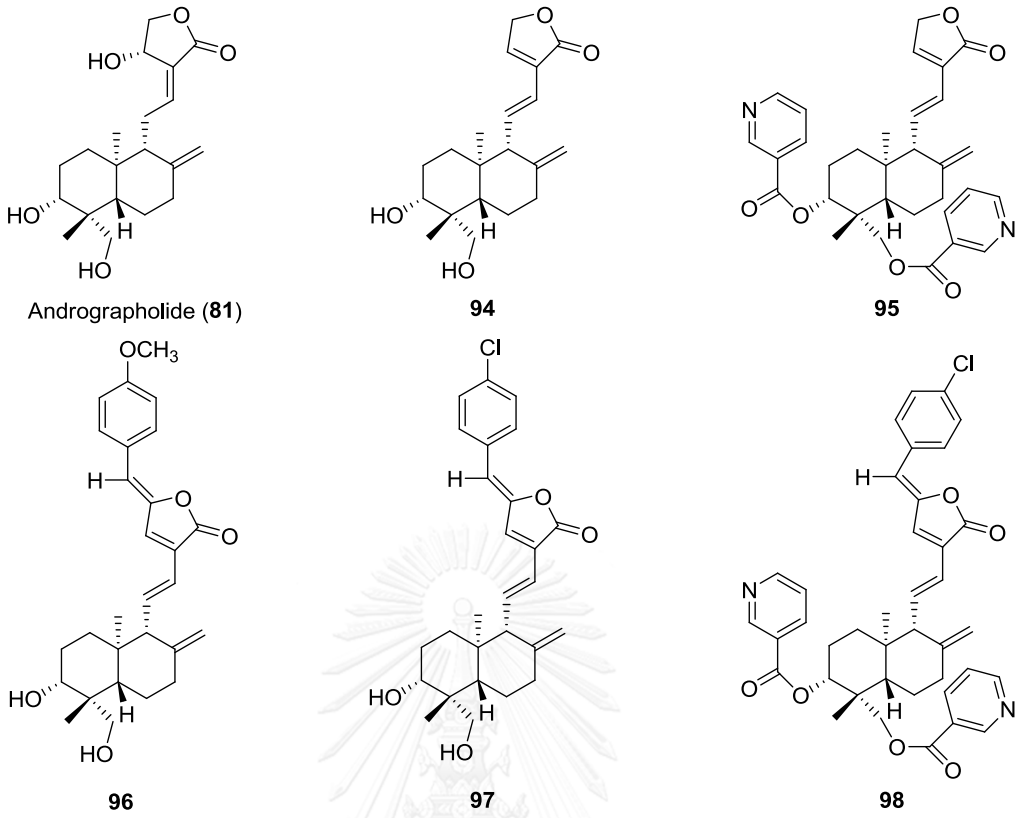

Figure 4.3 Chemical structures of andrographolide (**81**) and its derivatives (**94**-**98**).

In 2012 Sirion and co-worker studied cytotoxic activities of 19 andrographolide derivatives with the modification at the three hydroxyl groups. A number of the andrographolide derivatives demonstrated much higher cytotoxicity than that of the **81** on cancer cells comprising P-388 (murine leukaemia cell line), KB (human epidermoid carcinoma of the mouth), COL-2 (human colon cancer), MCF-7 (human breast cancer), LU-1 (human lung cancer) and ASK (rat glioma) cells. The semi-synthetic analogue **115** bearing triphenylmethoxyl group at C-19 was found to be the most potent derivative against the tested cancer cells by ED_{50} values ranging from 0.45 to 2.86 μM. Their structure–activity relationships (SARs) revealed the introduction of silyl ether or triphenylmethyl ether group into C-19 of the **81** led to increase in the cytotoxic activity. Moreover, the presence of one acetyl group at C-3 or C-14 of **101** and **106** led to a dramatic increase in the cytotoxicity as compared with compound **99** [85].

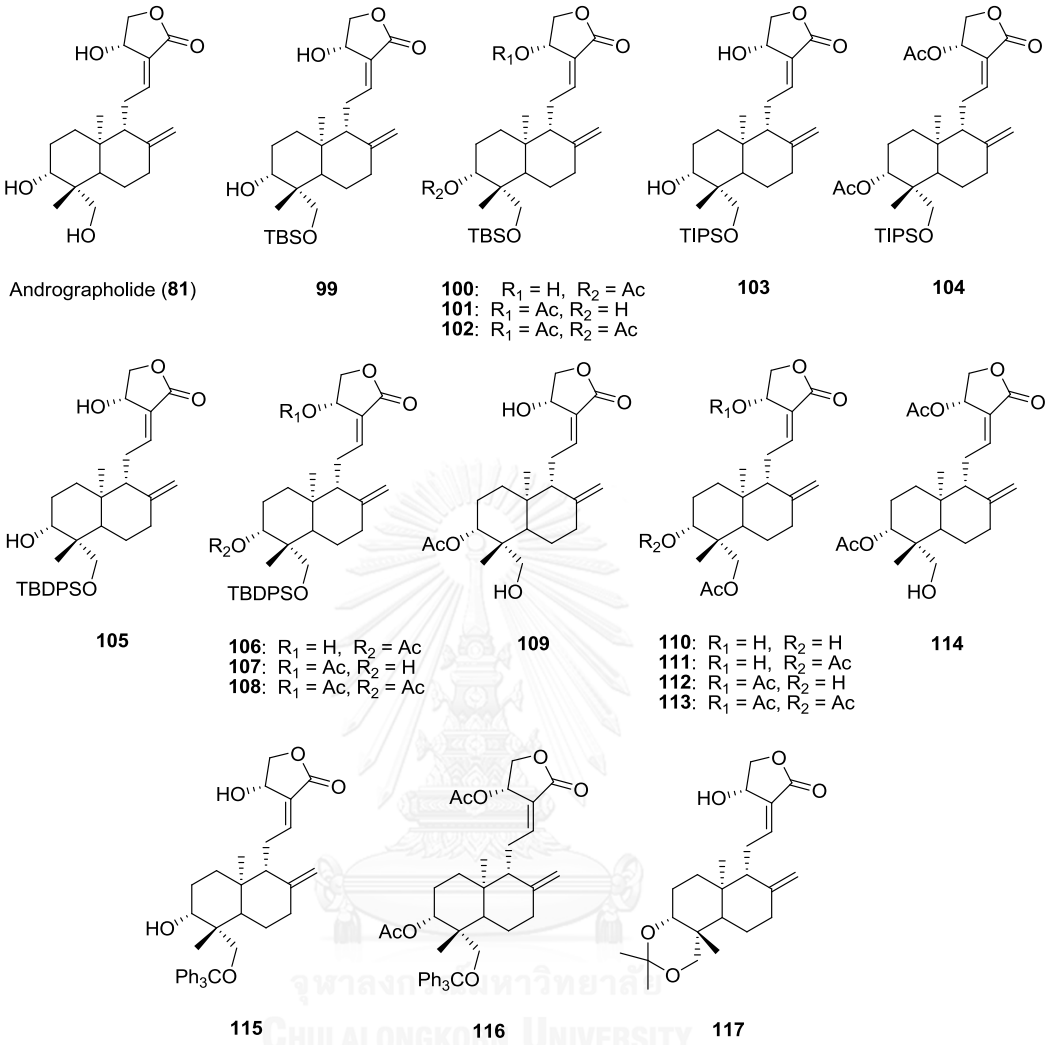

Figure 4.4 Chemical structures of andrographolide (**81**) and its derivatives (**99-117**).

In 2013 Wong and co-worker studied the anti-lipid droplets accumulation (LDA) activity of series of limonoids, ceramicines A-L (**118-129**) which isolated from the barks of *Chisocheton ceramicus*, along with their semisynthetic derivatives (**130-138**). As a results of the structure activity relationship study, natural ceramicines B (**119**) exhibited the highest inhibition of LDA in MC3T3-G2/PA6 cells (IC_{50} = 1.8 μM). The presence of an oxygen atom at C-7 of **119** may be a very important structural feature for anti-LDA activity, but modification at C-7 of the derivative **137** resulted in a decrease of activity. Moreover, etherification and esterification of 7-OH (**130-135**) led to decrease in LDA inhibitory activity [86].

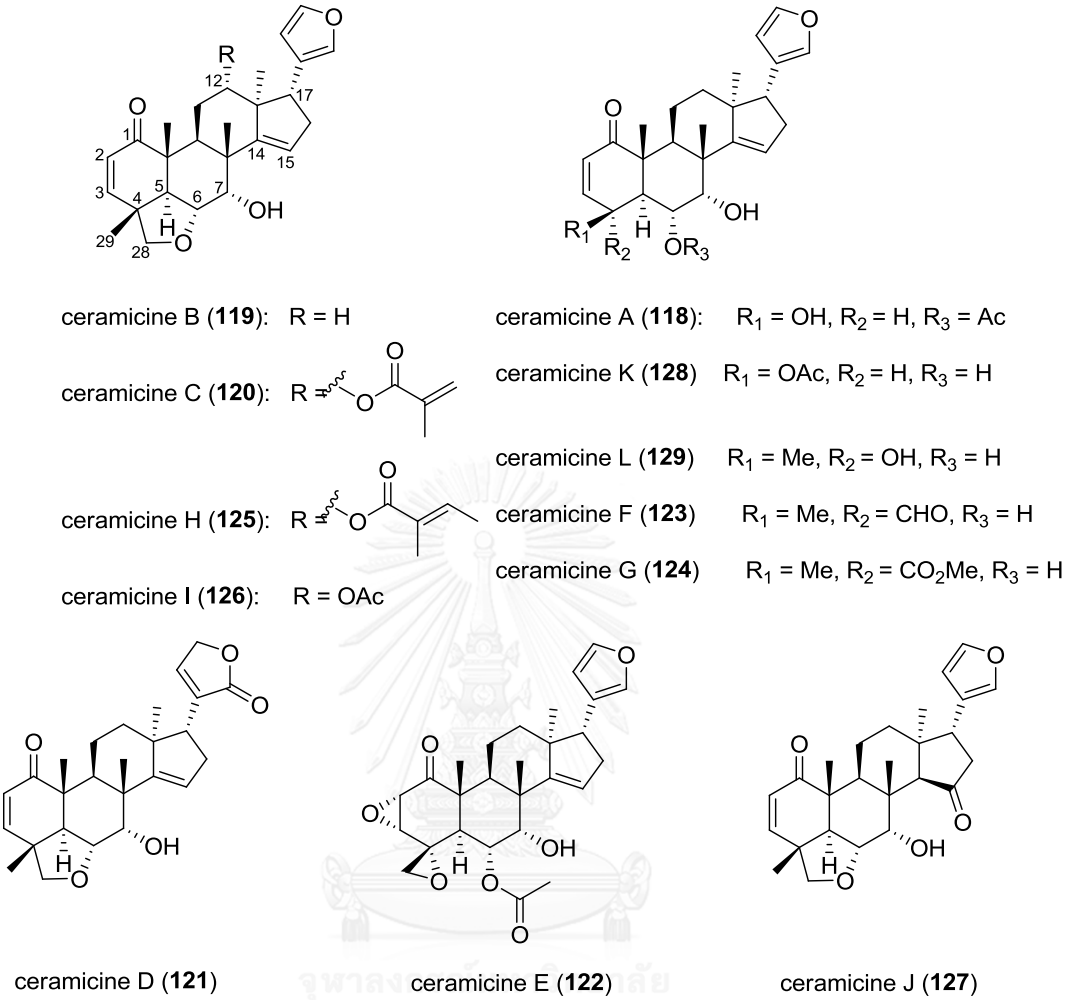

Figure 4.5 Chemical structure of ceramicines A-L (**118-129**).

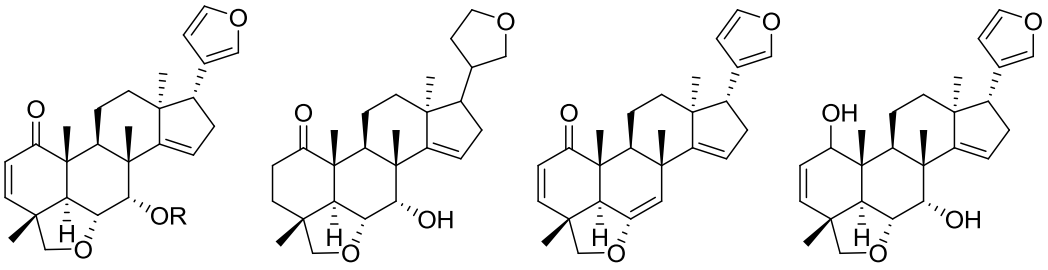

130 : R = Et
131 : R = CH_2OCH_3
132 : R = Ac
133 : R = $COCF_3$
134 : R = Bz

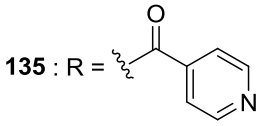

135 : R =

136 **137** **138**

Figure 4.6 Chemical structures of ceramicine derivatives (**130-138**).

4.3 Experiments

4.3.1 General Experimental Procedures

4.3.1.1 Nuclear magnetic resonance spectrometer (NMR)

The NMR spectra were recorded in $CDCl_3$, CD_3OD, and $(CD_3)_2SO$ using a Bruker AV400 and Varian Mecury 400 plus spectrometer at 400 MHz for ^{1}H NMR and 100 MHz for ^{13}C NMR using TMS (tetramethylsilane) as internal standard.

.4.3.2 Chemicals

4.3.2.1 Solvent and chemicals

Reagents and solvents used below were obtained from commercial sources and when required were purified. Two starting materials, dysobinin (**80**) were isolated from the seeds of *C. siamensis*, and andrographolide (**81**) were isolated from the leaves of *A. paniculata*.

4.3.2.2 Chromatography

Merck's silica gel 60 No. 9385 was used as adsorbent for open column chromatography. Merck's thin layer chromatography (TLC) aluminum and glass sheets, silica gel 60 F_{254} precoated, 20x20 cm, layer thickness 0.2 mm were used for TLC analysis. Detection was visualized under ultraviolet light at wavelengths of 254 nm and dipped with $(NH_4)_6Mo_7O_{24}$ in 5% H_2SO_4 solution.

4.3.3 Anti-inflammatory assay and Cytotoxic assay

The anti-inflammatory effect and cytotoxic activity data was obtained by the same manner with 3.3.3 and cytotoxic activity was also performed by the same method with 3.3.4.

4.3.4 Synthesis of dysobinin derivatives

Synthesis of derivative **139**

Dysobinin (**80**) (100 mg, 0.2022 mmol) and K_2CO_3 (41.92 mg, 0.3033 mmol) in aqueous methanol (10 mL) were stirred for at 55°C for 24 h. After completion of the reaction, the mixture was acidified with HCl (1 N) and then the mixture was extracted with Et_2O (3×10 mL). The combined ether phases were dried over anhydrous Na_2SO_4 and evaporated in vacuo. The crude product was chromatographed on silica gel eluted with a gradient of EtOAc : hexane (30%-50%) to yield compound **139 (**83.0 mg, 99% yield); ^{1}H NMR (400 MHz, CD_3OD); δ_H 7.40 (s, 1H), 7.30 (s, 1H), 7.25 (d, *J* = 6.8 Hz, 1H), 6.32 (s, 1H), 5.80 (d, *J* = 6.4 Hz, 1H), 5.53 (d, *J* = 1.2 Hz, 1H), 4.15 (dd, *J* = 7.6, 1.6 Hz, 1H), 3.87 (d, *J* = 2.0 Hz, 1H), 2.82 (m, 1H), 2.58 (m, 1H), 2.35 (dd, *J* = 4.8, 2.4 Hz, 1H), 2.32 (dd, *J* = 4.8, 2.4 Hz, 1H), 2.30 (d, *J* = 7.6 Hz, 1H), 2.23 (dd, *J* = 8.0, 4.4 Hz, 1H), 1.95 (m, 1H), 1.88 (m, 1H), 1.69 (m, 2H), 1.38 (s, 3H), 1.31 (s. 3H), 1.19 (s, 3H), 1.10 (s. 3H), 0.81 (s, 3H): ^{13}C NMR (100 MHz, CD_3OD); δ_C 209.1, 161.1, 161.0, 143.8, 141.1, 126.5, 126.0, 121.0, 112.2, 78.0, 69.3, 53.2, 50.0, 48.3, 46.9, 45.4, 42.1, 37.2, 36.0, 34.4, 32.7, 27.6, 21.5, 21.0×2, 17.6 [87].

Synthesis of derivative **140**

To a solution of $(COCl)_2$ (0.0041 mL, 0.0486 mmol) in dry CH_2Cl_2 (0.5 mL) under nitrogen was added dropwise at -80 °C a solution of DMSO (0.0086 mL, 0.1215 mmol) in CH_2Cl_2 (0.5 mL). After 10 min, the diol **139** (10 mg, 0.0243 mmol) dissolved in CH_2Cl_2 (0.25 mL) was added dropwise at -80 °C. After 1.5 h stirring at this temperature, Et_3N (0.0271 mL, 0.1944 mmol) was added and kept stirring at -80 °C for additional 5 h then the reaction was hydrolyzed with a 2:1 mixture of a saturated aqueous NH_4Cl solution and NH_3 (28% in water). The layers were separated, and the aqueous layer was extracted twice with CH_2Cl_2. The combined organic phases were dried over anhydrous Na_2SO_4 and the solvent was removed under reduced pressure, then the product was purified by column chromatography over silica gel using a mixture of EtOAc : hexane (40%) to give compound **140 (**8.26 mg, 83% yield); ^{1}H NMR (400 MHz, CD_3OD); δ_H 7.43 (t, *J* = 1.2 Hz, 1H), 7.35 (s, 1H), 7.26 (d, *J* = 6.8 Hz, 1H), 6.35 (s, 1H), 5.97 (dd, *J* = 2.4, 1.2 Hz, 1H), 5.90 (d, *J* = 6.8 Hz, 1H), 4.89 (s, 1H), 2.88 (dd, *J* = 7.6, 4.8 Hz, 1H), 2.63 (m, 1H), 2.40 (m, 1H), 2.16 (dd, *J* = 8.0, 3.6 Hz, 1H), 2.07 (m, 1H), 1.98 (m, 1H), 1.94 (d, *J* = 8.8 Hz, 2H), 1.90 (m, 1H), 1.79 (m, 1H), 1.51 (s, 3H), 1.47 (s, 3H), 1.38 (s, 3H), 1.32 (s, 3H), 0.84 (s, 3H): ^{13}C NMR (100 MHz, CD_3OD) δ_C 211.9, 207.5, 159.0, 154.1, 143.9, 141.2, 127.8, 127.0, 125.8, 112.1, 111.5, 72.7, 59.2, 53.2, 52.5, 47.6, 45.9, 41.4, 35.9, 34.8, 32.2, 28.0×2, 22.3, 21.1, 20.8, 18.5.

Synthesis of derivative **141**

A solution of **80** (10 mg, 0.0243 mmol) in CH_2Cl_2 (1 mL) was treated with 2,2-dimethoxypropane (0.016 mL, 0.1349 mmol) and *p*-TsOH (1.65 mg, 0.0087 mmol) and stirred at room temperature for 3 h. The reaction was quenched with saturated $NaHCO_3$ aqueous solution (10 mL). The organic layer was separated and the aqueous layer was extracted with $CHCl_3$ (2×10 mL). The combined organic layer was dried over Na_2SO_4 and concentrated under reduced pressure. The crude product was subjected to column chromatography on a silica gel eluting with a mixture of EtOAc : hexane (30%) to afford compound **141** (2.51 mg, 23% yield); ^{1}H NMR (400 MHz, CD_3OD) δ_H 7.43 (s, 1H), 7.34 (s, 1H) 7.31 (d, *J* = 6.8 Hz, 1H), 6.35 (s, 1H), 5.86 (d, *J* = 6.8 Hz, 1H), 5.49 (d, *J*= 1.6 Hz, 1H), 4.87 (s, 1H), 4.55 (dd, *J* = 7.2, 2.8 Hz, 1H), 4.38 (d,

J = 3.2 Hz, 1H), 2.85 (dd, *J* = 7.2, 4.8 Hz, 1H), 2.60 (m, 1H), 2.35 (m, 1H), 2.25 (dd, *J* = 7.6, 4.4 Hz, 1H), 2.12 (d, *J* = 7.2 Hz, 1H), 2.07 (m, 1H), 1.93 (m, 1H), 1.80 (m,1H), 1.69 (m, 1H), 1.45 (s, 3H), 1.38 (s. 3H), 1.35 (s, 3H), 1.34 (s, 3H), 1.30 (s, 3H), 1.12 (s. 3H), 0.82 (s, 3H): ^{13}C NMR (100 MHz, CD_3OD) δ_C 207.9, 160.3, 160.2, 143.8, 141.1, 126.6, 126.0, 121.2, 112.2, 109.2, 81.8, 75.4, 53.0, 52.2, 46.9, 41.8, 41.4, 38.9, 35.7, 34.2, 32.8, 30.6, 29.3, 26.7, 22.2, 21.5, 20.5, 18.0 [88].

Synthesis of derivatives **142-143**

A solution of **80** (30 mg, 0.0607 mmol) in a 2:1 mixture of methanol and chloroform (4 mL) was stirred under nitrogen atmosphere at 0 °C. Cerium trichloride heptahydrate (45.23 mg, 0.1214 mmol) was added, followed by the slow addition of sodium borohydride (2.30 mg, 0.0607 mmol). The reaction mixture was stirred for 6 h and quenched by the addition of a solution of 1% aqueous acetic acid. The reaction mixture was extracted 3 times with CH_2Cl_2. The combined organic layers were dried (Na_2SO_4), filtered, and concentrated. The resulting white solid was dissolved in minimal CH_2Cl_2 then purified by SiO_2 column chromatography using acetone-dichloromethane mixture as an eluent to give compounds **142** and **143.**

Compound 142 (8.4 mg, 30% yield); ^{1}H NMR (400 MHz, $CDCl_3$); δ_H 7.36 (s, 1H), 7.22 (s, 1H), 6.26 (s, 1H), 5.86 (dd, *J* = 10.4, 2.0 Hz, 1H), 5.64 (dd, *J* = 12.0, 2.4 Hz, 1H), 5.35 (m, 3H), 3.91 (s, 1H), 2.76 (dd, *J* = 10.8, 7.6 Hz, 1H), 2.36 (m, 3H), 2.19 (d, *J* = 12.0 Hz, 1H), 2.09 (dd, *J* = 12.4, 7.2 Hz, 2H), 2.01 (s, 3H), 2.00 (s, 3H), 1.85 (m, 3H), 1.65 (m, 3H), 1.25 (s, 3H), 1.10 (s, 3H), 0.92 (s, 3H), 0.76 (s, 3H): ^{13}C NMR (100 MHz, $CDCl_3$) δ_C 170.4, 170.2, 159.9 142.5, 139.7, 137.1, 125.4, 119.1, 111.1, 76.6, 75.8, 70.1, 51.5, 48.5, 47.2, 43.5, 41.5, 40.3, 37.2, 34.4, 32.7, 30.0, 27.8, 21.5, 21.0, 20.1, 20.0, 18.1, 17.3, 14.1.

Compound 143 (7.7 mg, 25% yield); ^{1}H NMR (400 MHz, $CDCl_3$); δ_H 7.36 (s, 1H), 7.22 (s, 1H), 6.26 (s, 1H), 5.55 (dd, *J* = 12.0, 2.4 Hz, 1H), 5.32 (dd, *J* = 7.6, 2.0 Hz, 2H), 3.24 (m, 1H), 2.76 (dd, *J* = 10.8, 7.2 Hz, 1H), 2.34 (m, 3H), 2.02 (s, 3H), 2.01 (s, 3H), 1.94 (m, 3H), 1.79 (m, 4H), 1.67 (m, 2H), 1.26 (s, 3H), 1.12 (s, 3H), 1.04 (s, 3H), 0.88 (s, 1H), 0.83 (s, 3H), 0.77 (s, 3H): ^{13}C NMR (100 MHz, $CDCl_3$); δ_C 170.4, 170.2, 158.8,

142.5, 139.7, 124.7, 119.0, 111.1, 78.2, 76.0, 70.6, 51.5, 50.9, 43.1, 38.4, 37.8, 34.4, 32.7, 31.9, 30.2, 27.4, 26.8, 22.7, 21.6, 21.1, 19.9, 16.6, 16.4, 15.5, 14.1.

Synthesis of derivatives **144-145**

A solution of **139** (30 mg, 0.0731 mmol) in a 2:1 mixture of methanol and chloroform (4 mL) was stirred under nitrogen atmosphere at 0 °C. Cerium trichloride heptahydrate (54.47 mg, 0.1462 mmol) was added, followed by the slow addition of sodium borohydride (2.77 mg, 0.0731 mmol). The reaction mixture was stirred for 6 h and quenched by the addition of a solution of 1% aqueous acetic acid. The reaction mixture was extracted 3 times with CH_2Cl_2. The combined organic layers were dried (Na_2SO_4), filtered, and concentrated. The resulting white solid was dissolved in minimal CH_2Cl_2 then purified by SiO_2 column chromatography using acetone-dichloromethane mixture as an eluent to give compounds **144** and **145.**

Compound 144 (7.2 mg, 23% yield); ^{1}H NMR (400 MHz, $CDCl_3$); δ_H 7.38 (s, 1H), 7.25 (s, 1H), 6.28 (s, 1H), 5.78 (dd, *J* = 10.4, 2.0 Hz, 1H), 5.54 (d, *J* = 2.4 Hz, 1H), 5.36 (dd, *J* = 10.4, 2.0 Hz, 1H), 4.27 (d, *J* = 10.8 Hz, 1H), 3.93 (d, *J* = 2.4 Hz, 1H), 3.91 (t, *J* = 2.0 Hz, 1H), 2.83 (dd, *J* = 10.8, 7.2 Hz, 1H), 2.57 (m, 1H), 2.40 (m, 2H), 2.01 (m, 2H), 1.85 (m, 3H), 1.67 (m, 2H), 1.32 (s, 3H), 1.26 (s, 3H), 1.17 (s, 3H), 1.12 (s, 3H), 0.88 (t, *J* = 6.4 Hz, 1H), 0.78 (s, 3H) : ^{13}C NMR (100 MHz, $CDCl_3$) δ_C 161.8, 142.6, 139.7, 136.9, 125.5, 124.3, 119.6, 111.0, 77.1, 76.9, 69.7, 51.6, 49.2, 47.4, 44.9, 41.4, 38.9, 37.6, 34.3, 32.3, 31.9, 30.4, 28.0, 19.9, 17.8, 17.1 [89].

Compound 145 (5.0 mg, 16% yield); ^{1}H NMR (400 MHz, $CDCl_3$); δ_H 7.37 (s, 1H), 7.25 (s, 1H), 6.28 (s, 1H), 5.53 (d, *J* = 2.4 Hz, 1H), 4.18 (dd, *J* = 11.2, 1.6 Hz, 1H), 3.91 (d, *J* = 2.8 Hz, 1H), 3.22 (dd, *J* = 11.6 Hz, 1H), 2.82 (dd, *J* = 11.2, 7.6 Hz, 1H), 2.57 (m, 1H), 2.42 (m, 1H), 1.83 (m, 3H), 1.69-1.50 (m, 6H), 1.31 (s, 3H), 1.25 (s. 3H), 1.15 (s, 3H), 0.99 (s, 3H), 0.95 (s, 3H), 0.89-0.83 (m, 1H), 0.80 (s, 3H) : ^{13}C NMR (100 MHz, $CDCl_3$) δ_C 161.7, 142.6, 139.7, 124.4, 119.5, 111.0, 78.6, 77.2, 69.8, 51.7, 51.5, 47.4, 41.6, 39.2, 38.9, 37.8, 34.3, 32.3, 30.4, 29.7, 27.5, 26.8, 19.9, 16.5, 16.2, 15.2 [90].

4.3.5 Synthesis of andrographolide derivatives

Synthesis of derivatives **146-148**

A solution of andrographolide (**81**) (100 mg, 0.2853 mmol) in CH_2Cl_2 (8 mL) were added. Acetic anhydride (0.5 mL, 0.5706 mmol) and a catalyst amount of DMAP (34.86 mg, 0.2853 mmol) at room temperature stirring for 30 min. The solution was quenched by the addition of H_2O (10 mL) and extracted with CH_2Cl_2 (2×10 mL). The organic layer were dried over anhydrous Na_2SO_4, then removed the solvent by evaporation to furnish the crude product. The crude product was further purified by SiO_2 column chromatography with a mixture of EtOAc : hexane (30%-50%) to give compounds **146**, **147** and **148.**

Compound 146 (101.8 mg, 74% yield); ^{1}H NMR (400 MHz, $CDCl_3$); δ_H 6.95 (t, *J* = 5.6 Hz, 1H), 5.88 (d, *J* = 6.0 Hz, 1H), 4.86 (s. 2H), 4.56 (dd, *J* = 11.6, 4.0 Hz, 1H), 4.48 (s. 1H), 4.32 (d, *J* = 11.6 Hz, 1H), 4.21 (dd, *J* = 11.2, 6.0 Hz, 1H), 4.08 (d, *J* = 11.6 Hz, 1H), 1.96-1.65 (m, 6H), 2.08 (s, 3H), 2.00 (s. 6H), 1.31 (m, 5H), 0.71 (s, 3H), 0.99 (s, 3H) : ^{13}C NMR (100 MHz, $CDCl_3$) δ_C 170.7, 170.3×3, 149.9, 146.4 124.0, 108.7, 79.5, 71.4, 67.7, 64.5, 55.7, 55.1, 41.2, 38.8, 37.8, 36.9, 25.1, 24.5, 24.1, 21.6, 21.0×2, 20.6, 14.4 [85].

Compound 147 (17.9 mg, 13% yield); ^{1}H NMR (400 MHz, $CDCl_3$); δ_H 7.00 (m, 1H), 5.92 (d, *J* = 6.0 Hz, 1H), 4.89 (s, 2H), 4.66 (dd, *J* = 12.4, 4.8 Hz, 1H), 4.51 (m, 2H), 4.25 (dd, *J* = 11.2, 2.0 Hz, 1H), 4.24 (dd, *J* = 11.2, 2.0 Hz, 1H), 4.13 (d, *J* = 12.0 Hz, 1H), 3.38 (d, *J* = 11.6 Hz, 1H), 2.44 (m ,2H), 2.43 (m, 1H), 2.11 (s, 3H), 2.09 (s, 3H), 1.86 (m, 2H), 1.84 (m, 1H) 1.77 (m, 1H), 1.31 (m, 2H), 1.08 (s, 3H), 0.69 (s, 3H) : ^{13}C NMR (100 MHz, $CDCl_3$) δ_C 170.4, 150.1, 169.7, 169.0, 146.5, 124.0, 109.0, 82.3, 71.5, 67.7, 63.5, 55.7, 55.4, 42.6, 38.8, 37.6, 36.9, 25.3, 24.2, 23.9, 22.4, 21.3, 20.7, 14.9 [85].

Compound 148 (13.8 mg, 10% yield); ^{1}H NMR (400 MHz, $CDCl_3$) δ_H 7.00 (t, *J* = 5.6 Hz, 1H), 5.92 (d, *J* = 6.0 Hz, 1H), 4.89 (s, 2H), 4.57-4.51 (m, 2H), 4.32 (d, *J* = 11.6 Hz, 1H), 4.12 (d, *J* = 11.6 Hz, 1H), 3.33 (dd, *J* = 11.2, 2.0 Hz, 2H), 2.12 (s, 3H), 1.88-1.64 (m, 4H), 2.05 (s, 3H), 1.98 (m, 1H), 1.88-1.64 (m. 2H), 1.61 (br s, 2H), 1.45 (dd, *J* = 12.8, 4.0 Hz, 2H), 1.25 (m , 1H), 1.15 (s, 3H), 0.71 (s, 3H) : ^{13}C NMR (100 MHz, $CDCl_3$)

δ_C 170.9, 170.5, 169.0, 150.3, 148.0, 124.0, 108.8, 78.8, 71.6, 67.8, 64.9, 55.9, 55.3, 42.4 39.0, 37.8, 37.3, 27.8, 25.2, 24.2, 22.5, 21.0, 20.7, 14.7 [85].

Synthesis of derivative **149**

Andrographolide (100 mg, 0.2853 mmol) in $CHCl_3$ (5 mL) was cooled to 0 °C, then *m*CPBA (73.86 mg, 0.4280 mmol) was added and the reaction was stirred for 2 h. After completion of the reaction, the mixture was successively washed with saturated Na_2CO_3, brine, and water successively. The $CHCl_3$ phase was dried over aqueous Na_2SO_4, filtered, and concentrated to give crude product. The crude product was purified by column chromatography over silica gel using EtOAc (100%) and then MeOH: EtOAc (10%) to give compound **149** (63.27 mg, 57% yield); ^{1}H NMR (400 MHz, $CDCl_3$); δ_H 6.79 (dd, J = 11.2, 5.6 Hz, 1H), 4.98 (d, J = 3.6 Hz, 1H), 4.37 (dd, *J* = 10.0, 5.6 Hz, 1H), 4.26 (d, J = 10.4 Hz, 1H), 3.50 (dd, J = 10.8, 4.8 Hz, 1H), 3.34 (t, J = 7.6 Hz, 1H), 3.00 (d, J = 6.8 Hz, 1H), 2.66 (d, J = 3.6 Hz, 2H), 1.96-1.73 (m, 4H), 1.51-1.41 (m, 4H), 1.29 (m, 2H), 1.26 (s, 3H), 1.23-1.16 (m, 2H), 0.82 (s, 3H) : ^{13}C NMR (100 MHz, $CDCl_3$) δ_C 170.1, 145.8, 129.2, 80.2, 73.6, 65.2, 63.8, 60.2 54.6, 53.4, 50.9, 42.7, 39.8, 36.8, 35.9, 27.4, 22.7, 21.3, 19.6, 15.1 [91].

Synthesis of derivatives **150-151**

Andrographolide (100 mg, 0.2853 mmol) and PDC (53.86 mg, 0.1427 mmol) in $CHCl_3$ (8 mL) were stirred for 3 h at room temperature. The reaction mixture was filtered through cotton. The filter cake was washed with $CHCl_3$. The combined $CHCl_3$ phase was extracted with brine and water, and dried with anhydrous Na_2SO_4. The solvent was evaporated to afford the crude product. The crude product was subjected to column chromatography over silica gel eluted with a gradient of MeOH : CH_2Cl_2 (2.5% - 4%) to give compounds **150** and **151**.

Compound 150 (28 mg, 24% yield); ^{1}H NMR (400 MHz, $CDCl_3$); δ_H 9.75 (s, 1H), 7.28 (s, 2H), 4.98 (s, 3H), 4.78 (s, 1H), 4.54 (d, *J* = 5.6 Hz, 1H), 3.22 (m, 1H), 3.01 (d, *J* = 10.4 Hz, 1H), 2.50 (m, 2H), 2.04 (m, 1H), 1.97 (m, 1H), 1.93 (m, 1H), 1.89 (m, 2H), 1.84 (m, 1H), 1.82 (m, 1H), 1.64 (m ,2H), 1.27 (s, 3H), 1.16 (m, 1H), 0.63 (s, 3H) : ^{13}C

NMR (100 MHz, $CDCl_3$) δ_C 207.5, 172.9, 147.5, 145.2, 136.2, 108.4, 77.1, 70.4, 67.4, 55.7, 52.8, 52.0, 39.8, 38.1, 36.9, 30.5, 28.6, 24.1, 19.4, 13.7.

Compound 151 (31.9 mg, 22% yield); ^{1}H NMR (400 MHz, $CDCl_3$); δ_H 4.98 (s, 1H), 4.84 (s, 2H), 4.81 (s, 1H), 4.54 (m, 1H), 3.88 (d, *J* = 11.2 Hz, 1H), 3.46 (m, 1H), 2.55 (m, 2H), 2.04 (m, 1H), 2.02 (m, 1H), 1.95 (m, 1H), 1.91 (m, 1H), 1.85 (d, *J* = 3.2 Hz, 1H), 1.85 (d, *J* = 3.2 Hz, 1H), 1.82 (d, *J* = 3.2 Hz, 1H), 1.78 (m, 1H), 1.75 (m, 1H), 1.73 (m, 1H), 1.23 (s, 3H), 0.79 (s, 3H) : ^{13}C NMR (100 MHz, $CDCl_3$) δ_C 218.1, 172.8, 147.5, 145.3, 136.0, 108.6, 70.5, 67.6, 65.6, 55.7, 52.3, 51.9, 39.3, 37.9, 36.5, 34.9, 30.7, 25.0, 22.0, 14.8.

Synthesis of derivative **152**

A solution of andrographolide (**81**) (250 mg, 0.2853 mmol) in CH_2Cl_2 (10 mL) was treated with 2,2-dimethoxypropane (0.2 mL, 1.5834 mmol) and *p*-TsOH (19.54 mg, 0.2568 mmol), then stirred at 65 °C for 24 h. The reaction was quenched with saturated $NaHCO_3$ aqueous solution (10 mL). The organic layer was separated and the aqueous layer was extracted with CH_2Cl_2 (2×10 mL). The combined organic layer was dried anhydrous over Na_2SO_4 and concentrated to give the crude product. The crude product was chromatographed on a silica gel using EtOAc : hexane (50% - 100%) to give compound **152** (120.5 mg, 32% yield); ^{1}H NMR (400 MHz, $CDCl_3$) δ_H 6.76 (t, *J* = 6.8 Hz, 1H), 5.03 (t, *J* = 8.0 Hz, 1H), 4.85 (s, 1H), 4.43 (s, 1H), 4.18 (m, 1H), 3.83 (t, *J* = 8.4 Hz, 1H), 3.70 (s, 3H), 3.47 (m, 1H), 3.32 (d, *J* = 11.2 Hz, 2H), 2.68 (m, 2H), 2.52 (m, 1H), 2.00 (m, 1H), 1.81 (m,1H), 1.79 (m, 2H), 1.75 (m, 1H), 1.50 (s, 1H), 1.40 (s, 3H), 1.25 (s, 3H). 1.23 (m, 2H), 0.67 (s, 3H) : ^{13}C NMR (100 MHz, $CDCl_3$) δ_C 167.0, 147.9, 147.1, 127.5, 109.4, 108.8, 80.6, 73.4, 68.9, 64.2, 56.8, 55.3, 51.7, 42.9, 39.0, 37.9, 37.1, 28.3, 26.3 25.3, 23.9, 23.8, 22.7, 15.3.

Synthesis of derivatives **153-154**

Benzoyl chloride (0.03 mL, 0.3139 mmol) was slowly added to a mixture of andrographolide (**81**) (50 mg, 0.1427 mmol), triethylamine (0.1 mL, 0.7135 mmol), and dimethylaminopyridine (DMAP; 1.75 mg, 0.0143 mmol) in anhydrous CH_2Cl_2 (5 mL) at 0 ℃. The reaction mixture was stirred for 8 h at room temperature

and quenched by the addition of MeOH. The reaction mixture was diluted with CH_2Cl_2 (5 mL) and washed with 1 N HCl (4 mL), satd. $NaHCO_3$ (4 mL), and brine (4 mL). The dried solution (Na_2SO_4) was then evaporated under reduced pressure to give the crude product. The crude product was further purified by column chromatography MeOH : CH_2Cl_2 (1% - 5%) to give compounds **153** and **154**.

Compound 153 (7.5 mg, 12% yield); ^{1}H NMR (400 MHz, $CDCl_3$) δ_H 8.00 (d, *J* = 7.2 Hz, 2H), 7.56 (t, *J* = 7.2 Hz, 1H), 7.44 (t, *J* = 7.6 Hz, 2H), 7.18 (s, 1H), 6.89 (dd, *J* = 15.6, 10.0 Hz, 1H), 6.14 (d, *J* = 16.0 Hz, 1H), 4.80 (s, 2H), 4.60 (m, 1H), 4.55 (m, 2H), 4.40 (d, *J* = 11.6 Hz, 1H), 3.39 (dd, *J* = 11.6, 4.8 Hz, 1H), 2.48 (m, 1H), 2.36 (d , *J* = 10.0 Hz, 1H), 2.07 (m, 1H), 1.93 (m, 1H), 1.76 (m, 1H), 1.60 (m, 1H), 1.56 (m, 1H), 1.32 (m, 1H), 1.28 (s, 3H), 1.20 (m. 1H), 0.91 (s, 3H) : ^{13}C NMR (100 MHz, $CDCl_3$) δ_C 172.2, 166.7, 147.9, 142.8, 135.9, 133.0, 130.2, 129.5×2, 128.5×2, 129.6, 121.2, 109.3, 79.2, 69.5, 65.4, 61.7, 54.9, 43.0, 38.8, 38.6, 36.7, 27.8, 23.7, 22.6, 15.6.

Compound 154 (15 mg, 24% yield); ^{1}H NMR (400 MHz, $CDCl_3$) δ_H 7.97 (d, *J* = 7.6 Hz, 2H), 7.57 (t, *J* = 7.2 Hz, 2H), 7.45 (t, *J* = 7.6 Hz, 2H), 7.17 (s, 1H), 6.94 (m, 1H), 6.15 (d, *J* = 15.6 Hz, 1H), 4.95 (dd, *J* = 10.8, 5.6 Hz, 1H), 4.82 (s, 1H), 4.57 (s, 1H), 4.27 (d, *J* = 11.6 Hz, 2H), 3.58 (t, *J* = 10.0 Hz, 2H), 2.38 (d, *J* = 10.0 Hz, 1H), 1.97 (m. 1H), 1.88 (m, 2H), 1.51 (m, 2H), 1.40 (m, 1H), 1.31 (m, 1H), 1.15 (s, 3H), 0.09 (s, 3H) : ^{13}C NMR (100 MHz, $CDCl_3$) δ_C 170.4, 165.9, 147.9, 143.1, 135.8, 133.1, 130.3, 129.3×2, 128.7×2, 129.2, 121.4, 109.4, 82.9, 69.5, 63.8, 61.7, 55.2, 43.1, 38.6, 38.3, 36.6, 24.3, 23.4, 22.5, 15.6.

Synthesis of derivative **155**

To a magnetically stirred solution of andrographolide (**81)** (30 mg, 0.0856 mmol) in methanol (4 mL) was added gradually $NiCl_2{\cdot}6H_2O$ (26.24 mg, 0.1104 mmol) at room temperature. When the clear solution acquired a greenish color, the whole reaction mixture was brought to 0 °C and $NaBH_4$ (4.86 mg, 0.1284 mmol) was added portion wise. After the addition was completed, the solution was stirred for 30 min at 0 °C to room temperature. Methanol was removed by vacuum, and then extracted with ethyl acetate (3×20 mL), the organic layer was washed with water,

dried over anhydrous Na_2SO_4 and evaporated under reduced pressure. The residue was then chromatographed on SiO_2 eluted with a gradient of acetone : CH_2Cl_2 (20% - 50%) to give compound **155** (10.8 mg, 37% yield); ^{1}H NMR (400 MHz, $CDCl_3$) δ_H 4.84 (s, 1H), 4.60 (s.1H), 4.56 (m ,2H), 4.27 (m, 2H), 4.18 (d, *J* = 11.2 Hz, 1H), 3.48 (m, 1H), 3.31 (m, 1H), 2.44 (m, 1H), 2.40 (m, 1H), 1.94 (m, 1H), 1.84 (m, 1H), 1.83 (m, 1H), 1.82 (m, 3H), 1.63 (m, 1H), 1.60 (m, 1H), 1.58 (m, 1H), 1.52 (m, 1H), 1.25 (s, 2H), 1.24 (m, 1H), 1.23 (s, 3H), 1.19 (m, 2H), 0.63 (m, 1H) : ^{13}C NMR (100 MHz, $CDCl_3$) δ_C 147.3, 107.1, 80.7, 74.3, 69.3, 64.2, 56.7, 55.3, 45.7, 42.9, 39.1, 38.2, 37.0, 29.7, 28.3, 24.0, 22.9, 22.7, 22.0, 15.2.

Synthesis of derivative **156**

Andrographolide (**81**) (100 mg, 0.2853 mmol) was treated with conc. hydrochloric acid for 24 h. at room temperature. After the completion of reaction, the resultant mixture was poured into ice water (10 mL) and neutralized with aq. $NaHCO_3$, extracted with ethyl acetate (3×10 mL) and washed with water (3×10 mL). The organic layer was separated, dried over anhydrous Na_2SO_4 and concentrated. The residue was purified over a column of silica gel with MeOH : CH_2Cl_2 (4%) to give pale yellow solid, which was subsequently re-crystallized with methanol to give compound **156** (11.3 mg, 11% yield); ^{1}H NMR (400 MHz, $CDCl_3$) δ_H 7.28 (s, 1H), 4.79 (s, 2H), 4.68 (m, 1H), 3.45 (d *J* = 10.4 Hz, 1H), 2.84 (d, *J* = 70.8 Hz, 2H), 2.00 (m, 1H), 1.72 (m, 2H) 1.69 (m, 1H), 1.66 (m, 1H), 1.57 (m, 2H), 1.56 (m, 1H), 1.47 (m, 1H), 1.41 (m, 1H), 1.39 (m, 1H), 1.31 (m, 1H), 1.24 (s, 3H), 1.09 (s, 3H), 0.93 (s, 3H) : ^{13}C NMR (100 MHz, $CDCl_3$) δ_C 172.5, 143.2, 138,4, 82.7, 80.9, 73.1, 70.5, 64.2, 58.0, 52.7, 42.6, 39.1, 36.2, 35.7, 29.9, 27.5, 22.7, 20.3, 18.2, 16.4 [92].

Synthesis of derivatives **157-168**

A catalytic amount of *p*-Toluenesulfonic acid (0.0206 mmol) was added to a solution of benzene/DMSO (10 ml, 7.5:1), andrographolide (**81**) (0.0571 mmol) and 2, 2-dimethoxypropane or aldehyde (0.6338 mmol). The reaction mixture was then raised until reflux began. After completion of the reaction within 4 h (monitored by TLC), the mixture was cooled to room temperature and basified with

Et_3N (0.5 ml) in order to quench any remaining catalyst. The mixture was next diluted with benzene (10 ml) and washed with H_2O (3 ×10 ml). The organic layer was dried (anhydrous Na_2SO_4) and concentrated to furnish the crude product, which was further subjected to column chromatography over silica gel using a mixture of EtOAc : CH_2Cl_2 as eluent to give compounds **157** and **158**.

Compound 157 (81.7 mg, 73% yield); ^{1}H NMR (400 MHz, $CDCl_3$); δ_H 5.00 (t, *J* = 6.4 Hz, 1H), 6.92 (t, *J* = 5.6 Hz, 1H), 4.89 (s, 1H), 4.61 (s, 2H), 4.43 (dd, *J* = 10.4, 6.4 Hz, 1H), 4.24 (dd, *J* = 10.4, 2.0 Hz, 1H), 3.95 (d, *J* = 11.6 Hz, 1H), 3.47 (dd, *J* = 8.4, 3.2 Hz, 1H), 2.56 (t, *J* = 6.8 Hz, 2H), 2.00-1.94 (m, 2H), 1.87-1.70 (m, 3H), 1.40 (s, 4H), 1.35 (s, 3H), 1.31-1.22 (m, 4H), 1.18 (s, 3H), 0.94 (s, 3H):^{13}C NMR (100 MHz, $CDCl_3$) δ_C 170.3, 149.0, 147.0, 128.8, 109.0, 74.4×2, 66.0, 63.8, 56.0, 52.2, 43.9, 40.2, 38.4, 37.6, 26.1×2, 25.3, 24.9×2, 23.2, 16.1 [93].

Compound 158 (62.3 mg, 92% yield); ^{1}H NMR (400 MHz, $CDCl_3$); δ_H 7.33 (d, *J* = 8.4 Hz, 2H), 7.42 (d, *J* = 8.4 Hz, 2H), 6.97 (t, *J* = 6.8 Hz, 1H), 5.75 (s, 1H), 5.03 (br s, 1H), 4.92 (s, 1H), 4.63 (s, 1H), 4.46 (dd, *J* = 10.4, 6.0 Hz, 2H), 3.67 (dd, *J* = 12.8, 4.8 Hz, 2H), 2.57 (m, 1H), 2.31 (m, 1H), 2.04 (m, 1H), 2.01 (m, 1H), 1.91 (m, 1H), 1.84 (m, 1H), 1.61 (s, 2H), 1.46 (s, 3H), 1.31 (m, 3H), 1.30 (m ,2H), 1.29 (m, 1H), 0.87 (s, 3H) :^{13}C NMR (100 MHz, $CDCl_3$) δ_C 169.8, 148.7, 146.5, 137.5, 134.6, 128.5, 128.1×2, 127.7, 109.2, 108.1, 94.2, 74.3, 71.0, 66.3, 55.8, 54.9, 38.9, 37.6, 36.9, 36.1, 26.0, 24.8, 22.8, 21.7, 15.4 [94].

Compound 159 (7.7 mg, 28% yield); ^{1}H NMR (400 MHz, $CDCl_3$); δ_H 8.37 (s, 1H), 8.20 (m, 1H), 7.83 (d, *J* = 8.0 Hz, 1H), 7.54 (t, *J* = 8.0 Hz, 1H), 7.00 (m, 1H), 5.83 (s, 1H), 5.06 (t, *J* = 5.2 Hz, 1H) 4.94 (s, 1H), 4.64 (s, 1H), 4.48 (dd, *J* = 10.4, 6.0 Hz, 1H), 4.25 (m, 1H), 3.71 (dd, *J* = 12.8, 5.2 Hz, 1H), 3.63 (d, *J* = 11.2 Hz, 1H), 2.57 (m, 1H), 2.17 (s, 1H), 2.09 (m, 1H), 2.04 (s, 1H), 1.91 (m, 1H), 1.90 (m, 1H), 1.86 (m, 1H), 1.84 (m, 1H), 1.47 (s, 3H), 1.35 (m, 1H), 1.32 (m, 1H), 1.31 (m, 1H), 1.27 (m, 1H), 0.89 (s, 3H) :^{13}C NMR (100 MHz, $CDCl_3$) δ_C 170.0, 148.6, 147.8, 146.4, 140.9, 132.4, 129.3, 128.1, 123.7, 121.7, 109.3, 108.1, 93.6, 74.2, 69.6, 66.3, 55.8, 54.8, 38.9, 37.5, 36.1, 30.9, 26.0, 24.8, 22.8, 15.4 [95].

Compound 160 (14.1 mg, 56% yield); ^{1}H NMR (400 MHz, $CDCl_3$); δ_H 7.50 (m, 2H), 7.35 (m, 3H), 6.98 (m, 1H), 5.77 (s, 1H), 5.04 (m, 1H), 4.92 (s, 1H), 4.63 (s, 1H), 4.46, (dd, *J* = 10.4, 6.0 Hz, 1H), 4.24 (m, 1H), 3.68 (dd, *J* = 12.8, 4.8 Hz, 1H), 3.60 (d, *J* = 11.2 Hz, 1H), 2.57 (m, 1H), 2.18 (m, 1H), 2.09 (m, 1H), 2.01 (m, 1H), 1.91 (m, 1H), 1.84 (m, 1H), 1.77 (m, 1H), 1.70 (m, 1H), 1.57 (s, 1H), 1.49 (s, 3H), 1.34 (m, 1H), 1.31 (m, 1H), 1.29 (m, 1H), 1.24 (m, 1H), 0.88 (s, 3H) :^{13}C NMR (100 MHz, $CDCl_3$) δ_C 170.0, 148.7, 146.6, 138.9, 128.9×2, 128.3, 128.1, 126.2×2, 109.2×2, 95.2, 80.7, 74.2, 69.5, 55.8, 54.9, 38.9, 37.0, 37.6, 36.1, 26.1, 24.8, 22.8, 21.8, 15.4 [96].

Compound 161 (18.6 mg, 72% yield); ^{1}H NMR (400 MHz, $CDCl_3$); δ_H 7.20 (t, *J* = 8.0 Hz, 1H), 7.01 (m, 1H), 6.92 (m, 1H), 6.79 (dd, *J* = 8.0, 1.6 Hz, 2H), 5.70 (s, 1H), 5.00 (m, 1H), 4.91 (s, 1H), 4.63 (s, 1H), 4.44 (dd, *J* = 10.4, 6.0 Hz, 1H), 4.24 (d, *J* = 10.8 Hz, 1H), 3.65 (dd, *J* = 12.8, 5.2 Hz, 1H), 3.57 (d, *J* = 11.2 Hz, 1H), 2.60 s, 1H, 2.04 (m, 2H), 2.01 (m, 1H), 1.90 (m, 1H), 1.84 (m, 1H), 1.77 (s, 2H), 1.47 (s, 3H), 1.32 (m, 1H), 1.29 (m, 1H), 1.27 (m, 1H), 1.31 (m, 2H), 0.89 (s, 3H) :^{13}C NMR (100 MHz, $CDCl_3$) δ_C 170.1, 156.1, 148.6, 146.5, 140.4, 129.5, 128.2, 118.2, 116.0, 113.3, 109.2, 108.1, 95.0, 80.7, 74.4, 69.5, 66.1, 55.8, 54.8, 40.8, 38.9, 37.6, 26.0, 24.7, 22.8, 21.7, 15.3.

Compound 162 (9.7 mg, 35% yield); ^{1}H NMR (400 MHz, CD_3SOCD_3); δ_H 8.21 (d, *J* = 8.8 Hz, 2H), 7.66 (d , *J* = 8.8 Hz, 2H), 6.62 (t, *J* = 5.2 Hz, 1H), 5.98 (s, 1H), 5.71 (d, *J* = 6.0 Hz, 1H), 4.91 (t, *J* = 6.0 Hz, 1H), 4.65 (s, 1H), 4.38 (dd, *J* = 10.0, 6.0 Hz, 1H), 4.24 (d, *J* = 11.2 Hz, 1H), 3.61 (dd, *J* = 12.8, 4.8 Hz, 1H), 3.49 (d, *J* = 11.2 Hz, 1H), 2.77 (m, 1H), 2.53 (m, 2H), 2.18 (m, 1H), 2.01-1.61 (m, 6H), 1.34 (s, 3H), 1.29-1.17 (m, 3H), 0.79 (s, 3H) :^{13}C NMR (100 MHz, CD_3SOCD_3) δ_C 169.8, 129.0, 147.1, 145.9, 145.8, 127.5×2, 123.2×2, 109.2, 108.6, 92.8, 80.0, 74.1, 64.4, 54.9, 53.5, 38.3, 36.9, 36.4, 35.0, 25.3, 23.8, 22.2, 21.4, 14.7 [95].

Compound 163 (18.8 mg, 69% yield); ^{1}H NMR (400 MHz, $CDCl_3$); δ_H 7.40 (d, J = 7.2 Hz, 2H), 7.31 (t, J = 6.8 Hz, 3H), 6.75 (d, J = 16.0 Hz, 2H), 6.19 (dd, J = 16.4, 5.2 Hz, 1H), 5.41 (d, J = 4.8 Hz, 1H), 5.04 (t, J= 6.0 Hz, 1H), 4.92 (s, 2H), 4.62 (s, 1H), 4.47 (dd, J = 10.4, 6.0 Hz, 1H), 4.26 (dd, J = 10.4, 2.0 Hz, 1H), 3.60 (dd, J = 12.4, 4.8 Hz, 1H), 3.53 (d, J = 11.2 Hz, 1H), 2.58 (m, 2H), 2.45 (m, 1H), 2.36 (dd, J = 13.2, 3.2 Hz, 1H), 1.91 (m, 2H), 1.86 (m, 2H), 1.84 (m, 2H), 1.78 (m, 2H), 1.43 (s, 3H), 1.28 (m,

2H), 0.85 (s, 3H) : ^{13}C NMR (100 MHz, $CDCl_3$) δ_C 170.0, 133.4, 146.5, 136.1, 128.5×2, 128.1×2, 126.8, 126.1 111.4, 109.2, 148.7, 94.3, 74.2, 69.1, 66.3, 55.8, 54.9, 38.9, 37.6, 36.9, 36.1, 26.0, 24.8, 21.8, 15.3.

Compound 164 (11.2 mg, 43% yield); ^{1}H NMR (400 MHz, $CDCl_3$); δ_H 7.15 (m, 1H), 7.25 (m, 1H), 6.97 (m, 1H), 6.98 (m, 1H), 6.88 (m, 1H), 5.93 (s, 1H), 5.04 (br s, 1H), 4.93 (s, 1H), 4.64 (s, 1H), 4.47 (dd, J = 10.4, 6.0 Hz, 1H), 4.26 (m, 1H), 3.65 (d, J = 11.6 Hz, 2H), 2.57 (m, 1H), 2.07-1.81 (m, 7H), 1.48 (s, 3H), 1.35-1.24 (m, 7H) 0.88 (s, 1H) : ^{13}C NMR (100 MHz, $CDCl_3$) δ_C 169.7, 155.4, 148.6, 146.3, 130.4, 128.1, 128.0, 121.9, 119.7, 117.3, 109.5, 108.1, 96.7, 81.0, 74.2, 66.3, 55.7, 54.8, 38.9, 37.5, 37.0, 35.9, 26.1, 24.8, 22.8, 21.5, 15.3.

Compound 165 (12.2 mg, 44% yield); ^{1}H NMR (400 MHz, $CDCl_3$); δ_H 6.96 (m, 1H), 5.09 (m, 1H), 5.03 (m, 1H), 4.90 (s, 1H), 4.86 (t, *J* = 5.6 Hz, 1H), 4.60 (s, 1H) 4.46 (dd, *J* = 10.4, 6.0 Hz, 1H), 4.26 (dd, *J* = 10.4, 2.0 Hz, 1H), 3.48 (dd, *J* = 12.8, 4.8 Hz,1H), 3.43 (d, *J* = 11.2 Hz, 1H), 2.43 (m, 1H), 2.29-2.25 (m, 1H), 1.96 (m, 2H), 1.92 (m, 2H), 1.84 (m, 1H), 1.82 (m, 3H), 1.75 (m, 2H), 1.74 (m, 2H), 1.71 (m, 2H), 1.67 (br s, 3H), 1.61 (br s, 1H), 1.40 (m, 2H), 1.36 (s, 3H), 1.26-1.17 (m, 1H), 1.17 (m, 2H), 0.86 (m, 3H), 0.82 (s, 3H) : ^{13}C NMR (100 MHz, $CDCl_3$) δ_C 169.8, 148.8, 146.7, 131.1, 128.0, 124.8, 109.6, 109.1, 90.0, 74.9, 74.3, 66.3, 55.8, 54.8, 42.3, 42.2, 38.9, 37.6, 37.5, 37.0, 28.4, 25.4, 25.3, 26.1, 24.8×2, 22.8, 21.8, 17.6, 15.3.

Compound 166 (10.1 mg, 45% yield); ^{1}H NMR (400 MHz, $CDCl_3$); δ_H 6.98 (t, *J* = 7.2 Hz, 1H), 5.04 (t, *J* = 6.4 Hz, 1H), 4.91 (s, 1H), 4.74 (t, *J* = 4.8 Hz, 1H), 4.60 (s, 1H), 4.46 (dd, *J* = 10.4, 6.0 Hz, 1H), 4.26 (dd, *J* = 10.8, 2.0 Hz, 1H), 3.49 (dd, *J* = 12.4, 4.8 Hz, 1H), 3.44 (d, *J* = 11.2 Hz, 1H), 2.57 (m, 2H), 2.43 (m, 1H), 2.28 (dd, *J* = 13.6, 3.2 Hz, 1H), 1.97 (d , *J* = 7.2 Hz, 1H), 1.87 (m, 1H), 1.84 (m, 1H)1.70 (m, 1H), 1.63 (m, 2H), 1.56 (m, 1H), 1.55 (m, 1H), 1.37 (s, 3H), 1.22 (m, 1H), 1.21 (m, 1H), 1.19 (m, 1H), 1.17 (m, 1H), 0.93 (t, *J* = 7.2 Hz, 3H), 0.82 (s, 3H) : ^{13}C NMR (100 MHz, $CDCl_3$) δ_C 170.1, 146.6, 129.1, 110.6, 109.1, 148.8, 96.1, 79.9, 74.2, 66.3, 55.8, 54.8, 38.9, 37.0, 37.6, 36.2, 28.2, 26.0, 24.8, 22.8, 21.8, 15.3, 8.07.

Compound 167 (12.8 mg, 55% yield); ^{1}H NMR (400 MHz, $CDCl_3$); δ_H 6.97 (t, *J* = 6.8 Hz, 1H), 5.03 (m, 1H), 4.90 (s, 1H), 4.80 (t, *J* = 4.8 Hz, 1H), 4.60 (s, 1H), 4.46 (dd, *J* = 10.4, 6.0 Hz, 1H), 4.26 (dd, *J* = 10.4, 1.6 Hz, 1H), 4.03 (d, *J* = 11.6 Hz, 1H), 3.50-3.41 (m, 2H), 2.59-2.52 (m, 2H), 2.43 (m, 1H), 2.31-2.17 (m, 2H), 2.01-1.96 (m, 1H), 1.86-1.79 (m, 3H), 1.67 (m, 1H), 1.60 (br d, *J* = 5.2 Hz, 3H), 1.57-1.53 (m, 2H), 1.45-1.38 (m, 2H), 1.36 (s, 3H), 1.27-1.18 (m, 4H), 0.91 (t, *J* = 7.2 Hz, 3H), 0.81 (s, 3H) : ^{13}C NMR (100 MHz, $CDCl_3$) δ_C 148.8, 146.6 128.0, 109.1, 95.1, 79.9, 74.2, 69.0, 66.3, 55.8, 54.8, 38.9, 37.6, 37.2, 37.0, 36.1, 26.0, 24.8, 22.8, 21.8, 17.2, 15.3, 14.0 [97].

Compound 168 (25.7 mg, 86% yield); ^{1}H NMR (400 MHz, $CDCl_3$); δ_H 7.53 (d, *J* = 8.0 Hz, 2H), 7.25 (d, *J* = 8.0 Hz, 2H), 6.99 (m, 3H), 5.77 (s, 1H), 5.05 (t, *J* = 6.4 Hz, 1H), 4.93 (s, 1H), 4.63 (m, 1H), 4.47 (dd, *J* = 10.4 Hz, 1H), 4.26 (m, 1H), 3.68 (dd, *J* = 12.8, 4,8 Hz, 1H), 3.60 (d, *J* = 11.2 Hz, 1H), 2.58 (m, 1H), 2.45 (m, 1H), 2.04 (m, 1H), 2.01 (m, 1H), 1.91 (m, 1H), 1.84 (m, 1H), 1.55 (s, 1H), 1.48 (s. 3H), 1.32 (m, 1H), 1.31 (m, 1H), 1.30 (m, 1H), 1.29 (m, 1H), 1.27 (m, 1H), 1.25 (m, 2H), 0.88 (s. 3H) : ^{13}C NMR (100 MHz, $CDCl_3$) δ_C 170.1, 148.7, 146.5, 137.7, 129.7, 129.6, 127.8×2, 120.8×2, 109.3, 108.1, 94.3, 88.2, 80.8, 74.2, 69.5, 66.4, 55.8, 54.9, 38.9, 37.6, 34.3, 26.0, 24.8, 21.8, 15.4.

Synthesis of derivative **169**

Compound **146** (20 mg, 0.0420 mmol), K_2CO_3 (8.17 mg, 0.0630 mmol) in aqueous methanol (5 mL) were combined and stirred for 10 min at 0°C. Then, the reaction was acidified with HCl (1 N) and subsequently extracted with CH_2Cl_2 (3×10 mL). The combined organic phases were dried over anhydrous Na_2SO_4 and evaporated under reduce pressure. The crude product was chromatographed on silica gel eluted with a mixture of EtOAc : hexane (40%) to give compound **169** (8.1 mg, 44% yield); ^{1}H NMR (400 MHz, $CDCl_3$); δ_H 6.95 (t, *J* = 6.8 Hz, 1H), 5.03 (t, *J* = 6.0 Hz, 1H), 4.91 (s, 1H), 4.61 (s, 1H), 4.59 (dd, *J* = 13.2, 6.4 Hz, 1H), 4.46 (dd, *J* = 10.4, 6.0 Hz, 1H), 4.38 (d, *J* = 11.6 Hz, 1H), 4.25 (dd, *J* = 10.4, 2.0 Hz, 1H), 4.11 (d, *J* = 11.6 Hz, 1H), 2..57-2.53 (m, 2H), 2.45-2.39 (m, 2H), 2.04 (s, 6H), 1.96-1.70 (m, 4H), 1.62 (s, 1H), 1.52 (dd, 12.8, 4.0 Hz, 1H), 1.38-1.31 (m, 2H), 1.03 (s, 3H), 0.78 (s, 3H) : ^{13}C NMR (100 MHz, $CDCl_3$) δ_C 170.9, 170.6, 169.8, 148.5, 146.4, 128.2, 108.9, 79.8, 74.3, 66.2, 64.7, 56.0, 55.3, 41.3, 39.0, 37.9, 37.1, 24.6, 24.2, 22.7, 21.1, 21.0, 14.5 [85].

Synthesis of derivative **170**

Compound **157** (50 mg, 0.1280 mmol), and PDC (24.08 mg, 0.0640 mmol) in $CHCl_3$ (4 mL) were stirred for 7 h at room temperature, then added more PDC (0.1920 mmol) and stirred for 1 h. The reaction mixture was filtrated through cotton. The filter cake was washed with $CHCl_3$. The combined $CHCl_3$ phase was extracted with brine and water then dried with anhydrous Na_2SO_4. The solvent was evaporated to furnish the crude extract, which was further purified by column chromatography over silica gel eluted with a gradient of EtOAc : CH_2Cl_2 (2%-5%) to give compound **170** (5.7 mg, 11% yield) ^{1}H NMR (400 MHz, $CDCl_3$); δ_H 7.28 (s, 1H), 4.93 (s, 1H), 4.83 (t, *J* = 38.4 Hz, 2H), 4.77 (m, 1H), 4.54 (m, 1H), 3.95 (d, *J* = 11.6 Hz, 1H), 3.16 (d, *J* = 11.6 Hz, 1H), 3.47 (m, 1H), 2.41 (m, 1H), 2.00 (m, 1H), 1.98 (m, 1H), 1.94 (m, 1H), 1.77 (m, 1H), 1.75 (m, 1H), 1.72 (m, 1H), 1.63 (d, *J* = 10.4 Hz, 1H), 1.40 (s, 3H), 1.36 (s, 3H), 1.23 (m, 1H), 1.19 (s, 3H), 0.90 (s, 3H) : ^{13}C NMR (100 MHz, $CDCl_3$) δ_C 172.9, 148.7, 145.1, 136.2, 108.0, 99.1, 76.4, 70.4, 67.8, 63.9, 53.3, 52.5, 38.8, 38.1, 37.9, 34.3, 30.5, 27.2, 26.1, 25.3, 25.0, 23.5, 16.3.

4.4 Results and Discussion

4.4.1 Semisynthesis and Anti-inflammatory Activity of Dysobinin Derivatives

In our searching for new anti-inflammatory agents from plant natural products, dysobinin, a limonoid from *Chisocheton siamensis*, was selected for their structure-activity relationship study on anti-inflammatory activity. It was because its structure was similar to that of gedunin-type limonoid, except for the lactone ring D replaced by a five-membered ring. Additionally, it displayed an acceptable effect on NO production in LPS and IFN-γ-activated murine macrophage RAW264.7 cell lines in preliminary screening (at 10 μM), with less toxicity. A series of dysobinin derivatives (**139-145**) were synthesized by starting from dysobinin (**80**) (Figure 4.1) and subsequently investigated for their anti-inflammatory activity.

As shown in Figure 4.7, deacetylation of **80** by treatment with K_2CO_3 in aqueous MeOH gave diol **139** in relatively high yield (99%), and subsequent Swern

oxidation of **139** to yielded ketone **140**. Only 7-OH was oxidized to ketone group, this might be because of steric effect from dimethyl functionality at C-4 on 6-OH. Alternatively, diol **139** was reacted with 2,2-dimethoxypropane in the presence of a catalytic amount of *p*-TsOH to form acetonide derivative **141**. Next, dysobinin (**80**) was subjected to the reduction with $NaBH_4$ in the presence of $CeCl_3.7H_2O$, and this reaction provided two derivatives (**142**-**143**), including the reduction on α,β-unsaturated ketone system and only a ketone group, in the yield ratio of around 1:1. Finally, reduction of **139** used the same reaction condition gave compounds **144**-**145**.

Further, all semisynthetic derivatives as well as dysobinin (**80**) were examined for their inhibition on NO production in activated macrophage RAW264.7 cells at three different doses, 2.5, 5 and 10 μM (Figure 4.8). Subsequently, their toxicity against cell lines was assayed by MTT assay at the same doses, and the results showed all compounds did not display any cytotoxicity at any doses tested (Figure 4.9). Their IC_{50} values were calculated and shown in Table 4.1. As seen in Table 4.1, diol **139** and ketoalcohol **140** exhibited the most potent activity with IC_{50} values of 3.92 and 4.40 μM, respectively, as well as more potent than dysobinin, the original compound. When the diol group was protected by acetonide, the activity was significantly decreased. It was thus suggested that the 6-OH and 7-OH were required for their activity. This could also be seen from the oxidation of 7-OH to ketone group as in **140**, which caused slightly decrease in activity. In the case of the reduced four derivatives **142**-**145**, particularly derivatives **143**-**145**, they significant loss their activity, compared to dysobinin, although two of them bearing diol functionality at C-6 and C-7. This clearly indicated that, not only diol, but an α,β-unsaturated ketone moiety was also required for their anti-inflammatory activity.

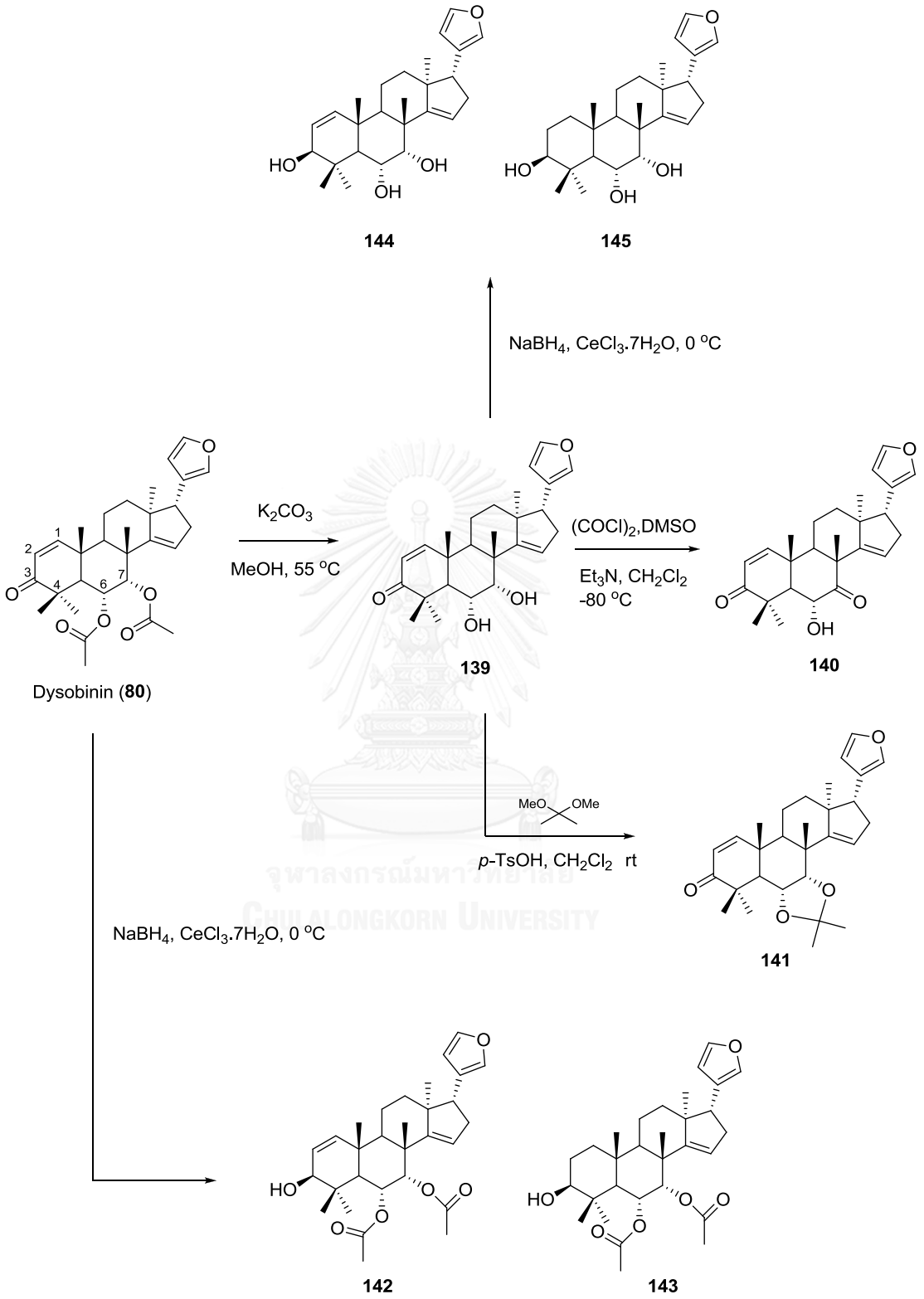

Figure 4.7 Chemical reactions of dysobinin to yield derivatives **139-145**.

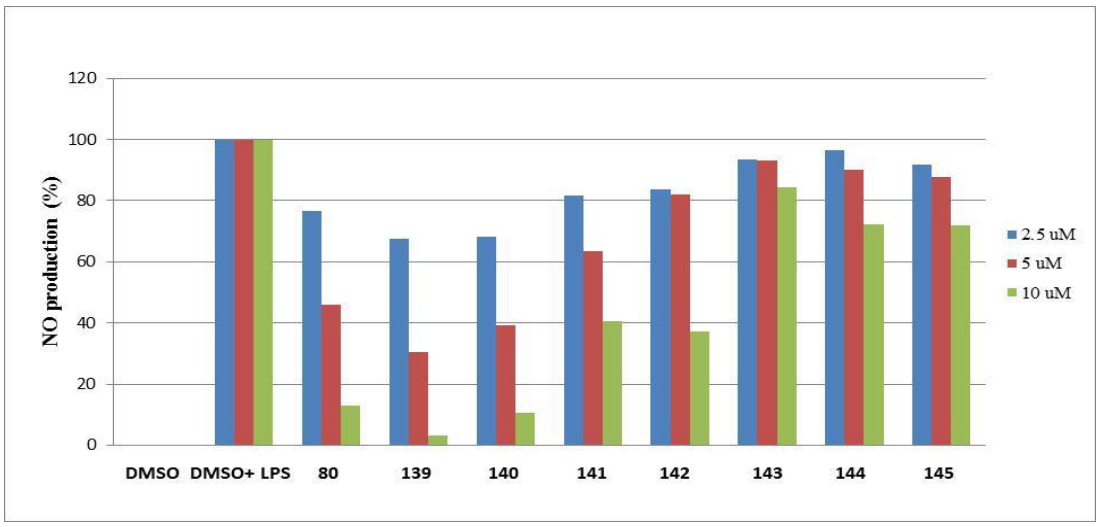

Figure 4.8 Percentage production of nitric oxide (NO) in LPS and IFN-γ stimulated murine macrophages RAW264.7 in the presence of dysobinin (**80**) and its derivatives (**139-145**).

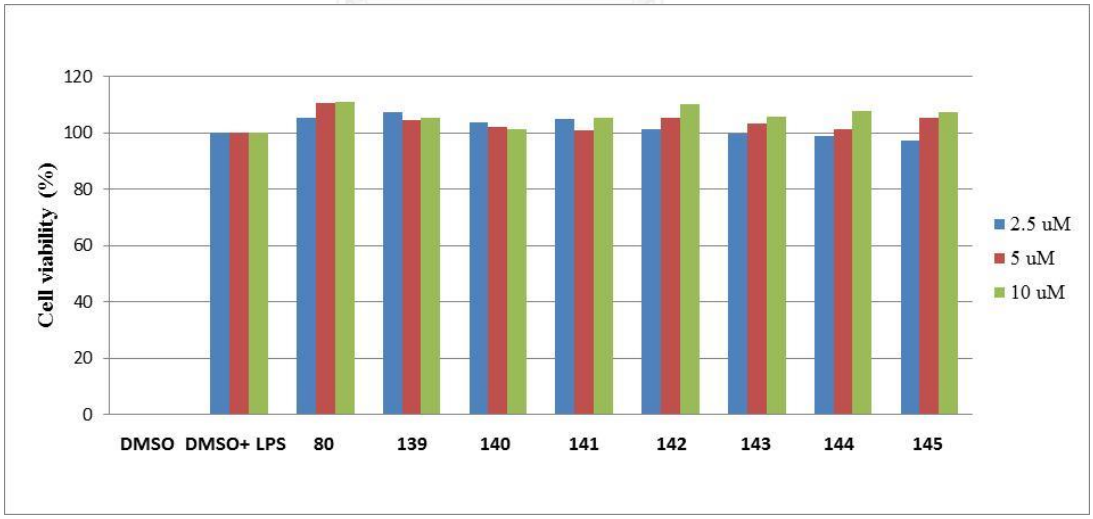

Figure 4.9 Cytotoxicity of dysobinin (**80**) and its derivatives (**139-145**) in LPS and IFN-γ stimulated murine macrophages RAW264.7.

Table 4.1 Inhibitory effect of dysobinin and its derivatives on nitric oxide production in stimulated murine macrophage RAW264.7 cell lines.

Compounds	IC_{50} (μM)
80	5.24
139	3.92
140	4.40
141	8.07
142	8.50
143	> 10
144	> 10
145	> 10

4.4.2 Semisynthesis and Anti-inflammatory Activity of Andrographolide Derivatives

The second series selected for structure activity relationship was andrographolide derivatives. This was because it was stated that andrographolide (**81**) restrains nitric oxide synthesis by suppressing iNOS protein expression activated by LPS and IFN-γ in RAW264.7 cell lines [98, 99]. Similarly, semisynthesis of andrographolide derivatives was performed by a number of chemical reactions. Acetylation of **81** with acetic anhydride in the presence of catalytic amounts of DMAP yielded three acetylated products, **146**-**148**, while subsequent deacetylation of **146** with K_2CO_3 provided only two acetoxy derivative **169**. When andrographolide was reacted with *m*CPBA, the epoxidation of $\Delta^{8,17}$ occurred and gave epoxide **149**. Oxidation with PDC gave one aldehyde (**150**) and one ketone (**151**) derivatives. Surprisingly, treatment of andrographolide with 2,2-dimethoxypropane in the presence of *p*-TsOH in CH_2Cl_2 gave acetonide derivative with 14-OH methylation (**152**), whereas treating with 2,2-dimethoxypropane in the presence of *p*-TsOH in benzene/DMSO yielded acetonide product (**157**). The latter reaction condition was further used for C-3,C-19 dihydroxy protection by using aldehydes in place of 2,2-

dimethoxypropane to give compounds **158**-**168**. Further oxidation of **157** with PDC provided derivative **170**. Next, andrographolide was treated with benzoyl chloride in the presence of DMAP and Et_3N to obtain ester derivatives **153** and **154**. Reduction of andrographolide with $NaBH_4$ in the presence of $NiCl_2.6H_2O$ led to ring opening of α-alkylidene-γ-butyrolactone to give alcohol **155**. Finally, andrographolide was heated with conc. HCl overnight to yield derivative **156**. The structures of all semisynthetic derivatives are presented in Figures 4.10-4.12

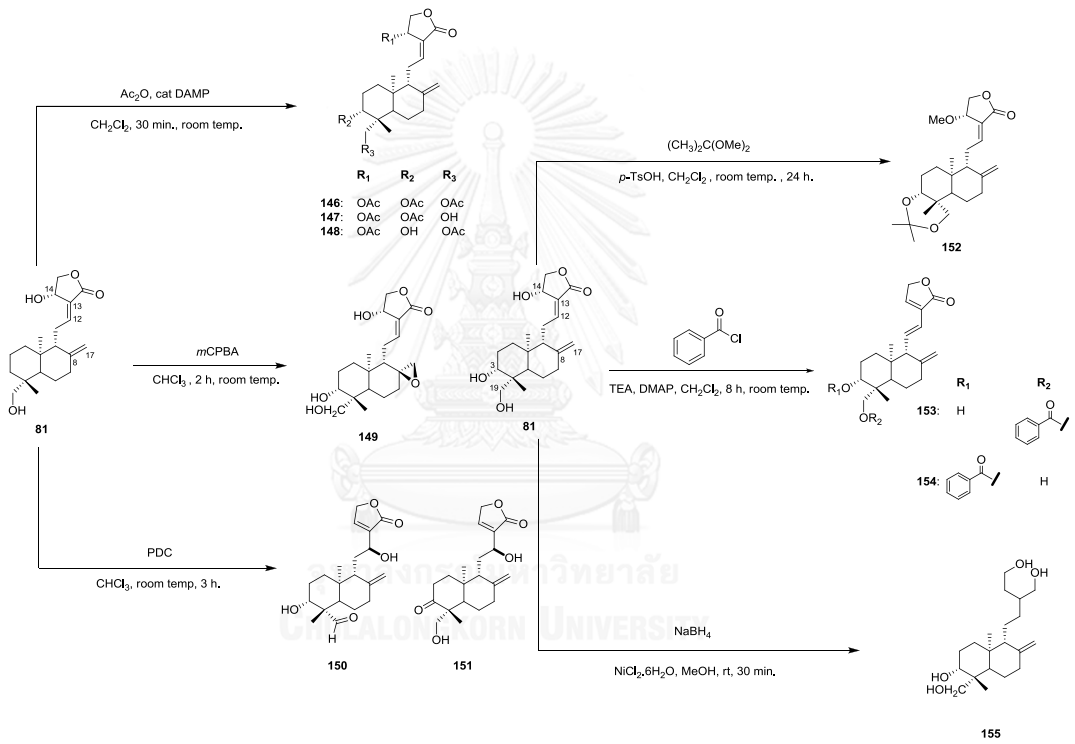

Figure 4.10 Chemical reactions of **81** to yield derivatives (**146-155**).

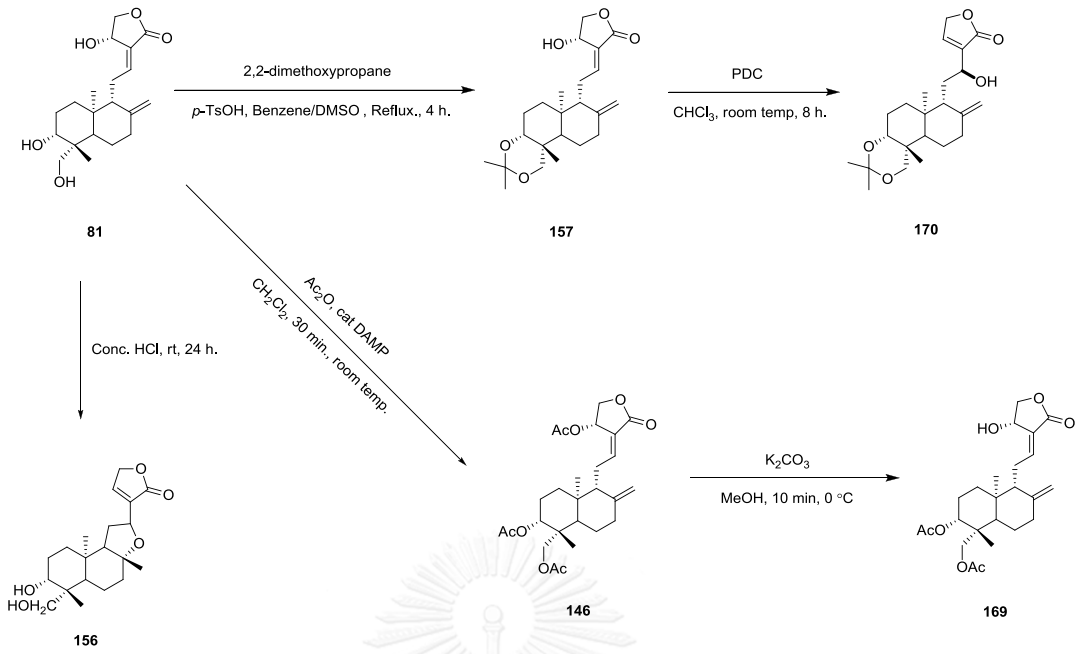

Figure 4.11 Chemical reactions of **81** to yield derivatives (**156-157, 169-170**).

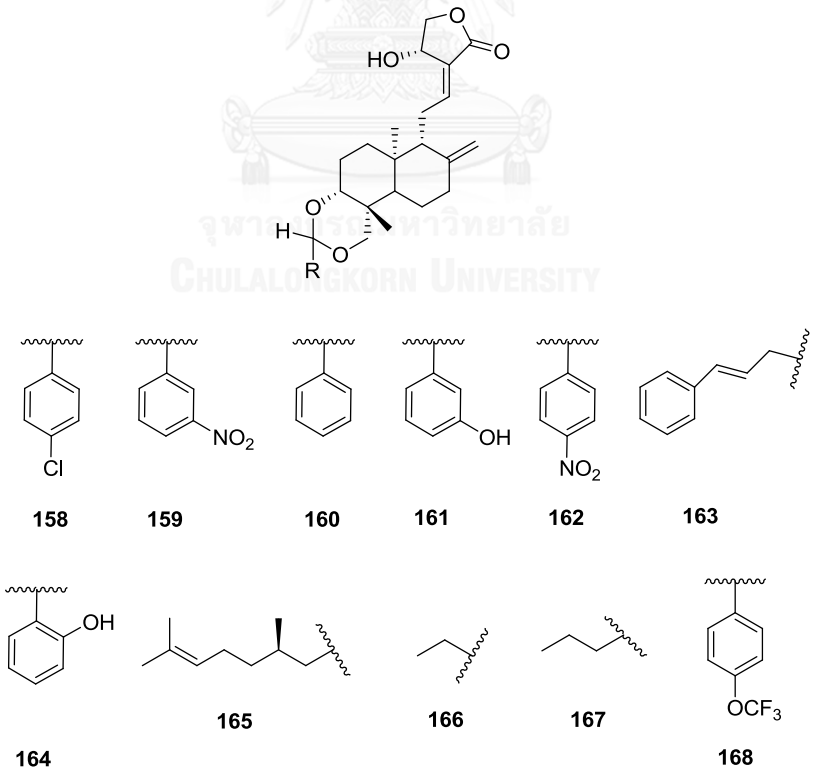

Figure 4.12 Chemical structure of andrographolide derivatives (**157-168**).

Similar to dysobinin compound series, andrographolide and its derivatives were subjected to NO inhibitory and MTT assay to assess their anti-inflammatory and cytotoxic activity. Based on the activity of andrographolide, the compounds were tested at three doses 1.25, 2.5 and 5.0 μM (Figures 4.13 and 4.14). Among them, acetylated derivative **147** showed the most potent activity with IC_{50} value of 2.71 μM, compared with a parent andrographolide (IC_{50} = 4.65 μM). These results roughly indicated that α-alkylidene-γ-butyrolactone, $\Delta^{8,17}$ exomethylene and $\Delta^{12,13}$ double bond were required for anti-inflammatory activity of this type compound. In addition, the results of percentage of NO production of the protective hydroxyl groups at C-3 and C-19 derivatives (**158-168**) revealed that different aliphatic or aromatic substitution derivatives gave contradictory NO inhibitory activity. The derivative **166** displayed good inhibitory activities against nitric oxide production with IC_{50} value of 2.76 μM. This study indicated that increasing the lipophilicity of andrographolide by the protection of 3, 19-hydroxyls reacted with aliphatic aldehyde with suitable length of alkyl chain may play a crucial role for anti-inflammatory effect of this compound series.

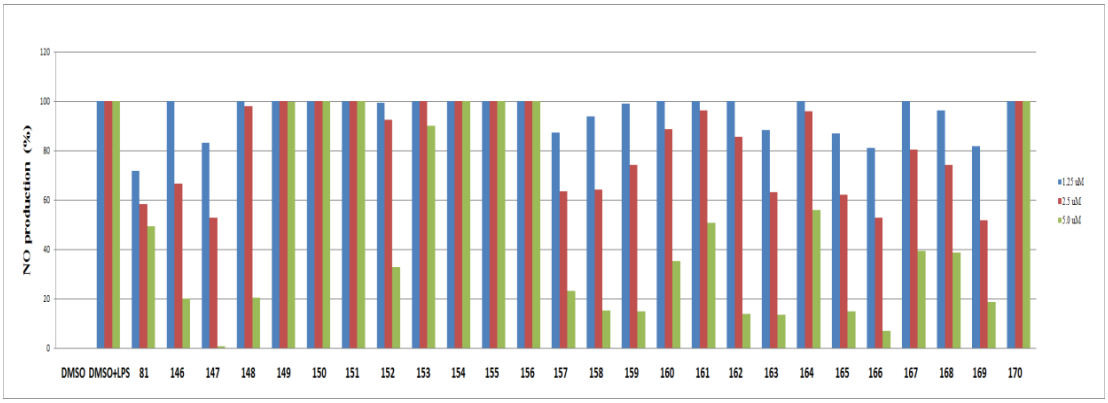

Figure 4.13 Percentage of nitric oxide (NO) in LPS and IFN-γ stimulated murine macrophages RAW264.7 in the presence of andrographolide (**81**) and its derivatives (**146-170**).

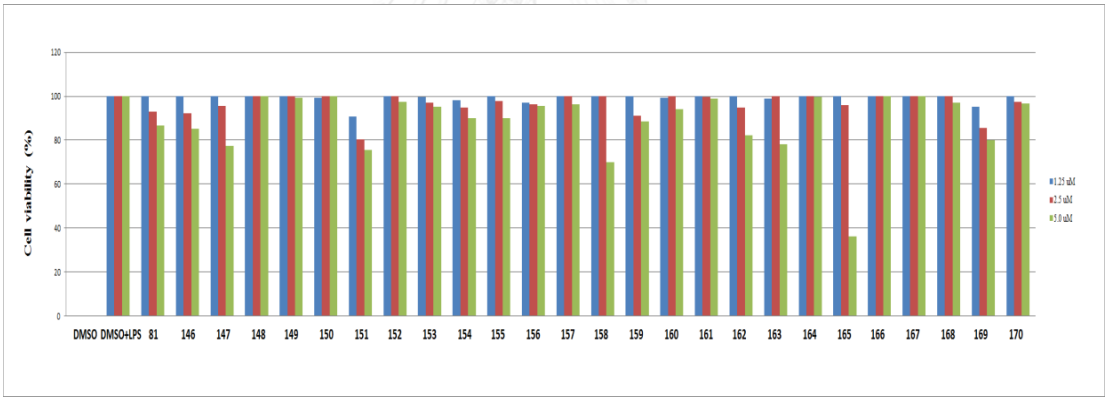

Figure 4.14 Cytotoxicity of andrographolide (**81**) and its derivatives (**146-170**) in LPS and IFN-γ stimulated murine macrophages RAW264.7.

Table 4.2 Inhibitory effect of andrographolide and its derivatives on nitric oxide production in stimulated murine macrophage RAW264.7 cell lines.

Compounds	IC_{50} (μM)
81	4.65
146	3.54
147	2.71
148	4.00
152	4.26
157	3.39
158	3.29
159	3.48
160	4.30
161	5.23
162	3.65
163	3.17
165	3.16
166	2.76
167	4.35
168	4.23
169	2.97

4.5 Conclusion

Seven semisynthetic derivatives (**139**-**145**) of dysobinin (**80**) were prepared by some chemical reactions, and study on their structure-activity relationship on anti-inflammatory activity was performed. It was found that diol derivative **139** exhibited the most potent activity, as well as the activity was significantly loss when an α,β-unsaturated ketone moiety was reduced. Therefore, it could be concluded that both diol and α,β-unsaturated ketone moieties played a crucial role for the anti-inflammatory activity of dysobinin series. In the case of compounds in

andrographolide series, the parent compound and acetylated derivatives provided the most potent activity. It could thus be concluded that α-alkylidene-γ-butyrolactone, $\Delta^{8,17}$ exomethylene and $\Delta^{12,13}$ double bond originally in parent compound played important role for anti-inflammatory activity.

CHAPTER V

CONCLUSION

The chromatographic separation of seeds of *X. rumphii* collected from Kudee Island led to the isolation of six new mexicanolides, xylorumphiins E-F (**42-43**), 2-Hydroxyxylorumphiin F (**44**), xylorumphiins G-I (**45-47**), and a new phragmalin, xylorumphiin J (**48**), together with three known derivatives namely xyloccensins X, E and K (**49-51**). Their structures were elucidated on the basis of spectroscopic methods. In order to clarify the full structure and establish the relative configuration of **45**, single-crystal X-ray diffraction analysis was performed.

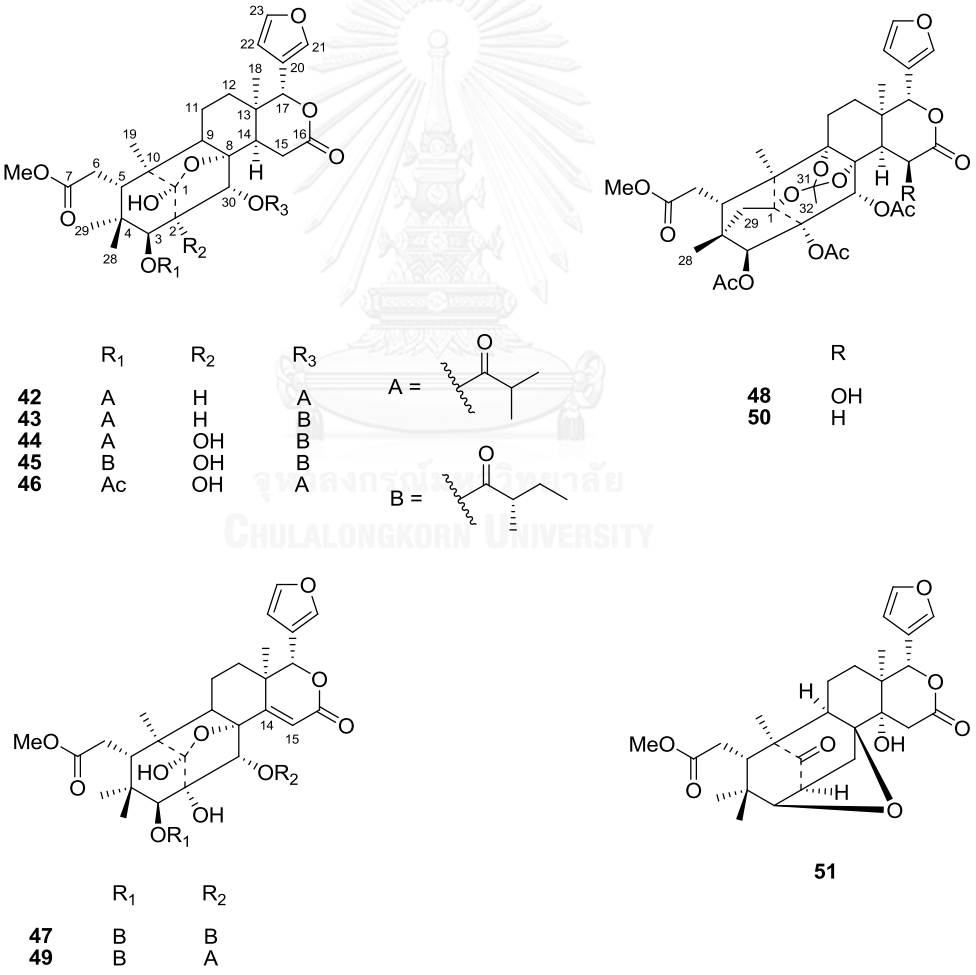

	R_1	R_2	R_3
42	A	H	A
43	A	H	B
44	A	OH	B
45	B	OH	B
46	Ac	OH	A

	R
48	OH
50	H

	R_1	R_2
47	B	B
49	B	A

51

Figure 5.1 Isolated limonoids from the seeds of *X. rumphii*.

In order to study the anti-inflammatory effect of limonoids from *Xylocarpus* plants, thirty-eight limonoids (**42-79**) obtained from seeds of *X. granatum, X. moluccensis* and *X. rumhiii* were examined for their anti-inflammatory activities by monitoring their inhibition of NO production in RAW264.7 murine macrophages co-stimulated with LPS and IFN-γ at doses of 25 and 50 μM. Among limonoids tested, only gedunin-type limonoid, 7-deacetylgedunin (**54**), displayed the most potent inhibitory activity, without any significant toxicity with an IC_{50} value of 4.85 μM. The suppression of NO production by **54** was correlated with the downregulation of mRNA and protein expression of inducible nitric oxide synthase (iNOS). Mechanistic studies revealed that the transcriptional activity of NF-κB and the activation of mitogen-activated protein kinases, stimulated with LPS and IFN-γ, were suppressed by **54**, which coincided with the inhibition of IκBα degradation and the suppression of p38, SAPK/JNK, and ERK1/2 signaling.

Seven semisynthetic derivatives (**139**-**145**) of dysobinin (**80**) were prepared by some chemical reactions, and study on their structure-activity relationship on anti-inflammatory activity was then performed. It was found that diol derivative **139** exhibited the most potent activity, as well as the activity was significantly loss when an α,β-unsaturated ketone moiety was reduced. Therefore, it could be concluded that both diol and α,β-unsaturated ketone moieties played a crucial role for the anti-inflammatory activity of dysobinin series. In the case of compounds in andrographolide series, the acetylated derivative **147** provided the most potent activity. It could thus be concluded that α-alkylidene-γ-butyrolactone, $\Delta^{8,17}$ exomethylene and $\Delta^{12,13}$ double bond originally in parent compound played important role for anti-inflammatory activity.

REFERENCES

[1] Giles, J.T., Post, W., Blumenthal, R.S., and Bathon, J.M. Therapy insight: Managing cardiovascular risk in patients with rheumatoid arthritis. Nature Clinical Practice Rheumatology 2(6) (2006): 320-329.

[2] Fridman, W.H., et al. Immune infiltration in human cancer: prognostic significance and disease control. Current topics in microbiology and immunology 344 (2011): 1-24.

[3] Bunimov, N. and Laneuville, O. Cyclooxygenase inhibitors: Instrumental drugs to understand cardiovascular homeostasis and arterial thrombosis. Cardiovascular and Hematological Disorders - Drug Targets 8(4) (2008): 268-277.

[4] Shah Biren, N., Nayak, B.S., Bhatt, S.P., Jalalpure, S.S., and Seth, A.K. The anti-inflammatory activity of the leaves of *Colocasia esculenta.* Saudi Pharmaceutical Journal 15(3-4) (2007): 228-232.

[5] Conney, A.H., et al. Inhibitory effect of curcumin and some related dietary compounds on tumor promotion and arachidonic acid metabolism in mouse skin. Advances in Enzyme Regulation 31 (1991): 385-388.

[6] Shah, B.N., Seth, A.K., and Maheshwari, K.M. A Review on Medicinal Plants as a Source of Anti-inflammatory agents. Research Journal of Medicinal plant 5(2) (2011): 101-115.

[7] Agnihotri, S., Wakode, S., and Agnihotri, A. An overview on anti-inflammatory properties and chemo-profiles of plants used in traditional medicine. Indian Journal of Natural Products and Resources 1(2) (2010): 150-167.

[8] Dinarello, C.A. Anti-inflammatory Agents: Present and Future. Cell 140(6) (2010): 935-50.

[9] Cragg, G.M. and Newman, D.J. Natural product drug discovery in the next millennium. Pharmaceutical Biology 39(SUPPL.) (2001): 8-17.

[10] Vane, J.R. and Botting, R.M. Mechanism of action of aspirin-like drugs. Seminars in Arthritis and Rheumatism 26(6 SUPPL. 1) (1997): 2-10.

[11] Chen, Y.C., Yang, L.L., and Lee, T.J.F. Oroxylin A inhibition of lipopolysaccharide-induced iNOS and COX-2 gene expression via suppression of nuclear factor-κB activation. Biochemical Pharmacology 59(11) (2000): 1445-1457.

[12] Barnes, P.J. and Karin, M. Nuclear factor-κB - A pivotal transcription factor in chronic inflammatory diseases. New England Journal of Medicine 336(15) (1997): 1066-1071.

[13] Li, Q. and Verma, I.M. NF- κ B regulation in the immune system. Nature Reviews Immunology 2(10) (2002): 725-734.

[14] Wu, J., Zhang, S., Song, Y., Xiao, Z., Xiao, Q., and Li, Q. Two new mexicanolides from the fruit of the Chinese mangrove *Xylocarpus granatum*. Zeitschrift fur Naturforschung - Section B Journal of Chemical Sciences 60(12) (2005): 1291-1294.

[15] Tan, Q.G. and Luo, X.D. Meliaceous limonoids: Chemistry and biological activities. Chemical Reviews 111(11) (2011): 7437-7522.

[16] Li, J., et al. Andhraxylocarpins A-E: Structurally intriguing limonoids from the true mangroves *Xylocarpus granatum* and *Xylocarpus moluccensis*. Chemistry - A European Journal 18(45) (2012): 14342-14351.

[17] Koul, O., Singh, G., Singh, R., Singh, J., Daniewski, W.M., and Berlozecki, S. Bioefficacy and mode-of-action of some limonoids of salannin group from *Azadirachta indica* A. Juss and their role in a multicomponent system against lepidopteran larvae. Journal of Biosciences 29(4) (2004): 409-416.

[18] Champagne, D.E., Koul, O., Isman, M.B., Scudder, G.G.E., and Neil Towers, G.H. Biological activity of limonoids from the Rutales. Phytochemistry 31(2) (1992): 377-394.

[19] Wu, J., Xiao, Q., Xu, J., Li, M.Y., Pan, J.Y., and Yang, M.H. Natural products from true mangrove flora: source, chemistry and bioactivities. Natural Product Reports 25 (2008): 955-981.

[20] Li, M.Y., et al. Granatumins A-G, limonoids from the seeds of a Krishna mangrove, *Xylocarpus granatum.* Journal of Natural Products 72(12) (2009): 2110-2114.

[21] Pudhom, K., Sommit, D., Nuclear, P., Ngamrojanavanich, N., and Petsom, A. Protoxylocarpins F - H, protolimonoids from seed kernels of *Xylocarpus granatum.* Journal of Natural Products 72(12) (2009): 2188-2191.

[22] Li, J., et al. Thaixylomolins A-C: Limonoids featuring two new motifs from the thai *Xylocarpus moluccensis.* Organic Letters 15(14) (2013): 3682-3685.

[23] Yang, M.H., Wang, J.S., Luo, J.G., Wang, X.B., and Kong, L.Y. Tetranortriterpenoids from *Chisocheton paniculatus.* Journal of Natural Products 72(11) (2009): 2014-2018.

[24] Mulholland, D.A., Parel, B., and Coombes, P.H. The chemistry of the Meliaceae and Ptaeroxylaceae of Southern and Eastern Africa and Madagascar. Current Organic Chemistry 4(10) (2000): 1011-1054.

[25] Phongmaykin, J., Kumamoto, T., Ishikawa, T., Suttisri, R., and Saifah, E. A new sesquiterpene and other terpenoid constituents of *Chisocheton penduliflorus.* Archives of Pharmacal Research 31(1) (2008): 21-27.

[26] Najmuldeen, I.A., et al. Chisomicines A-C, limonoids from *Chisocheton ceramicus.* Journal of Natural Products 74(5) (2011): 1313-1317.

[27] Maneerat, W., Laphookhieo, S., Koysomboon, S., and Chantrapromma, K. Antimalarial, antimycobacterial and cytotoxic limonoids from *Chisocheton siamensis.* Phytomedicine 15(12) (2008): 1130-1134.

[28] Saxena, S., Jain, D.C., Bhakuni, R.S., and Sharma, R.P. Chemistry and pharmacology of *Andrographis* species. Indian Drugs 35(8) (1998): 458-467.

[29] Xia, Y.F., et al. Andrographolide Attenuates Inflammation by Inhibition of NF-κB Activation through Covalent Modification of Reduced Cysteine 62 of p50. The Journal of Immunology 173(6) (2004): 4207-4217.

[30] Shen, Y.C., Chen, C.F., and Chiou, W.F. Andrographolide prevents oxygen radical production by human neutrophils: Possible mechanism(s) involved in its anti-inflammatory effect. British Journal of Pharmacology 135(2) (2002): 399-406.

[31] Bao, Z., et al. A novel antiinflammatory role for andrographolide in asthma via inhibition of the nuclear factor-kappaB pathway. American Journal of Respiratory and Critical Care Medicine 179(8) (2009): 657-65.

[32] Negi, A.S., Kumar, J.K., Luqman, S., Shanker, K., Gupta, M.M., and Khanuja, S.P. Recent advances in plant hepatoprotectives: a chemical and biological profile of some important leads. Medicinal Research Reviews 28(5) (2008): 746-72.

[33] Abu-Ghefreh, A.A., Canatan, H., and Ezeamuzie, C.I. *In vitro* and *in vivo* anti-inflammatory effects of andrographolide. International Immunopharmacology 9(3) (2009): 313-318.

[34] Lee, K.-C., Chang, H.-H., Chung, Y.-H., and Lee, T.-Y. Andrographolide acts as an anti-inflammatory agent in LPS-stimulated RAW264.7 macrophages by inhibiting STAT3-mediated suppression of the NF-κB pathway. Journal of Ethnopharmacology 135(3) (2011): 678-684.

[35] Lim, J.C.W., Chan, T.K., Ng, D.S., Sagineedu, S.R., Stanslas, J., and Wong, W.F. Andrographolide and its analogues: Versatile bioactive molecules for combating inflammation and cancer. Clinical and Experimental Pharmacology and Physiology 39(3) (2012): 300-310.

[36] Banerji, B. and Nigam, S.K. Wood constituents of Meliaceae: A review Fitoterapia 55 (1984): 3-36.

[37] Wu, J., Xiao, Q., and Li, Q. Limonoids from the Mangrove *Xylocarpus granatum.* Biochemical Systematics and Ecology 34(11) (2006): 838-841.

[38] Ximu, C. and Pongumphai, S. Preliminary revision of Swietenioideae (Meliaceae) in Thailand. Thai Journal of Forestry 13 (1994): 1-9.

[39] Yin, B., et al. Protolimonoids from the seeds of *Xylocarpus granatum.* Biochemical Systematics and Ecology 37(3) (2009): 218-220.

[40] Taylor, D.A.H. Limonoid extractives from *Xylocarpus moluccensis.* Phytochemistry 22(5) (1983): 1297-1299.

[41] Bandaranayake, W.M. Bioactivities, bioactive compounds and chemical constituents of mangrove plants. Wetlands Ecology and Management 10(6) (2002): 421-452.

[42] Sarker, S.D., Uddin, S.J., Shilpi, J.A., Rouf, R., Ferdous, M.E.M., and Nahar, L. Neuropharmacological properties of *Xylocarpus moluccensis.* Fitoterapia 78(2) (2007): 107-111.

[43] Shen, L.R., et al. Chemical constituents of plants from the genus *Xylocarpus.* Chemistry and Biodiversity 6(9) (2009): 1293-1308.

[44] Sarigaputi, C., Nuanyai, T., Teerawatananond, T., Pengpreecha, S., Muangsin, N., and Pudhom, K. Xylorumphiins A-D, mexicanolide limonoids from the seed kernels of *Xylocarpus rumphii.* Journal of Natural Products 73(8) (2010): 1456-1459.

[45] Wati Haron, N. and Mat Taha, R. Taxonomy, distribution and propagation of *Xylocarpus* species at carey island - The heritage island of Malaysia. in *Acta Horticulturae*. 2010. 997-1004.

[46] Wu, J., et al. Xyloccensins O and P, unique 8,9,30-phragmalin ortho esters from *Xylocarpus granatum.* Organic Letters 6(11) (2004): 1841-1844.

[47] Roy, A. and Saraf, S. Limonoids: Overview of significant bioactive triterpenes distributed in plants kingdom. Biological and Pharmaceutical Bulletin 29(2) (2006): 191-201.

[48] Aliero, B.L. Larvaecidal effects of aqueous extracts of *Azadirachta indica* (neem) on the larvae of *Anopheles mosquito.* African Journal of Biotechnology 2(9) (2003): 376-380.

[49] Lakshmi, V. and Gupta, P. An overview of the genus *Xylocarpus.* Natural product research 22(14) (2008): 1203-1230.

[50] Cui, J., Deng, Z., Xu, M., Proksch, P., Li, Q., and Lin, W. Protolimonoids and limonoids from the chinese mangrove plant *Xylocarpus granatum.* Helvetica Chimica Acta 92(1) (2009): 139-150.

[51] Chen, W., Shen, L., Li, M., Xiao, Q., Satyanandamurty, T., and Wu, J. Absolute configurations of new limonoids from a Krishna mangrove, *Xylocarpus granatum.* Fitoterapia 94 (2014): 108-113.

[52] Yin, S., Wang, X.N., Fan, C.Q., Lin, L.P., Ding, J., and Yue, J.M. Limonoids from the seeds of the marine mangrove *Xylocarpus granatum.* Journal of Natural Products 70(4) (2007): 682-685.

[53] Uddin, S.J., et al. Gedunin, a limonoid from *Xylocarpus granatum*, inhibits the growth of CaCo-2 colon cancer cell line *in vitro.* Phytotherapy Research 21(8) (2007): 757-761.

[54] Toume, K., et al. Xylogranin B: A potent Wnt signal inhibitory limonoid from *Xylocarpus granatum.* Organic Letters 15(23) (2013): 6106-6109.

[55] Wu, Y.B., et al. Xylomexicanins C and D, new mexicanolide-type limonoids from *Xylocarpus granatum.* Bioscience, Biotechnology and Biochemistry 77(4) (2013): 736-740.

[56] Pudhom, K., Sommit, D., Nuclear, P., Ngamrojanavanich, N., and Petsom, A. Moluccensins H-J, 30-ketophragmalin limonoids from *Xylocarpus moluccensis.* Journal of Natural Products 73(2) (2010): 263-266.

[57] Wisutsitthiwong, C., Buranaruk, C., Pudhom, K., and Palaga, T. The plant limonoid 7-oxo-deacetoxygedunin inhibits RANKL-induced osteoclastogenesis

by suppressing activation of the NF-κB and MAPK pathways. Biochemical and Biophysical Research Communications 415(2) (2011): 361-366.

[58] Ravangpai, W., et al. Limonoids from seeds of Thai *Xylocarpus moluccensis.* Bioorganic and Medicinal Chemistry Letters 21(15) (2011): 4485-4489.

[59] Brechbühler, S., Büchi, G., and Milne, G. The absolute configuration of the aflatoxins. Journal of Organic Chemistry 32(8) (1967): 2641-2642.

[60] Meyers, A.I., Knaus, G., and Kamata, K. Synthesis via 2-oxazolines. IV. An asymmetric synthesis of 2-methylalkanoic acids from a chiral oxazoline Journal of the American Chemical Society 96(1) (1974): 268-270.

[61] Connolly, J.D., MacLellan, M., Okorie, D.A., and Taylor, D.A.H. Limonoids from *Xylocarpus moluccensis* (Lam.) M. Roem. Journal of the Chemical Society, Perkin Transactions 1 (19) (1976): 1993-1996.

[62] Roy, A.D., et al. Xyloccensin X and Y, two new limonoids front xylocarpus molluccensis: NMR investigation in mixture. Magnetic Resonance in Chemistry 44(11) (2006): 1054-1057.

[63] Kokpol, U., et al. A limonoid from *Xylocarpus granatum.* Phytochemistry 41(3) (1996): 903-905.

[64] Naarding, P., Schoevers, R.A., Janzing, J.G.E., Jonker, C., Koudstaal, P.J., and Beekman, A.T.F. A study on symptom profiles of late-life depression: The influence of vascular, degenerative and inflammatory risk-indicators. Journal of Affective Disorders 88(2) (2005): 155-162.

[65] O'Neill, L.A.J., Bryant, C.E., and Doyle, S.L. Therapeutic targeting of toll-like receptors for infectious and inflammatory diseases and cancer. Pharmacological Reviews 61(2) (2009): 177-197.

[66] Okusawa, S., Gelfand, J.A., Ikejima, T., Connolly, R.J., and Dinarello, C.A. Interleukin 1 induces a shock-like state in rabbits. Synergism with tumor necrosis factor and the effect of cyclooxygenase inhibition. Journal of Clinical Investigation 81(4) (1988): 1162-1172.

[67] Wysocka, M., et al. Interleukin-12 is required for interferon-γ production and lethality in lipopolysaccharide-induced shock in mice. European Journal of Immunology 25(3) (1995): 672-676.

[68] Kröncke, K.D., Fehsel, K., and Kolb-Bachofen, V. Inducible nitric oxide synthase in human diseases. Clinical and Experimental Immunology 113(2) (1998): 147-156.

[69] Escribano, L., Akin, C., Castells, M., and Schwartz, L.B. Current options in the treatment of mast cell mediator-related symptoms in mastocytosis. Inflammation and Allergy - Drug Targets 5(1) (2006): 61-77.

[70] Perl, M., Chung, C.S., Garber, M., Huang, X., and Ayala, A. Contribution of anti-inflammatory/immune suppressive processes to the pathology of sepsis. Frontiers in Bioscience 11(1 P.1-446) (2006): 272-299.

[71] Wu, G. and Morris Jr, S.M. Arginine metabolism: Nitric oxide and beyond. Biochemical Journal 336(1) (1998): 1-17.

[72] Mollace, V., Muscoli, C., Masini, E., Cuzzocrea, S., and Salvemini, D. Modulation of prostaglandin biosynthesis by nitric oxide and nitric oxide donors. Pharmacological Reviews 57(2) (2005): 217-252.

[73] Ko, L. and Lagunoff, D. Depletion of mast cell ATP inhibits complement dependent cytotoxic histamine release. Experimental Cell Research 100(2) (1976): 313-321.

[74] Griesbacher, T. Kallikrein-kinin system in acute pancreatitis: Potential of B2-bradykinin antagonists and kallikrein inhibitors. Pharmacology 60(3) (2000): 113-120.

[75] Tani, K., et al. Thrombin enhances lung fibroblast proliferation in bleomycin-induced pulmonary fibrosis. American journal of respiratory cell and molecular biology 5(1) (1991): 34-40.

[76] Christie, M.J., Vaughan, C.W., and Ingram, S.L. Opioids, NSAIDS and 5-lipoxygenase inhibitors act synergistically in brain via arachidonic acid metabolism. Inflammation Research 48(1) (1999): 1-4.

[77] Kumar, H., Kawai, T., and Akira, S. Pathogen recognition by the innate immune system. International Reviews of Immunology 30(1) (2011): 16-34.

[78] McGettrick, A.F. and O'Neill, L.A. Localisation and trafficking of Toll-like receptors: an important mode of regulation. Current Opinion in Immunology 22(1) (2010): 20-27.

[79] Mogensen, T.H. Pathogen recognition and inflammatory signaling in innate immune defenses. Clinical Microbiology Reviews 22(2) (2009): 240-273.

[80] Pla, D., et al. Synthesis and structure-activity relationship study of potent cytotoxic analogues of the marine alkaloid lamellarin D. Journal of Medicinal Chemistry 49(11) (2006): 3257-3268.

[81] Lombardino, J.G. and Lowe, J.A. The role of the medicinal chemist in drug discovery - then and now. Nature Reviews Drug Discovery 3(10) (2004): 853-862.

[82] Manners, G.D. Citrus limonoids: Analysis, bioactivity, and biomedical prospects. Journal of Agricultural and Food Chemistry 55(21) (2007): 8285-8294.

[83] Das, B., et al. Synthesis, cytotoxicity, and structure-activity relationship (SAR) studies of andrographolide analogues as anti-cancer agent. Bioorganic and Medicinal Chemistry Letters 20(23) (2010): 6947-6950.

[84] Dai, G.F., et al. Anti-inflammatory effect of novel andrographolide derivatives through inhibition of NO and PGE_2 production. International Immunopharmacology 11(12) (2011): 2144-2149.

[85] Sirion, U., Kasemsook, S., Suksen, K., Piyachaturawat, P., Suksamrarn, A., and Saeeng, R. New substituted C-19-andrographolide analogues with potent cytotoxic activities. Bioorganic and Medicinal Chemistry Letters 22(1) (2012): 49-52.

[86] Wong, C.P., Deguchi, J., Nugroho, A.E., Kaneda, T., Hadi, A.H.A., and Morita, H. Ceramicines from *Chisocheton ceramicus* as lipid-droplets accumulation inhibitors. Bioorganic and Medicinal Chemistry Letters 23(6) (2013): 1786-1788.

[87] Singh, S., Garg, H.S., and Khanna, N.M. Dysobinin, a new tetranortriterpene from Dysoxylum binectariferum. Phytochemistry 15(12) (1976): 2001-2002.

[88] Siddiqui, S., Siddiqui, B.S., Faizi, S., and Mahmood, T. Isolation of a tetranortriterpenoid from Azadirachta indica. Phytochemistry 23(12) (1984): 2899-2901.

[89] Sarmaha, G.K., Bhattacharyyaa, N.K., Goswamia, B.N., Baruab, P., and Katakya, J.C.S. Derivatives of paniculatin and their antifungal activity. Journal of the Indian Chemical Society 80(12) (2003): 1163-1168.

[90] Bordoloi, M., Saikia, B., Mathur, R.K., and Nath Goswami, B. A meliacin from Chisocheton paniculatus. Phytochemistry 34(2) (1993): 583-584.

[91] Nanduri, S., et al. Synthesis and structure–activity relationships of andrographolide analogues as novel cytotoxic agents. Bioorganic & Medicinal Chemistry Letters 14(18) (2004): 4711-4717.

[92] Li, J., Huang, W., Zhang, H., Wang, X., and Zhou, H. Synthesis of andrographolide derivatives and their TNF-α and IL-6 expression inhibitory activities. Bioorganic and Medicinal Chemistry Letters 17(24) (2007): 6891-6894.

[93] Pandeti, S., Sonkar, R., Shukla, A., Bhatia, G., and Tadigoppula, N. Synthesis of new andrographolide derivatives and evaluation of their antidyslipidemic, LDL-oxidation and antioxidant activity. European Journal of Medicinal Chemistry 69 (2013): 439-448.

[94] Uttekar, M.M., et al. Anti-HIV activity of semisynthetic derivatives of andrographolide and computational study of HIV-1 gp120 protein binding. European Journal of Medicinal Chemistry 56 (2012): 368-374.

[95] Jada, S.R., Hamzah, A.S., Lajis, N.H., Saad, M.S., Stevens, M.F.G., and Stanslas, J. Semisynthesis and cytotoxic activities of andrographolide analogues. Journal of Enzyme Inhibition and Medicinal Chemistry 21(2) (2006): 145-155.

[96] Dai, G.F., Xu, H.W., Wang, J.F., Liu, F.W., and Liu, H.M. Studies on the novel α -glucosidase inhibitory activity and structure-activity relationships for andrographolide analogues. Bioorganic and Medicinal Chemistry Letters 16(10) (2006): 2710-2713.

[97] Dai, G.F., et al. The in vitro anti-tumor activities of andrographolide derivatives and the structure-activity relationships. Chinese Journal of New Drugs 20(4) (2011): 362-366.

[98] Chiou, W.F., Chen, C.F., and Lin, J.J. Mechanisms of suppression of inducible nitric oxide synthase (iNOS) expression in RAW 264.7 cells by andrographolide. British Journal of Pharmacology 129(8) (2000): 1553-1560.

[99] Vo, P.A., Lad, B., Tomlinson, J.A.P., Francis, S., and Ahluwalia, A. Autoregulatory role of endothelium-derived nitric oxide (NO) on lipopolysaccharide-induced vascular inducible NO synthase expression and function. Journal of Biological Chemistry 280(8) (2005): 7236-7243.

APPENDIX

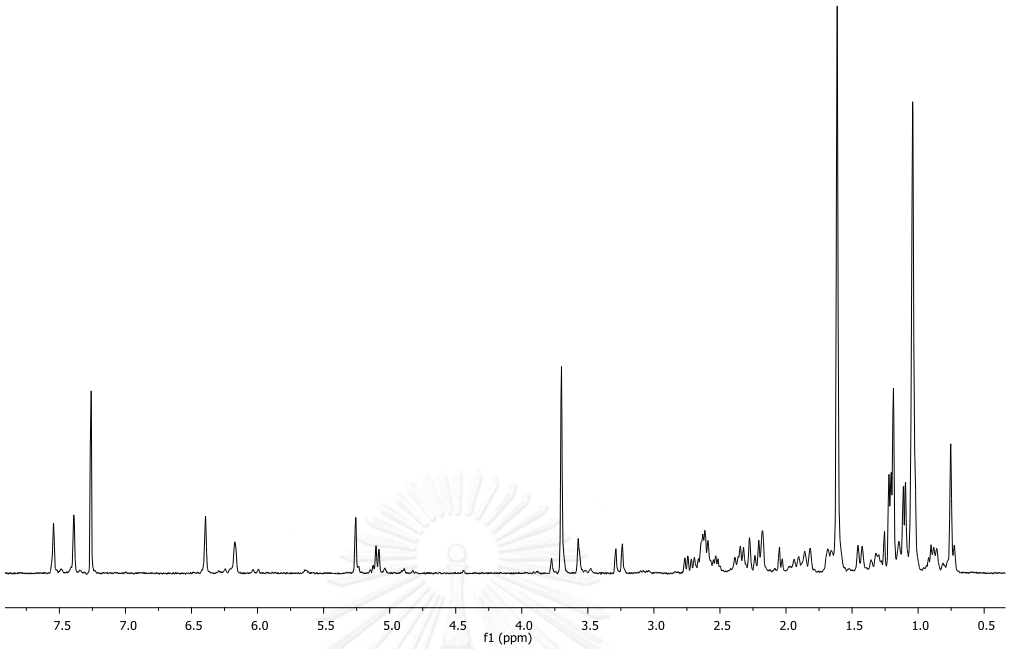

Figure A.1 ^{1}H NMR (400 MHz, $CDCl_3$) spectrum of compound **42**

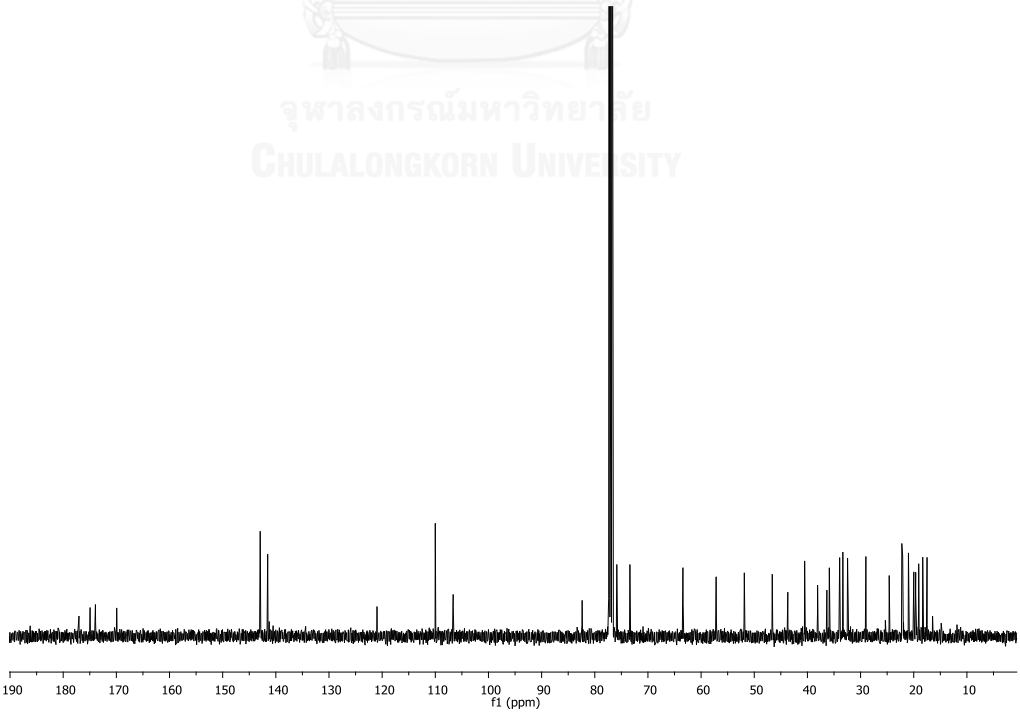

Figure A.2 ^{13}C NMR (100 MHz, $CDCl_3$) spectrum of compound **42**

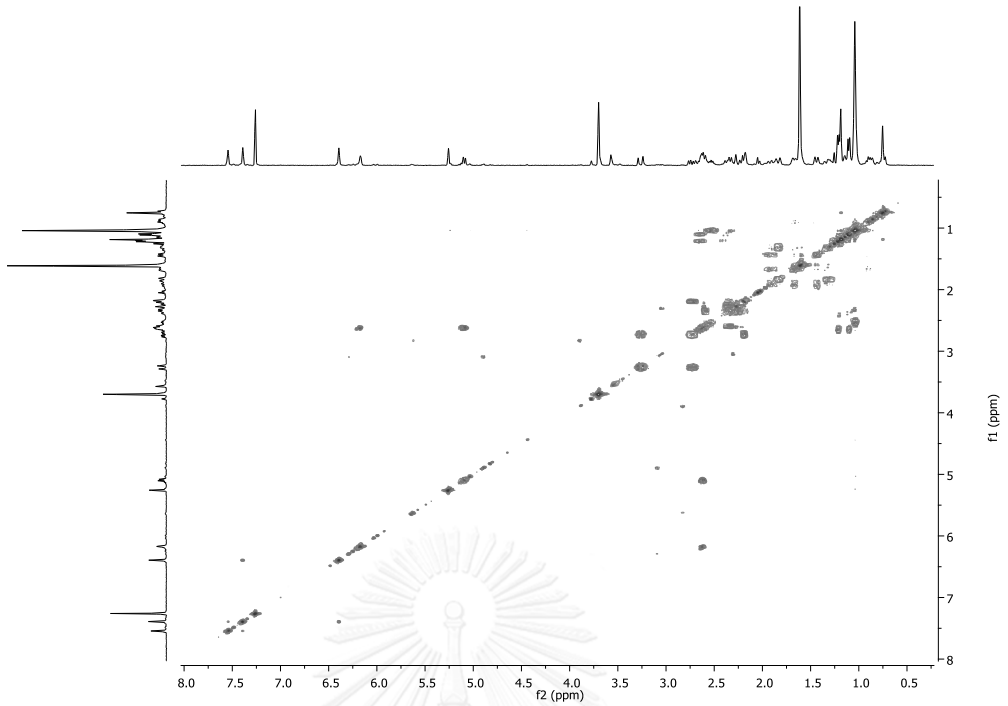

Figure A.3 ^{1}H-^{1}H COSY spectrum ($CDCl_3$) of compound **42**

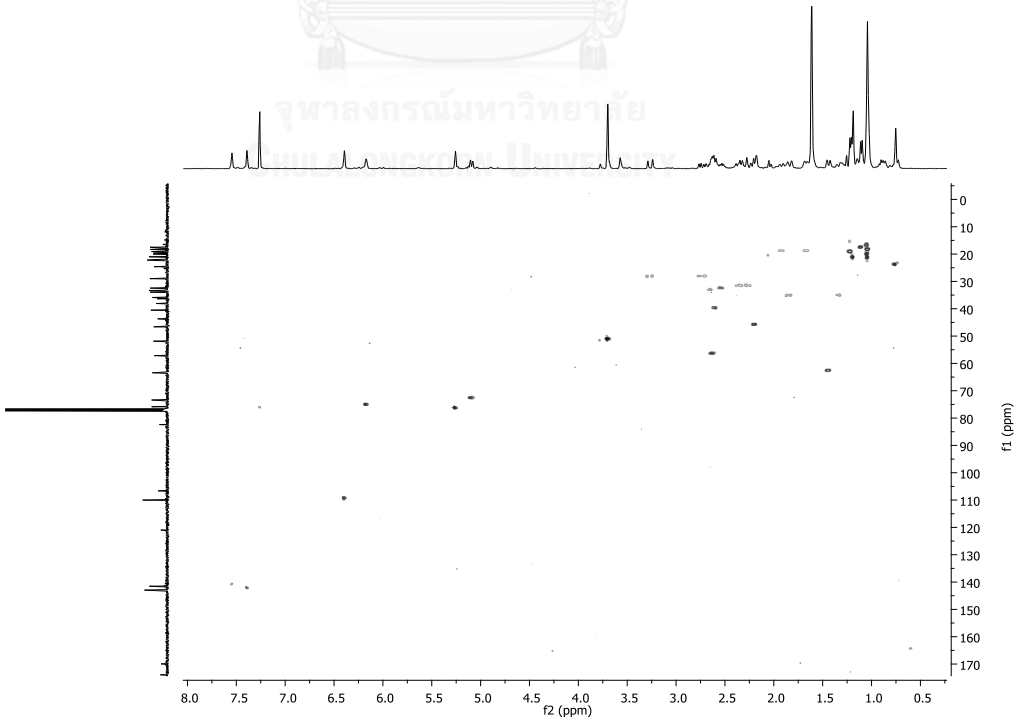

Figure A.4 HSQC spectrum ($CDCl_3$) of compound **42**

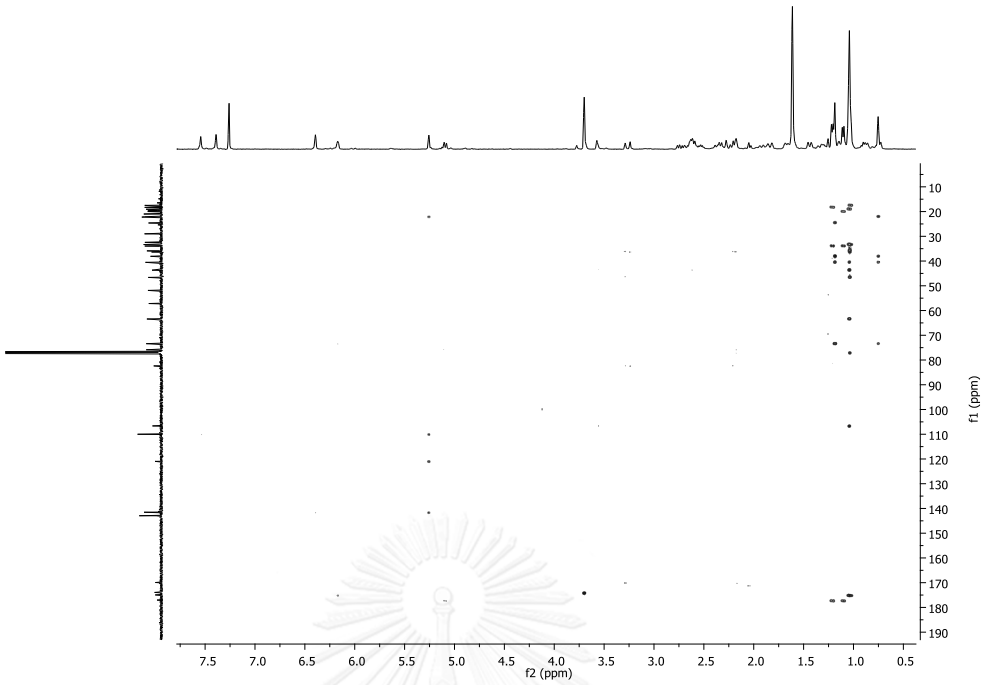

Figure A.5 HMBC spectrum ($CDCl_3$) of compound **42**

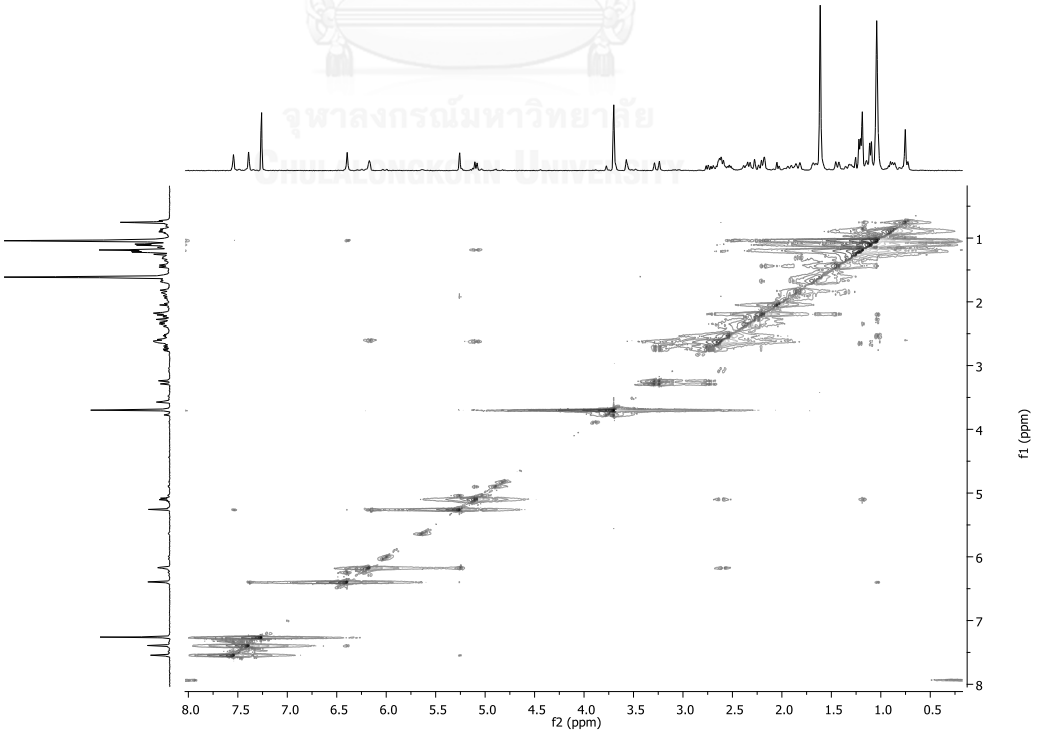

Figure A.6 NOESY spectrum ($CDCl_3$) of compound **42**

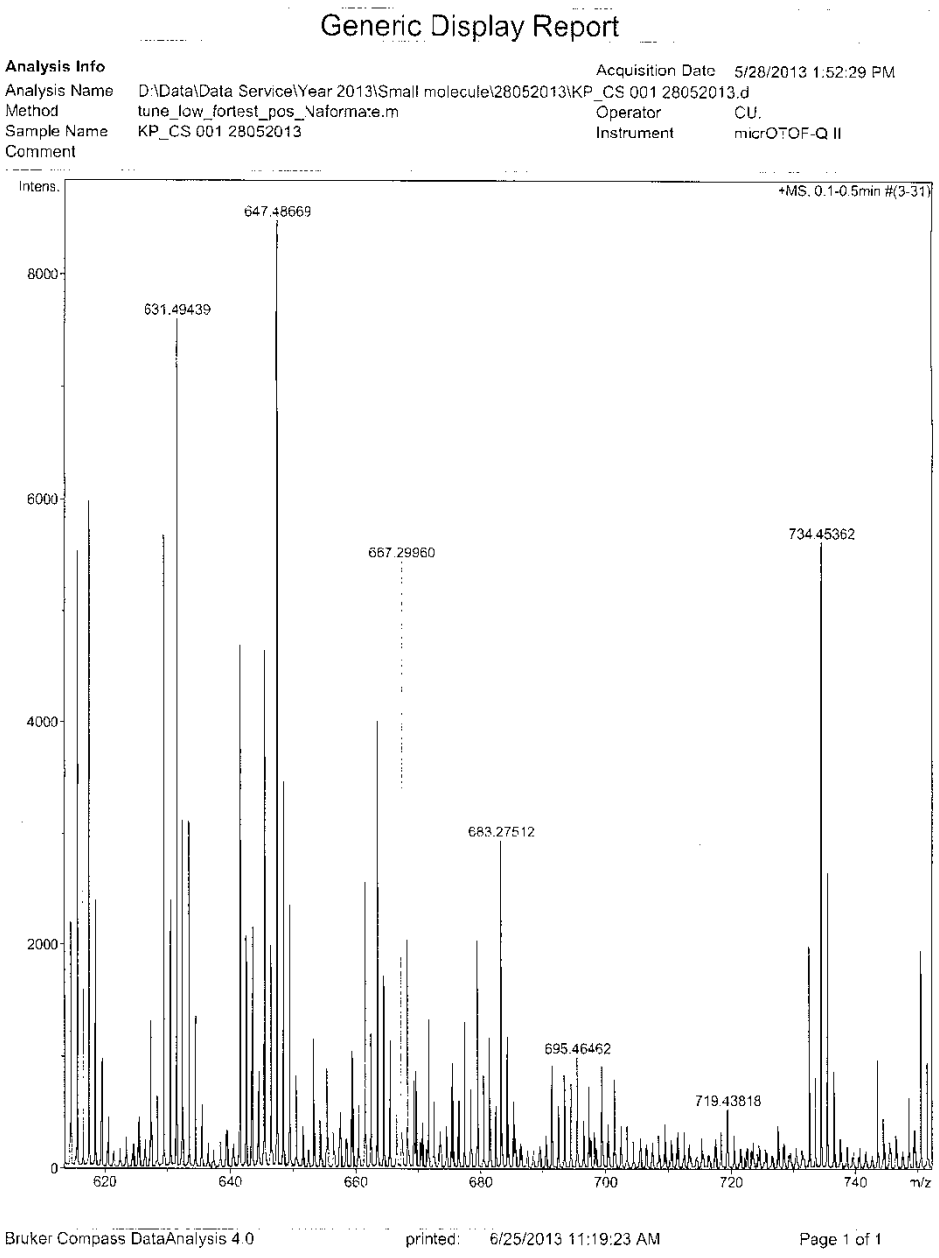

Figure A.7 HRESIMS Mass spectrum of compound **42**

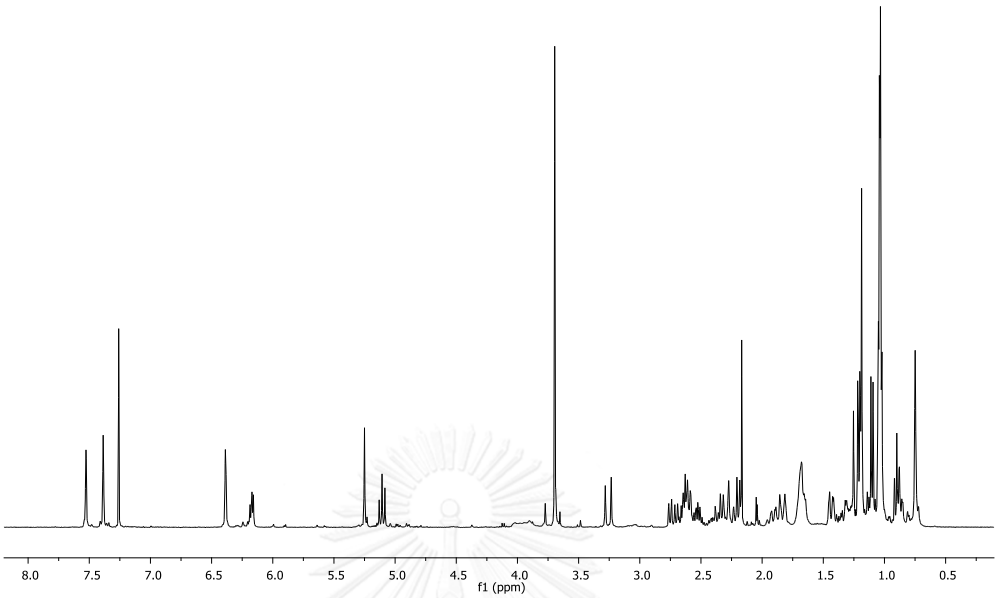

Figure A.8 ^{1}H NMR (400 MHz, $CDCl_3$) spectrum of compound **43**

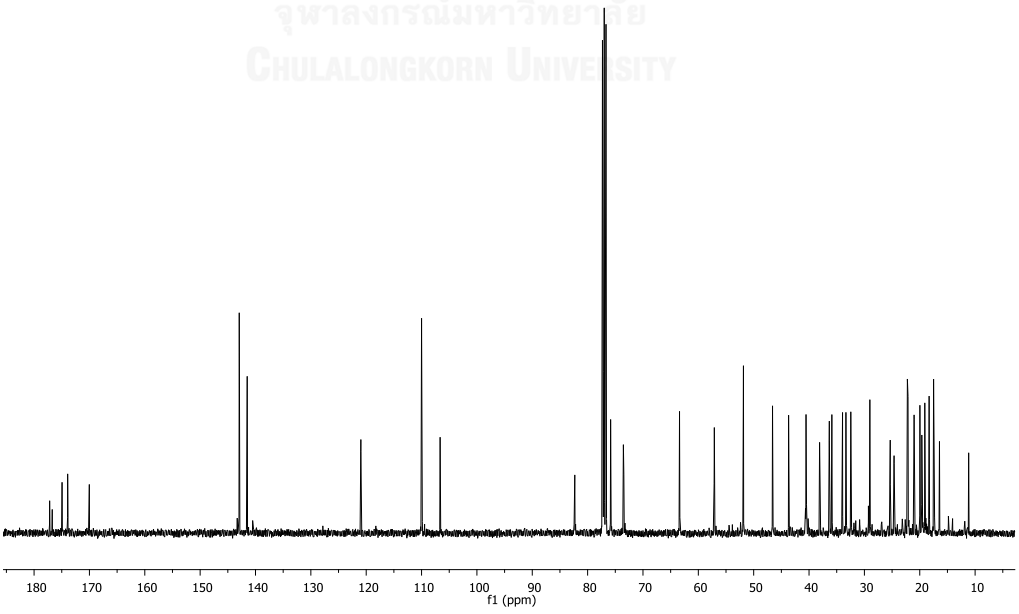

Figure A.9 ^{13}C NMR (100 MHz, $CDCl_3$) spectrum of compound **43**

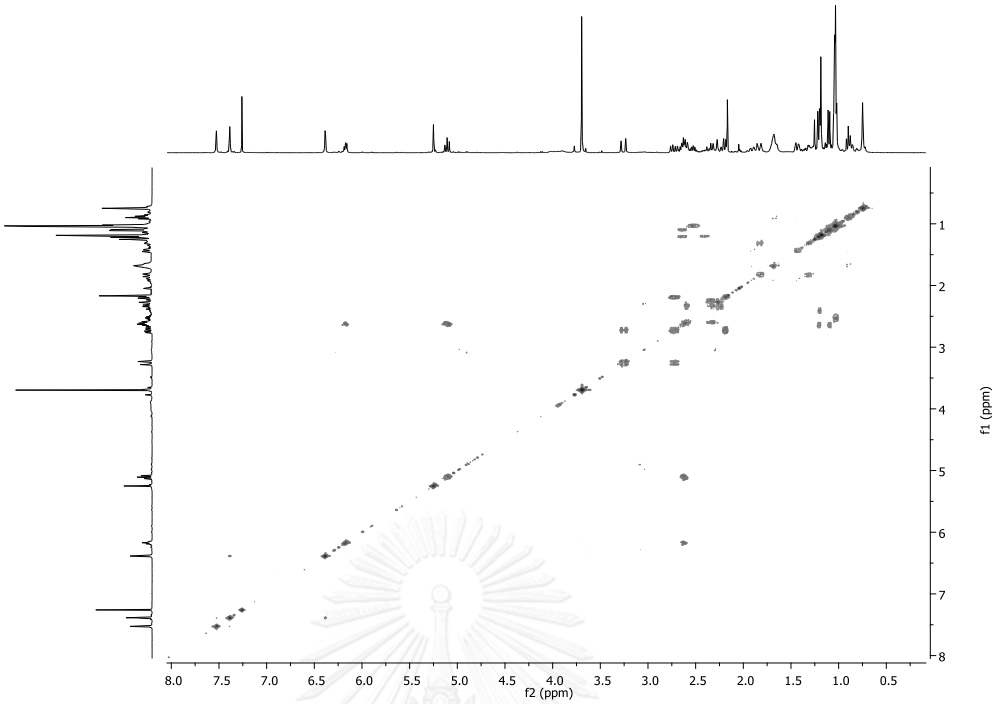

Figure A.10 ^{1}H-^{1}H COSY spectrum ($CDCl_3$) of compound **43**

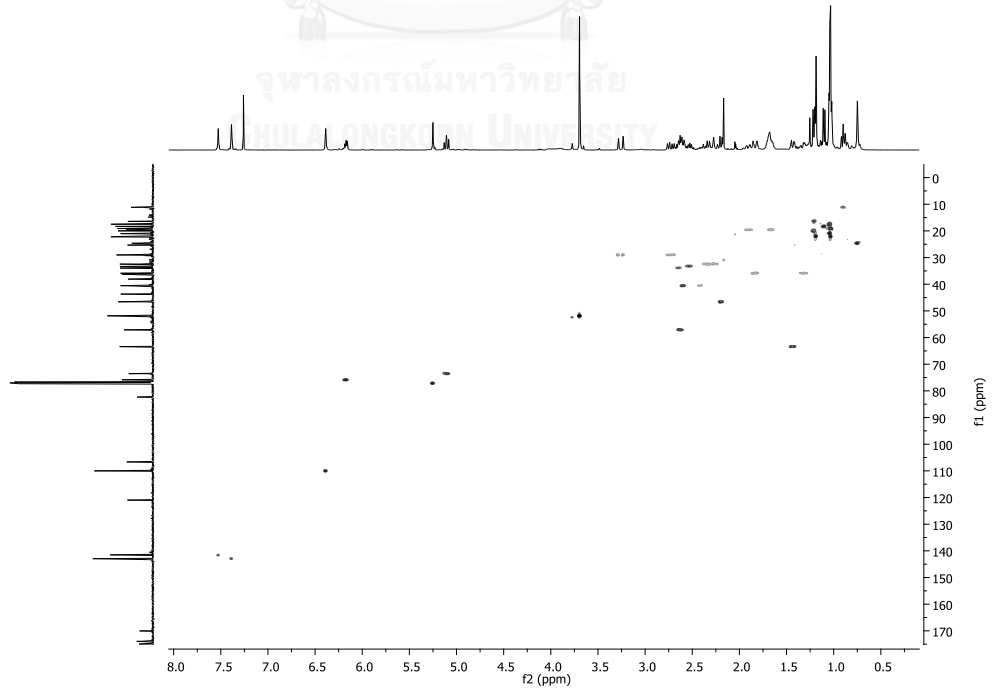

Figure A.11 HSQC spectrum ($CDCl_3$) of compound **43**

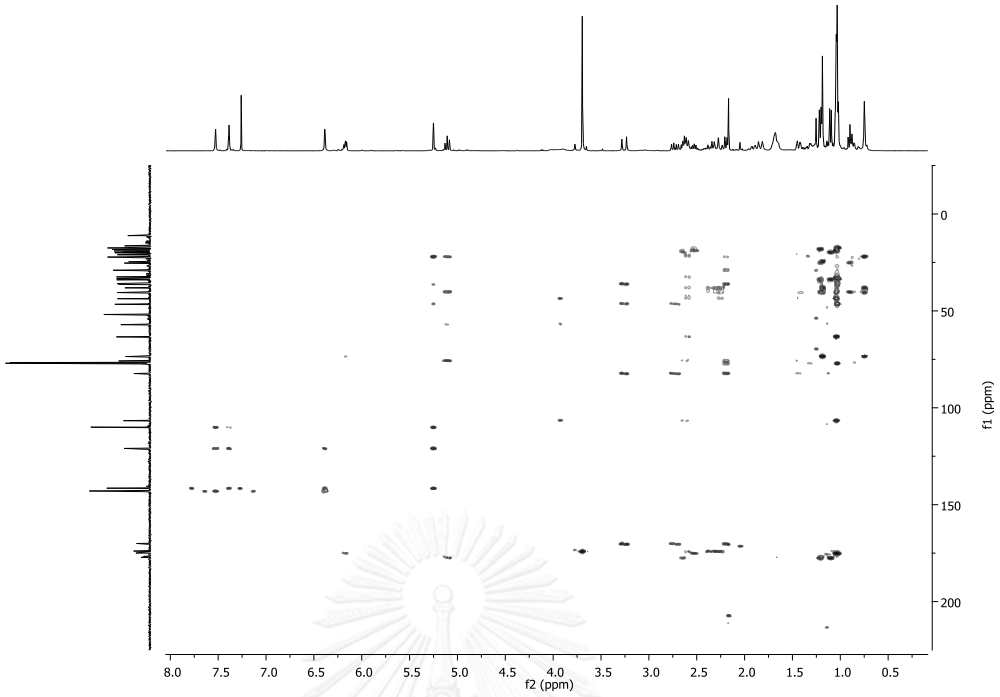

Figure A.12 HMBC spectrum ($CDCl_3$) of compound **43**

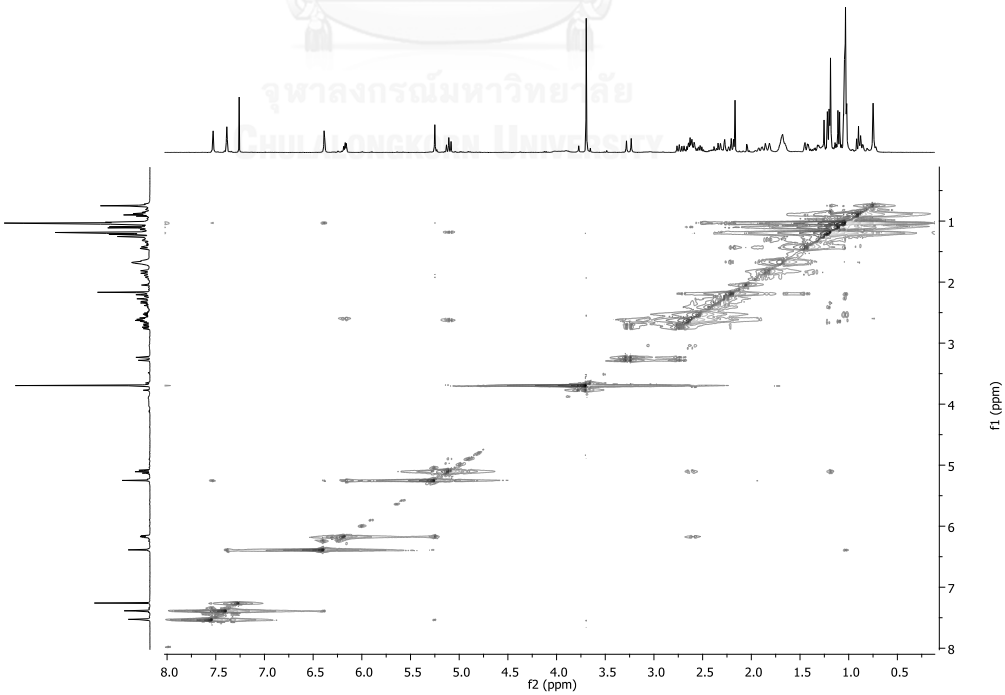

Figure A.13 NOESY spectrum ($CDCl_3$) of compound **43**

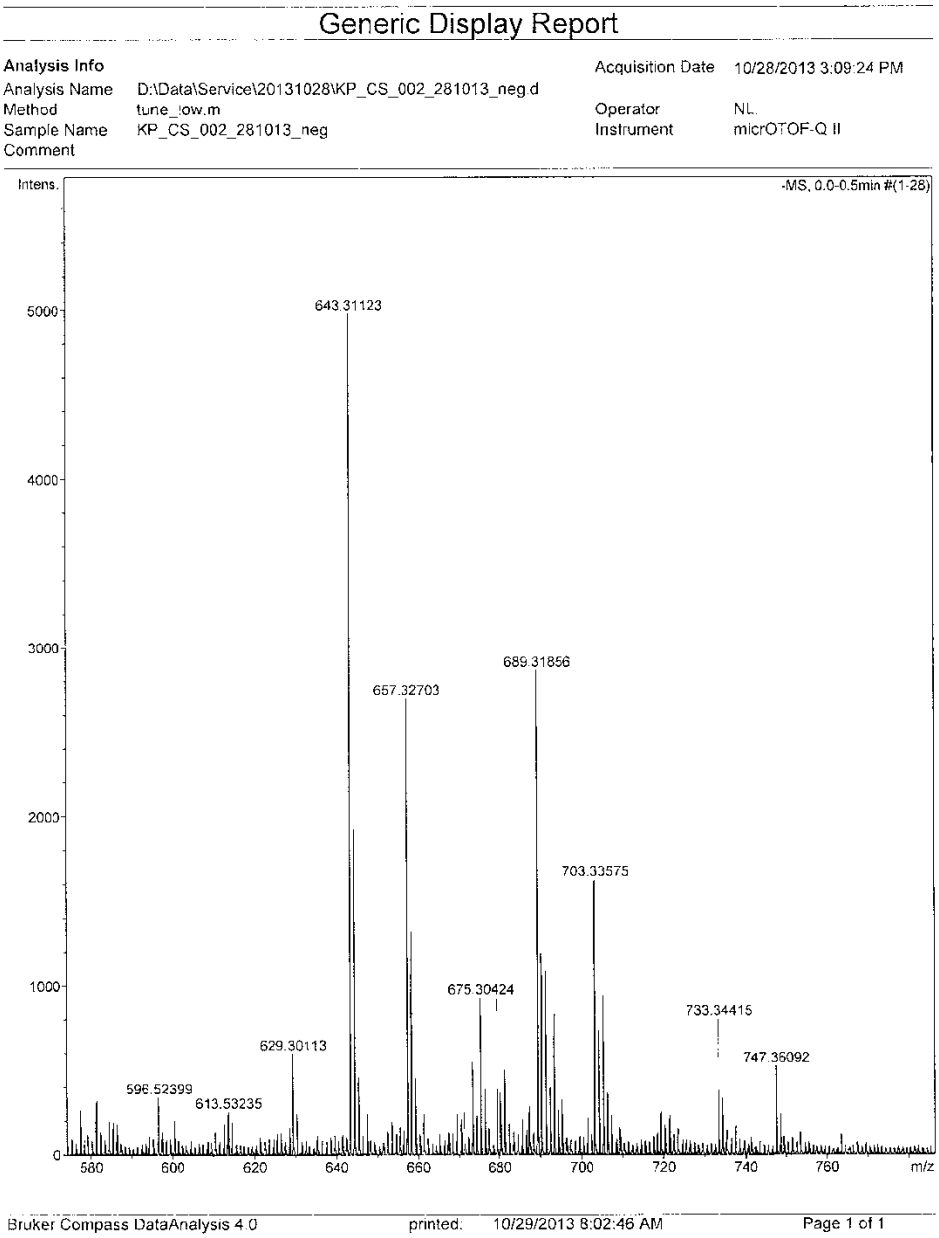

Figure A.14 HRESIMS Mass spectrum of compound **43**

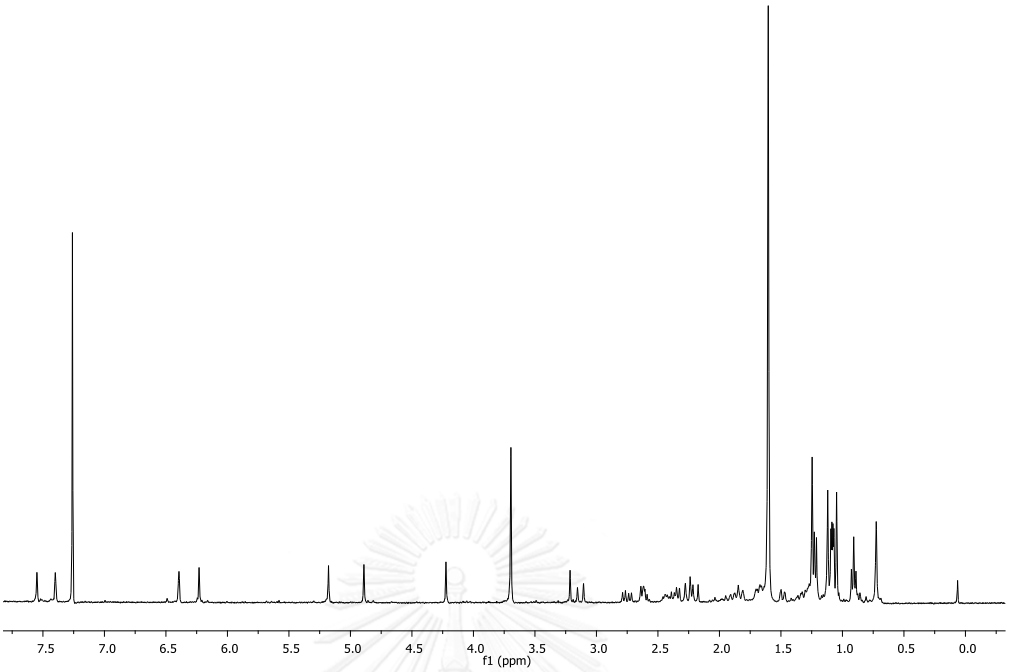

Figure A.15 ^{1}H NMR (400 MHz, $CDCl_3$) spectrum of compound **44**

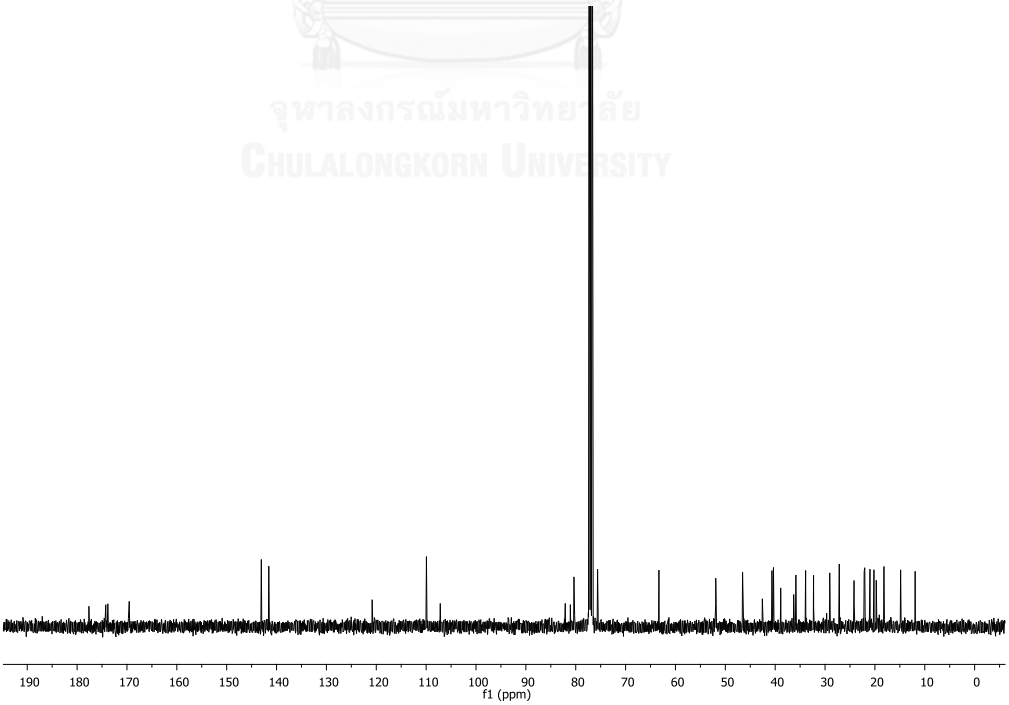

Figure A.16 ^{13}C NMR (100 MHz, $CDCl_3$) spectrum of compound **44**

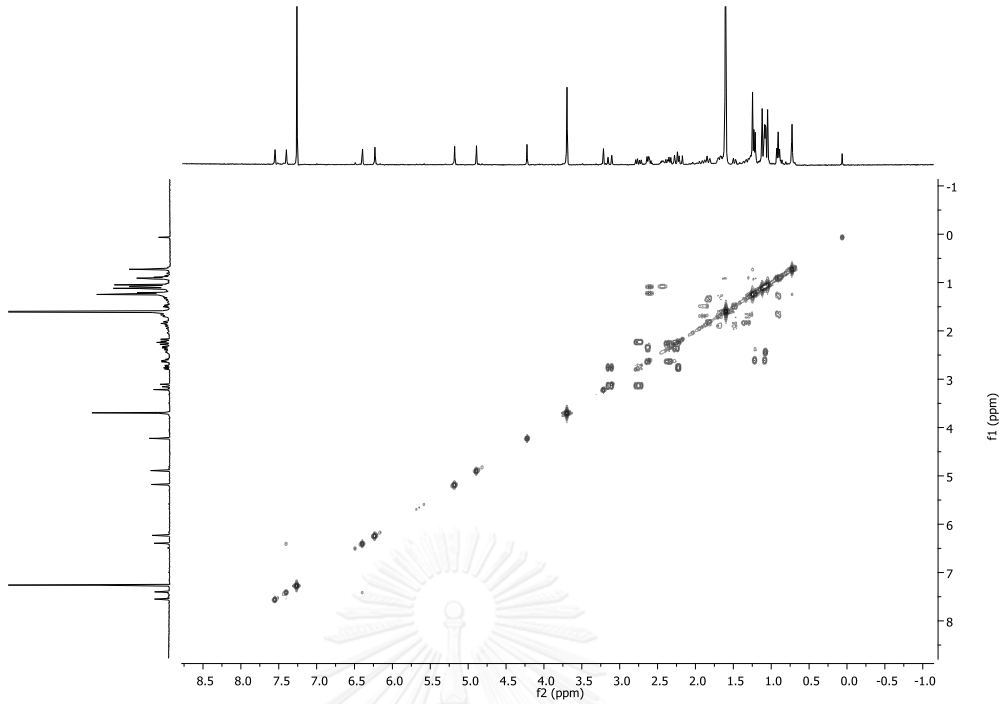

Figure A.17 ^{1}H-^{1}H COSY spectrum ($CDCl_3$) of compound **44**

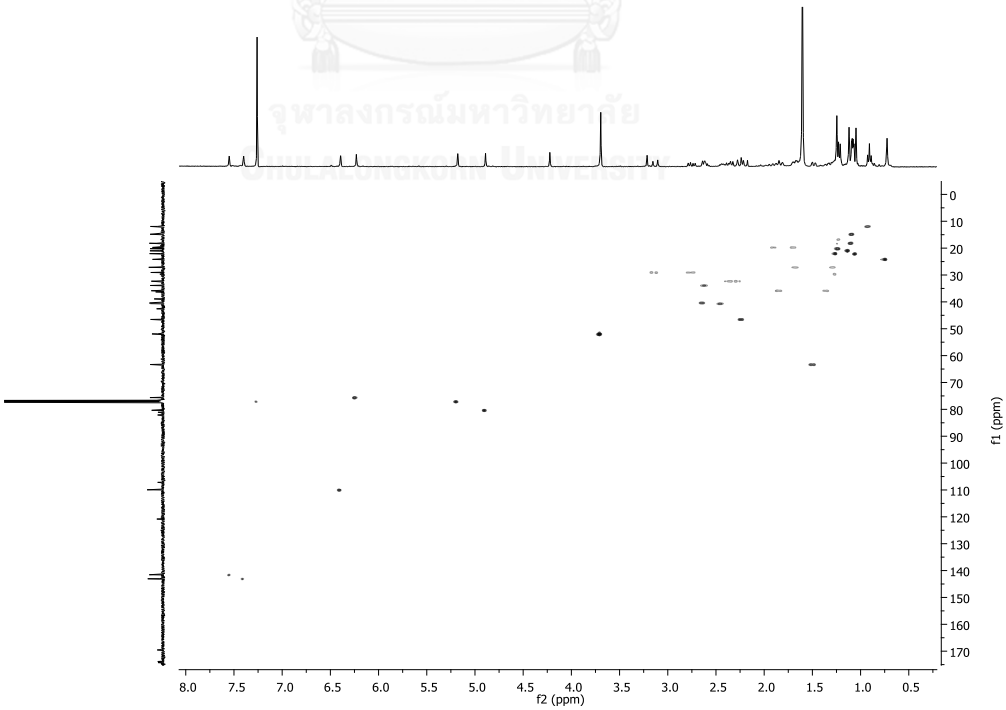

Figure A.18 HSQC spectrum ($CDCl_3$) of compound **44**

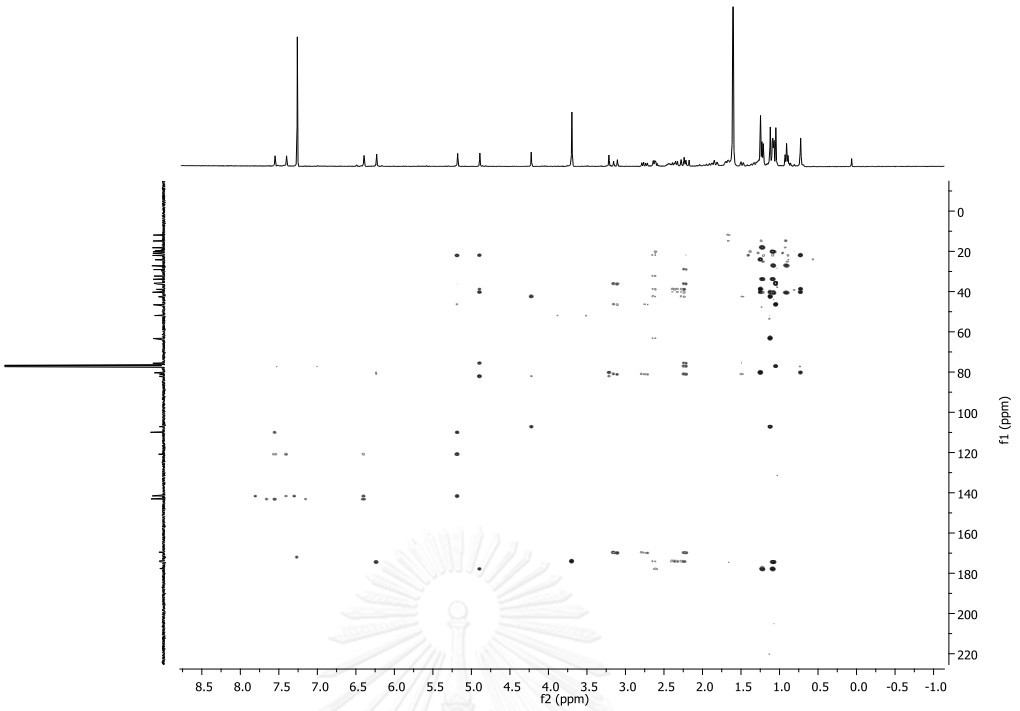

Figure A.19 HMBC spectrum ($CDCl_3$) of compound **44**

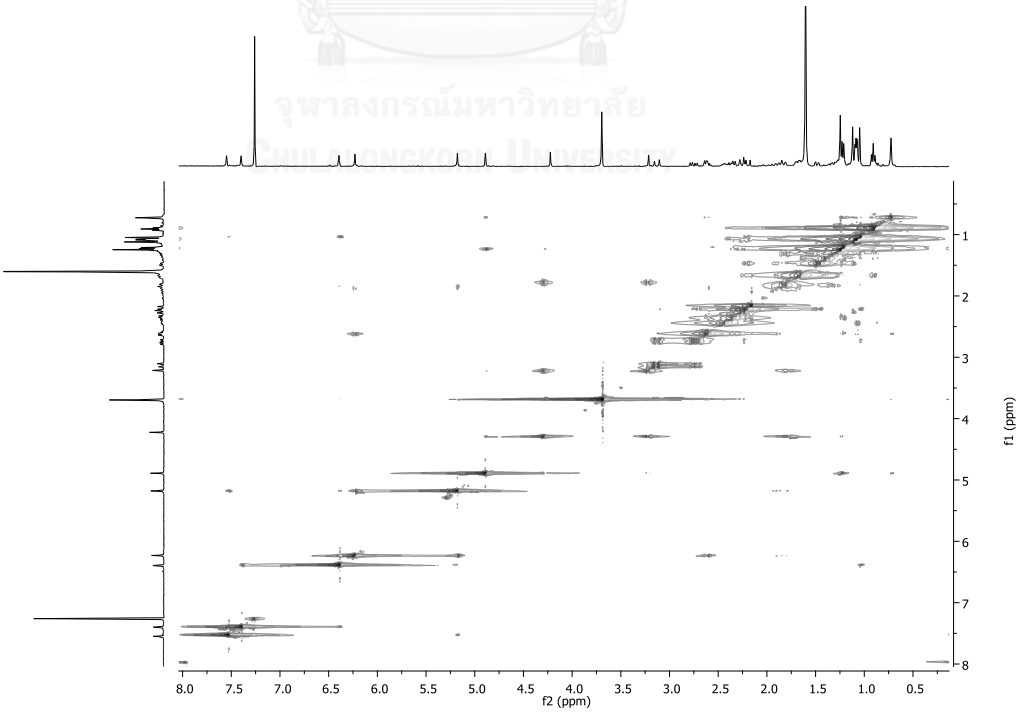

Figure A.20 NOESY spectrum ($CDCl_3$) of compound **44**

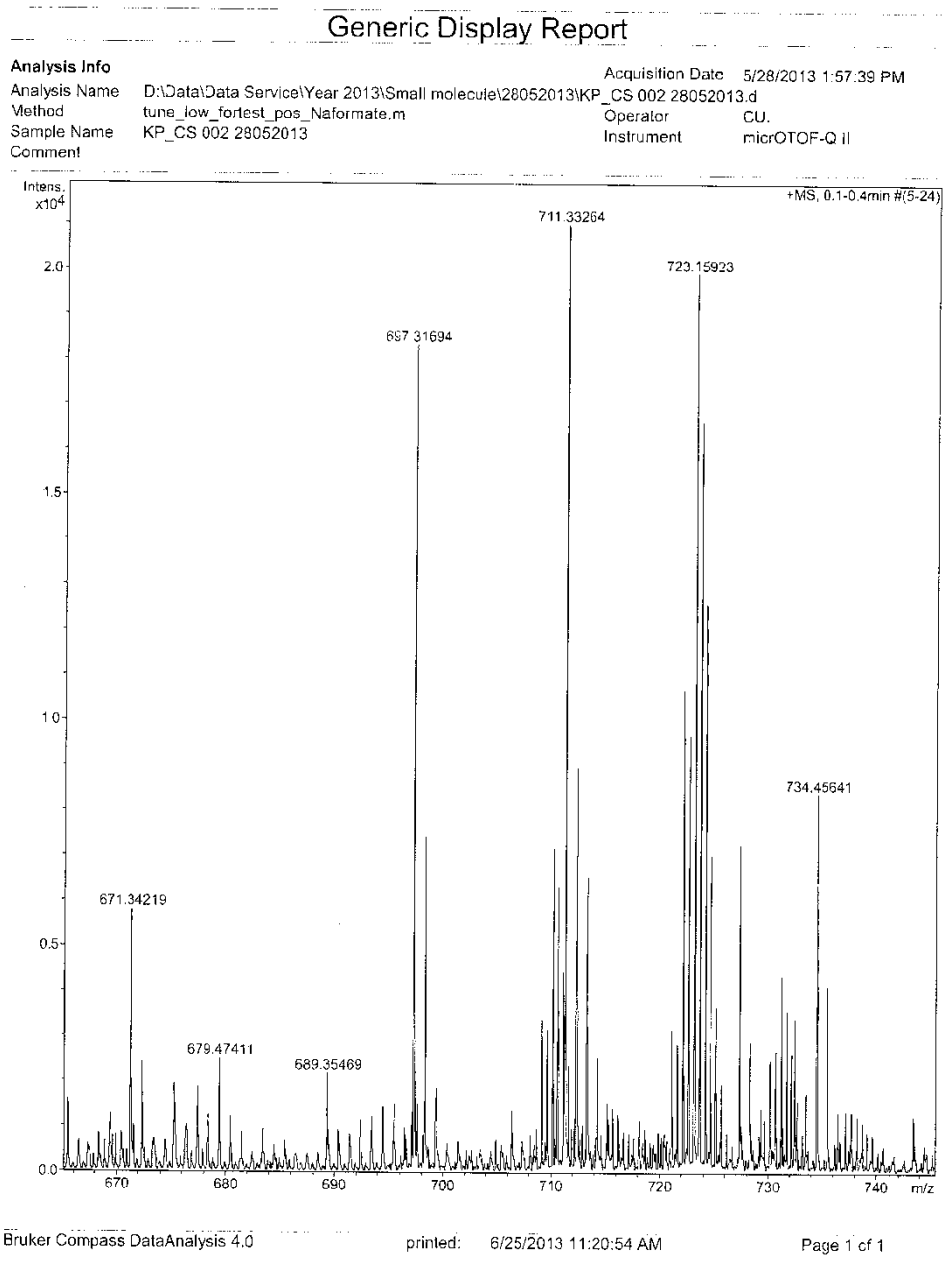

Figure A.21 HRESIMS Mass spectrum of compound **44**

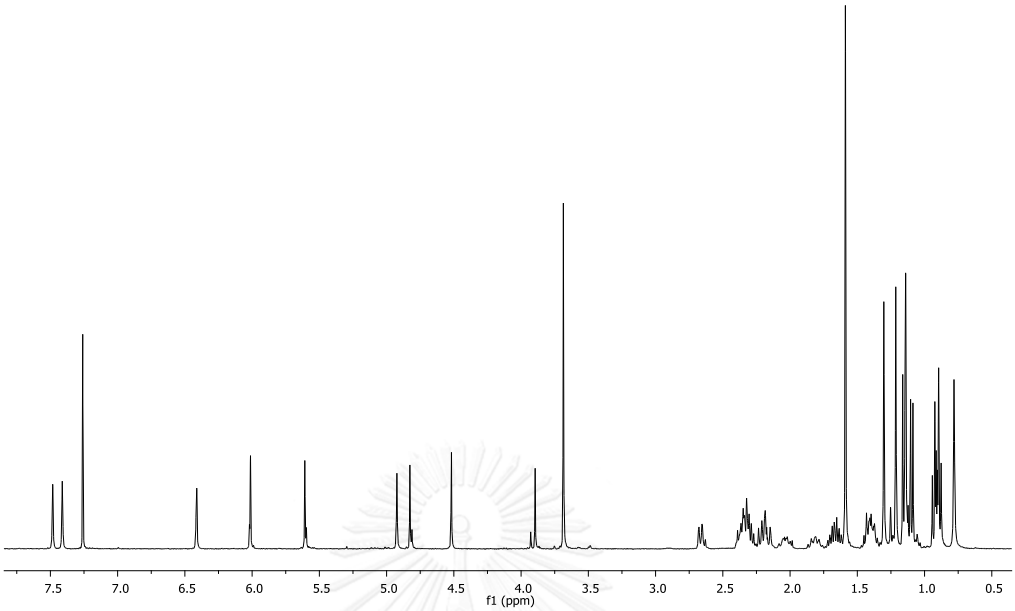

Figure A.22 ^{1}H NMR (400 MHz, $CDCl_3$) spectrum of compound **45**

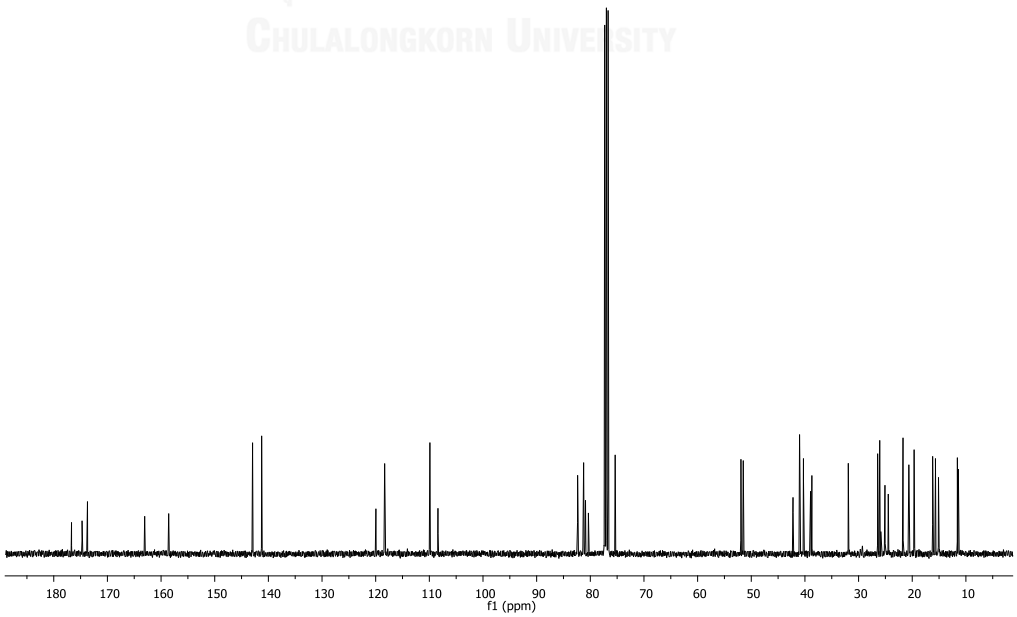

Figure A.23 ^{13}C NMR (100 MHz, $CDCl_3$) spectrum of compound **45**

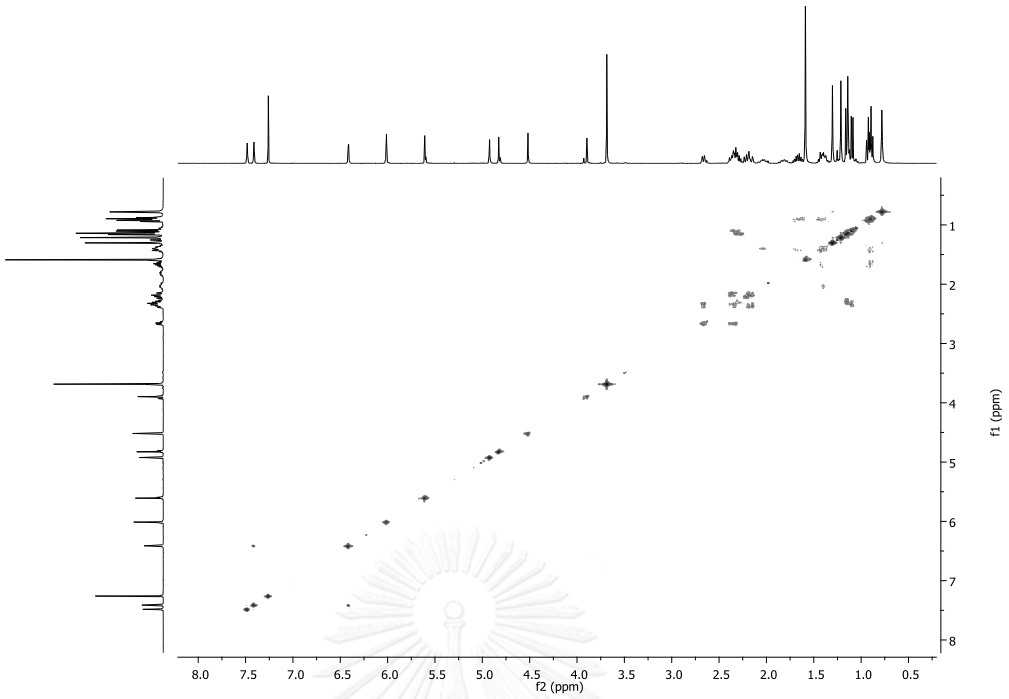

Figure A.24 ^{1}H-^{1}H COSY spectrum ($CDCl_3$) of compound **45**

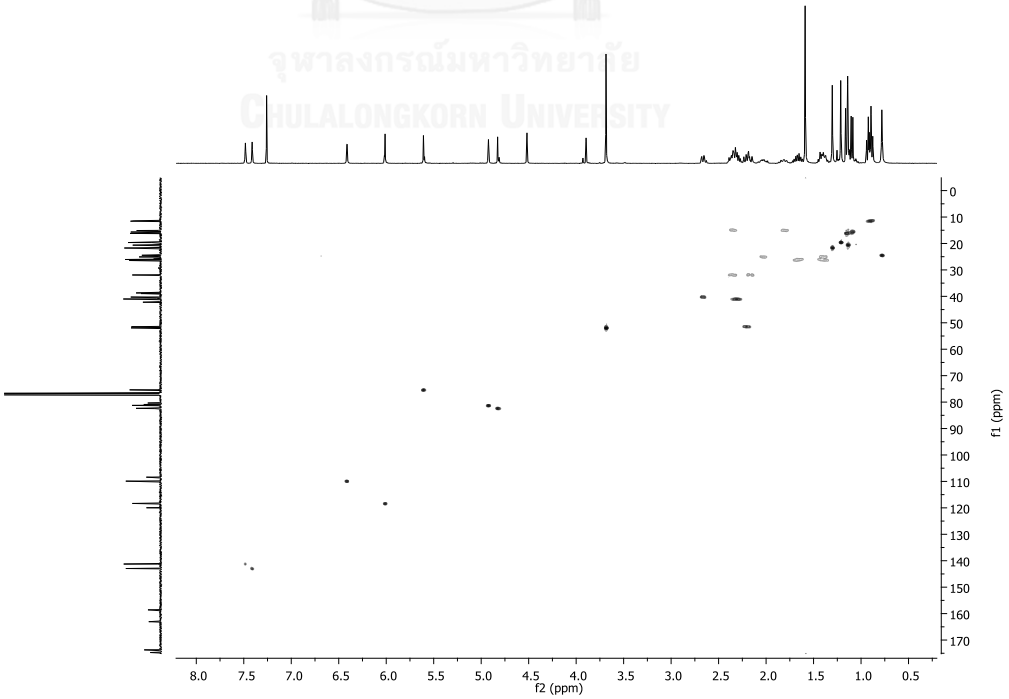

Figure A.25 HSQC spectrum ($CDCl_3$) of compound **45**

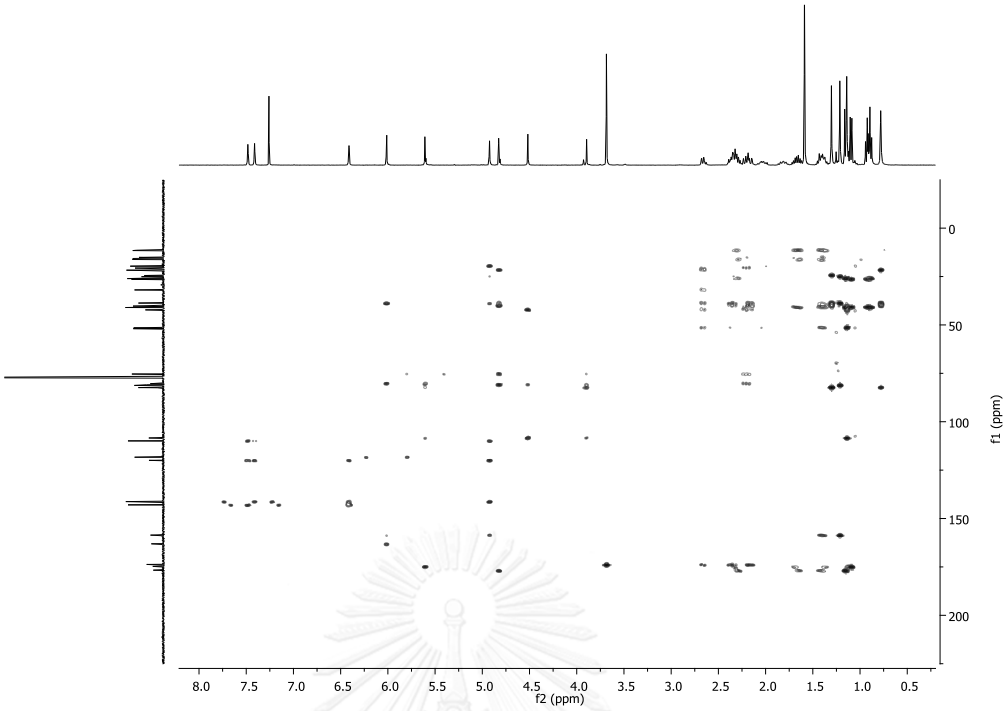

Figure A.26 HMBC spectrum ($CDCl_3$) of compound **45**

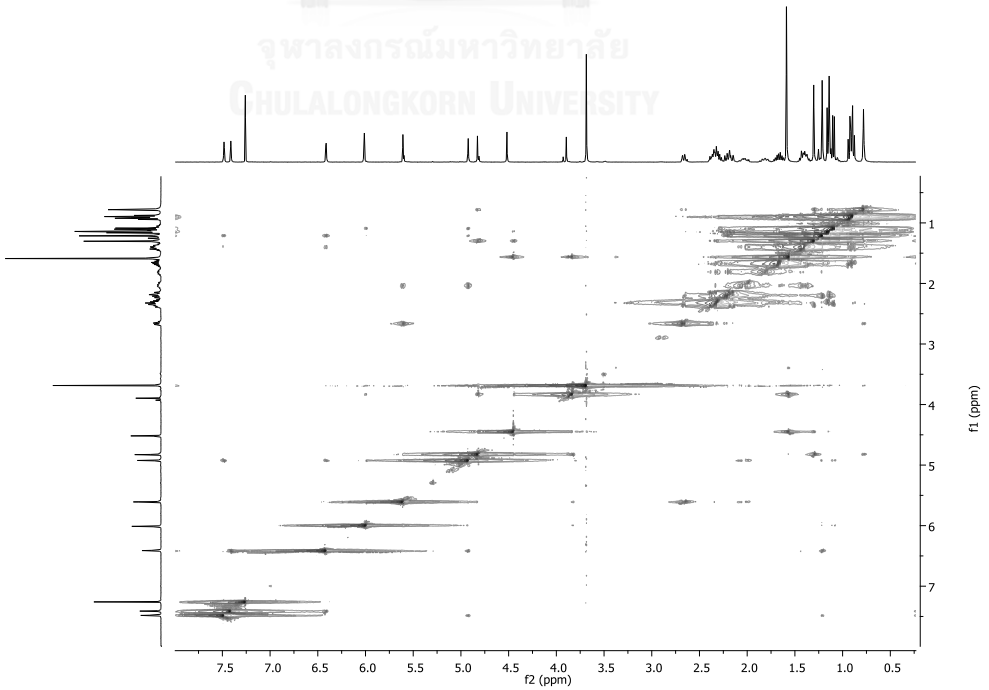

Figure A.27 NOESY spectrum ($CDCl_3$) of compound **45**

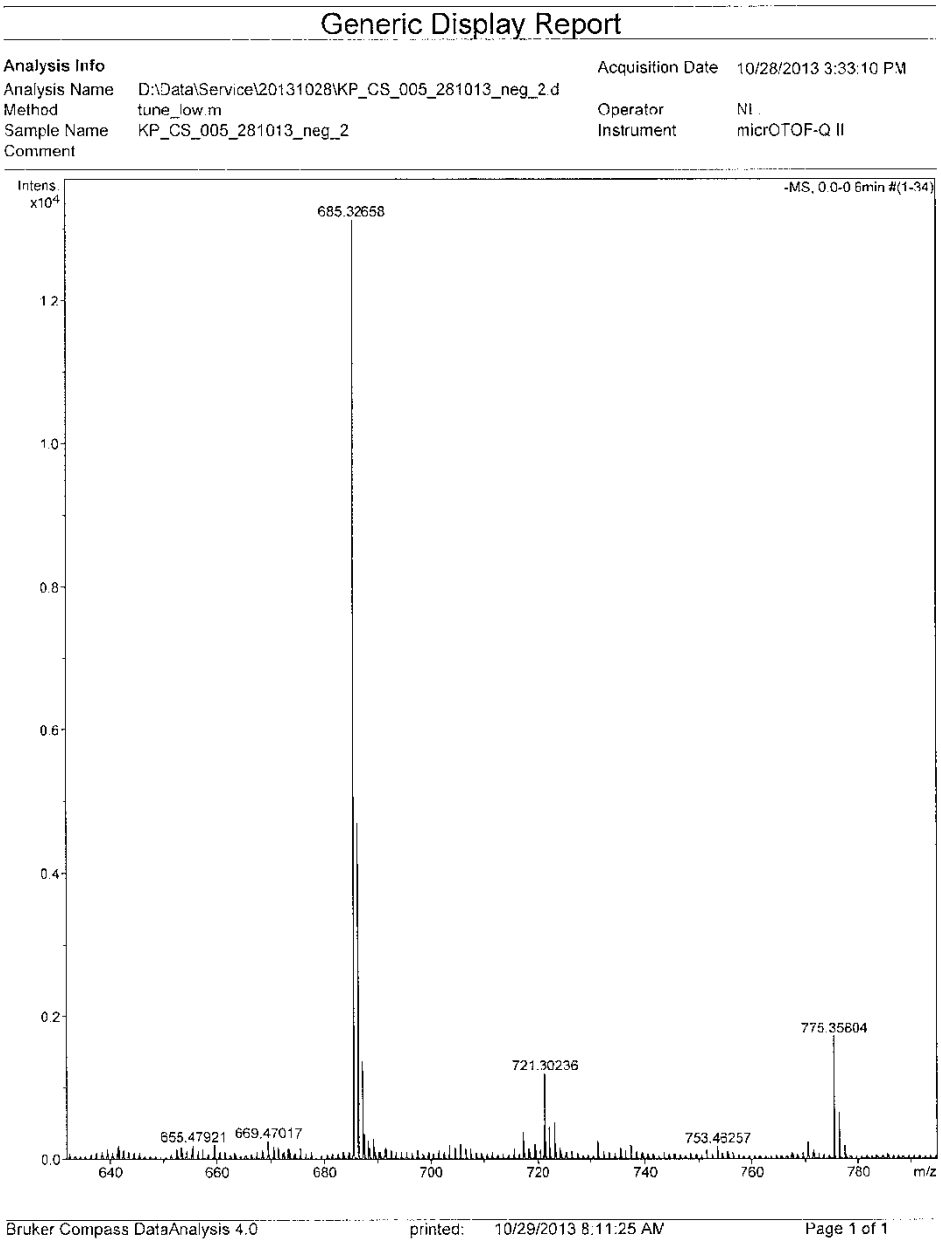

Figure A.28 HRESIMS Mass spectrum of compound **45**

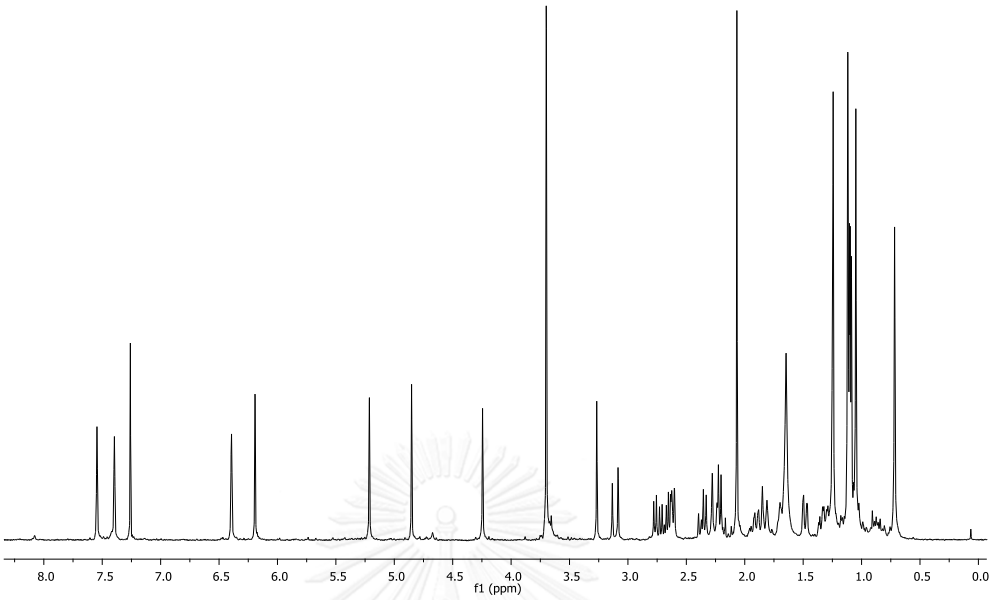

Figure A.29 ^{1}H (400 MHz, $CDCl_3$) NMR spectrum of compound **46**

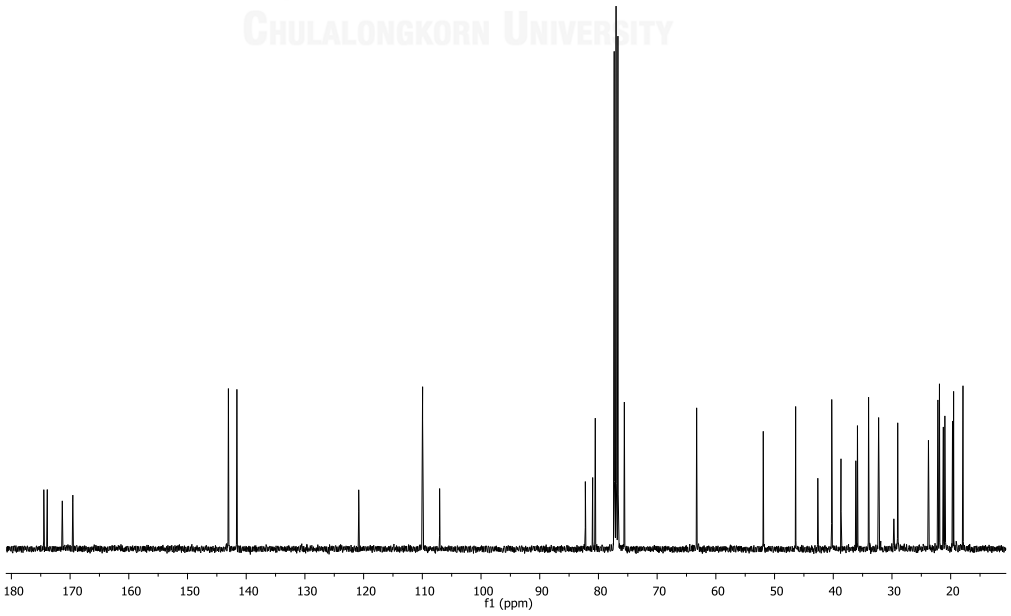

Figure A.30 ^{13}C NMR (100 MHz, $CDCl_3$) NMR spectrum of compound **46**

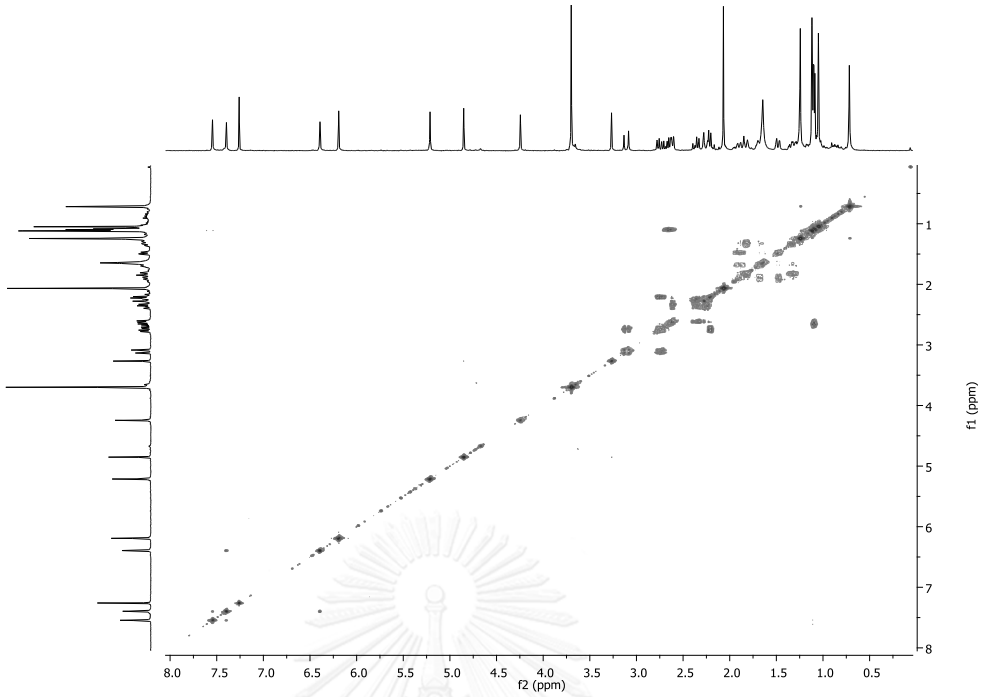

Figure A.31 ^{1}H-^{1}H COSY spectrum ($CDCl_3$) of compound **46**

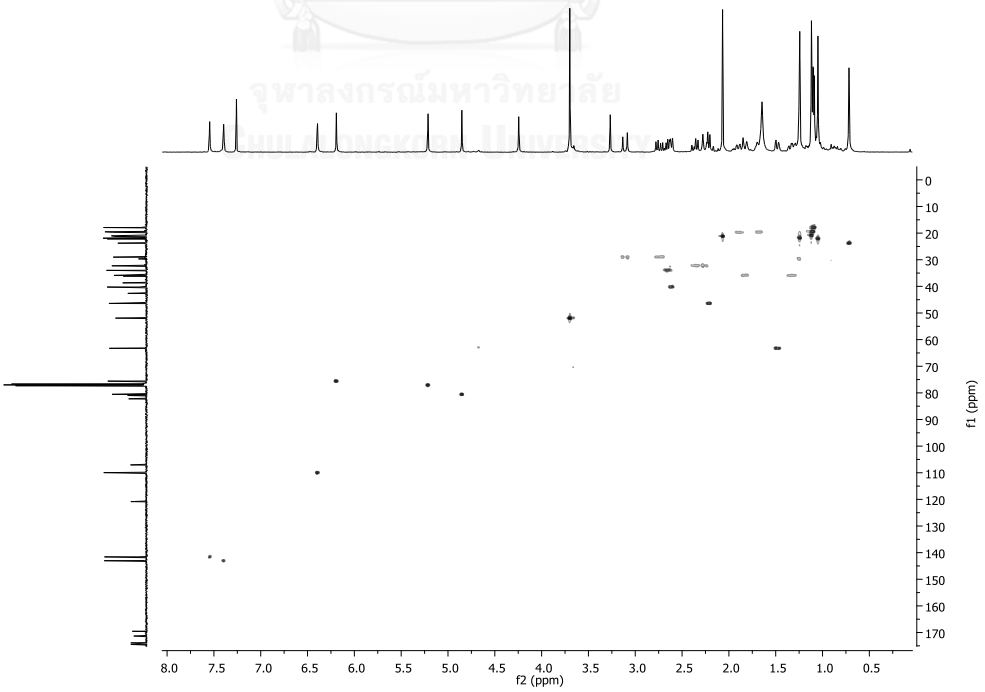

Figure A.32 HSQC spectrum ($CDCl_3$) of compound **46**

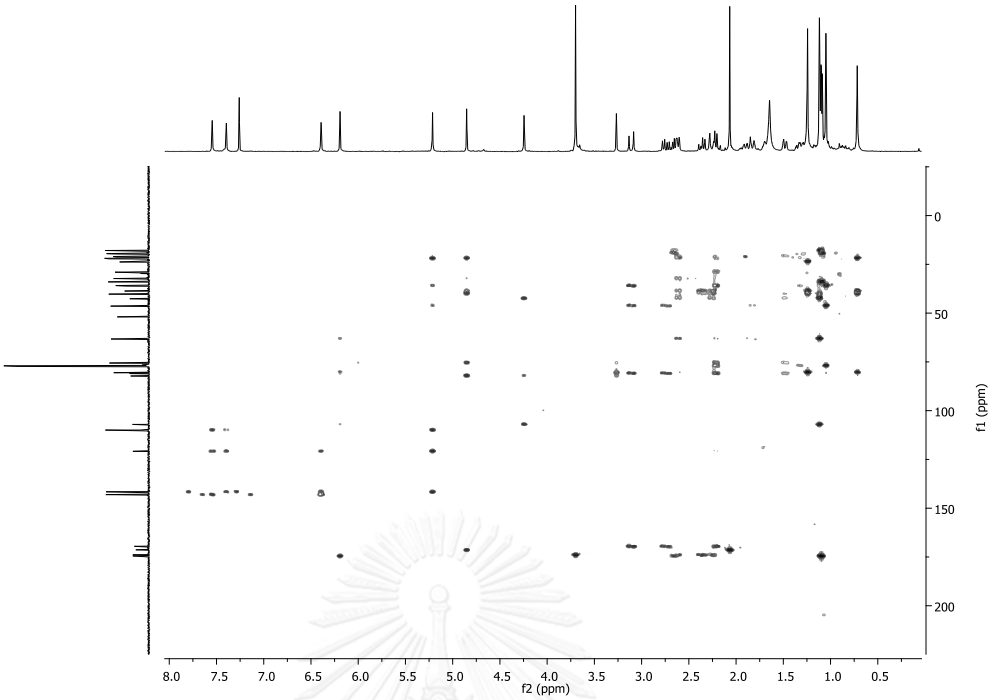

Figure A.33 HMBC spectrum ($CDCl_3$) of compound **46**

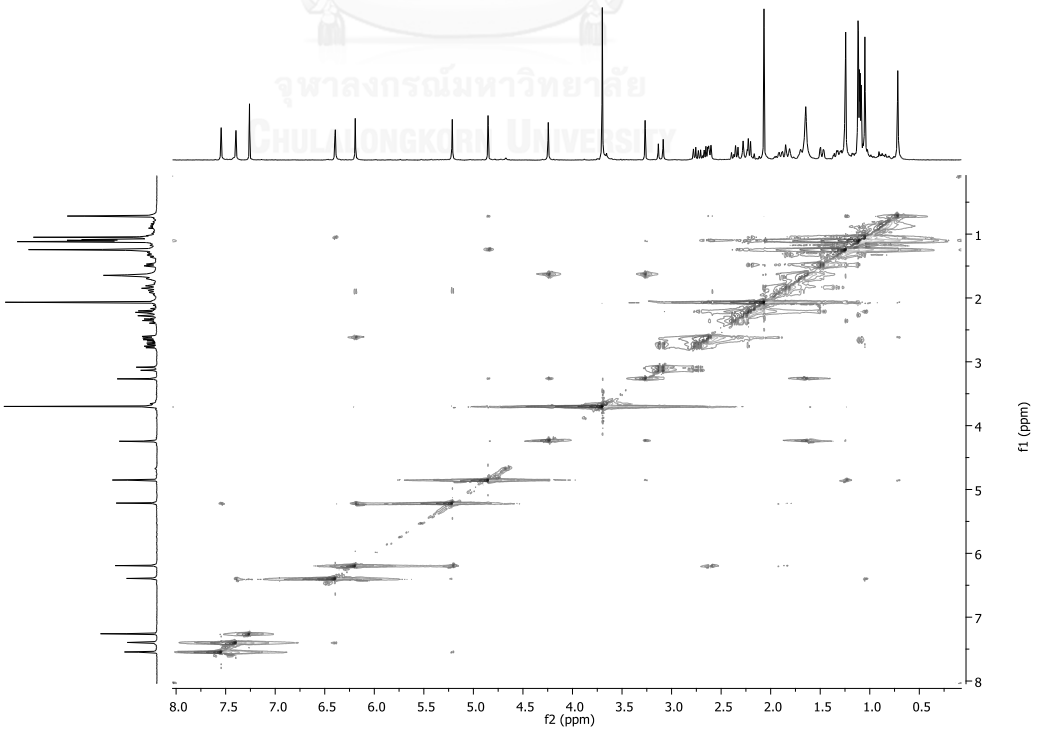

Figure A.34 NOESY spectrum ($CDCl_3$) of compound **46**

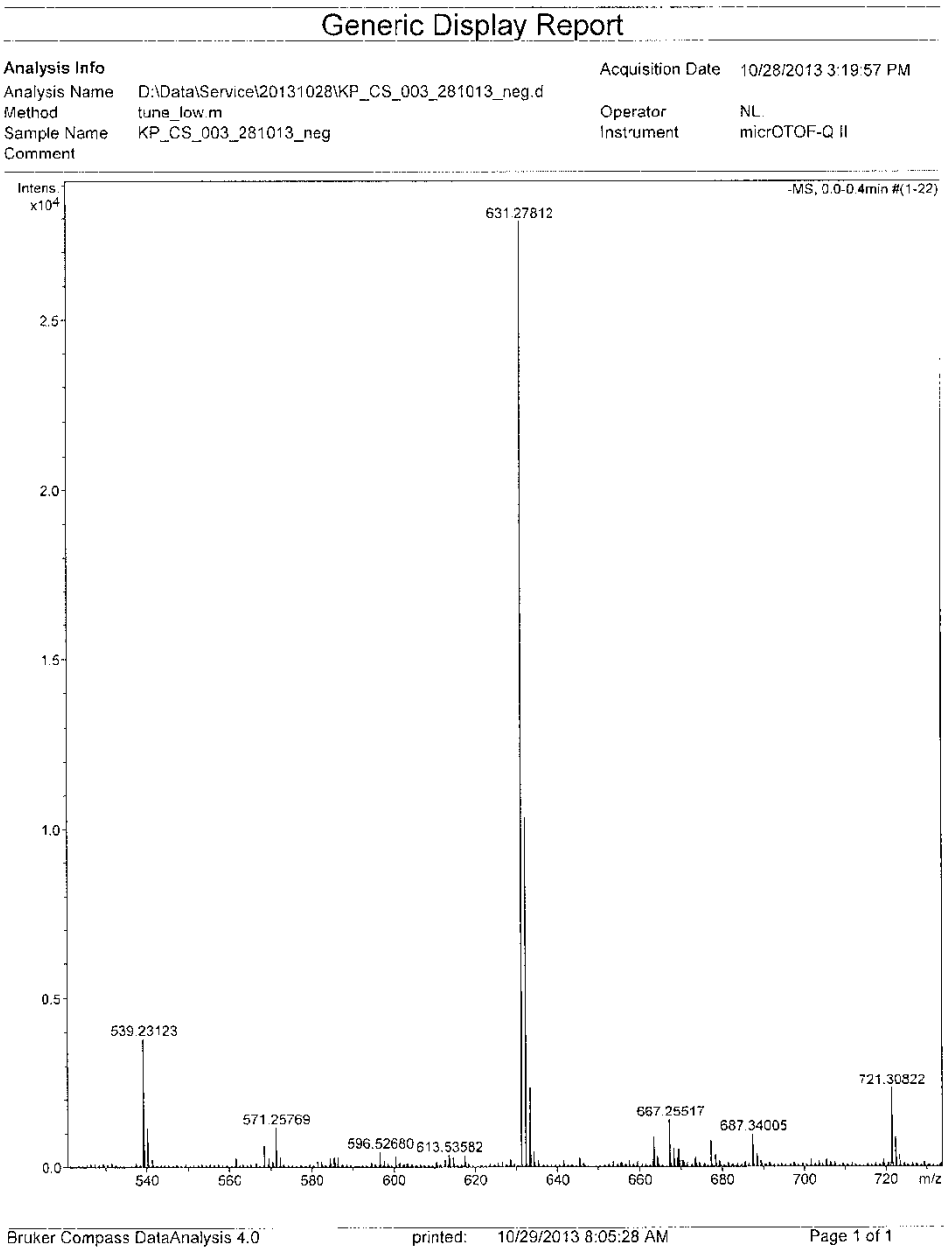

Figure A.35 HRESIMS Mass spectrum of compound **46**

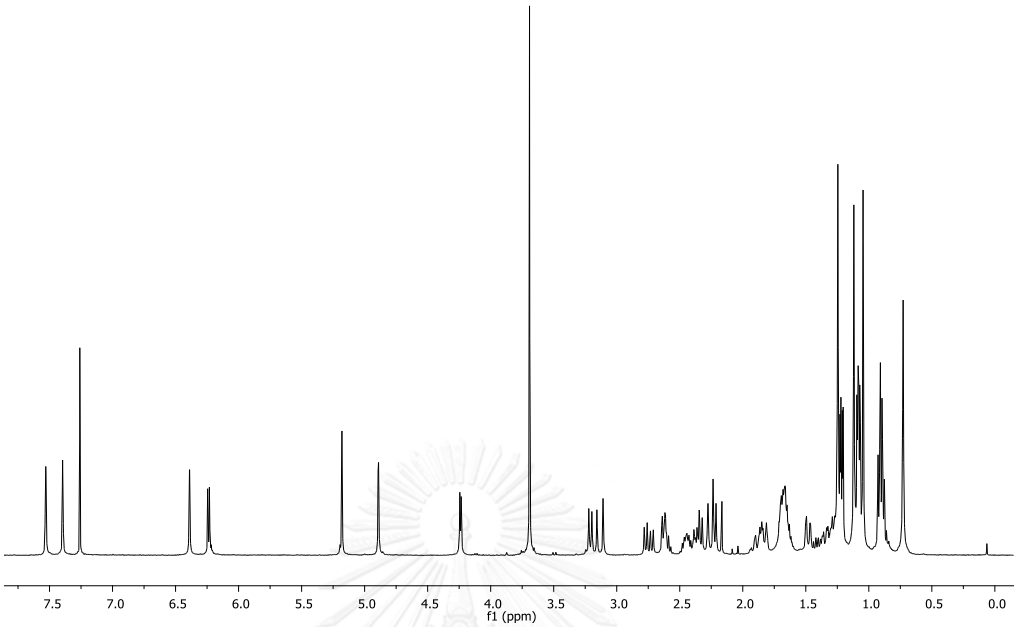

Figure A.36 ^{1}H NMR (400 MHz, $CDCl_3$) spectrum of compound **47**

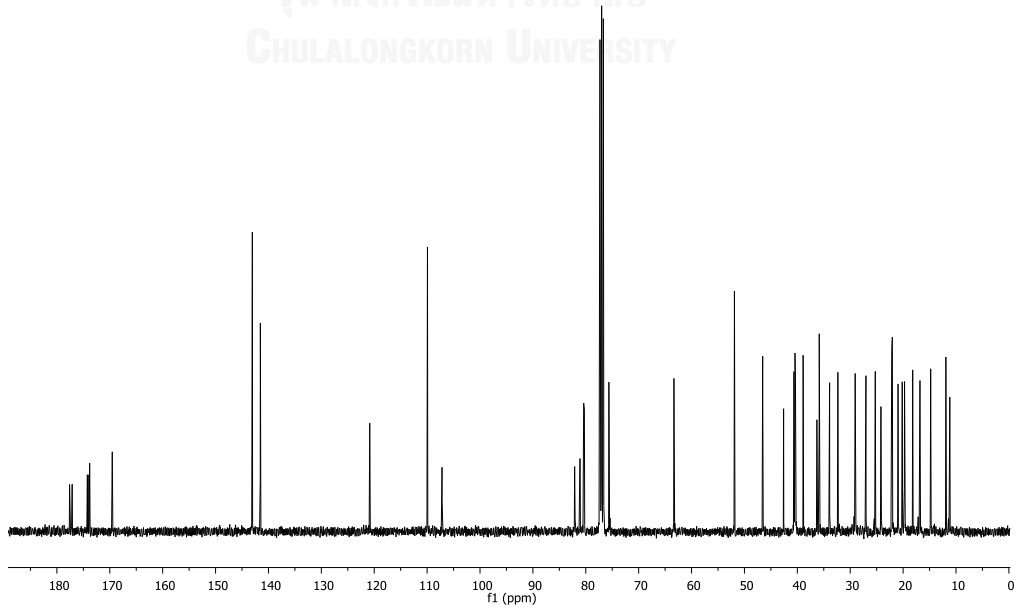

Figure A.37 ^{13}C NMR (100 MHz, $CDCl_3$) spectrum of compound **47**

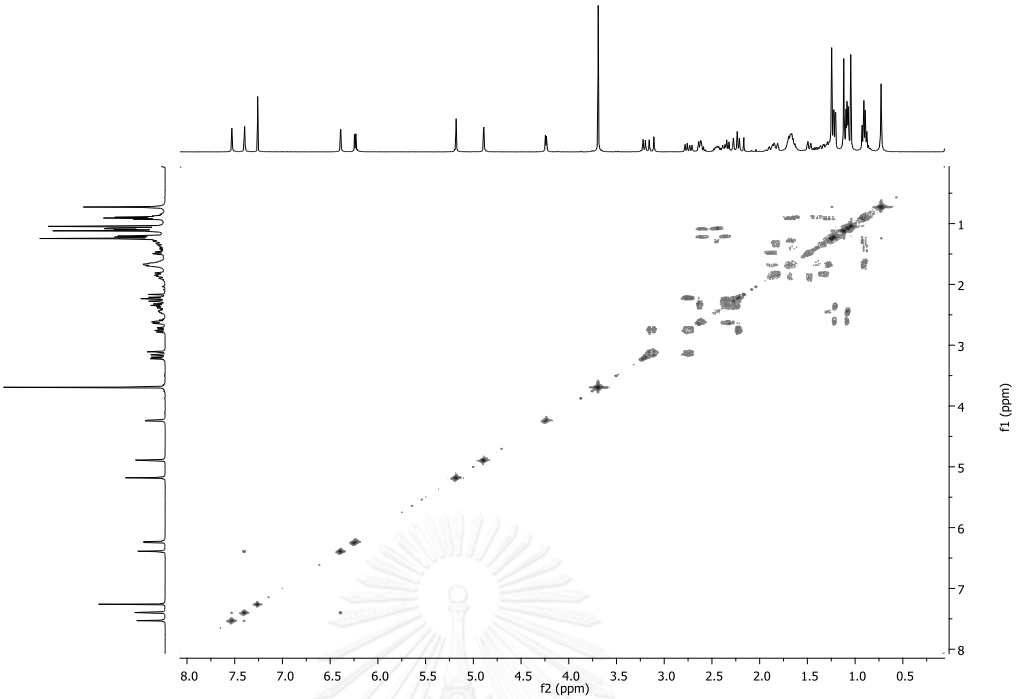

Figure A.38 ^{1}H-^{1}H COSY spectrum ($CDCl_3$) of compound **47**

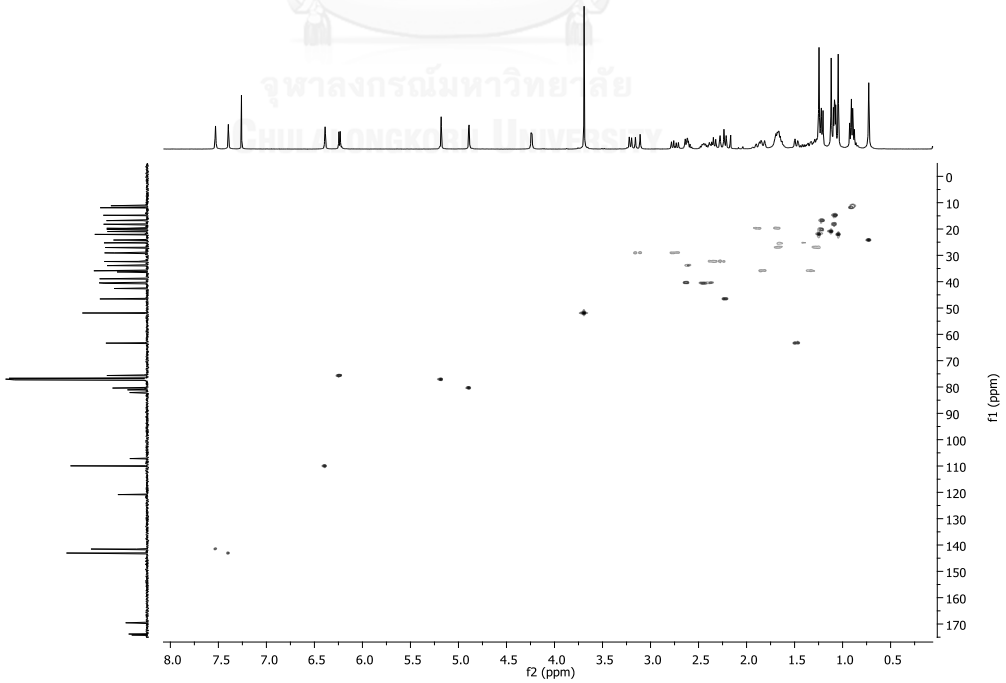

Figure A.39 HSQC spectrum ($CDCl_3$) of compound **47**

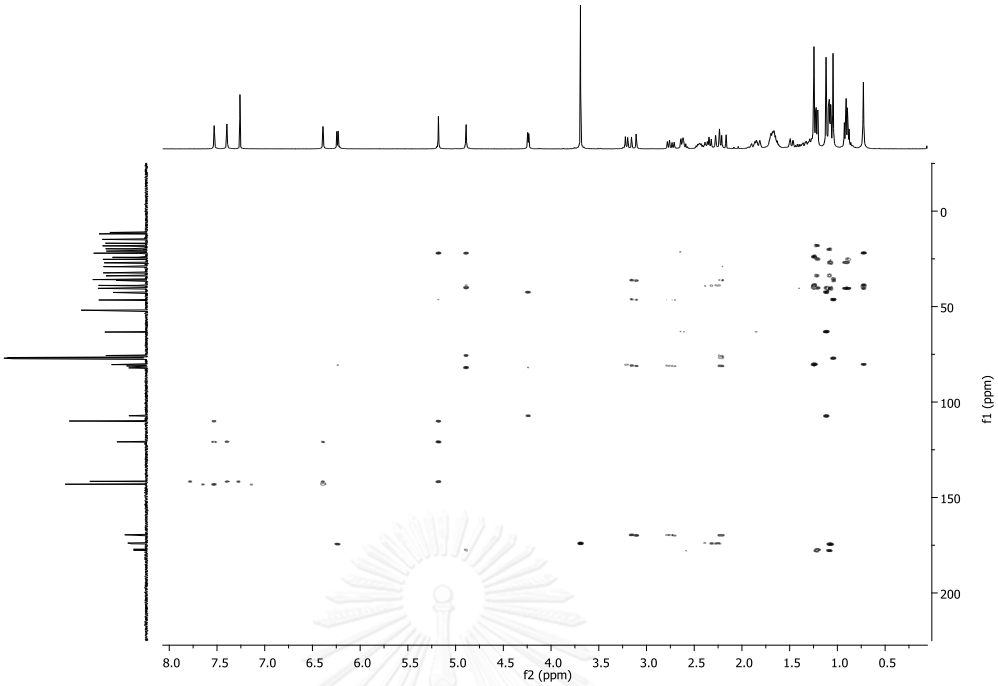

Figure A.40 HMBC spectrum ($CDCl_3$) of compound **47**

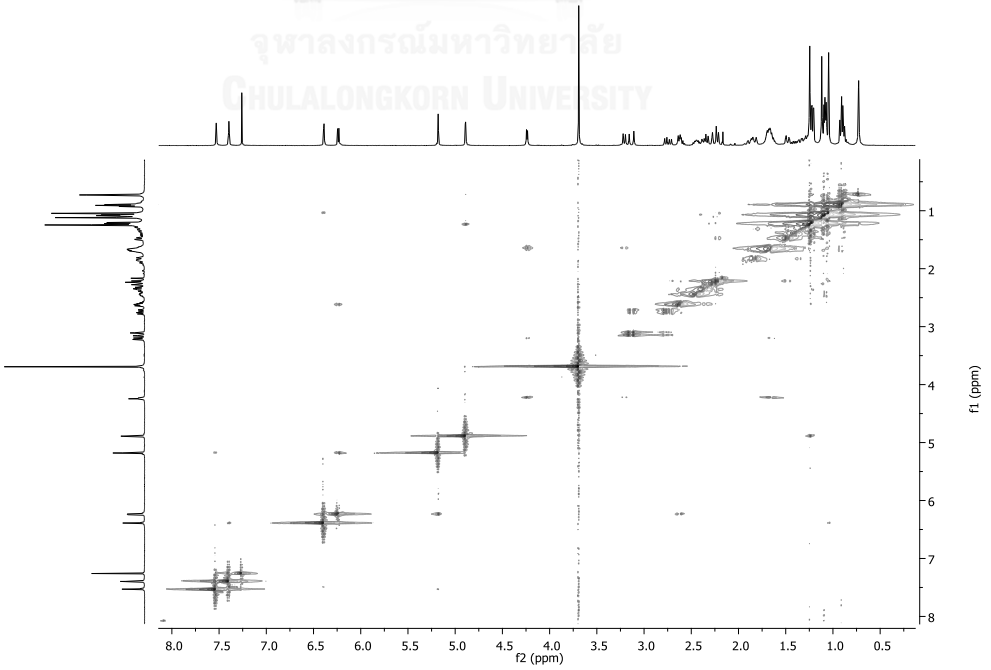

Figure A.41 NOESY spectrum ($CDCl_3$) of compound **47**

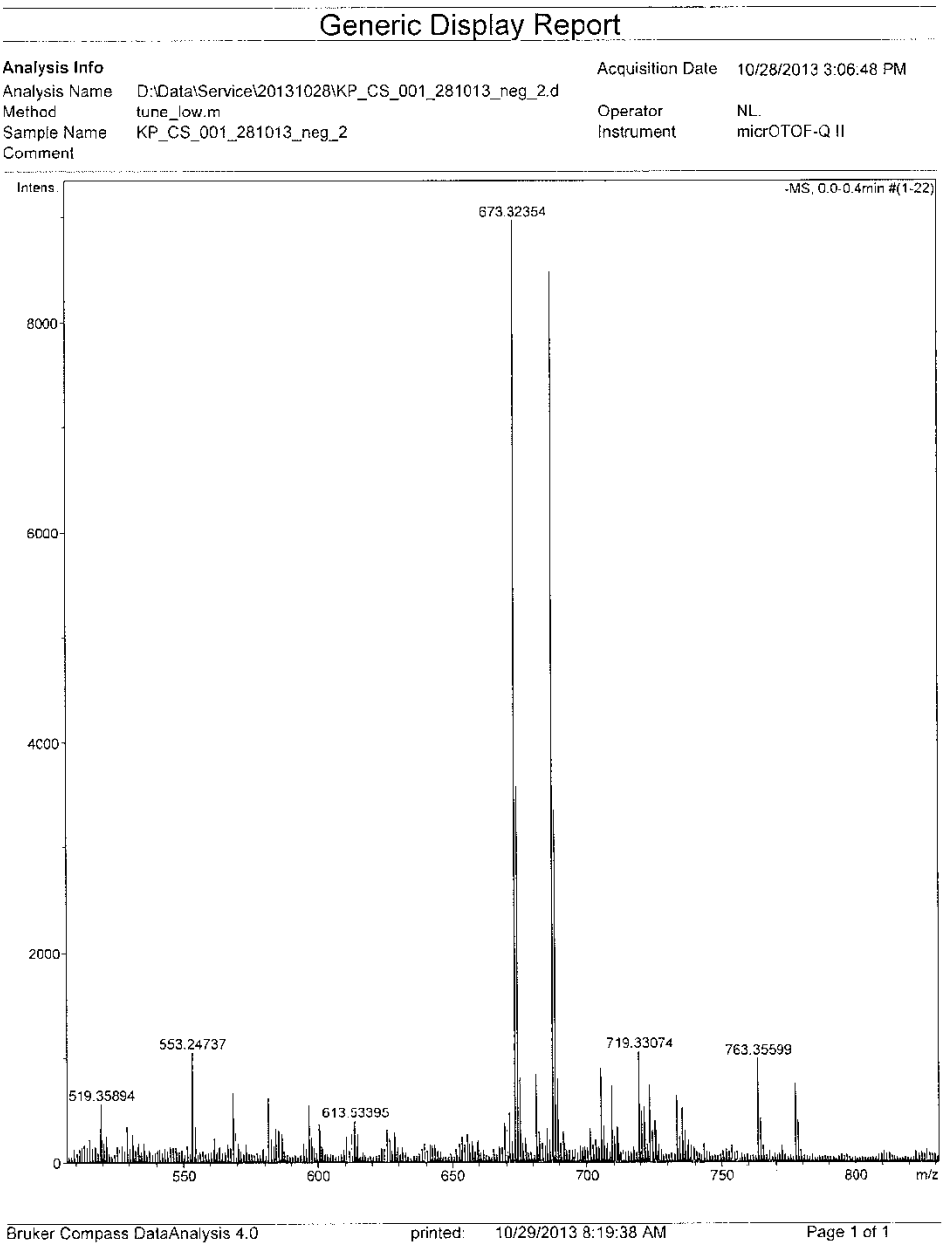

Figure A.42 HRESIMS Mass spectrum of compound **47**

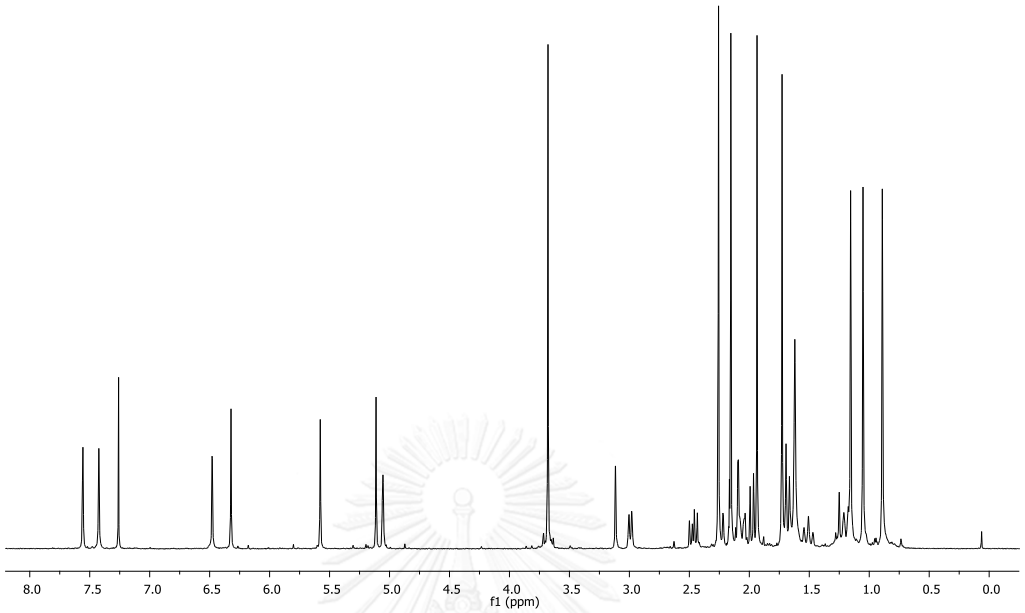

Figure A.43 ^{1}H NMR (400 MHz, $CDCl_3$) spectrum of compound **48**

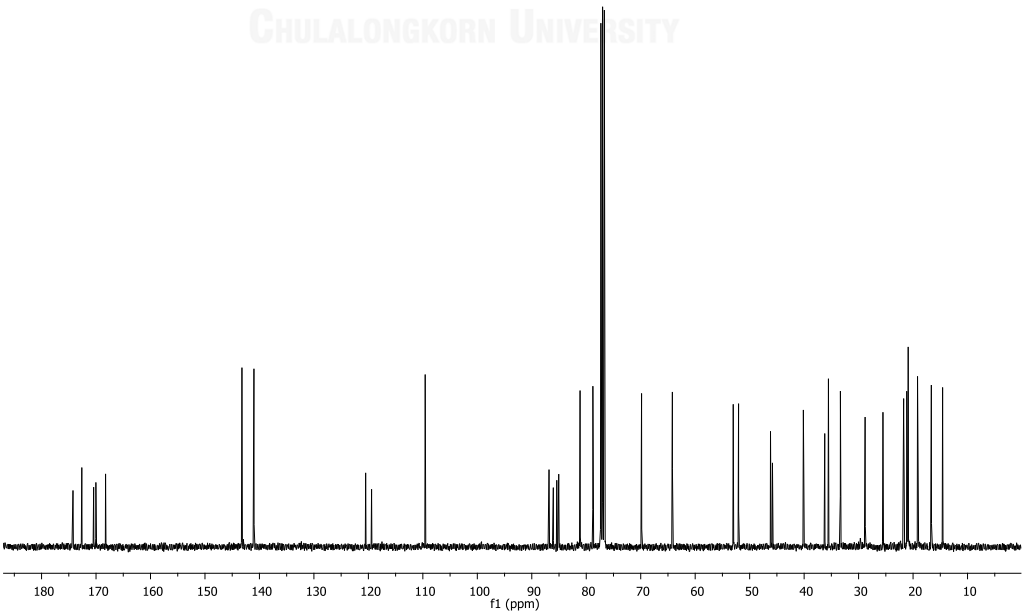

Figure A.44 ^{13}C NMR (100 MHz, $CDCl_3$) spectrum of compound **48**

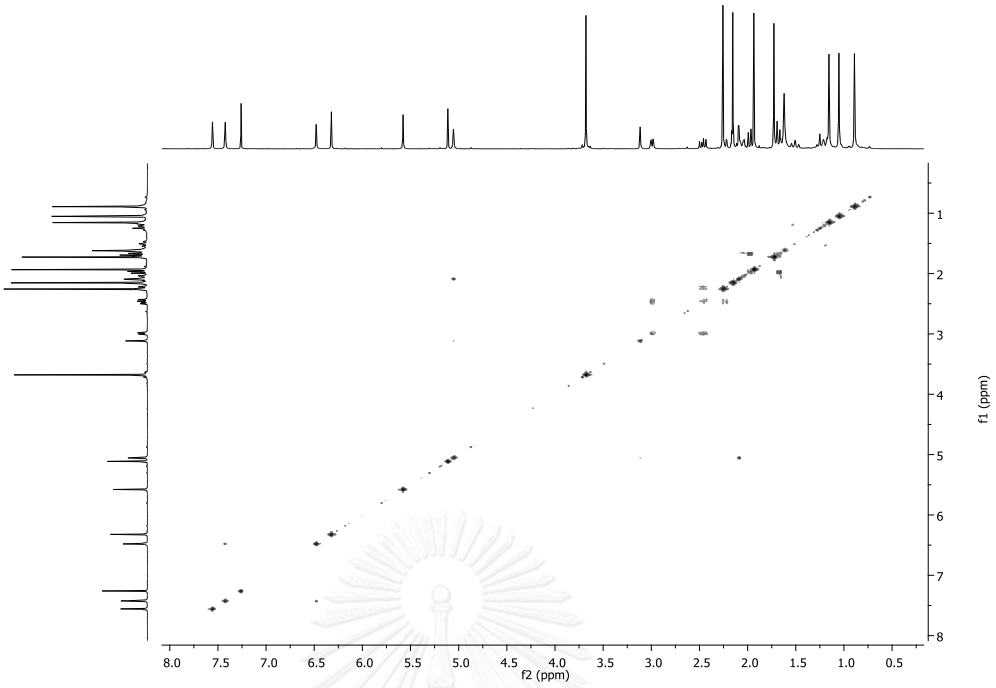

Figure A.45 ^{1}H-^{1}H COSY spectrum ($CDCl_3$) of compound **48**

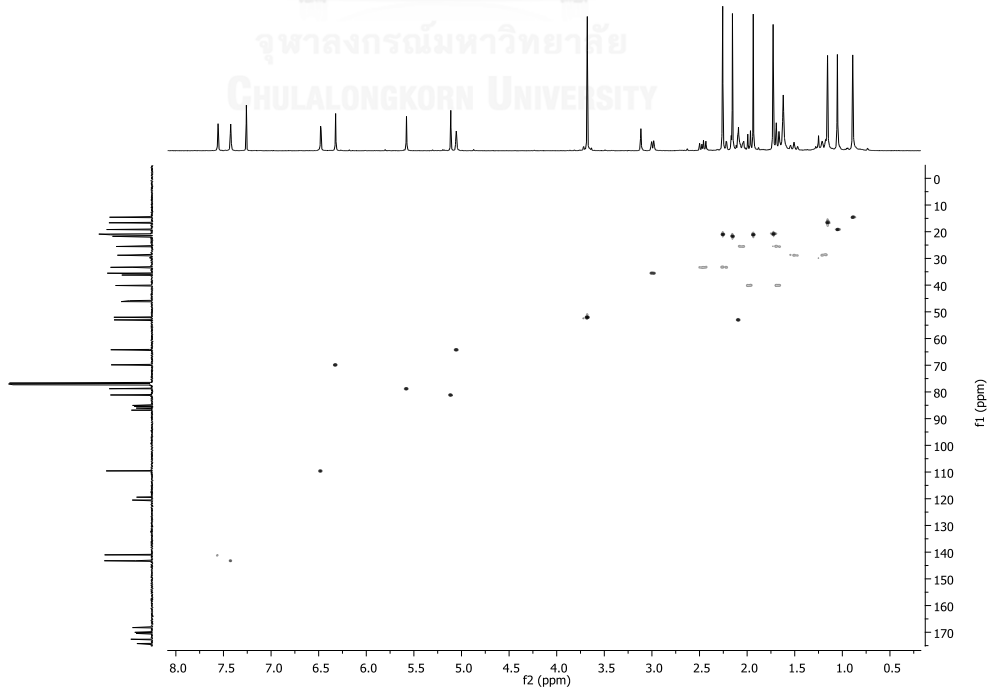

Figure A.46 HSQC spectrum ($CDCl_3$) of compound **48**

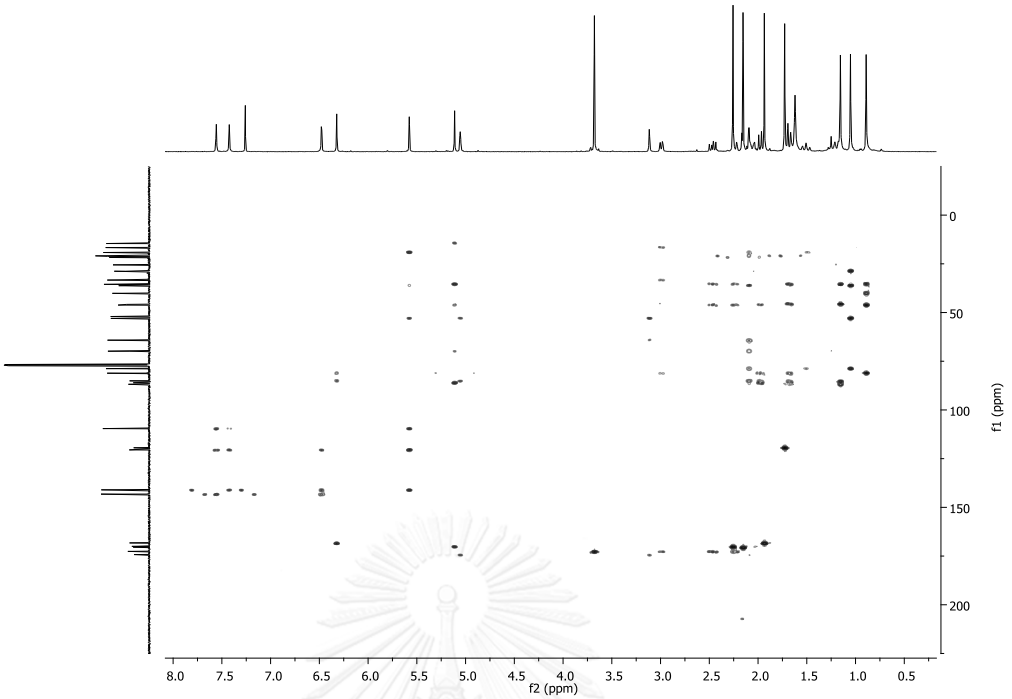

Figure A.47 HMBC spectrum ($CDCl_3$) of compound **48**

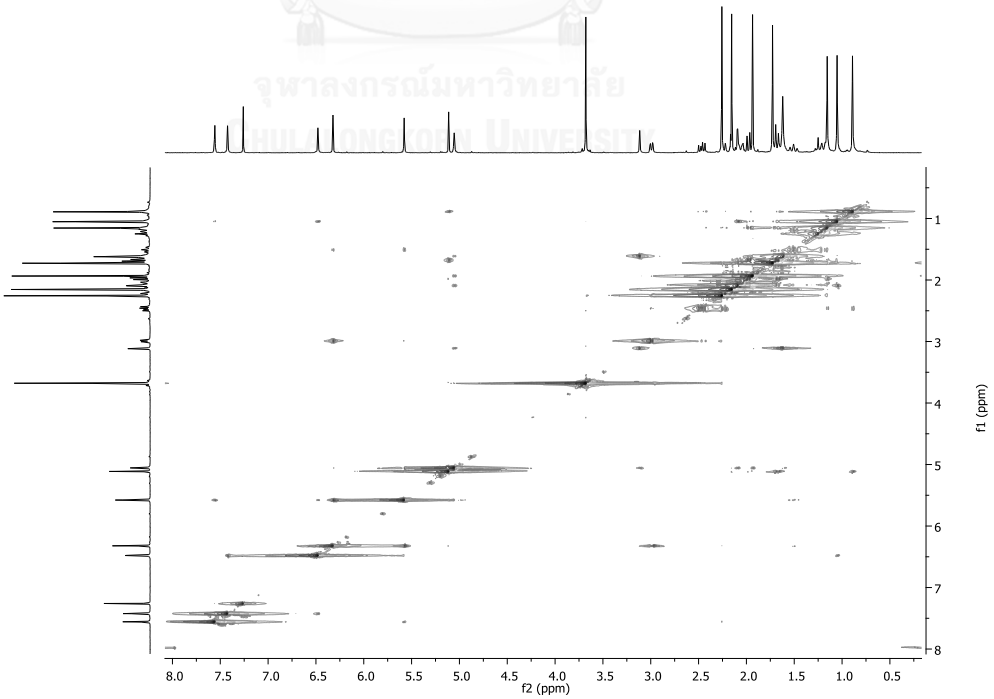

Figure A.48 NOESY spectrum ($CDCl_3$) of compound **48**

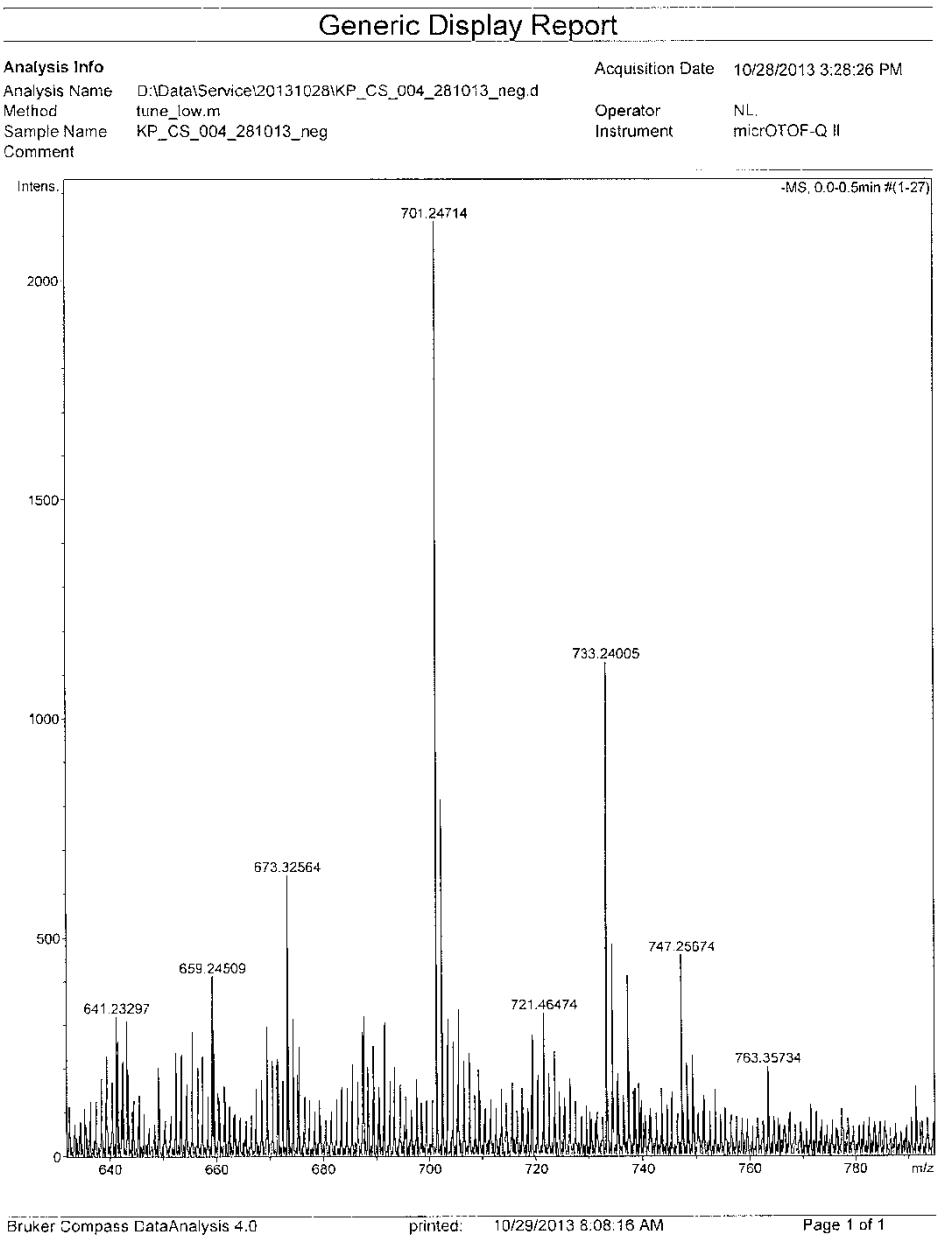

Figure A.49 HRESIMS Mass spectrum of compound **48**

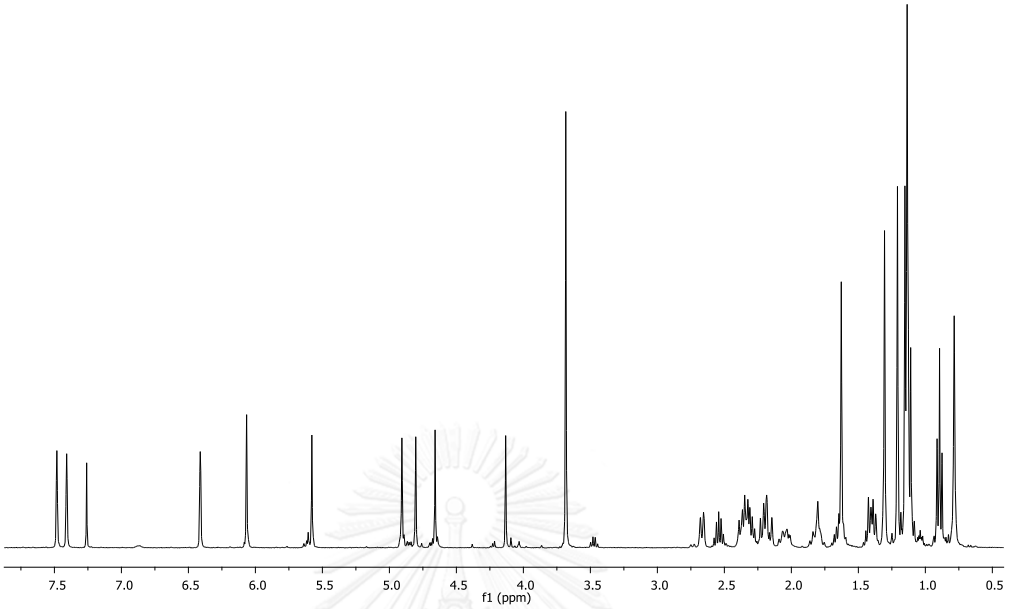

Figure A.50 ^{1}H NMR (400 MHz, $CDCl_3$) spectrum of compound **49**

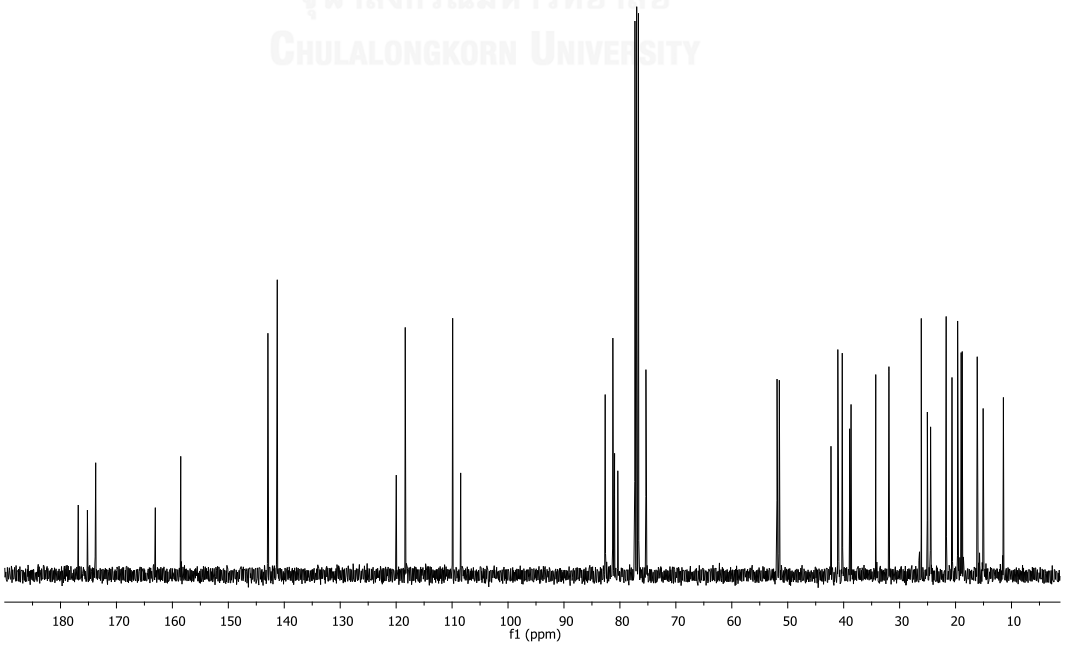

Figure A.51 ^{13}C NMR (100 MHz, $CDCl_3$) spectrum of compound **49**

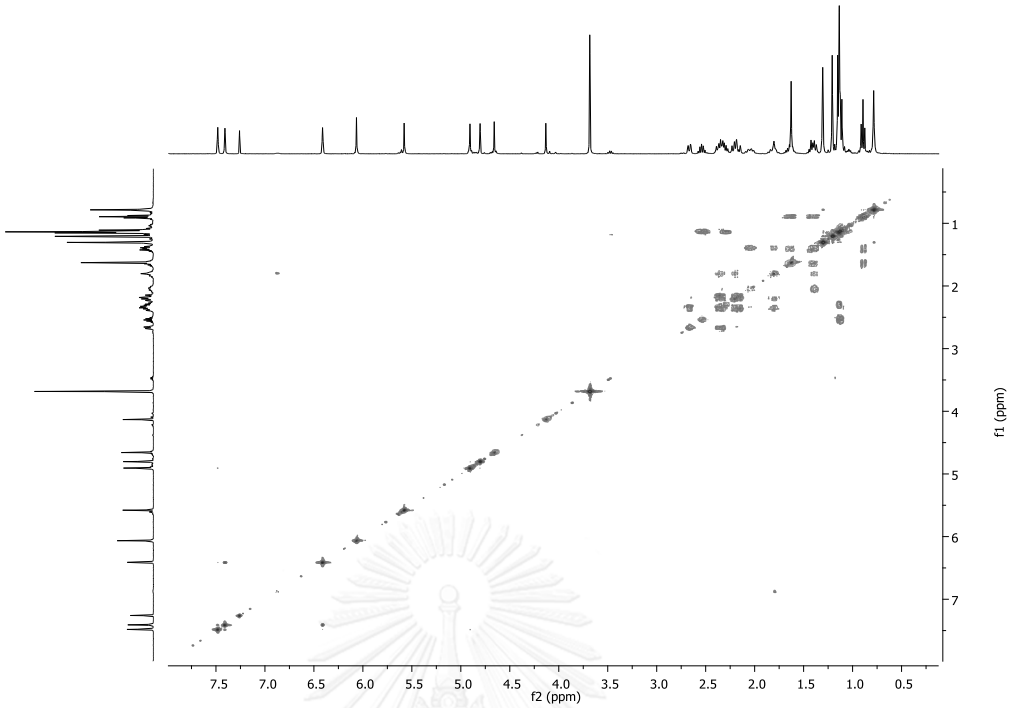

Figure A.52 ^{1}H-^{1}H COSY spectrum ($CDCl_3$) of compound **49**

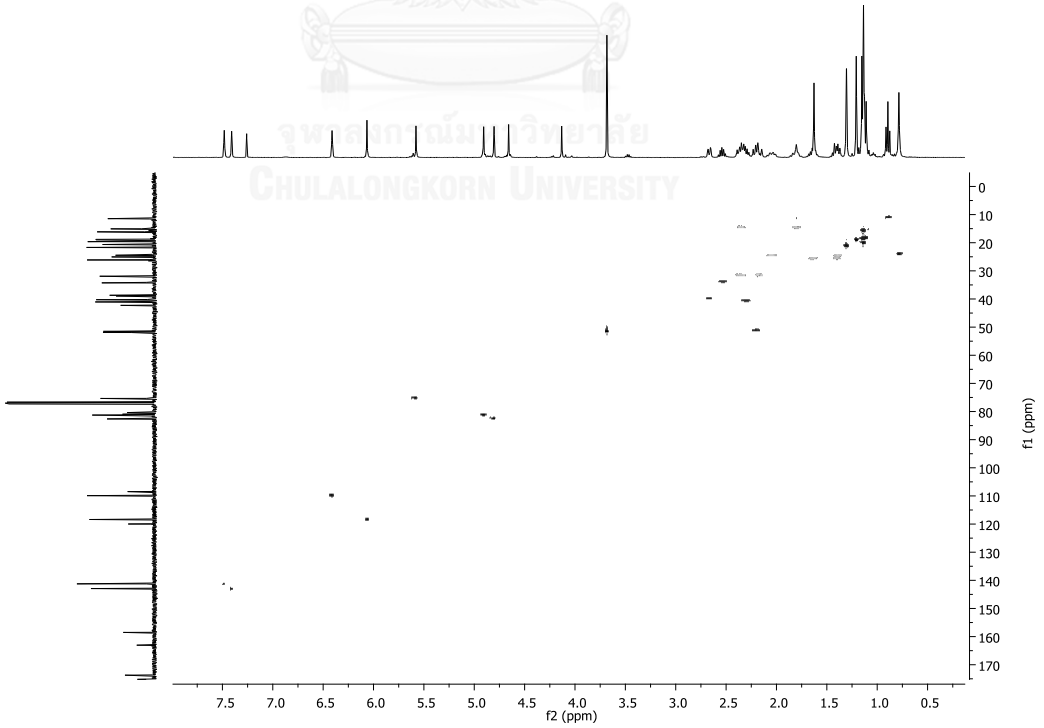

Figure A.53 HSQC spectrum ($CDCl_3$) of compound **49**

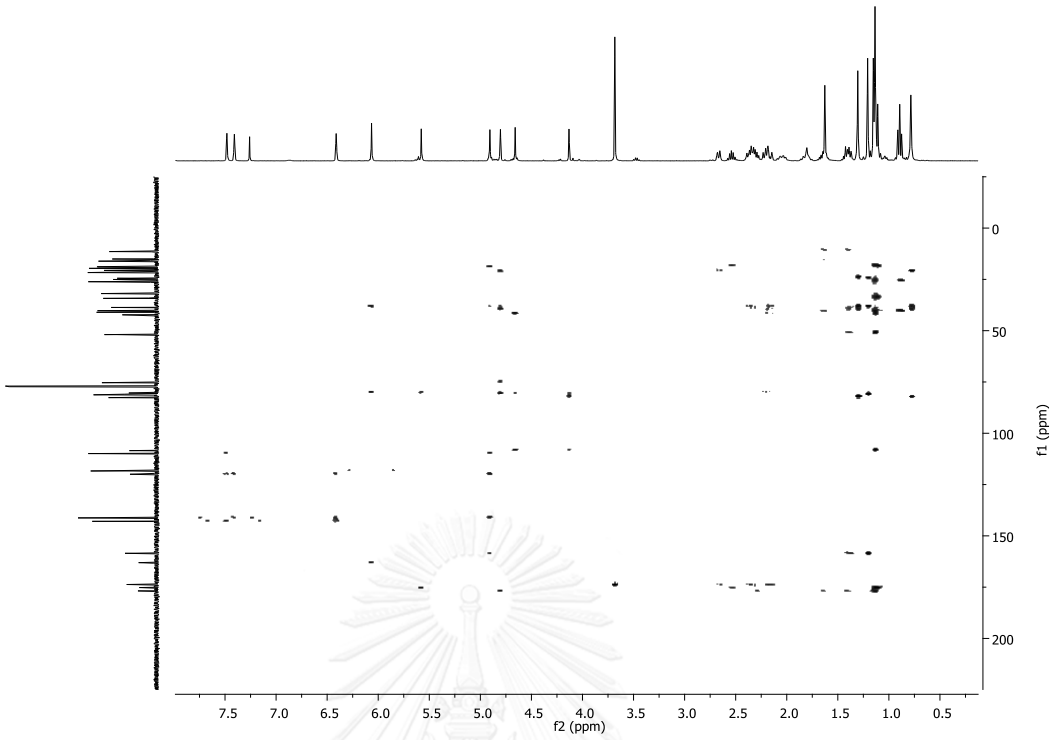

Figure A.54 HMBC spectrum ($CDCl_3$) of compound **49**

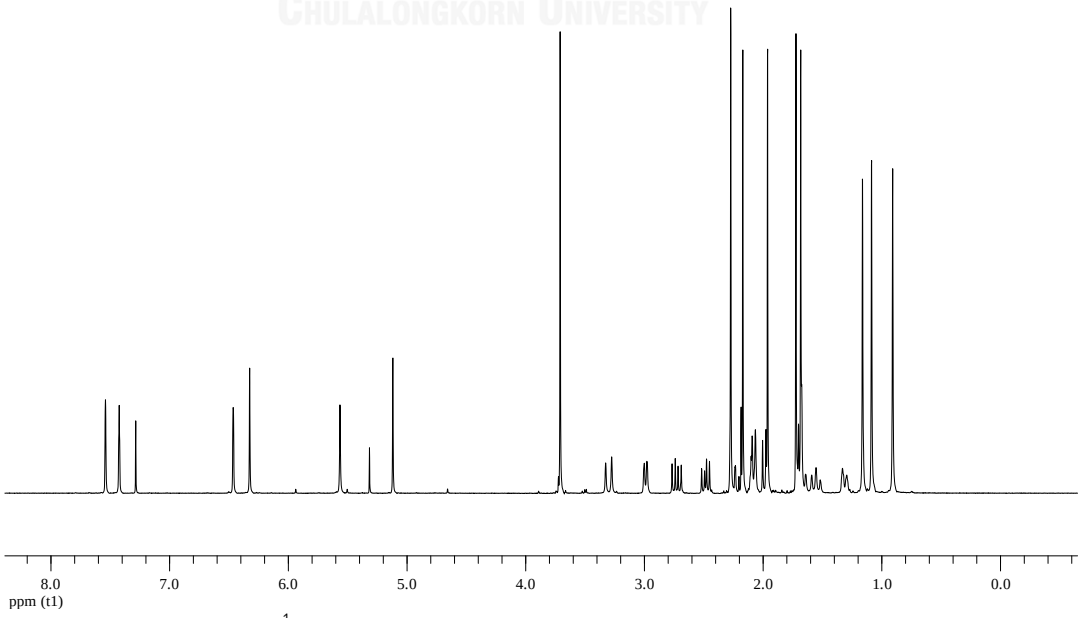

Figure A.55 ^{1}H NMR (400 MHz, $CDCl_3$) spectrum of compound **50**

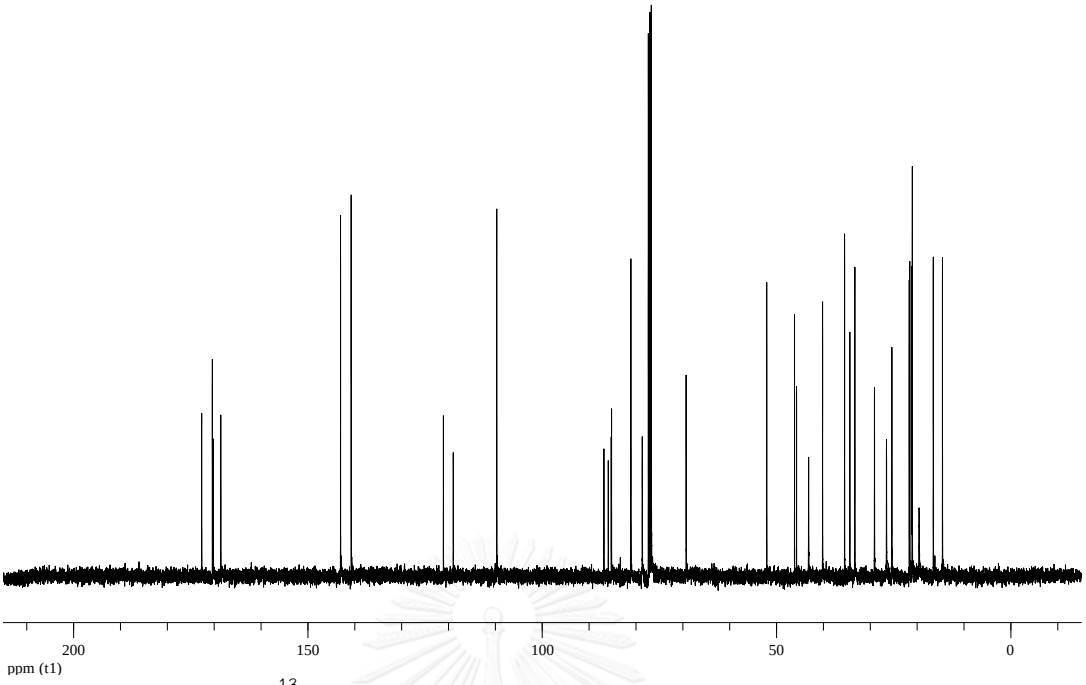

Figure A.56 ^{13}C NMR (100 MHz, $CDCl_3$) spectrum of compound **50**

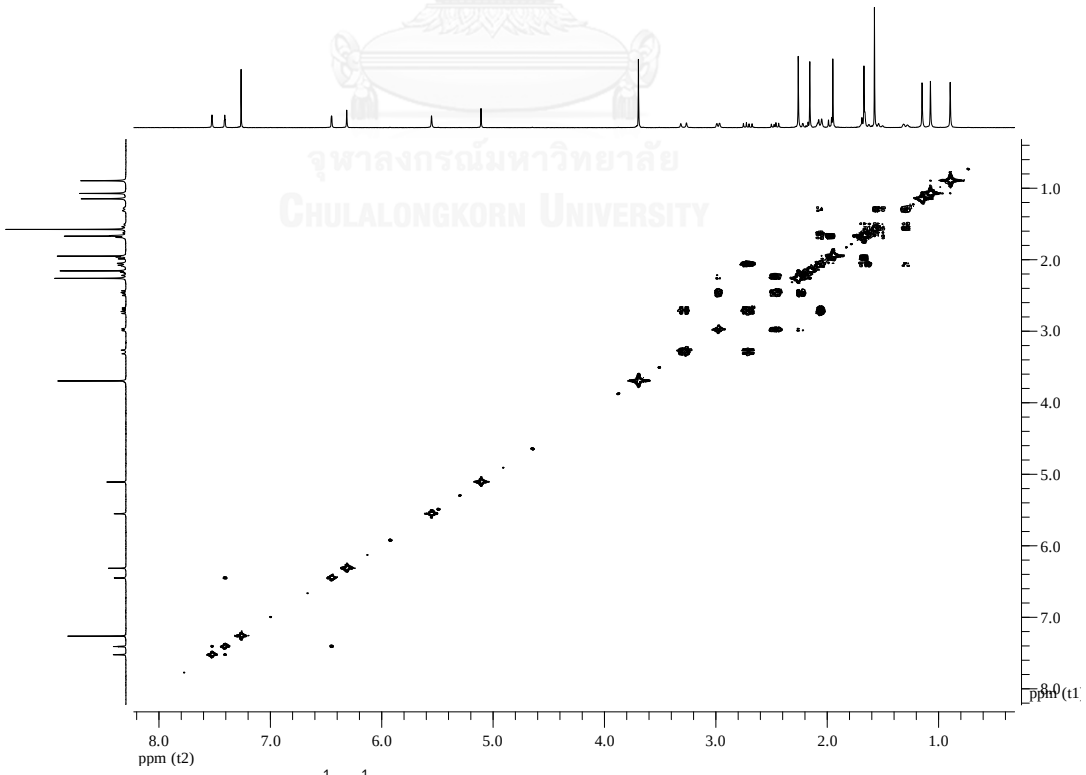

Figure A.57 ^{1}H-^{1}H COSY spectrum ($CDCl_3$) of compound **50**

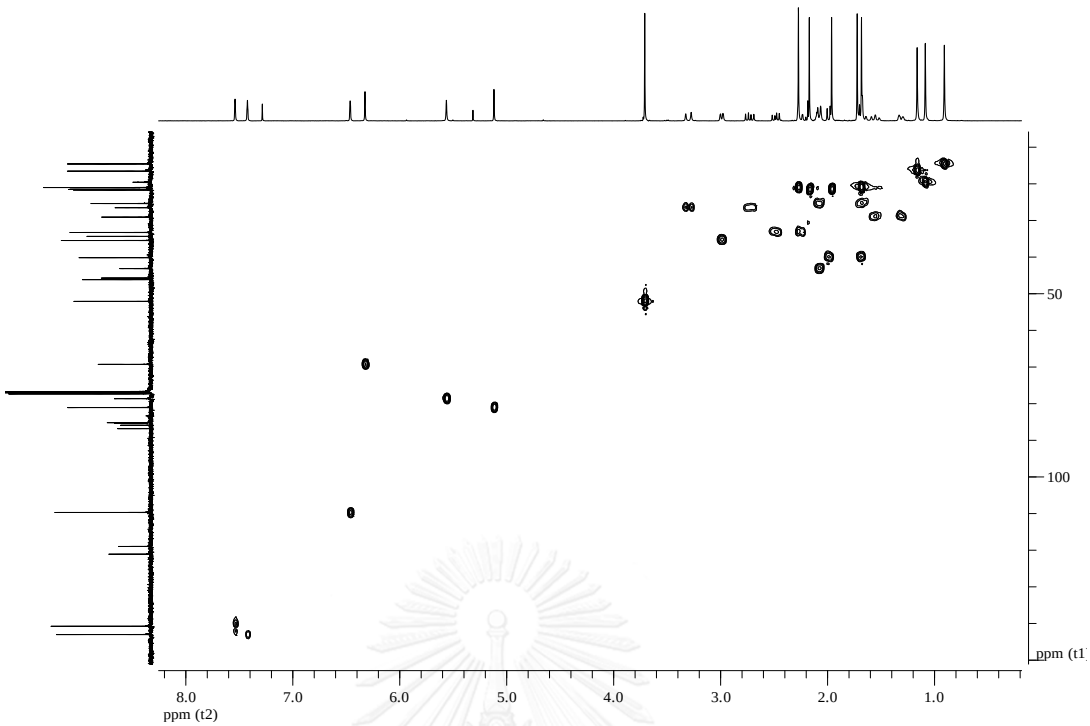

Figure A.58 HSQC spectrum of compound **50**

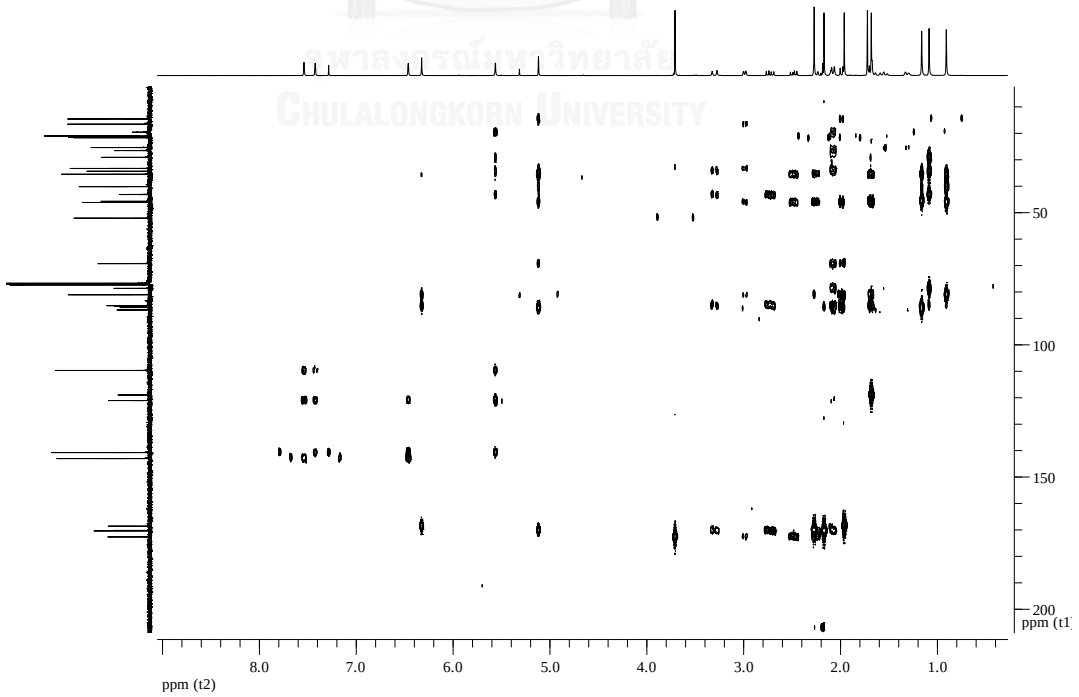

Figure A.59 HMBC spectrum ($CDCl_3$) of compound **50**

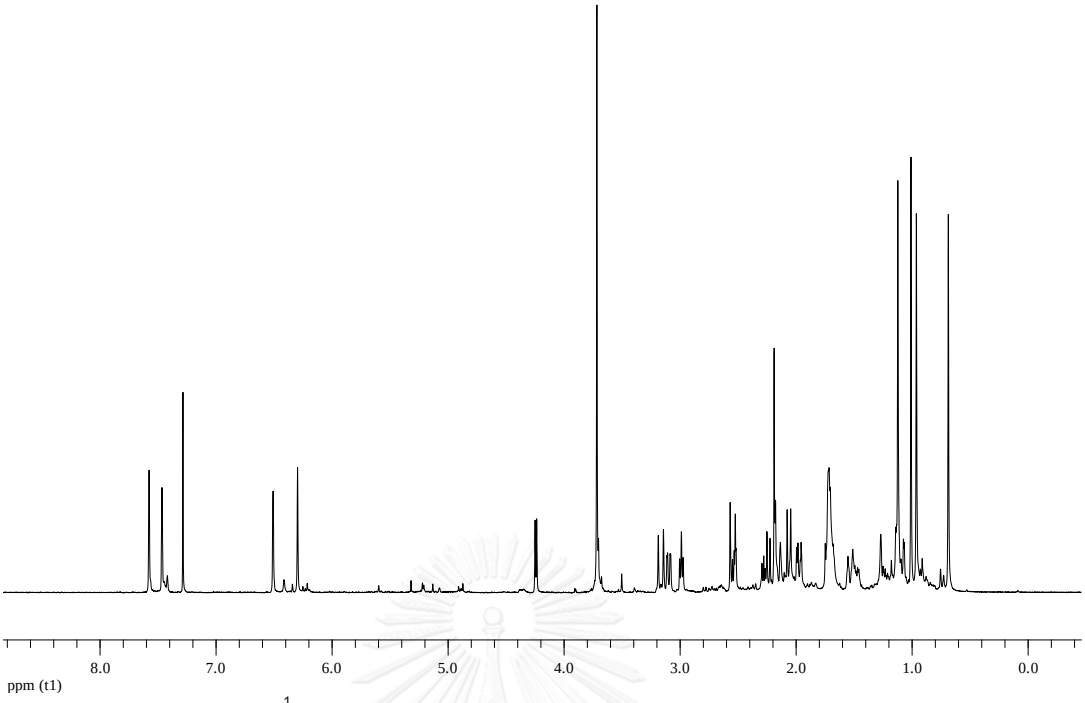

Figure A.60 ^{1}H NMR (400 MHz, $CDCl_3$) spectrum of compound **51**

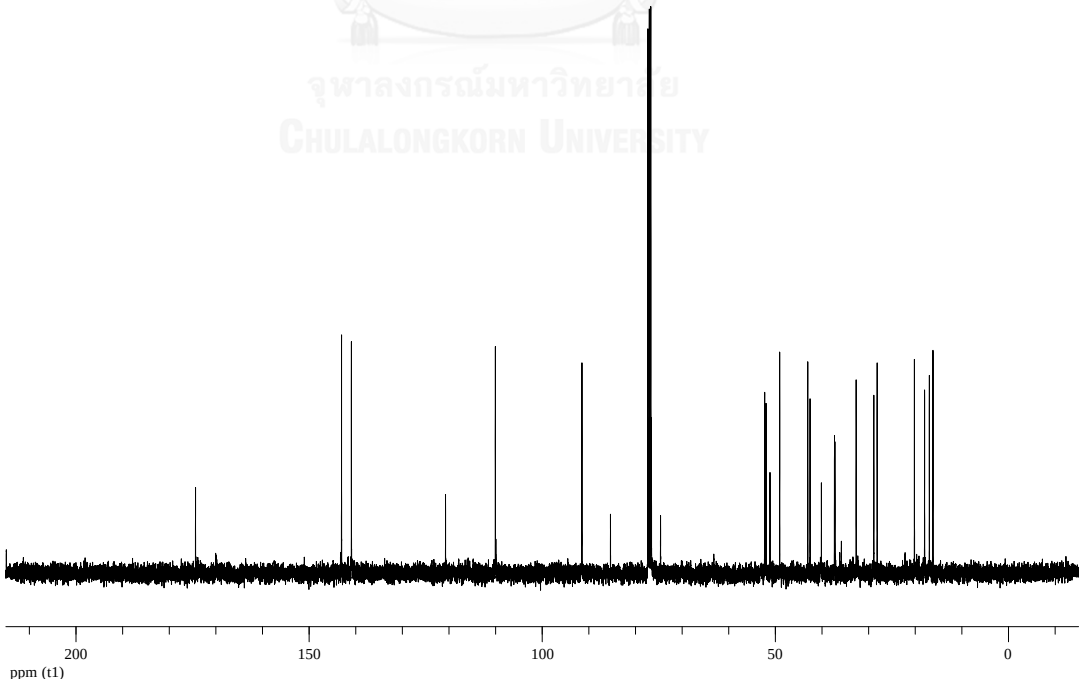

Figure A.61 ^{13}C NMR (100 MHz, $CDCl_3$) spectrum of compound **51**

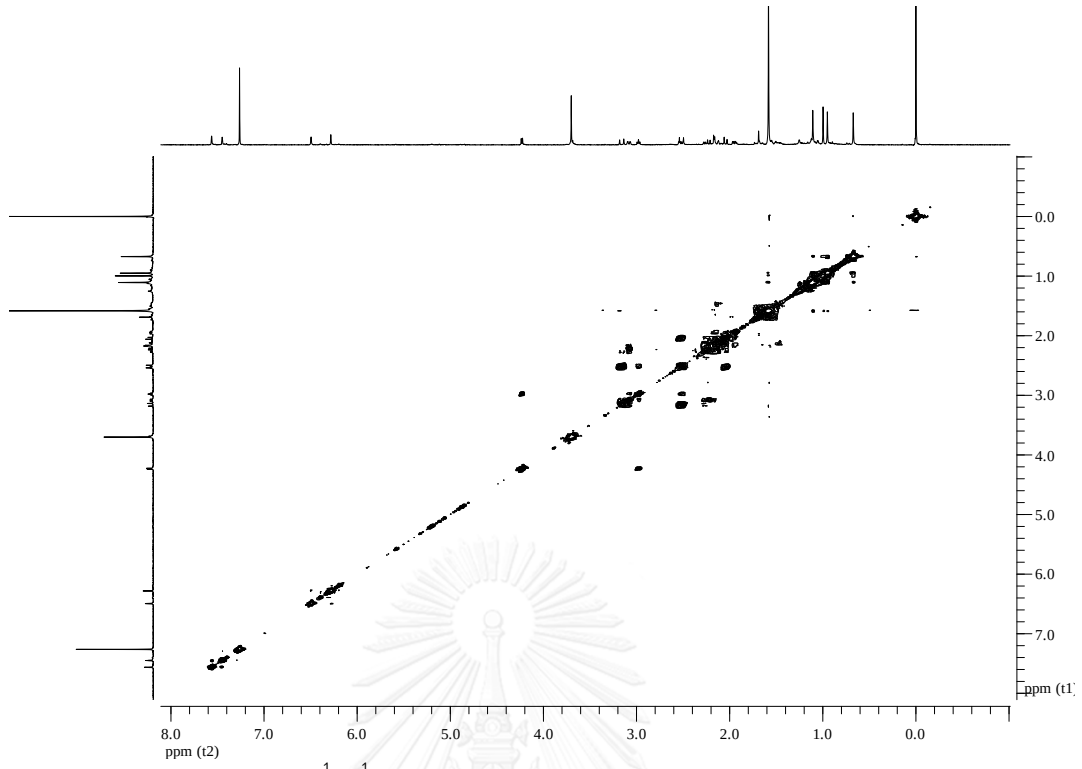

Figure A.62 ^{1}H-^{1}H COSY spectrum ($CDCl_3$) of compound **51**

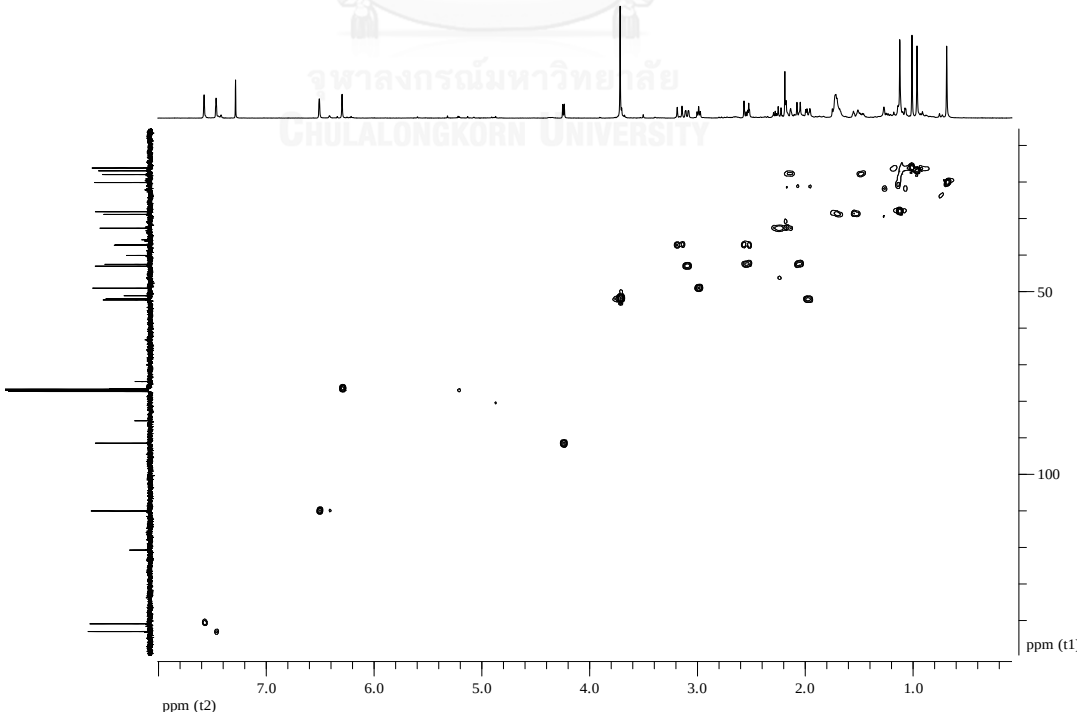

Figure A.63 HSQC spectrum of compound **51**

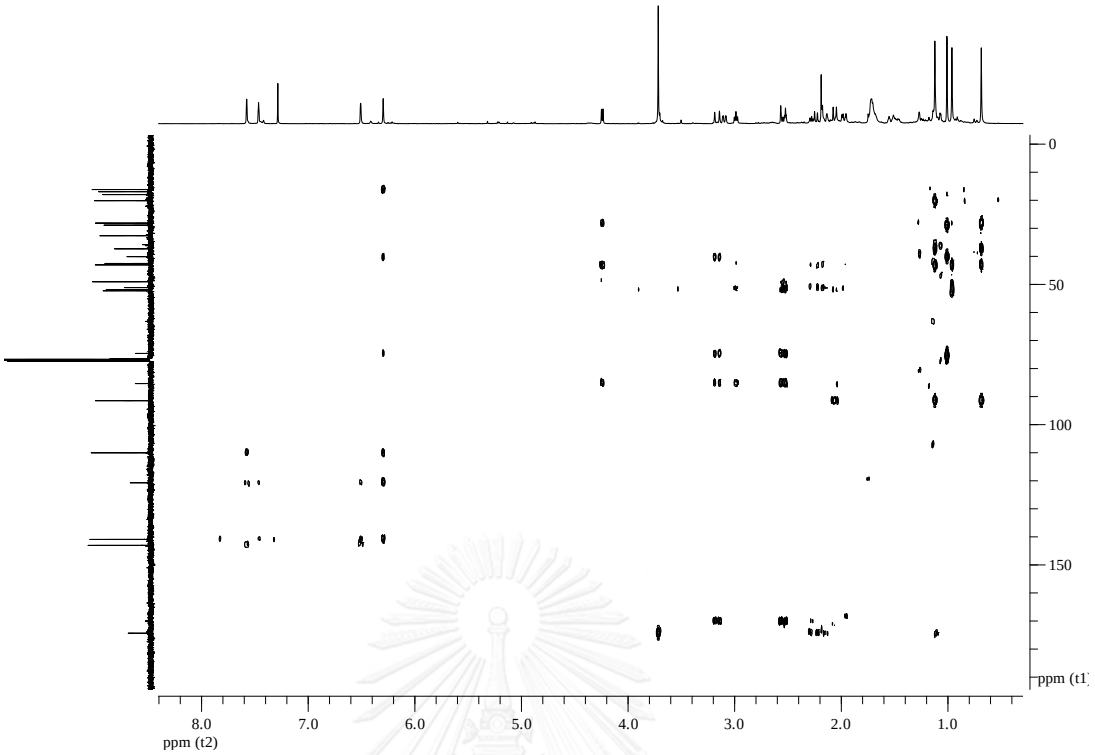

Figure A.64 HMBC spectrum ($CDCl_3$) of compound **51**

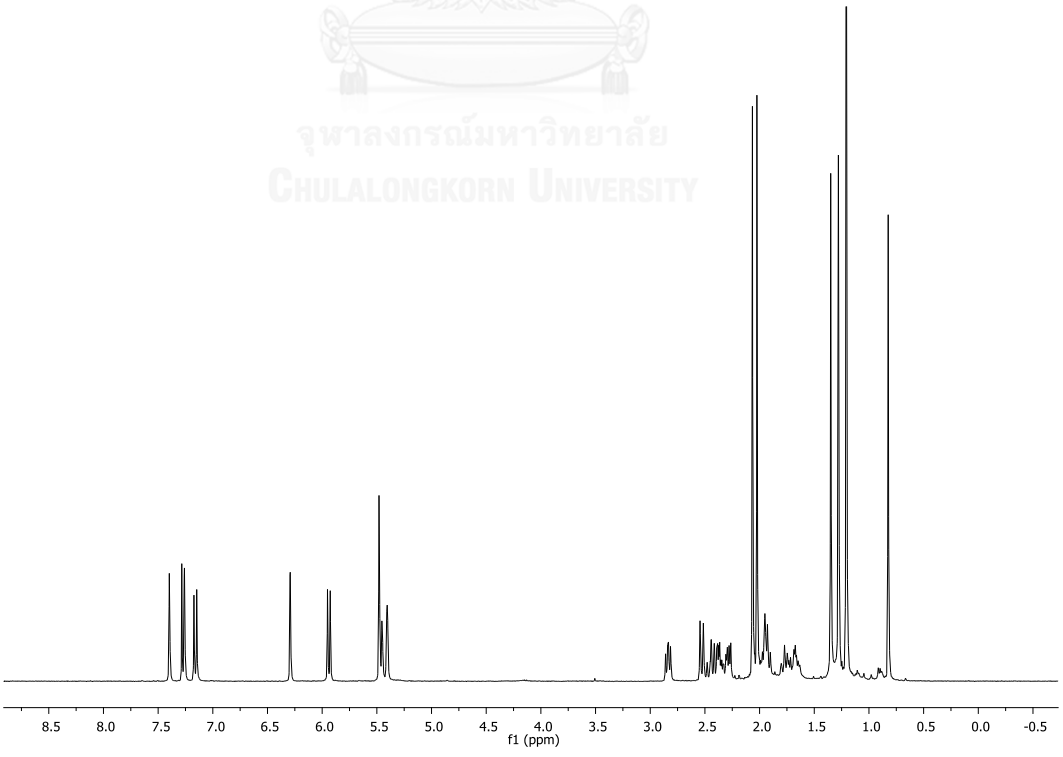

Figure A.65 ^{1}H NMR (400 MHz, $CDCl_3$) spectrum of compound **80**

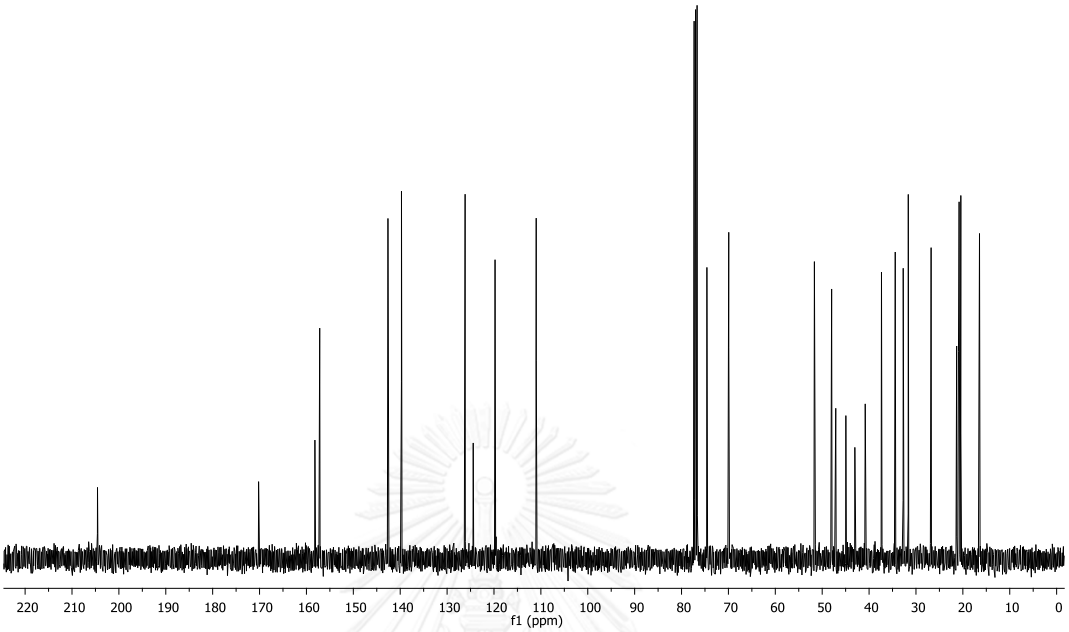

Figure A.66 ^{13}C NMR (100 MHz, $CDCl_3$) spectrum of compound **80**

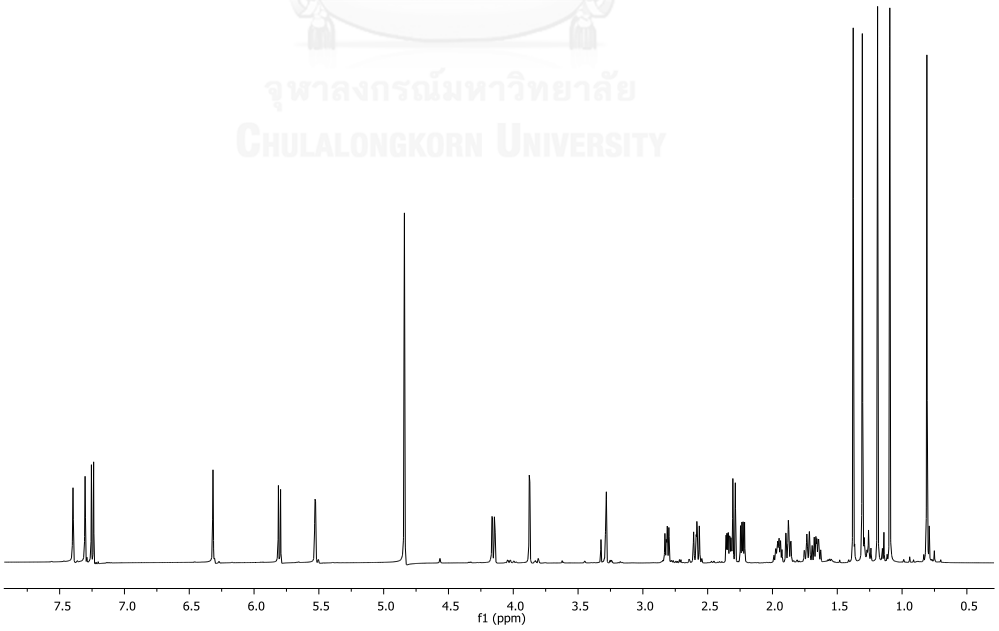

Figure A.67 ^{1}H NMR (400 MHz, CD_3OH) spectrum of compound **139**

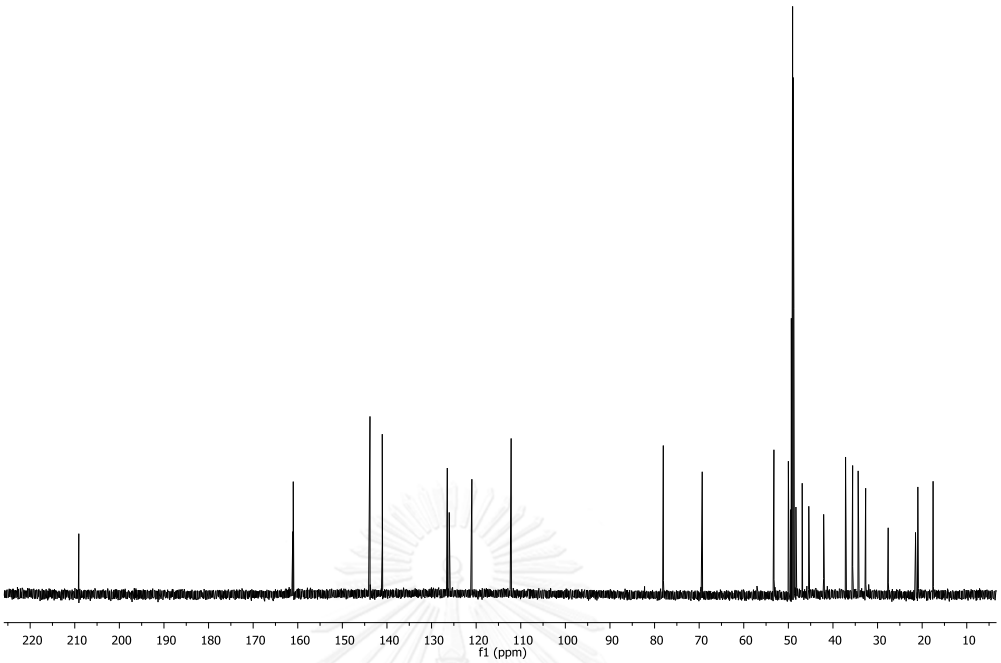

Figure A.68 ^{13}C NMR (100 MHz, CD_3OH) spectrum of compound **139**

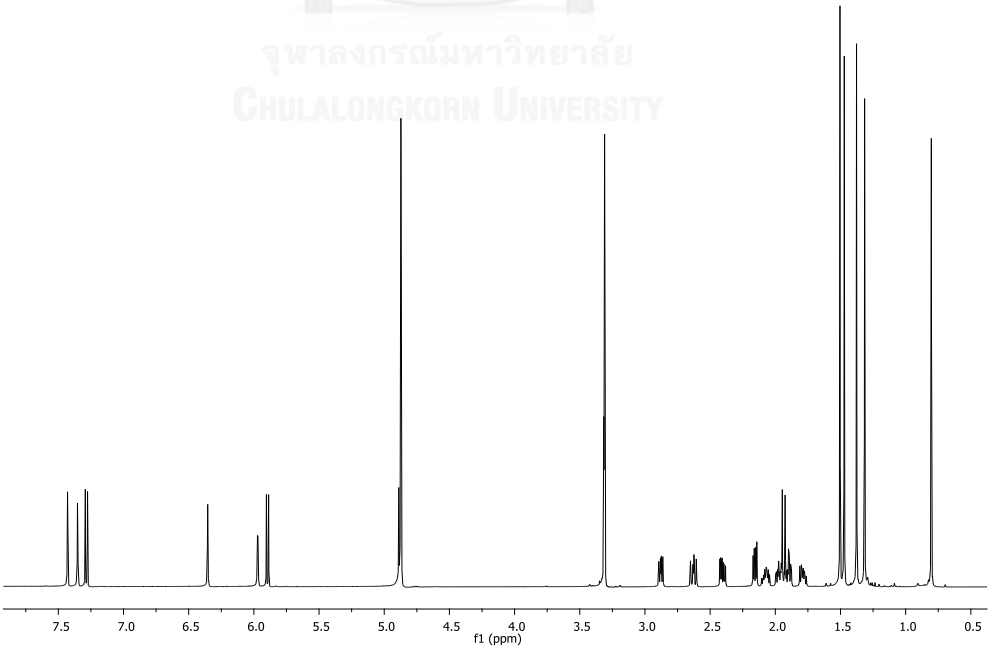

Figure A.69 ^{1}H NMR (400 MHz, CD_3OH) spectrum of compound **140**

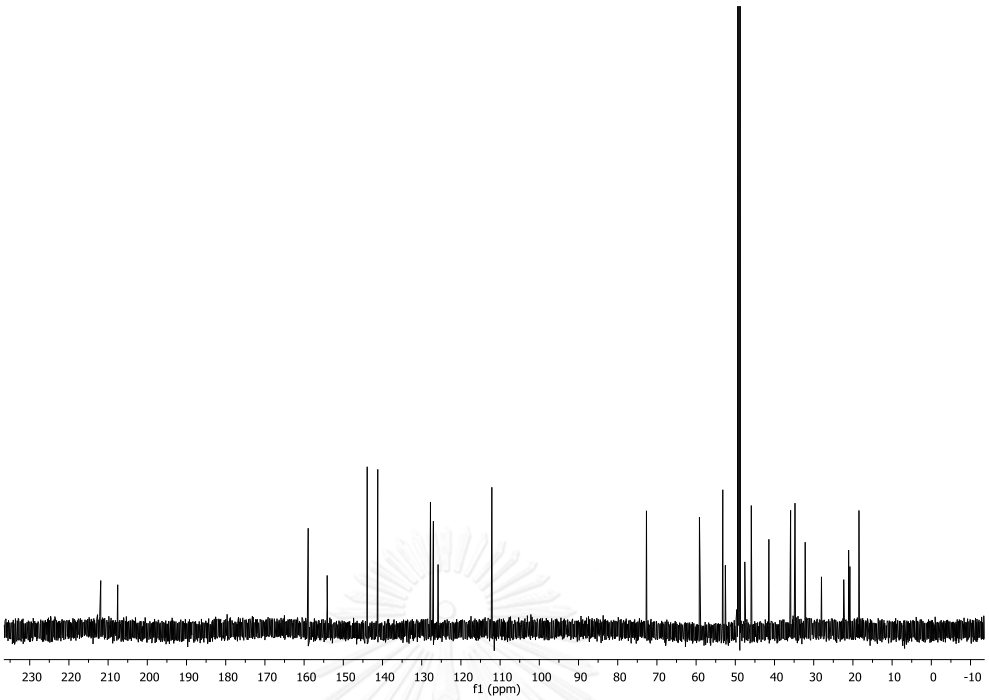

Figure A.70 ^{13}C NMR (100 MHz, CD_3OH) spectrum of compound **140**

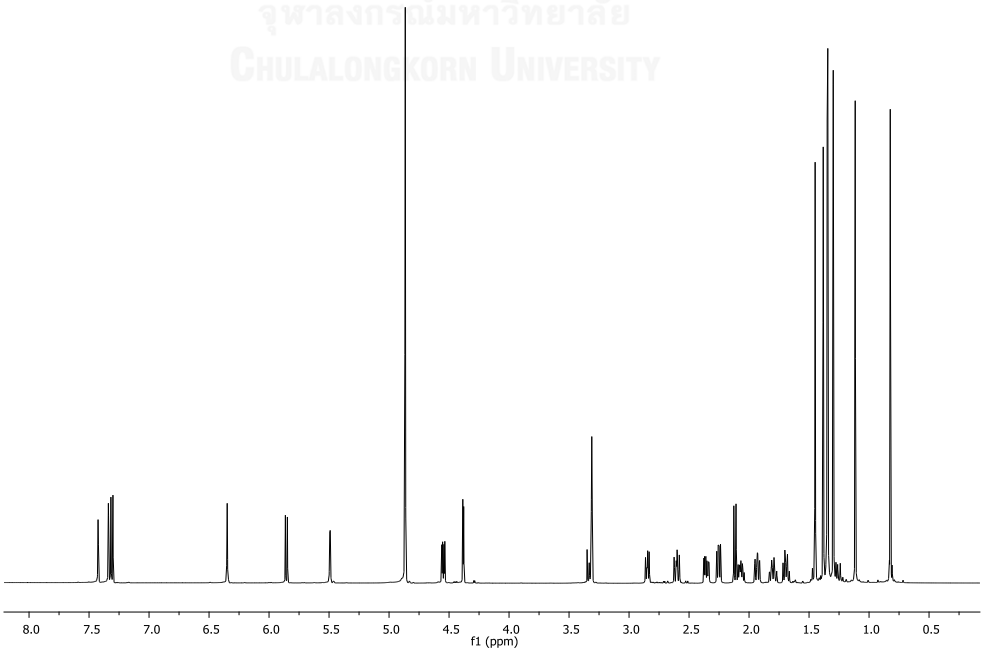

Figure A.71 ^{1}H NMR (400 MHz, CD_3OH) spectrum of compound **141**

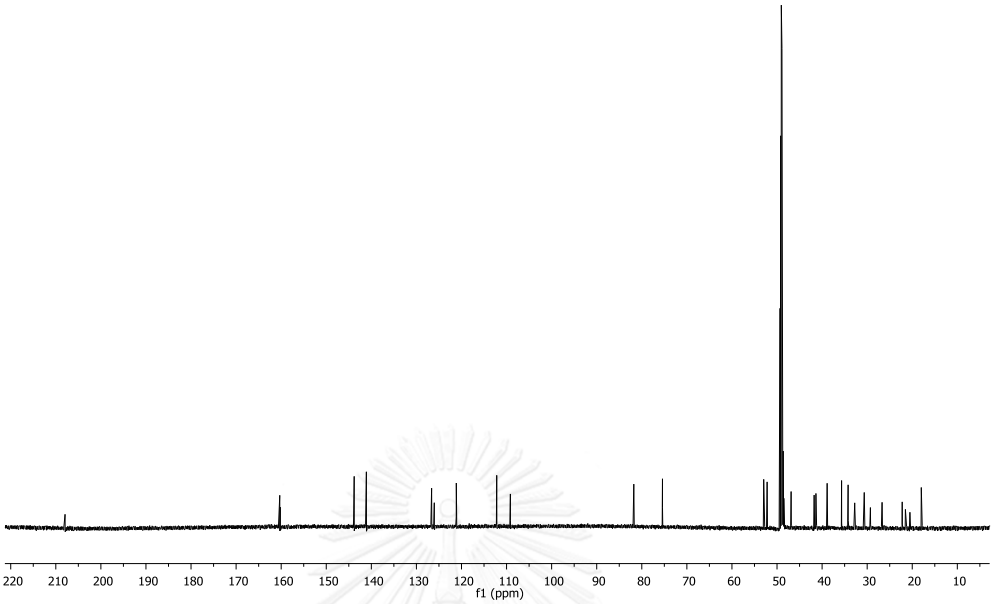

Figure A.72 ^{13}C NMR (100 MHz, CD_3OH) spectrum of compound **141**

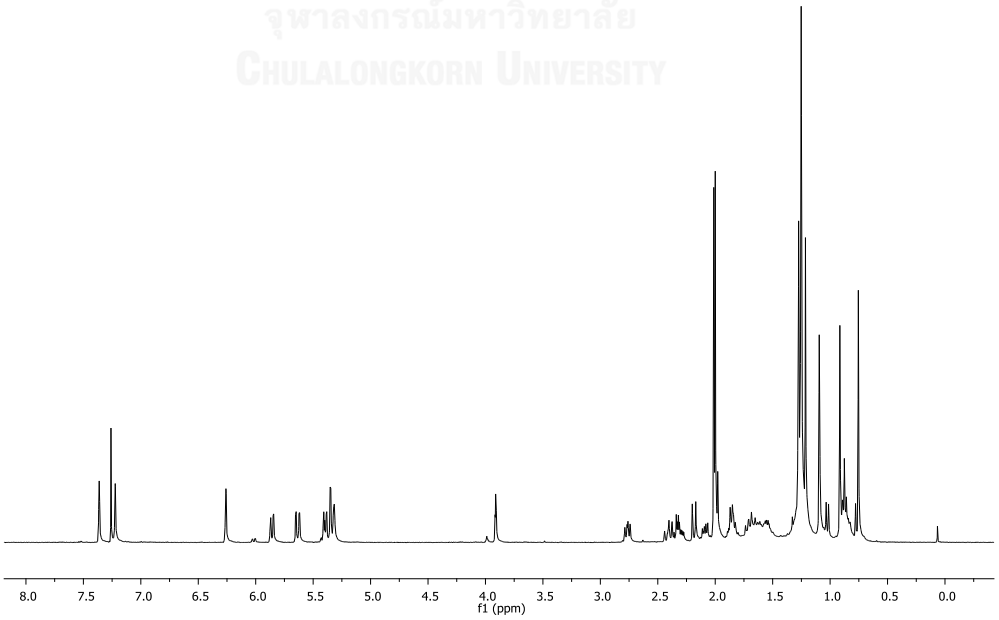

Figure A.73 ^{1}H NMR (400 MHz, $CDCl_3$) spectrum of compound **142**

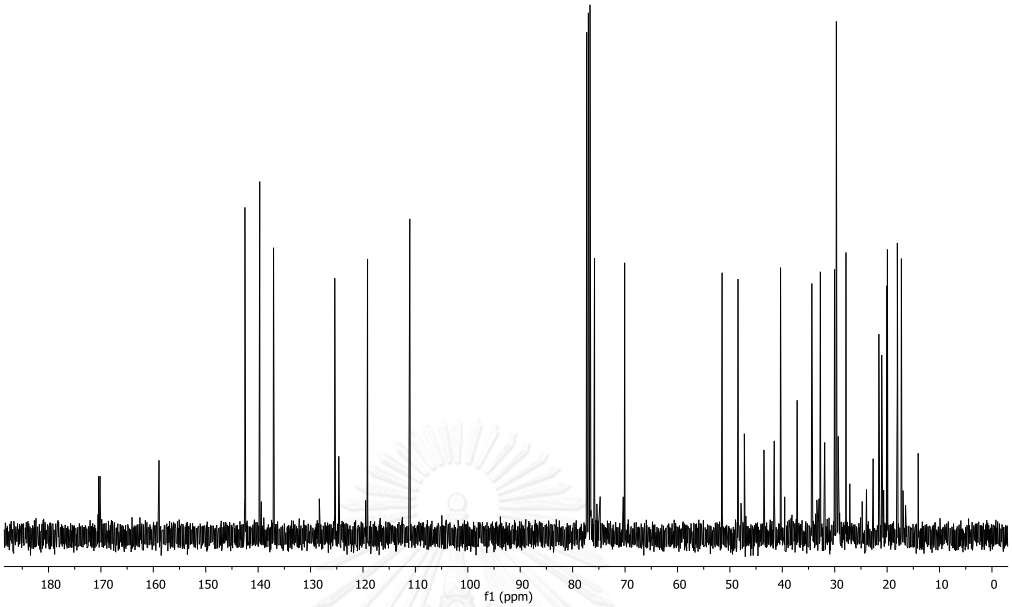

Figure A.74 ^{13}C NMR (100 MHz, $CDCl_3$) spectrum of compound **142**

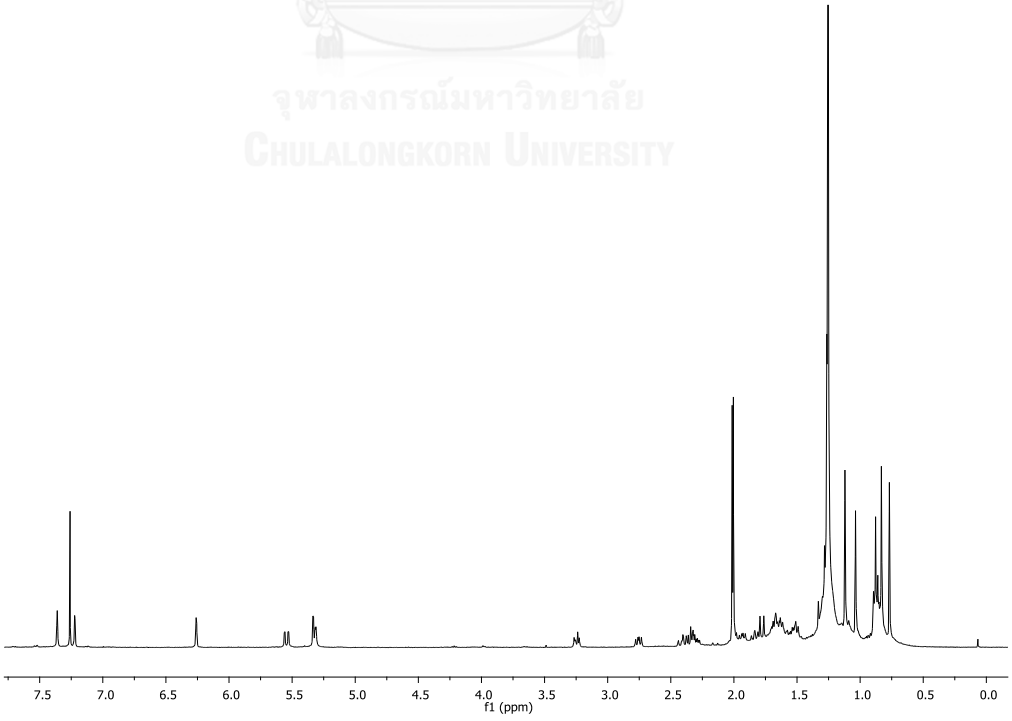

Figure A.75 ^{1}H NMR (400 MHz, $CDCl_3$) spectrum of compound **143**

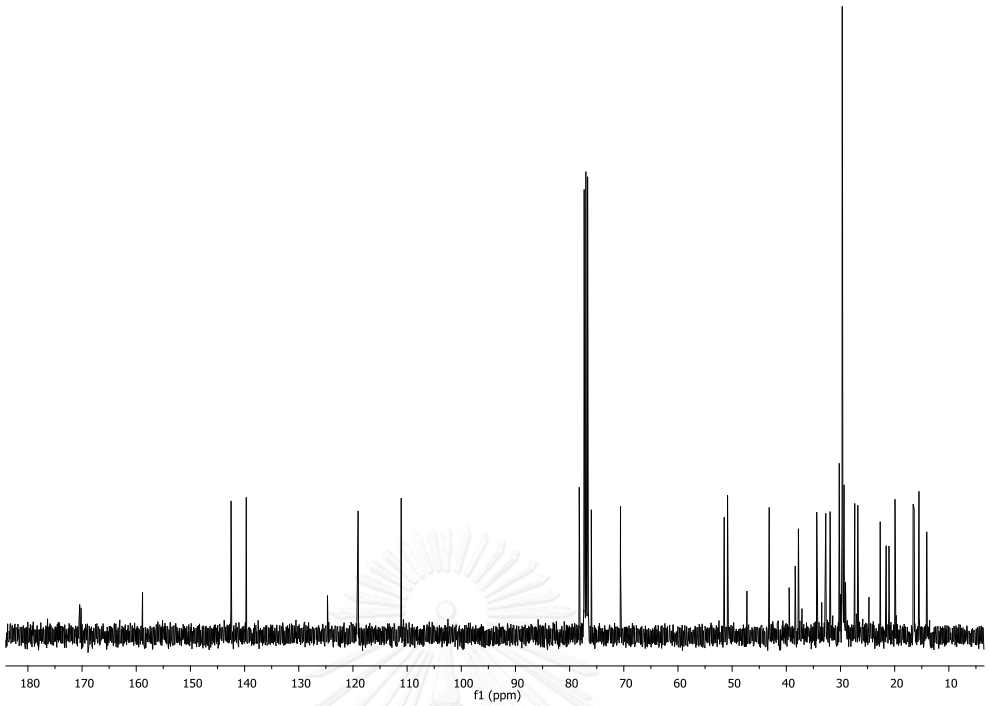

Figure A.76 ^{13}C NMR (100 MHz, $CDCl_3$) spectrum of compound **143**

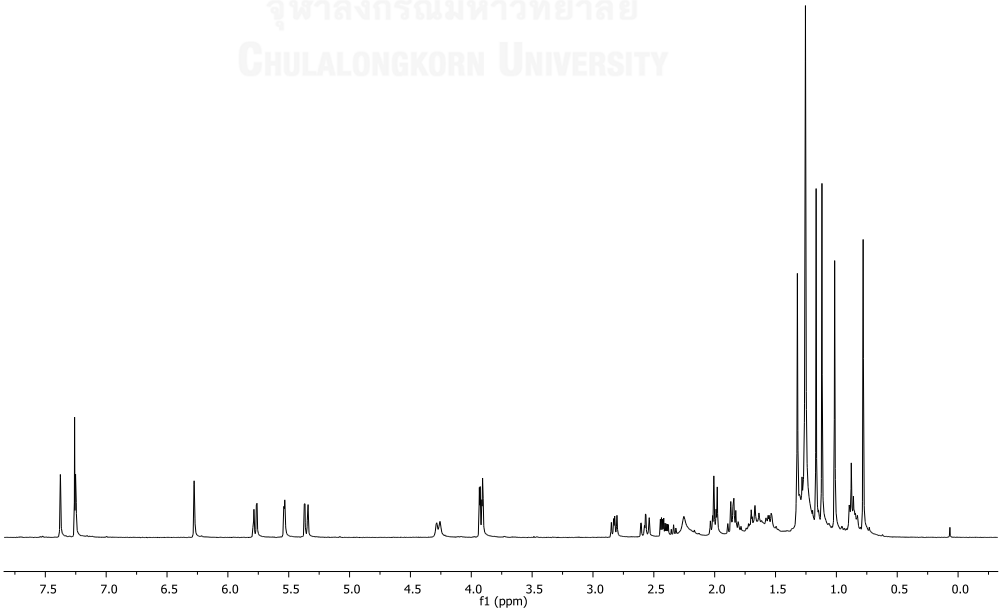

Figure A.77 ^{1}H NMR (400 MHz, $CDCl_3$) spectrum of compound **144**

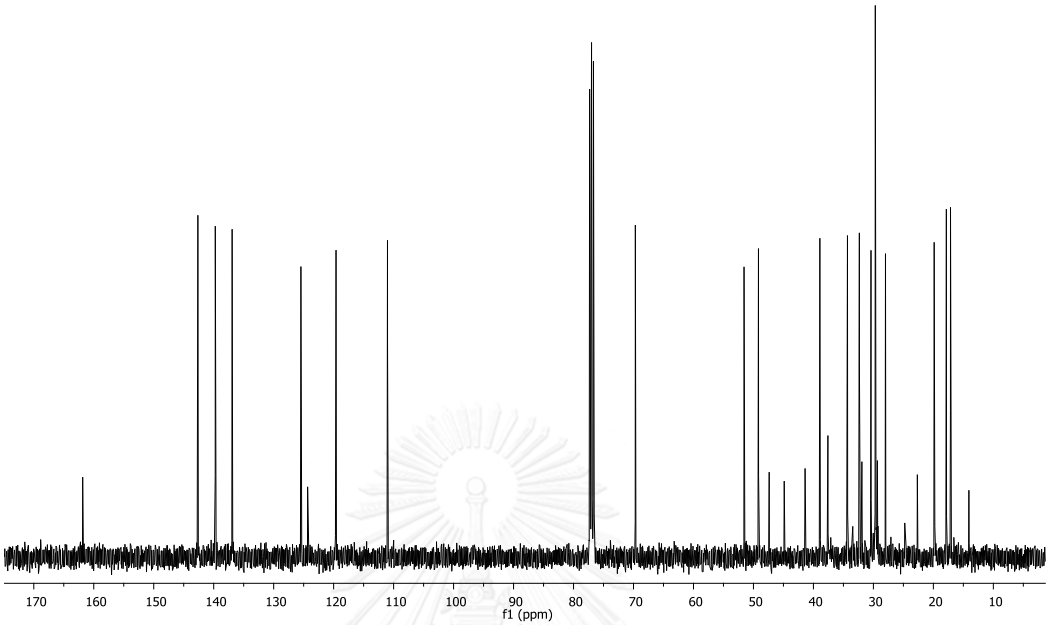

Figure A.78 ^{13}C NMR (100 MHz, $CDCl_3$) spectrum of compound **144**

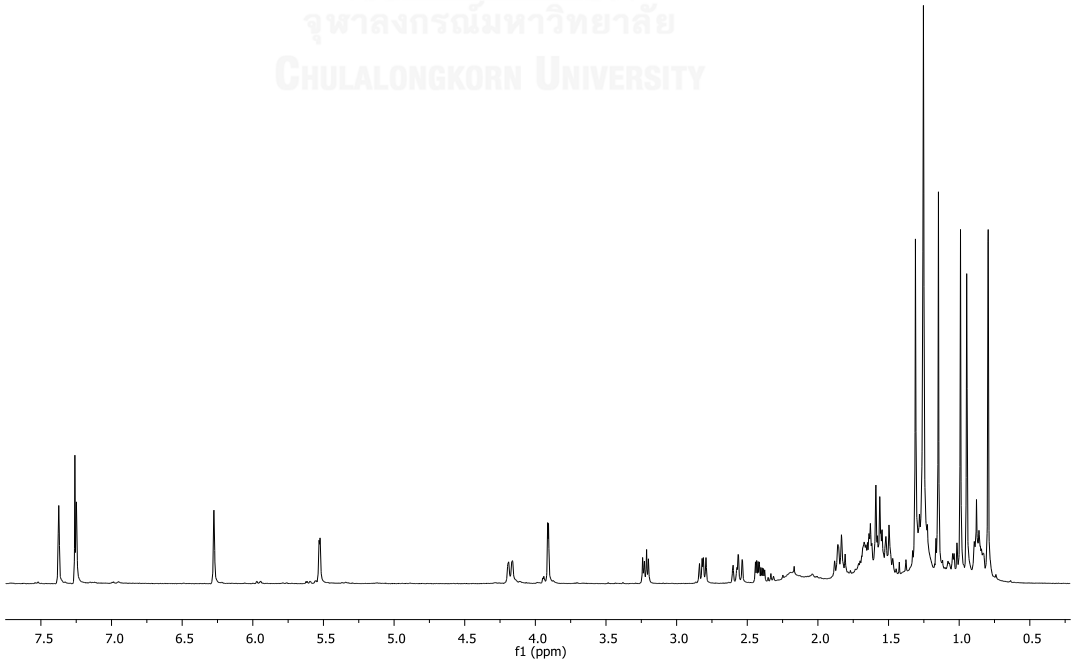

Figure A.79 ^{1}H NMR (400 MHz, $CDCl_3$) spectrum of compound **145**

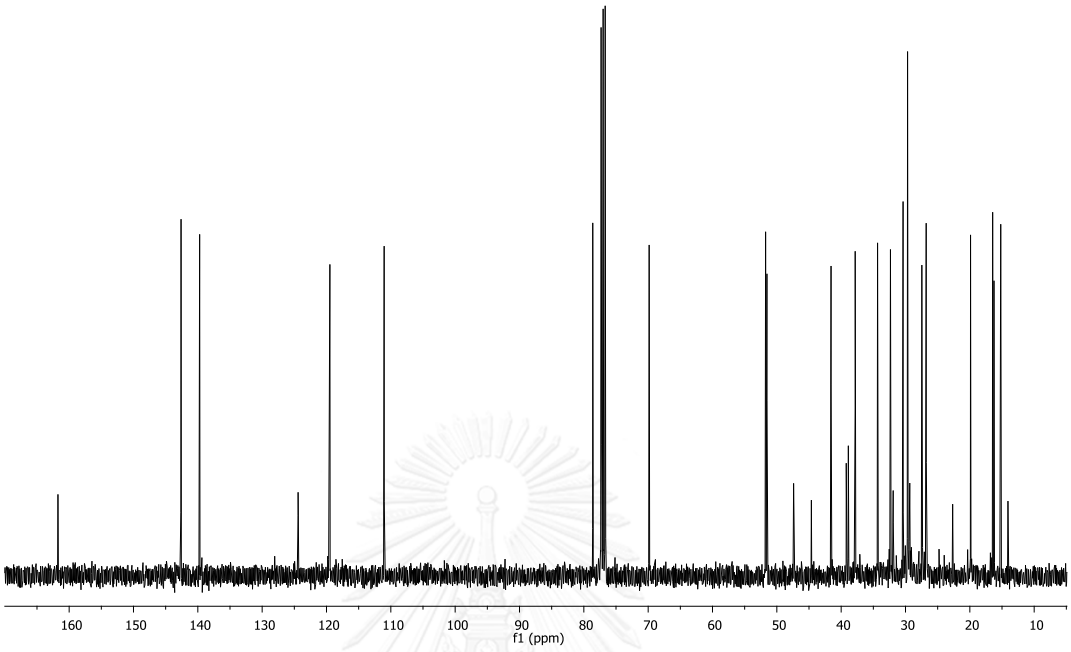

Figure A.80 ^{13}C NMR (100 MHz, $CDCl_3$) spectrum of compound **145**

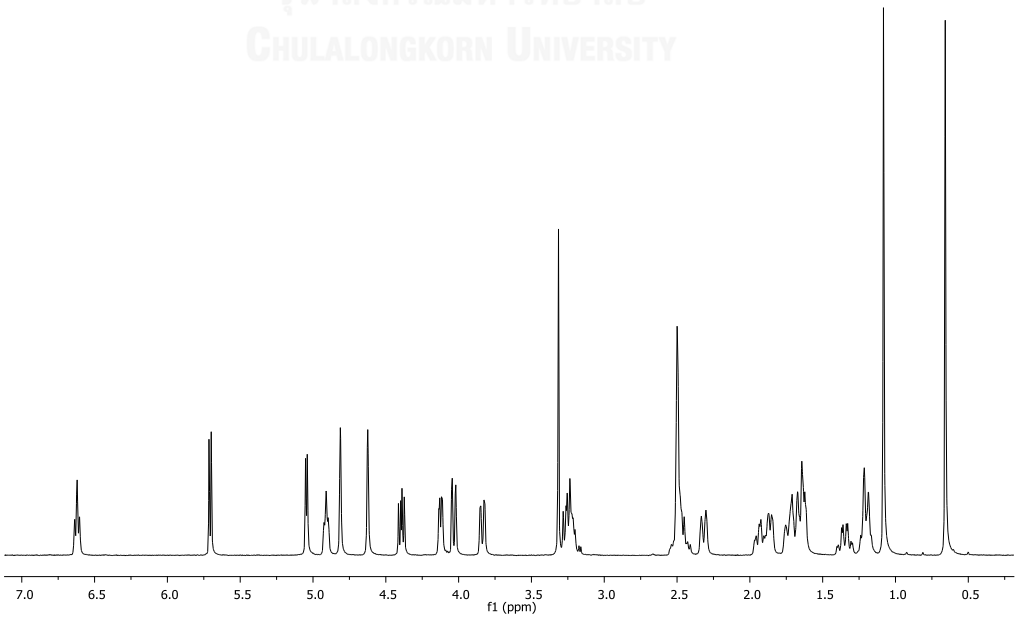

Figure A.81 ^{1}H NMR (400 MHz, $(CD_3)_2SO$) spectrum of compound **81**

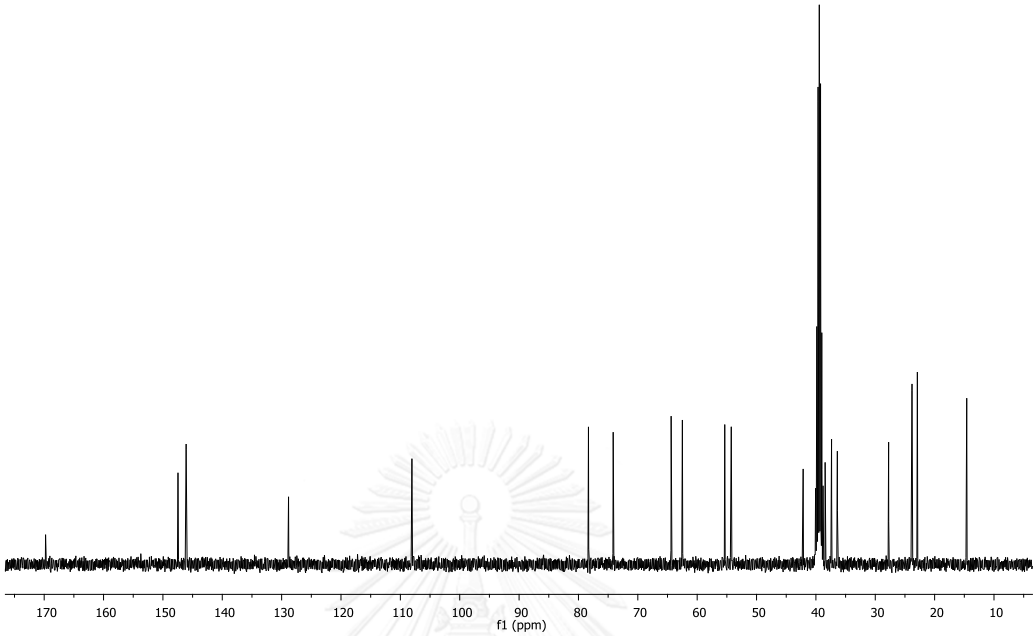

Figure A.82 ^{13}C NMR (100 MHz, $(CD_3)_2SO$) spectrum of compound **81**

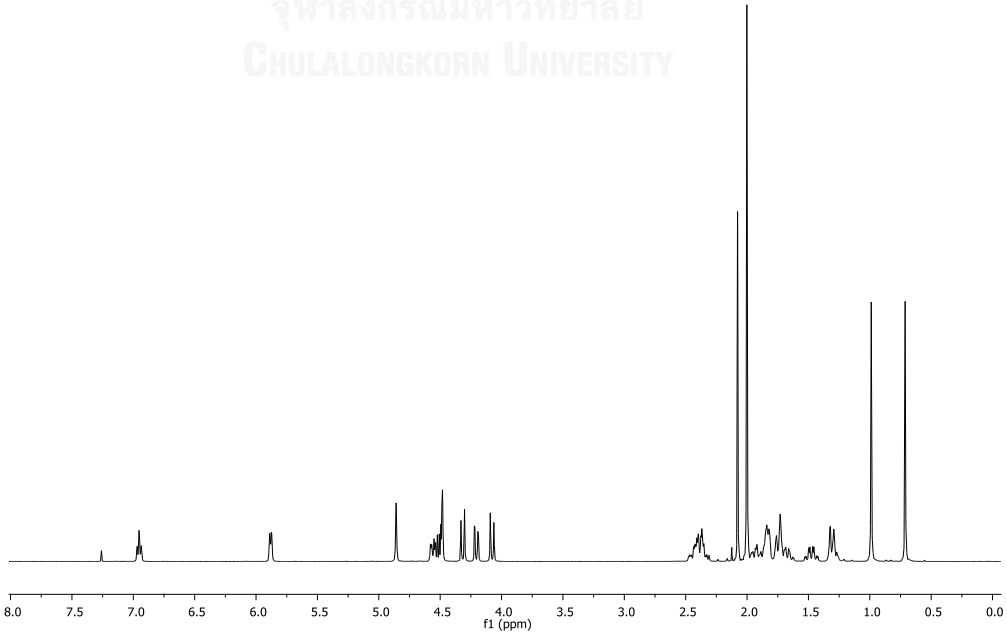

Figure A.83 ^{1}H NMR (400 MHz, $CDCl_3$) spectrum of compound **146**

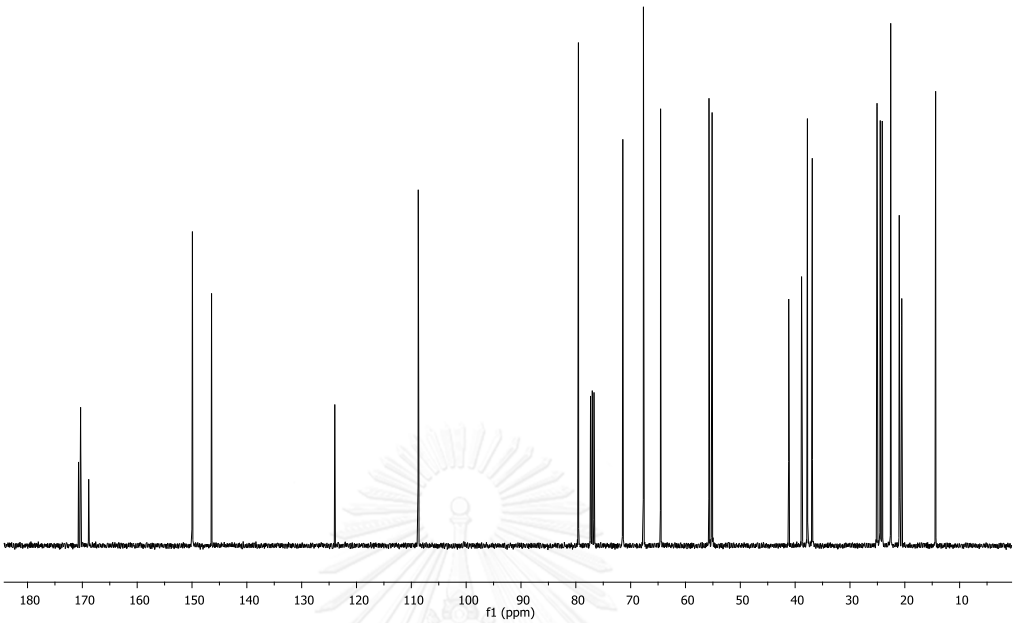

Figure A.84 ^{13}C NMR (100 MHz, $CDCl_3$) spectrum of compound **146**

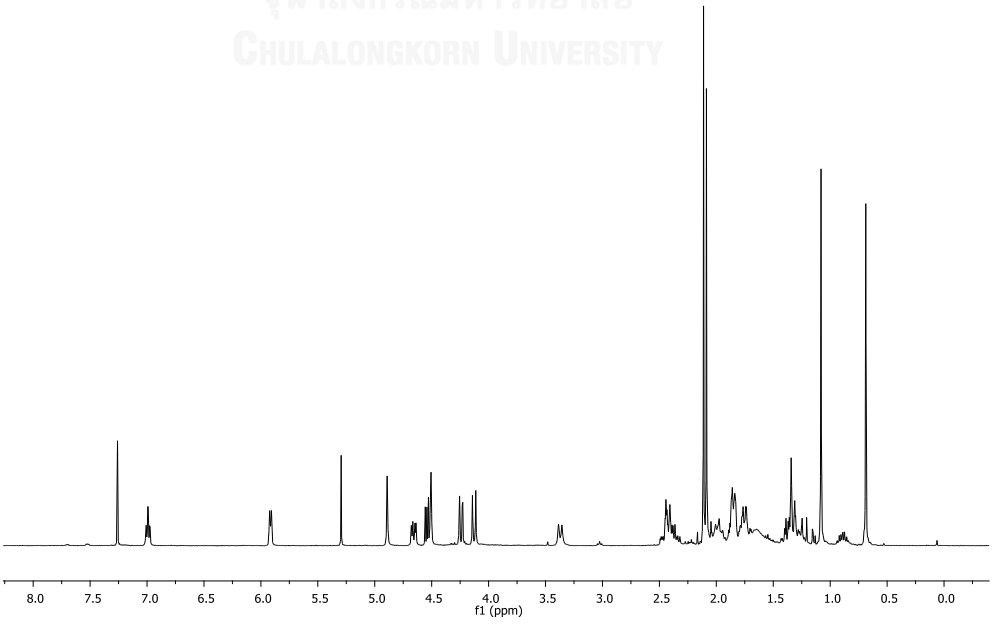

Figure A.85 ^{1}H NMR (400 MHz, $CDCl_3$) spectrum of compound **147**

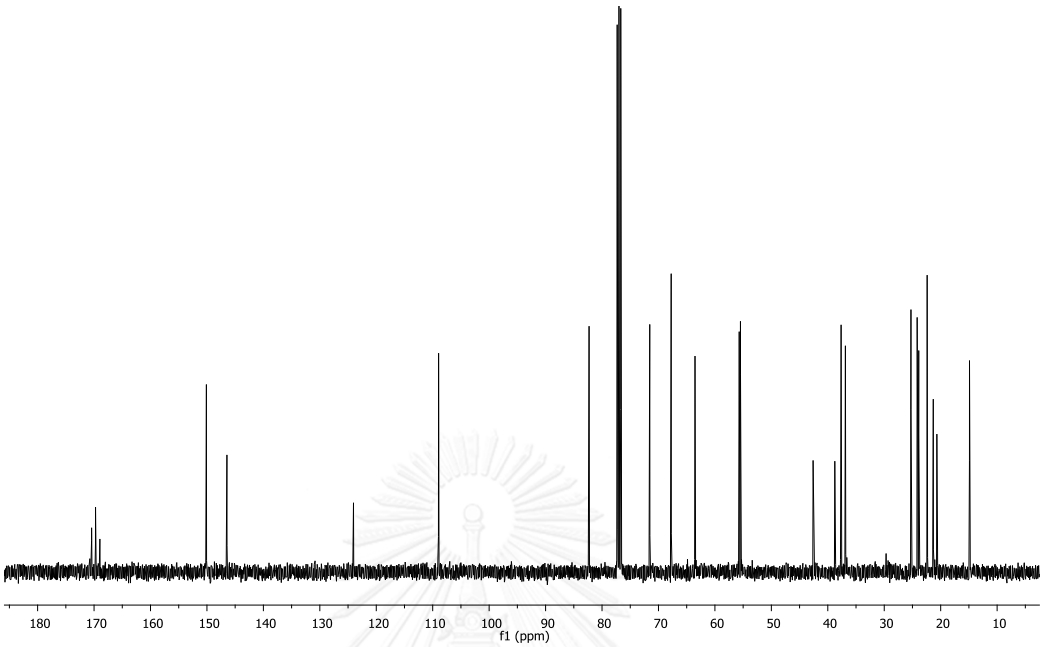

Figure A.86 ^{13}C NMR (100 MHz, $CDCl_3$) spectrum of compound **147**

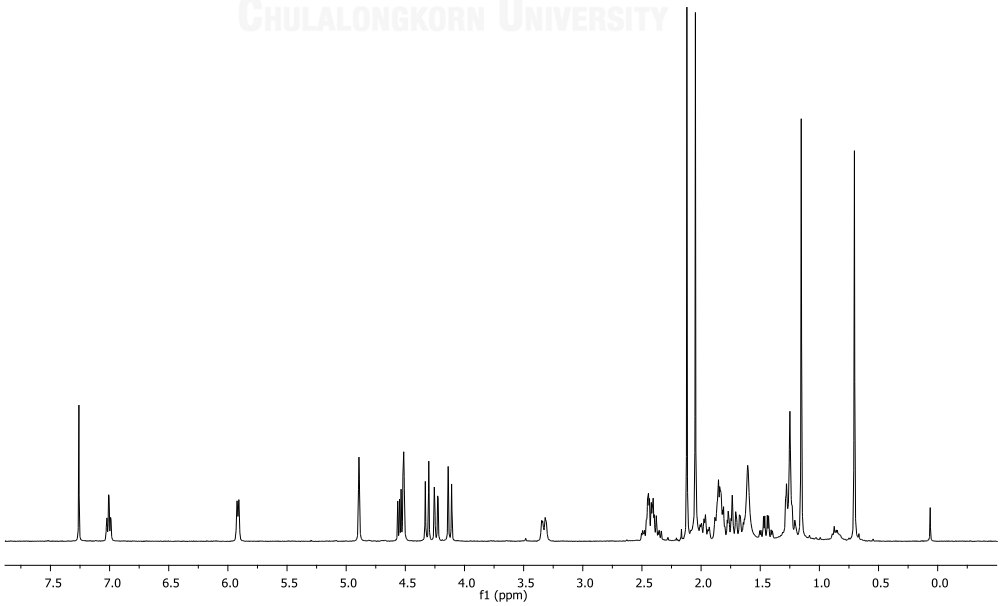

Figure A.87 ^{1}H NMR (400 MHz, $CDCl_3$) spectrum of compound **148**

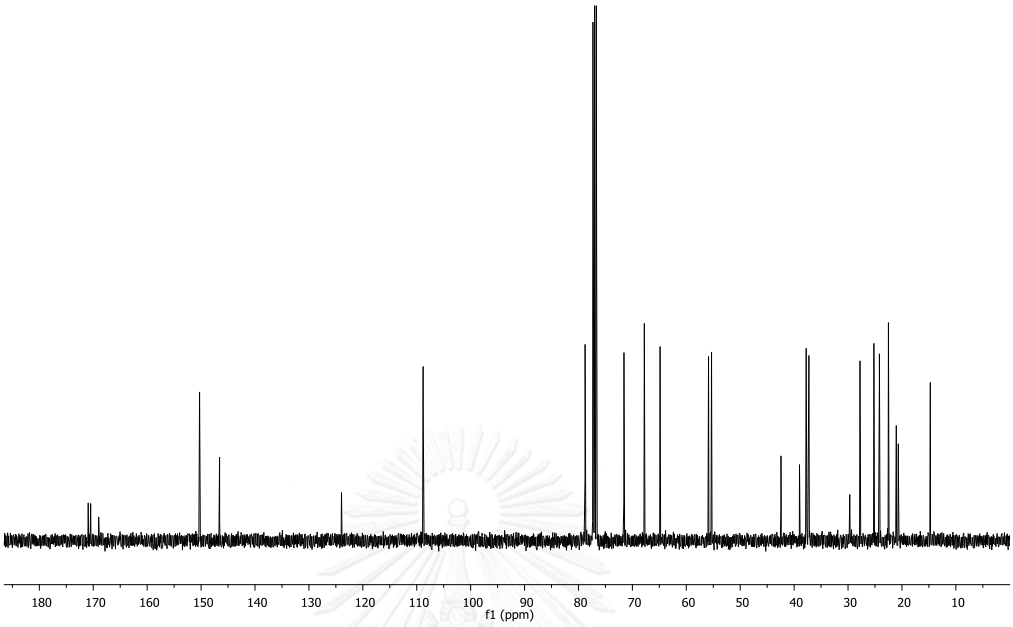

Figure A.88 ^{13}C NMR (100 MHz, $CDCl_3$) spectrum of compound **148**

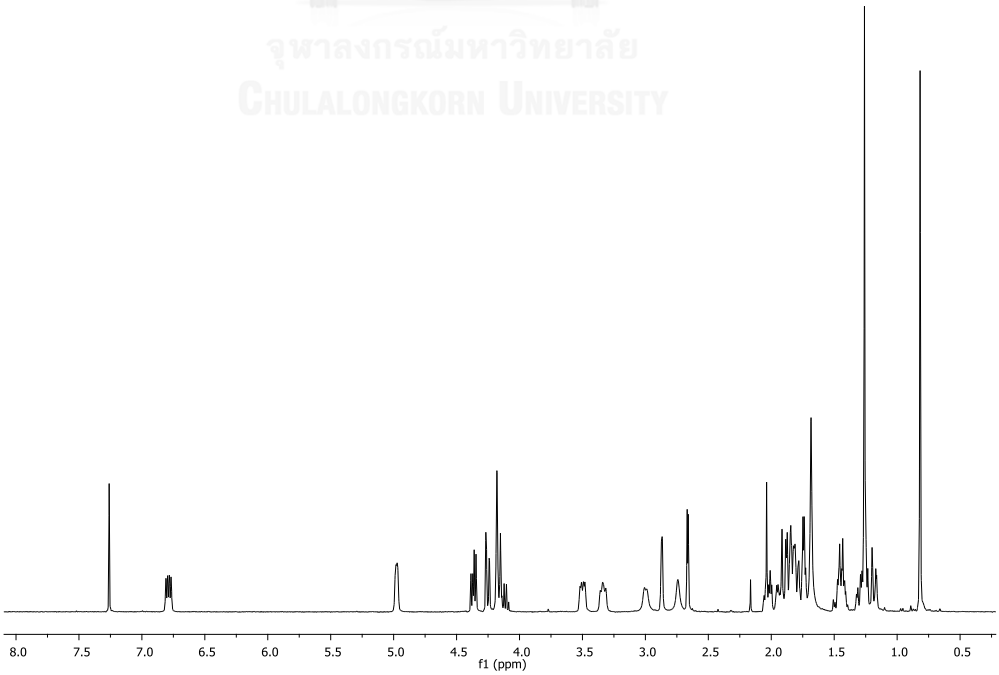

Figure A.89 ^{1}H NMR (400 MHz, $CDCl_3$) spectrum of compound **149**

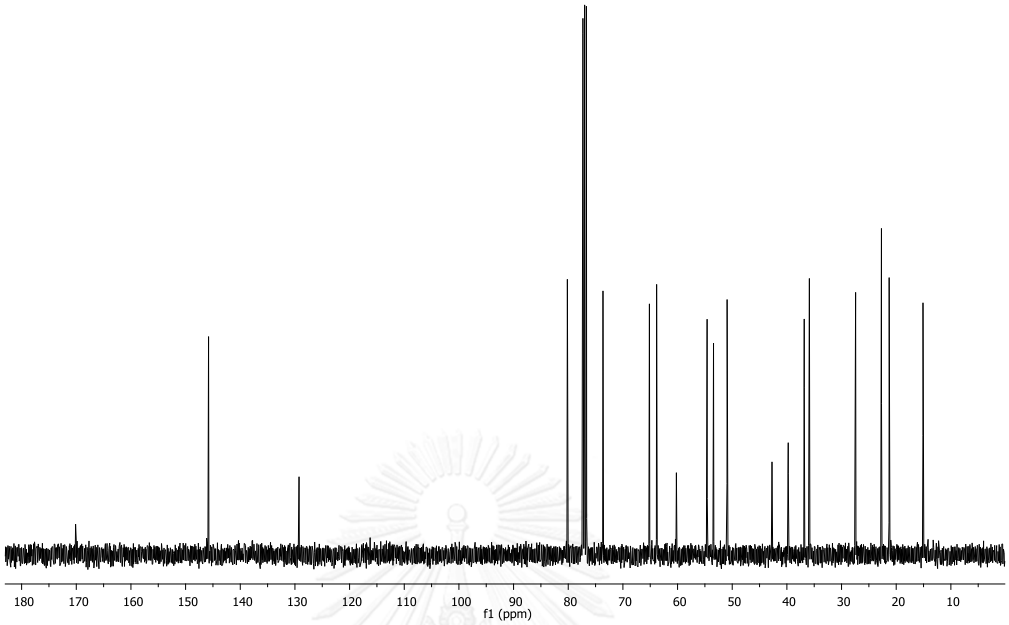

Figure A.90 ^{13}C NMR (100 MHz, $CDCl_3$) spectrum of compound **149**

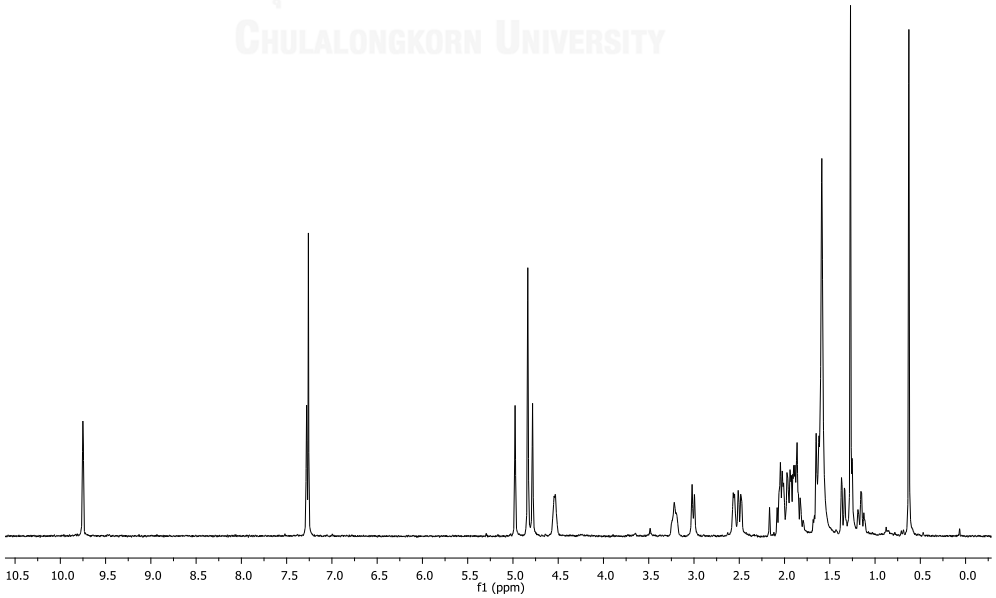

Figure A.91 ^{1}H NMR (400 MHz, $CDCl_3$) spectrum of compound **150**

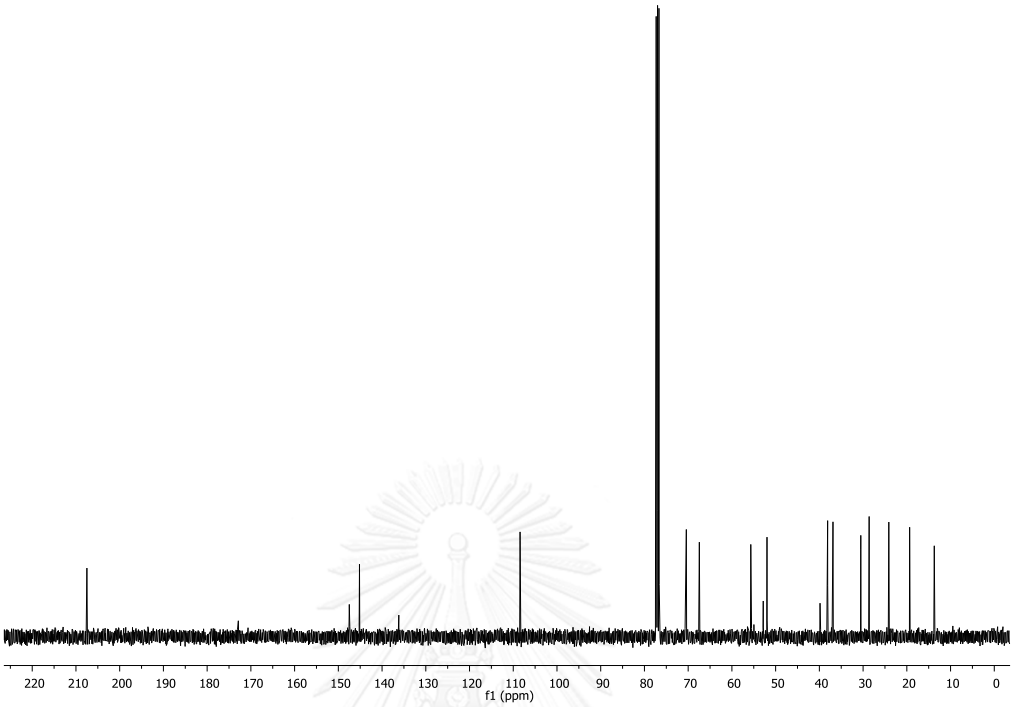

Figure A.92 ^{13}C NMR (100 MHz, $CDCl_3$) spectrum of compound **150**

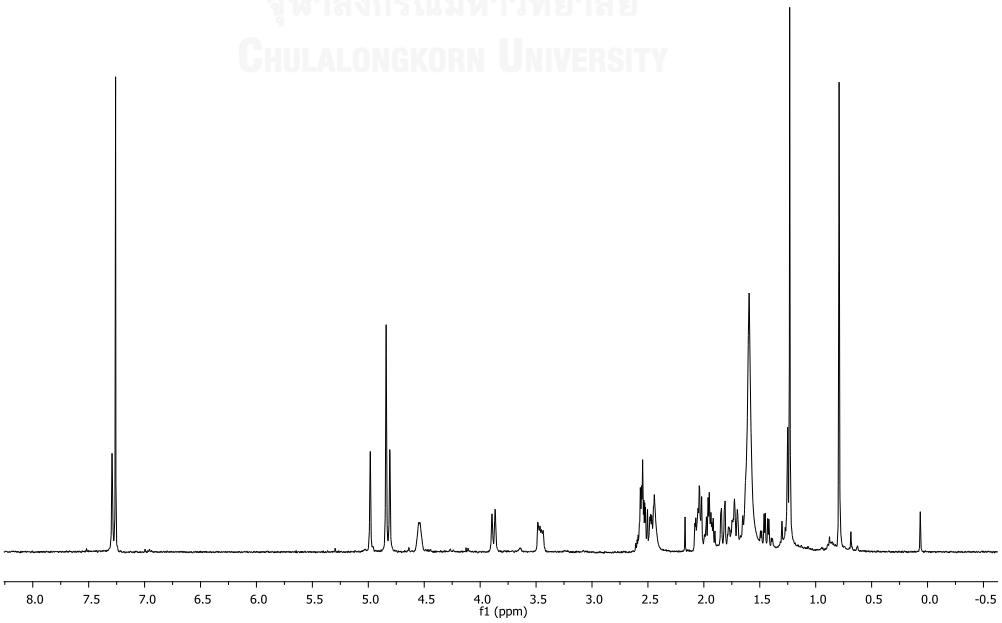

Figure A.93 ^{1}H NMR (400 MHz, $CDCl_3$) spectrum of compound **151**

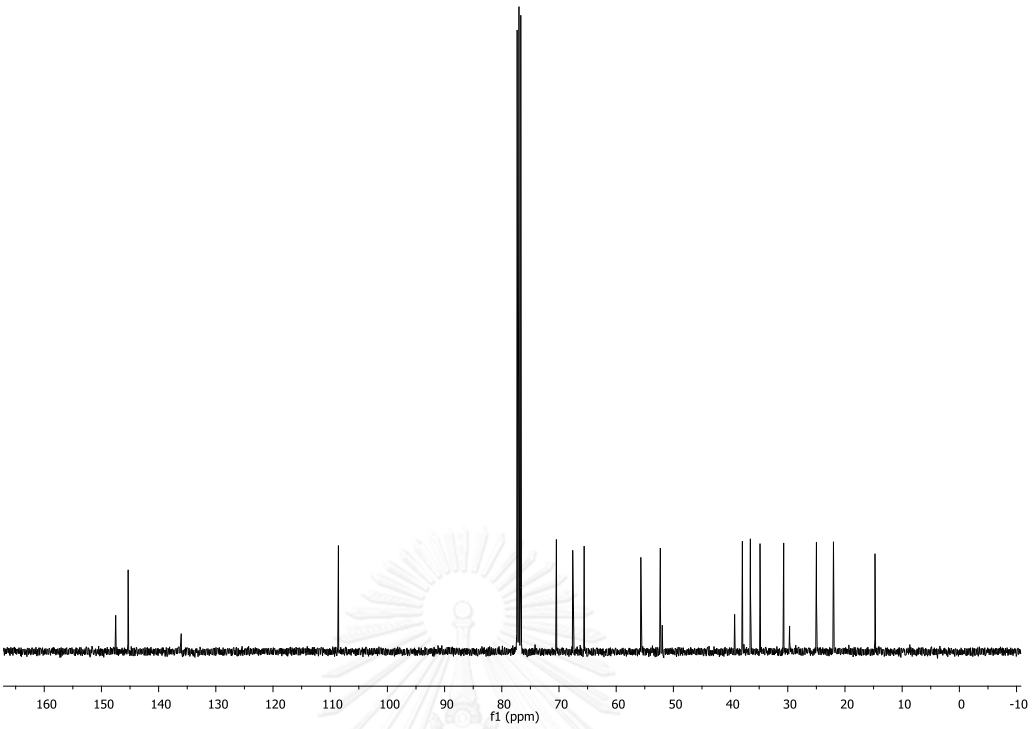

Figure A.94 ^{13}C NMR (100 MHz, $CDCl_3$) spectrum of compound **151**

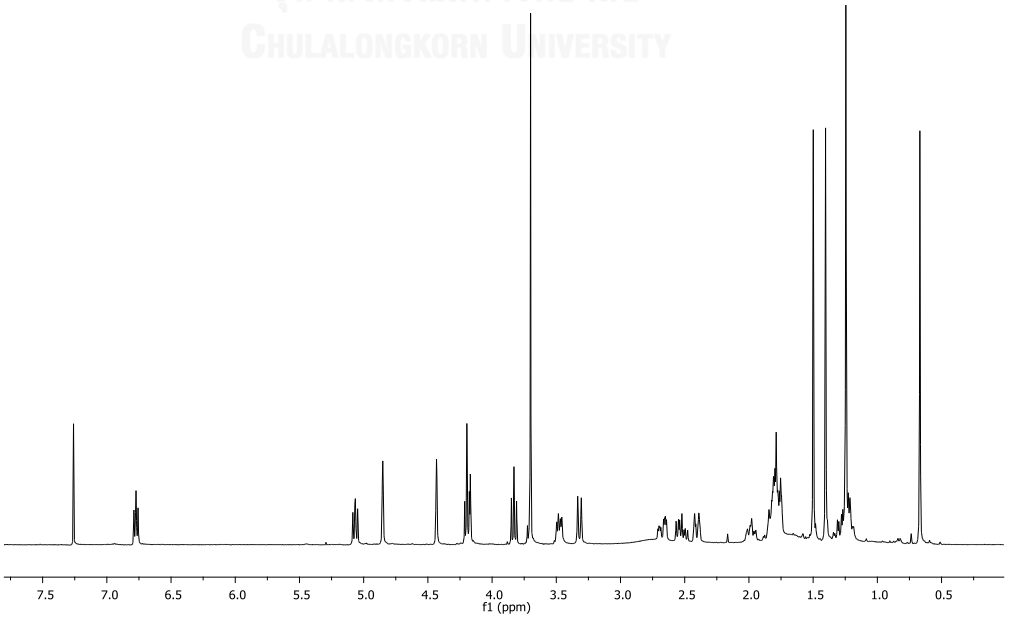

Figure A.95 ^{1}H NMR (400 MHz, $CDCl_3$) spectrum of compound **152**

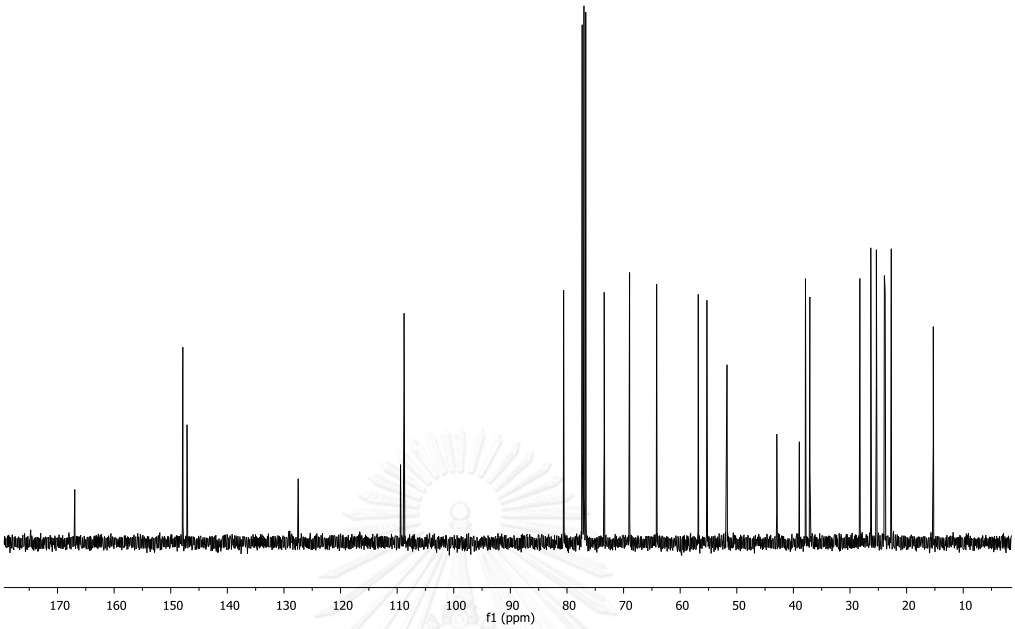

Figure A.96 ^{13}C NMR (100 MHz, $CDCl_3$) spectrum of compound **152**

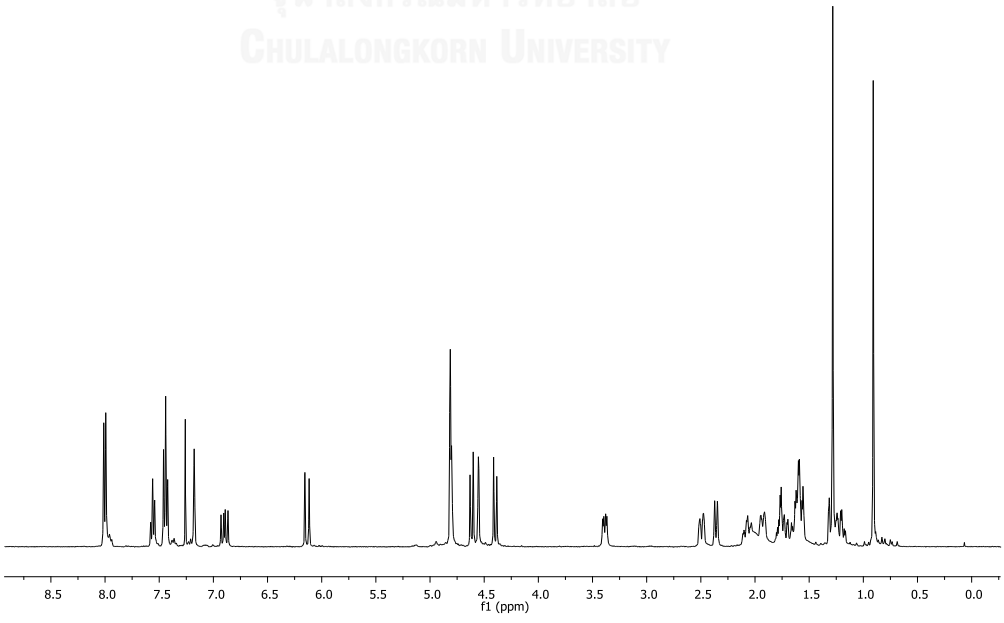

Figure A.97 ^{1}H NMR (400 MHz, $CDCl_3$) spectrum of compound **153**

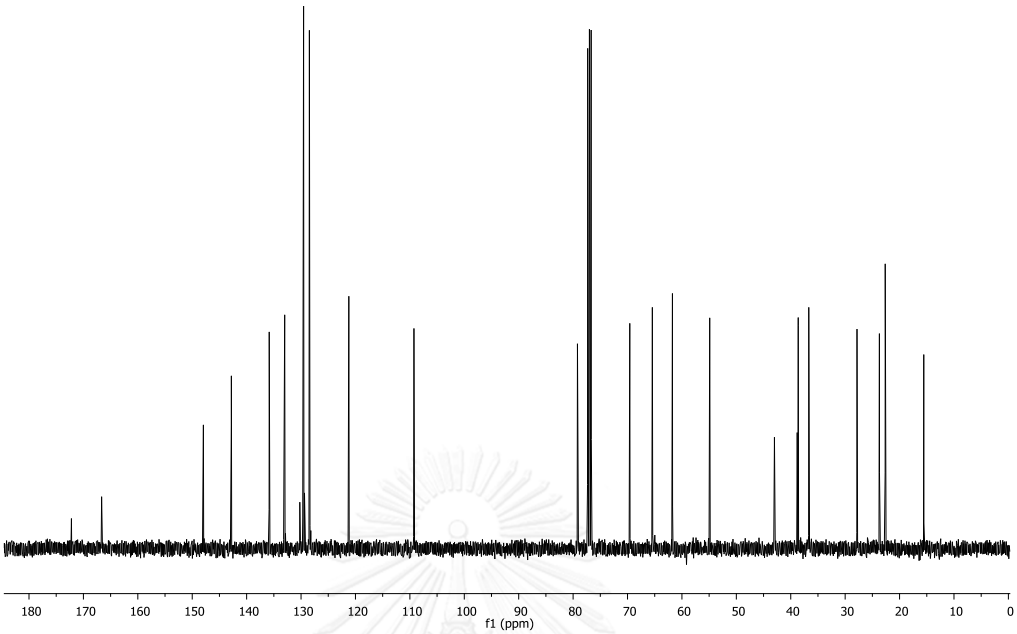

Figure A.98 ^{13}C NMR (100 MHz, $CDCl_3$) spectrum of compound **153**

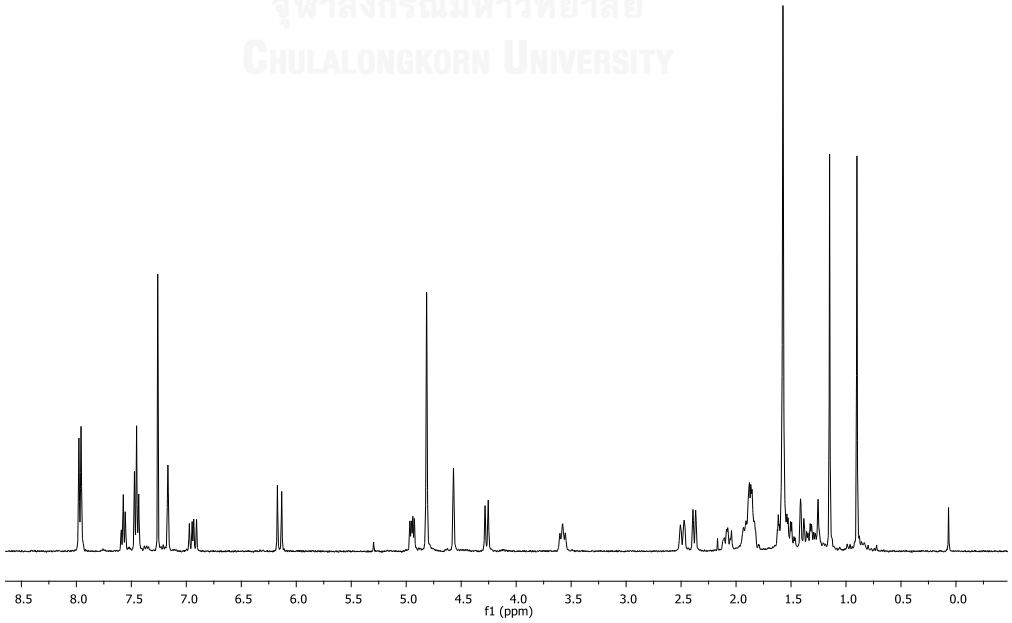

Figure A.99 ^{1}H NMR (400 MHz, $CDCl_3$) spectrum of compound **154**

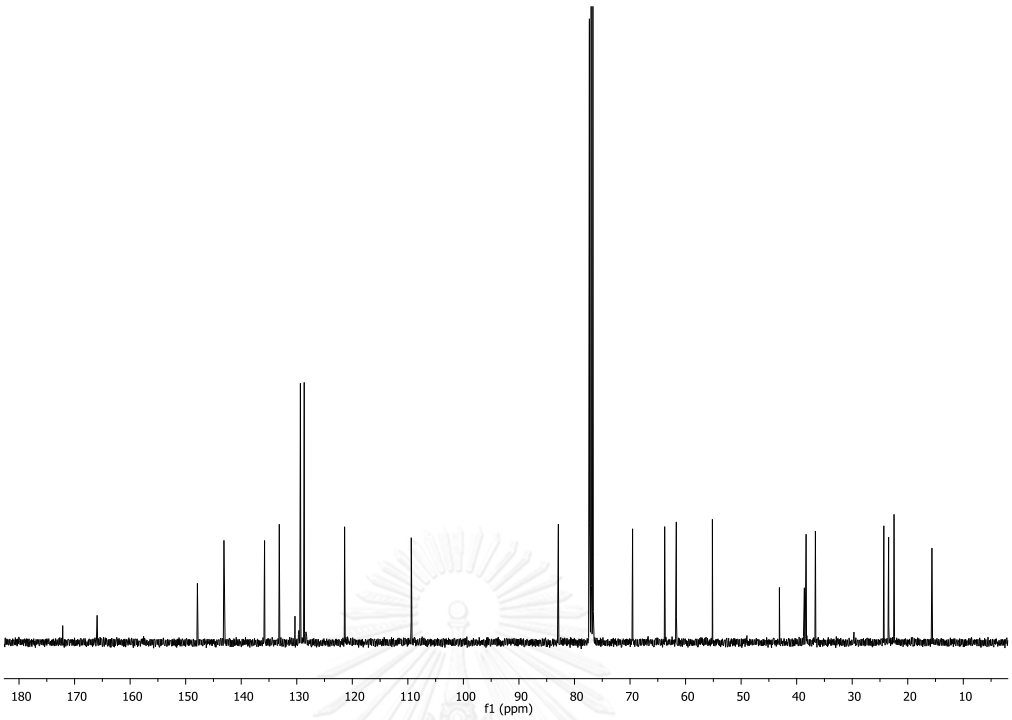

Figure A.100 ^{13}C NMR (100 MHz, $CDCl_3$) spectrum of compound **154**

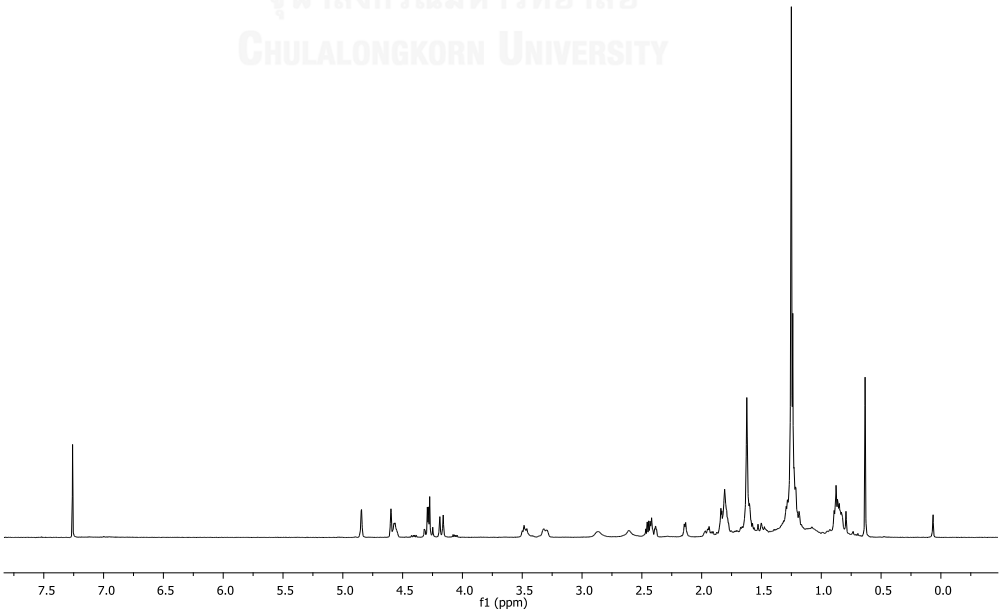

Figure A.101 ^{1}H NMR (400 MHz, $CDCl_3$) spectrum of compound **155**

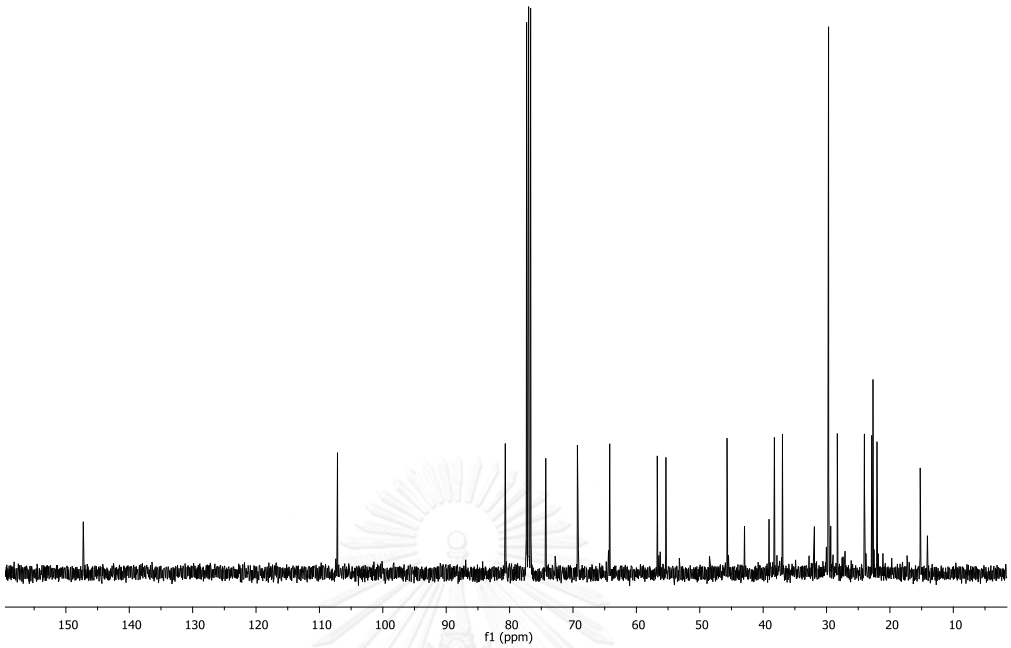

Figure A.102 ^{13}C NMR (100 MHz, $CDCl_3$) spectrum of compound **155**

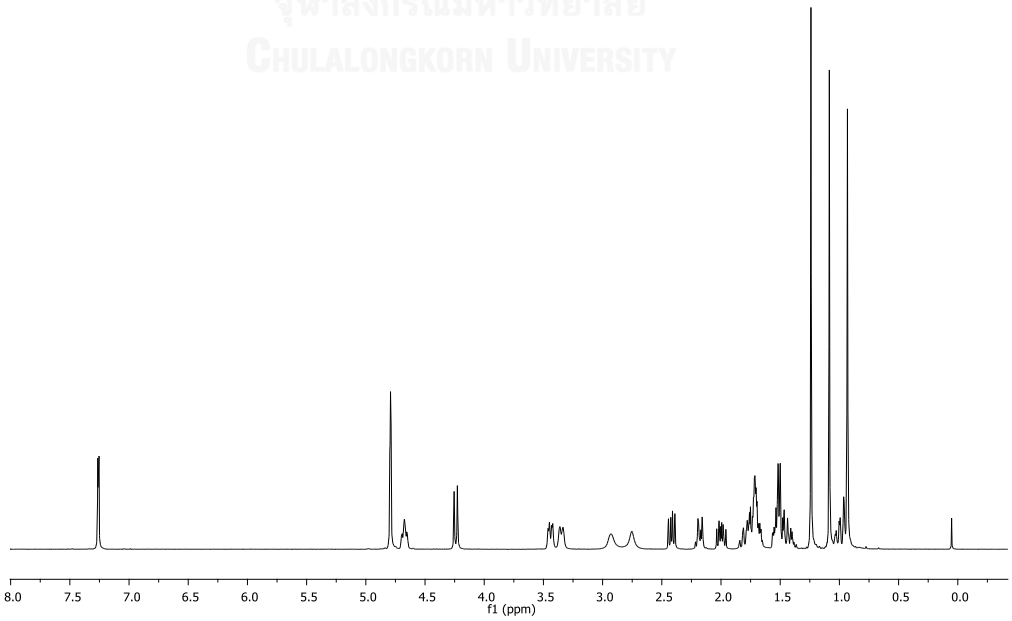

Figure A.103 ^{1}H NMR (400 MHz, $CDCl_3$) spectrum of compound **156**

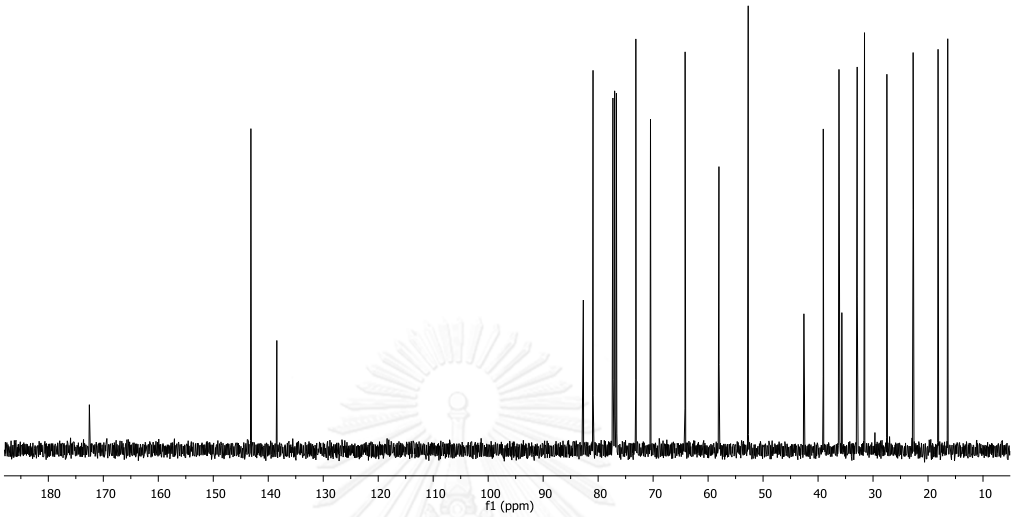

Figure A.104 ^{13}C NMR (100 MHz, $CDCl_3$) spectrum of compound **156**

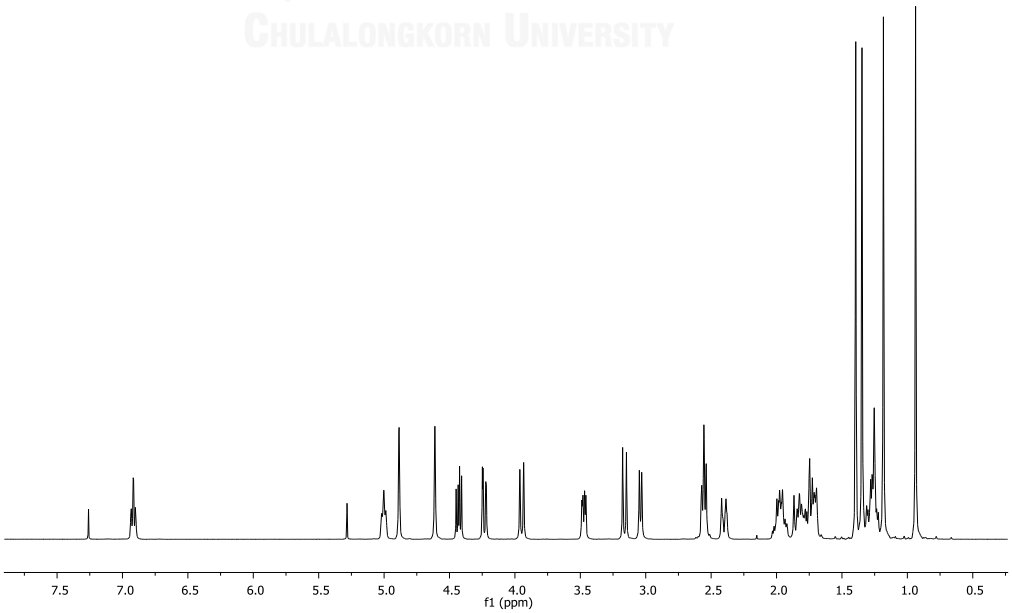

Figure A.105 ^{1}H NMR (400 MHz, $CDCl_3$) spectrum of compound **157**

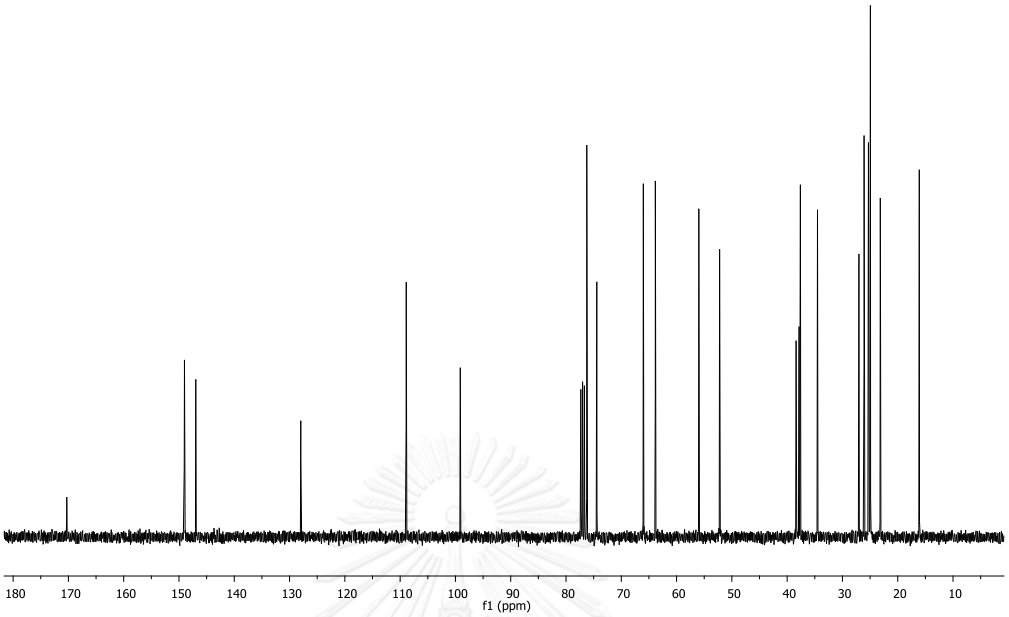

Figure A.106 ^{13}C NMR (100 MHz, $CDCl_3$) spectrum of compound **157**

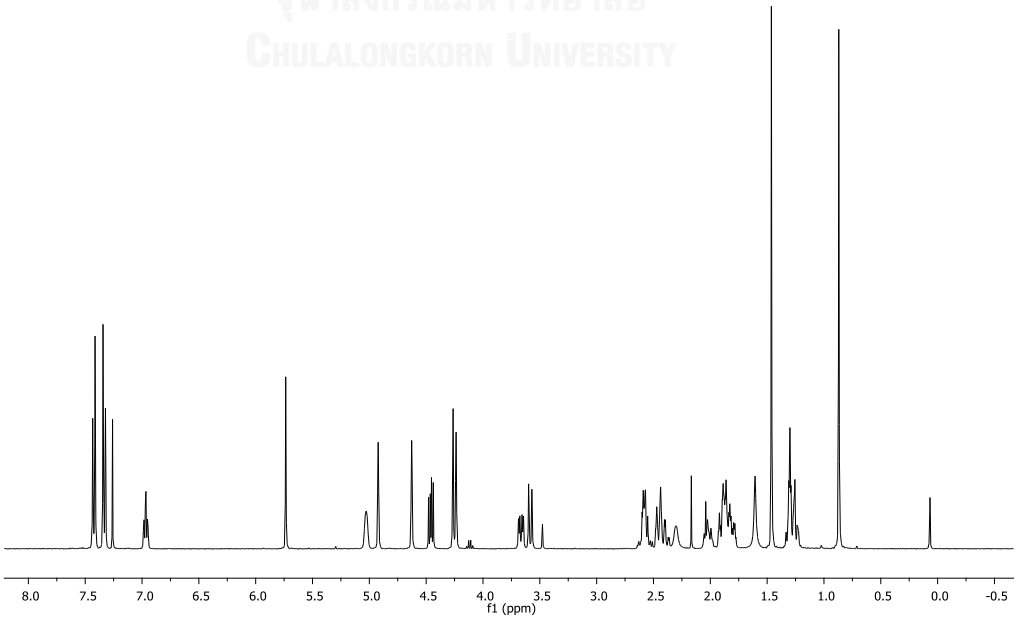

Figure A.107 ^{1}H NMR (400 MHz, $CDCl_3$) spectrum of compound **158**

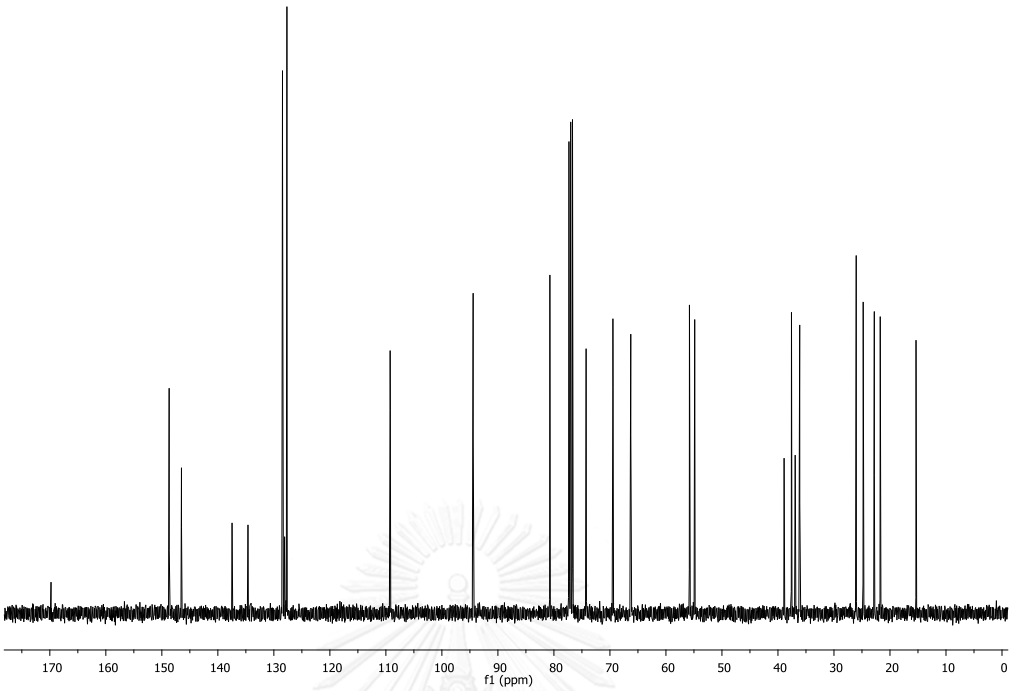

Figure A.108 ^{13}C NMR (100 MHz, $CDCl_3$) spectrum of compound **158**

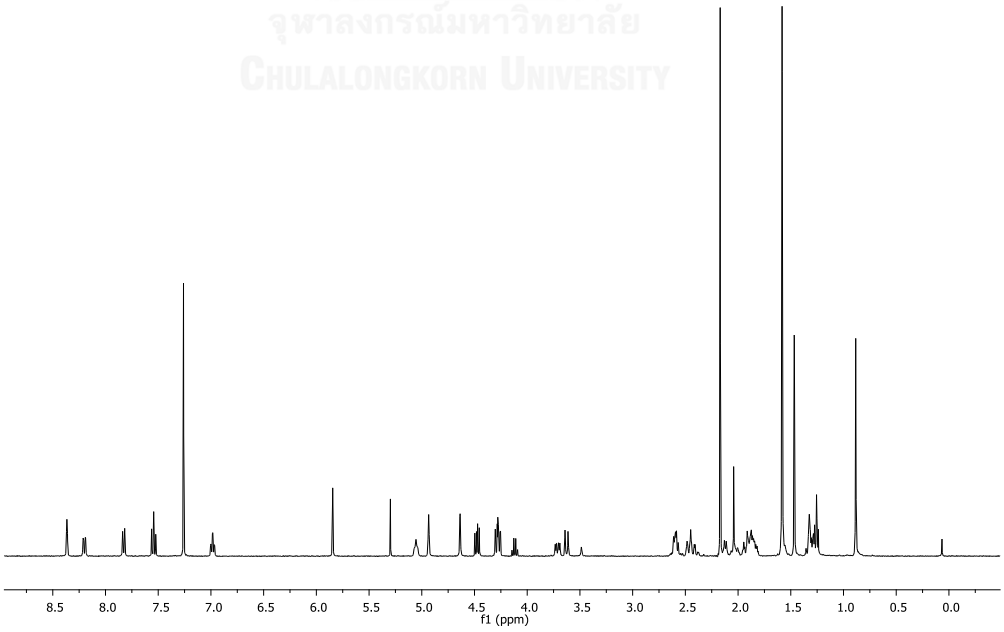

Figure A.109 ^{1}H NMR (400 MHz, $CDCl_3$) spectrum of compound **159**

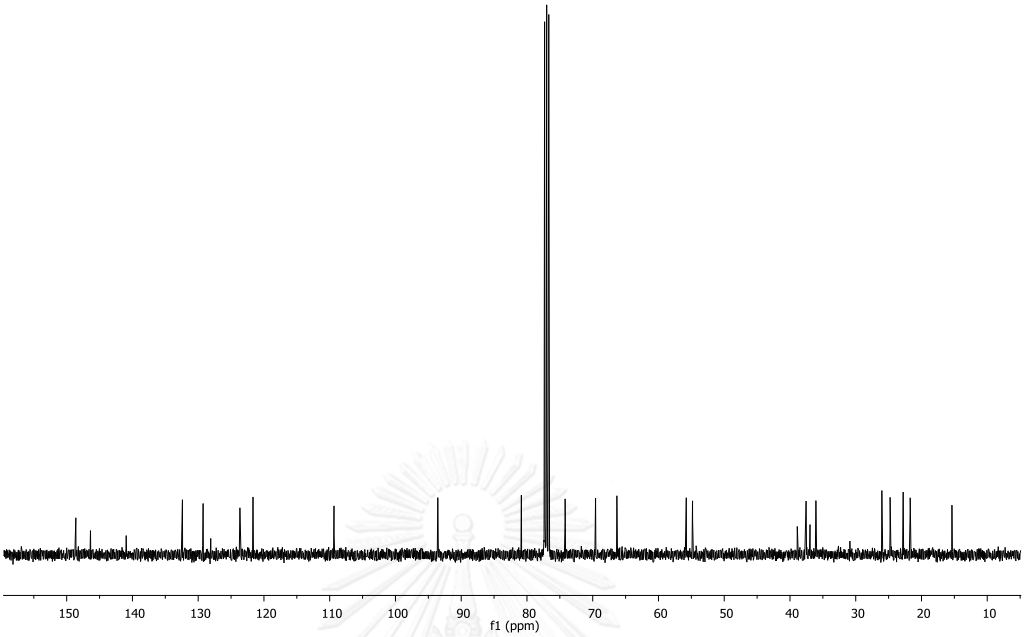

Figure A.110 ^{13}C NMR (100 MHz, $CDCl_3$) spectrum of compound **159**

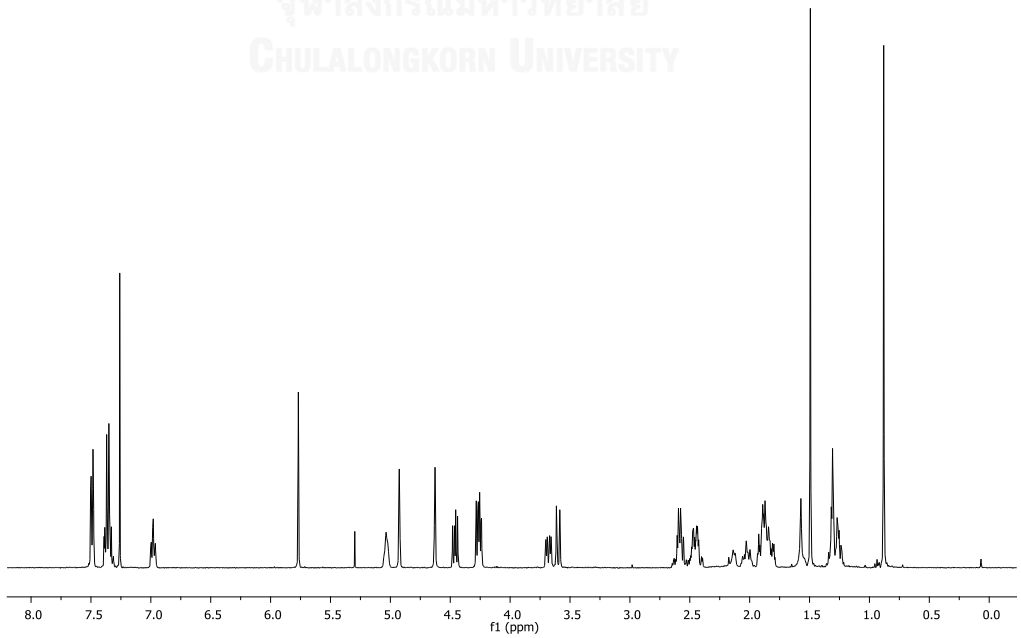

Figure A.111 ^{1}H NMR (400 MHz, $CDCl_3$) spectrum of compound **160**

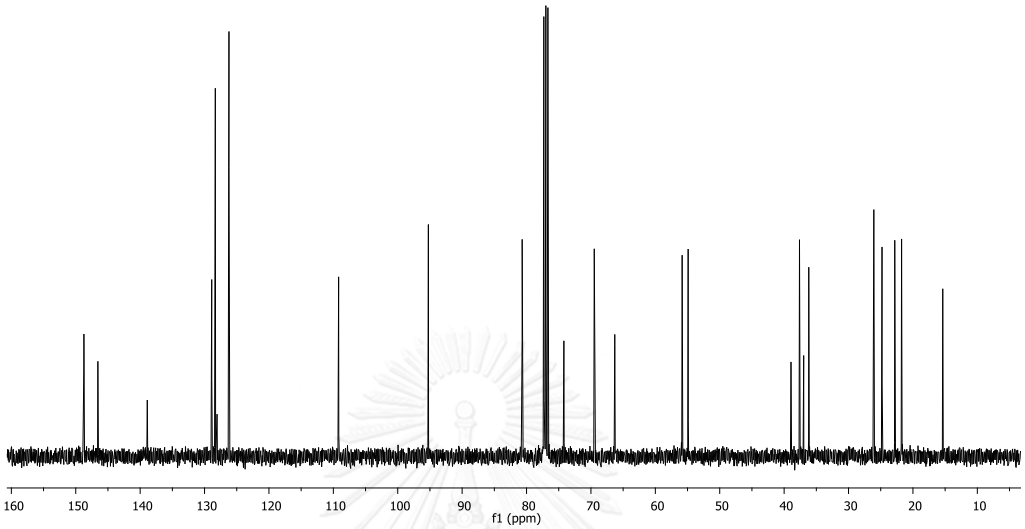

Figure A.112 ^{13}C NMR (100 MHz, $CDCl_3$) spectrum of compound **160**

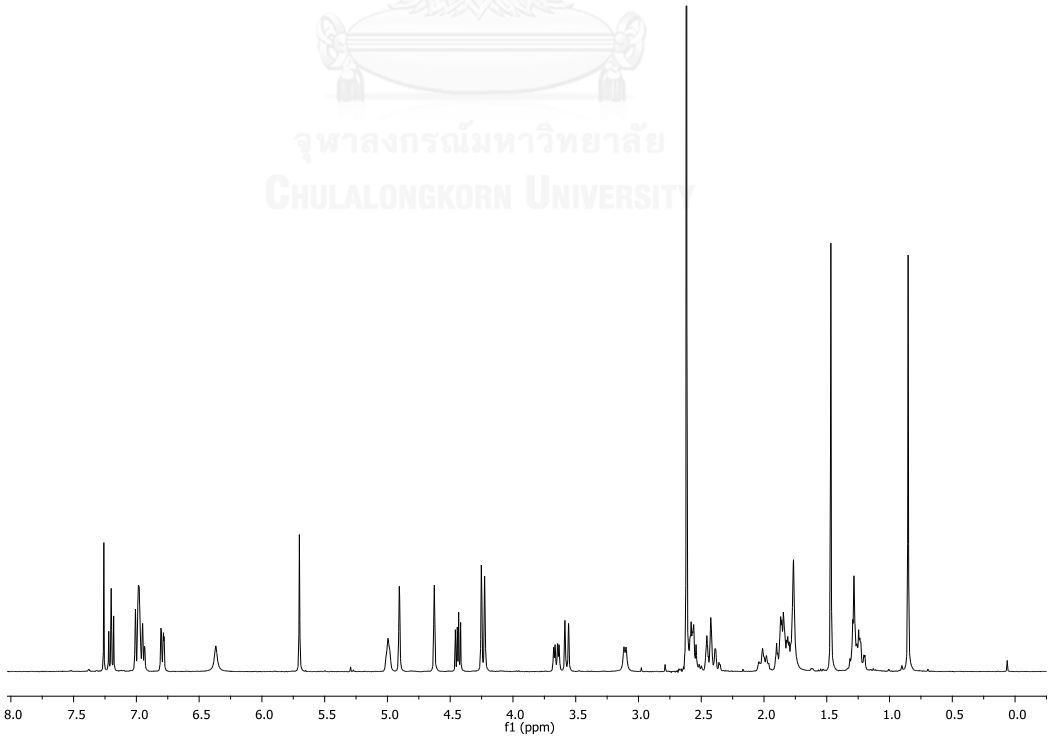

Figure A.113 ^{1}H NMR (400 MHz, $CDCl_3$) spectrum of compound **161**

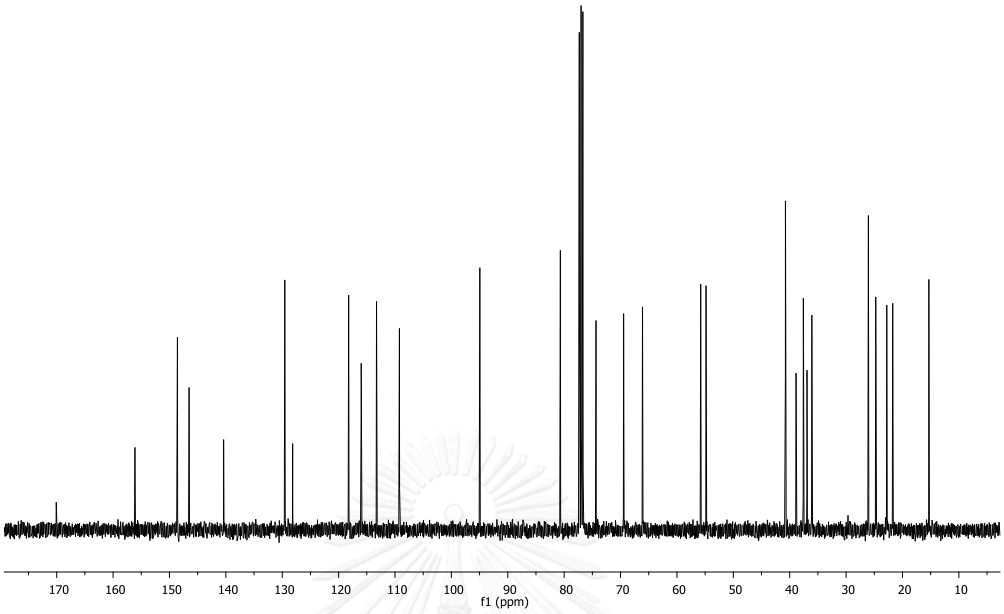

Figure A.114 ^{13}C NMR (100 MHz, $CDCl_3$) spectrum of compound **161**

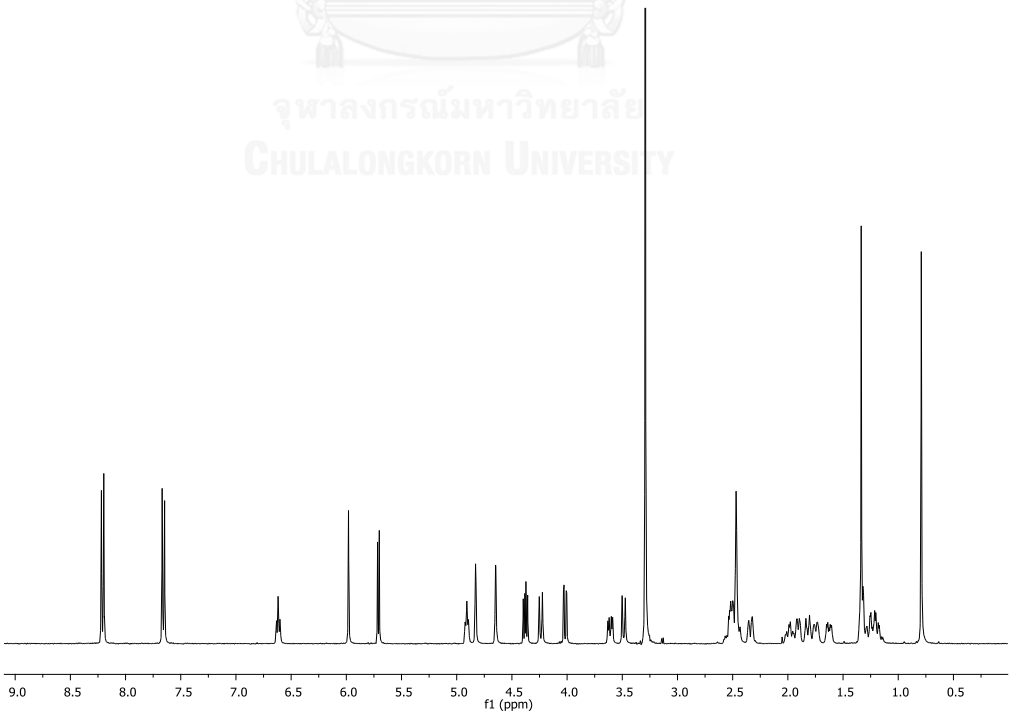

Figure A.115 ^{1}H NMR (400 MHz, $(CD_3)_2SO$) spectrum of compound **162**

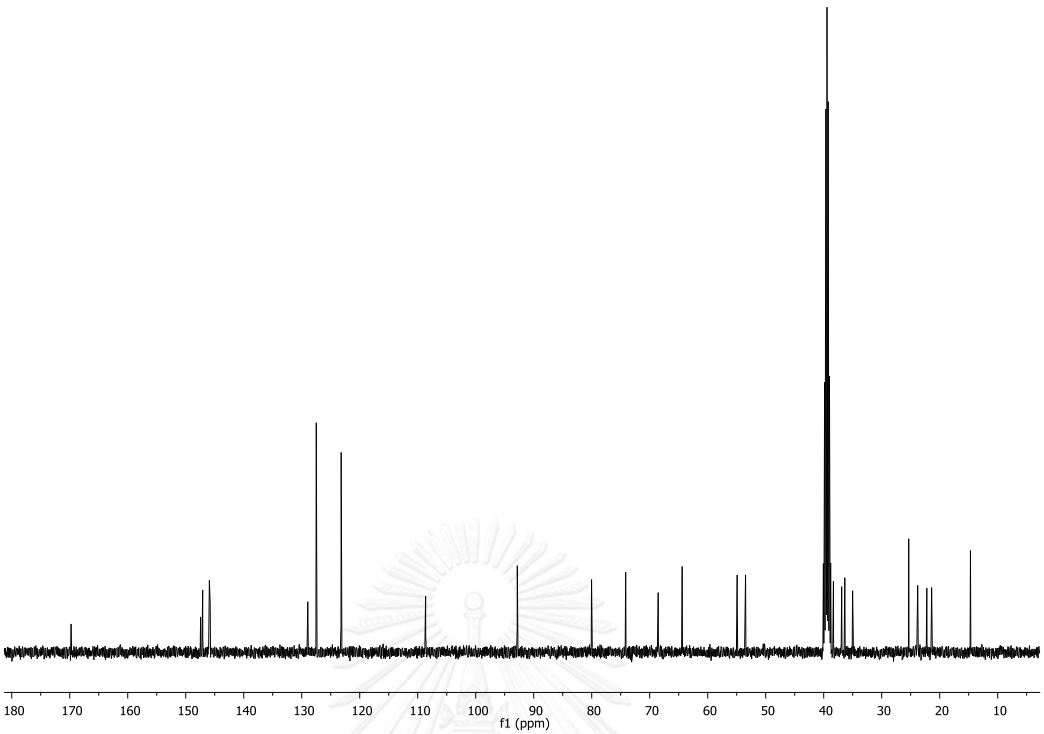

Figure A.116 ^{13}C NMR (100 MHz, $(CD_3)_2SO$) spectrum of compound **162**

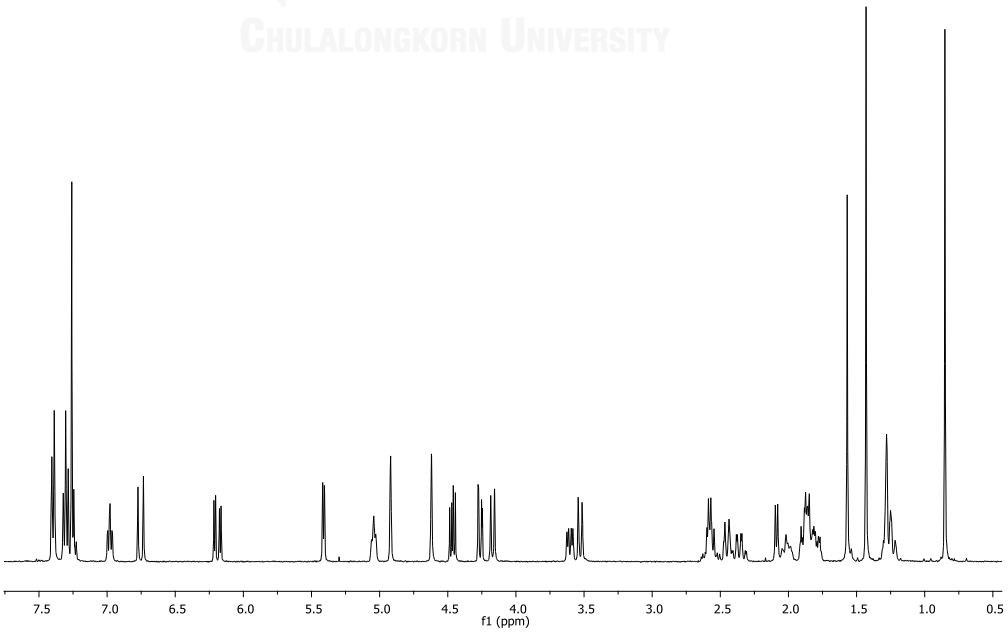

Figure A.117 ^{1}H NMR (400 MHz, $CDCl_3$) spectrum of compound **163**

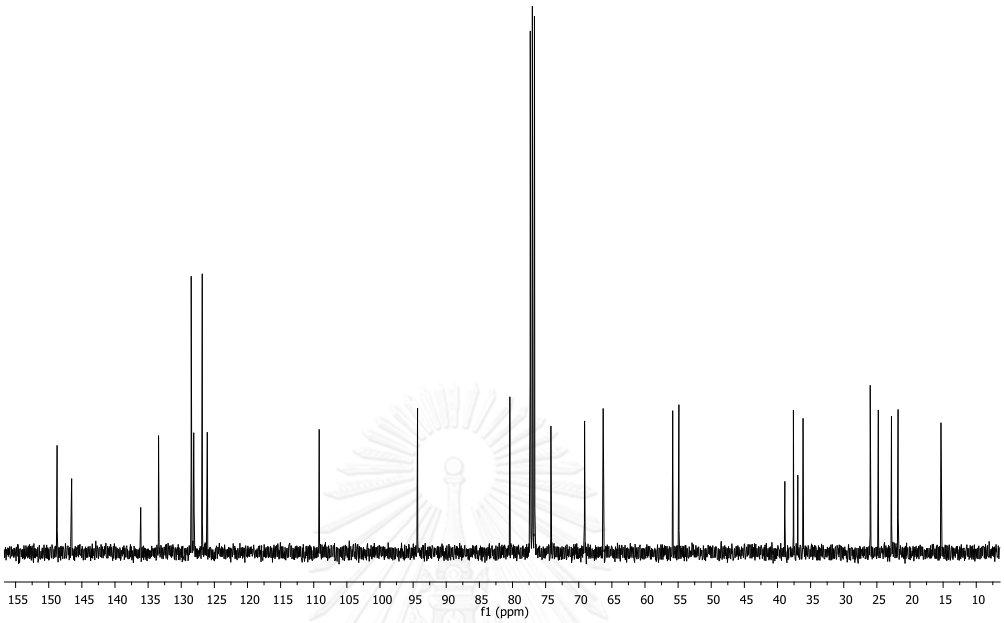

Figure A.118 ^{13}C NMR (100 MHz, $CDCl_3$) spectrum of compound **163**

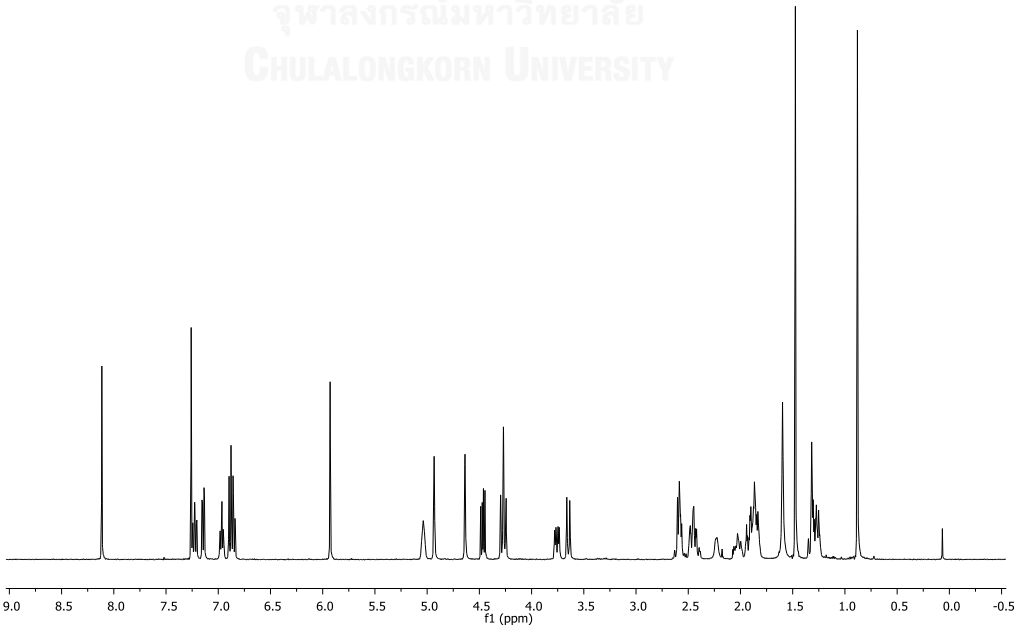

Figure A.119 ^{1}H NMR (400 MHz, $CDCl_3$) spectrum of compound **164**

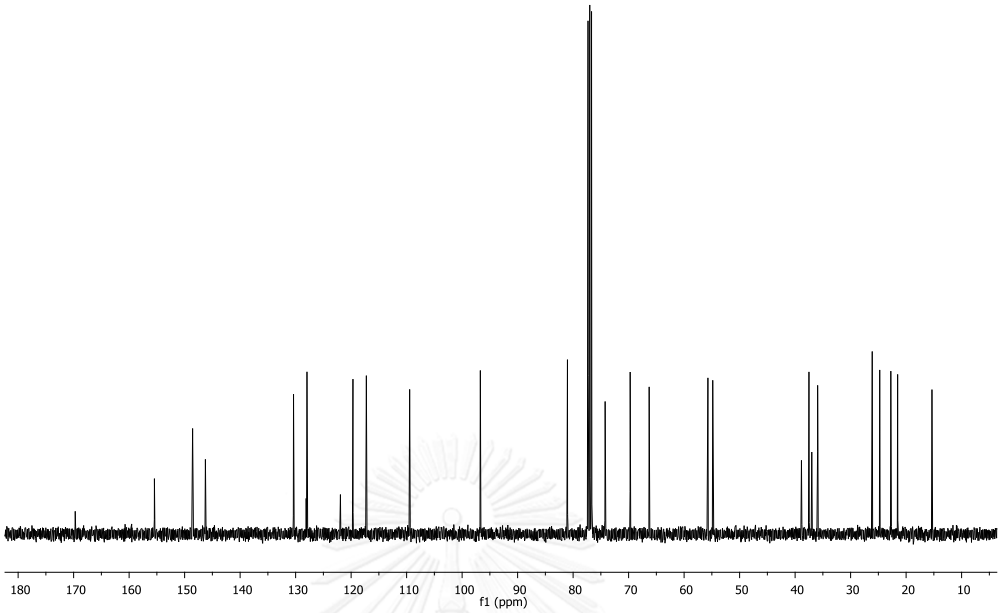

Figure A.120 ^{13}C NMR (100 MHz, $CDCl_3$) spectrum of compound **164**

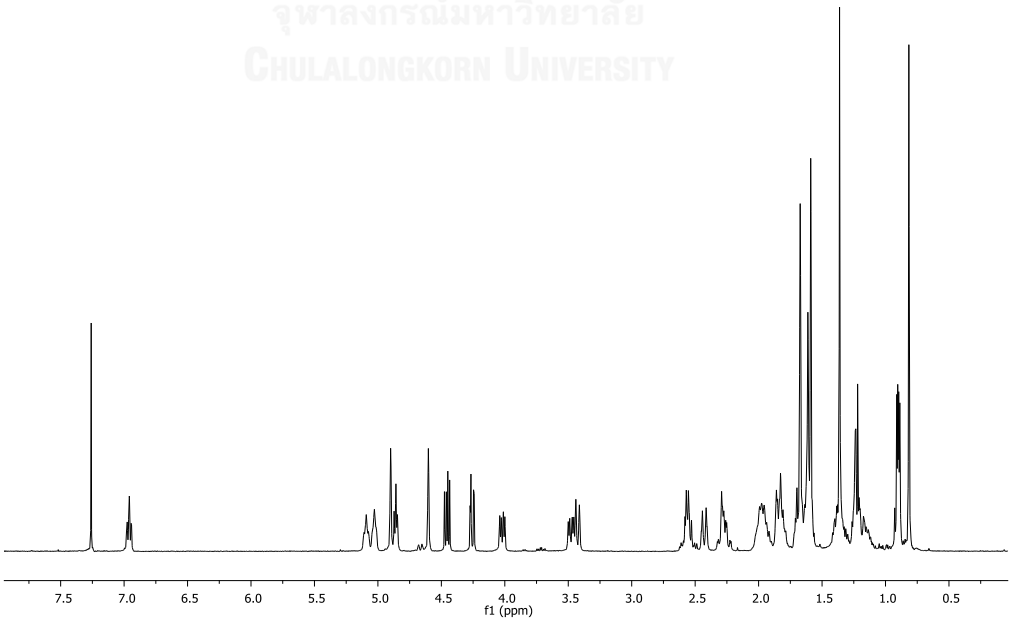

Figure A.121 ^{1}H NMR (400 MHz, $CDCl_3$) spectrum of compound **165**

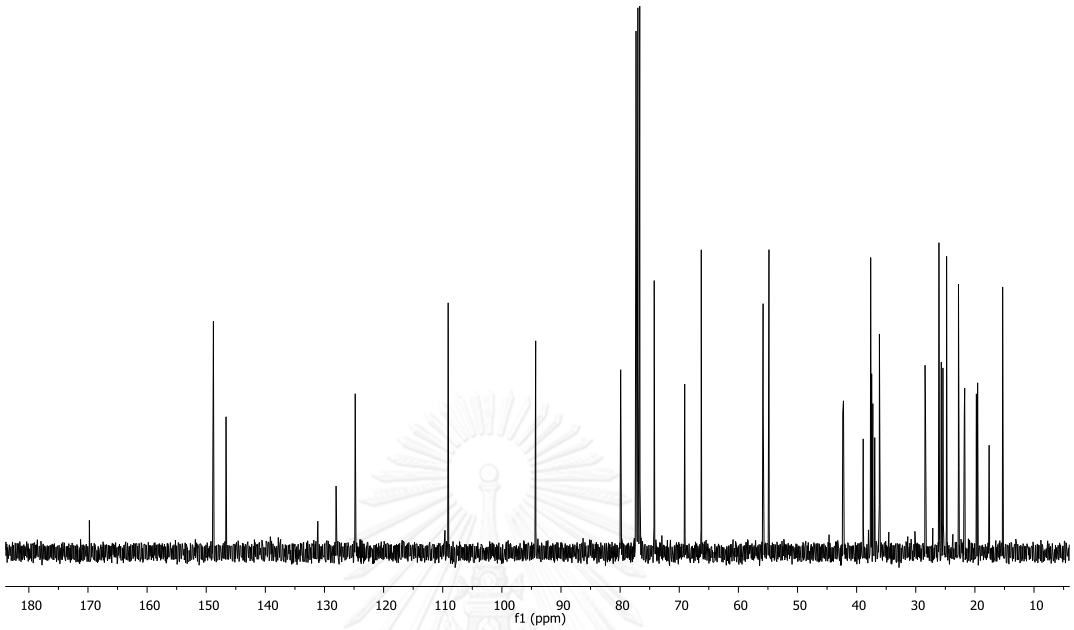

Figure A.122 ^{13}C NMR (100 MHz, $CDCl_3$) spectrum of compound **165**

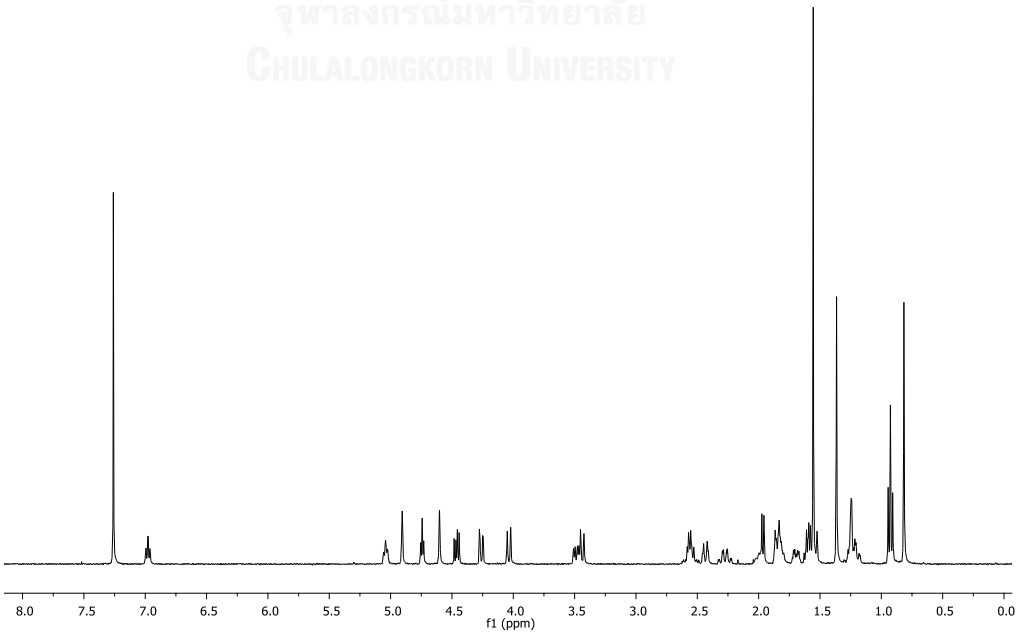

Figure A.123 ^{1}H NMR (400 MHz, $CDCl_3$) spectrum of compound **166**

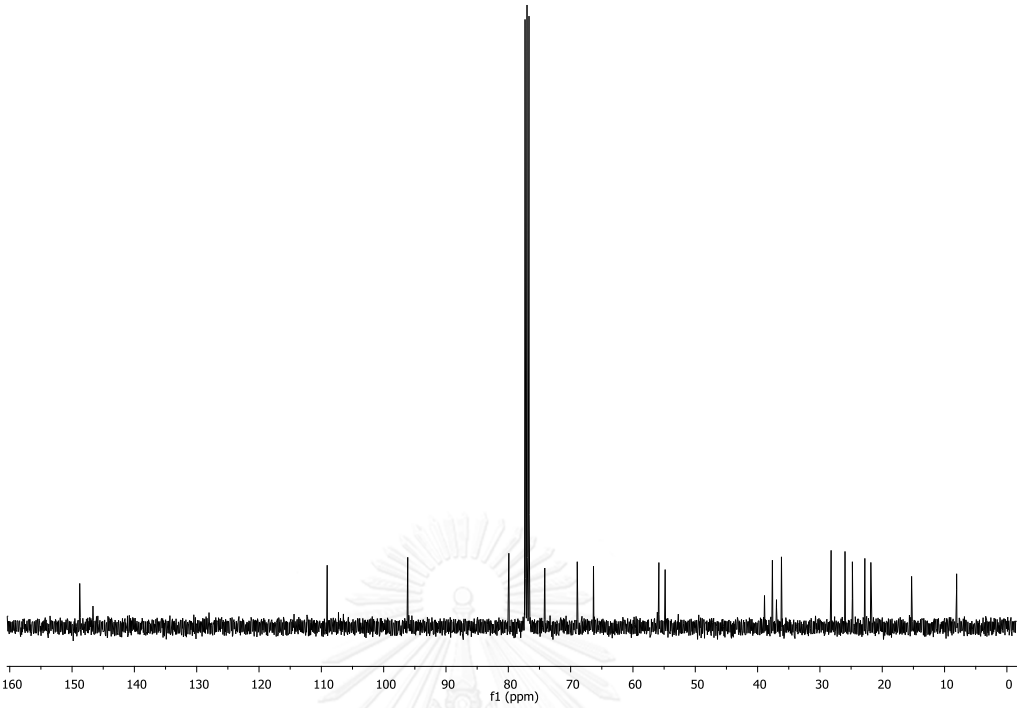

Figure A.124 ^{13}C NMR (100 MHz, $CDCl_3$) spectrum of compound **166**

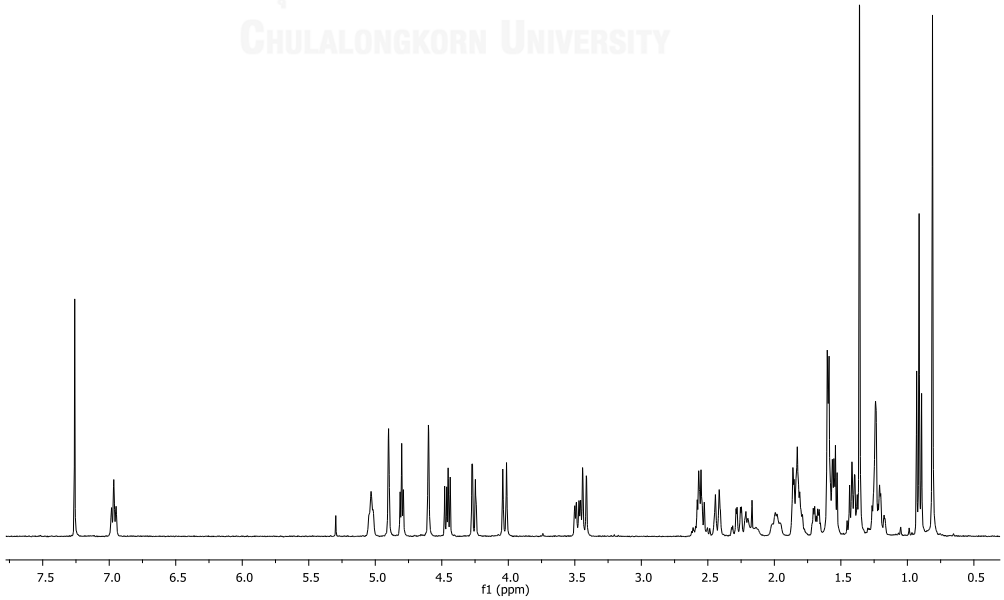

Figure A.125 ^{1}H NMR (400 MHz, $CDCl_3$) spectrum of compound **167**

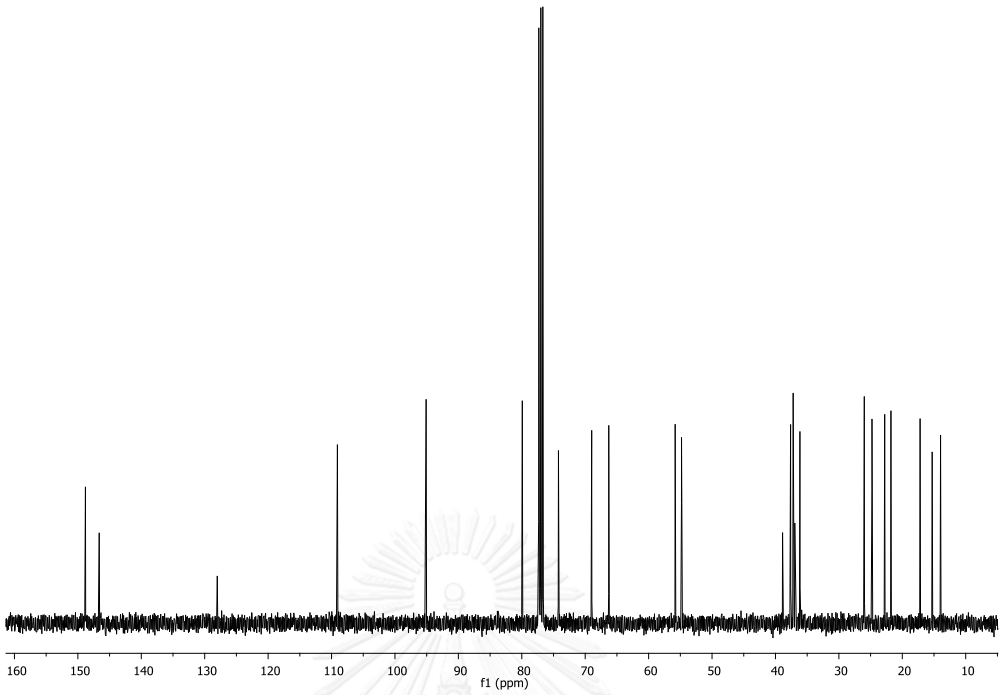

Figure A.126 ^{13}C NMR (100 MHz, $CDCl_3$) spectrum of compound **167**

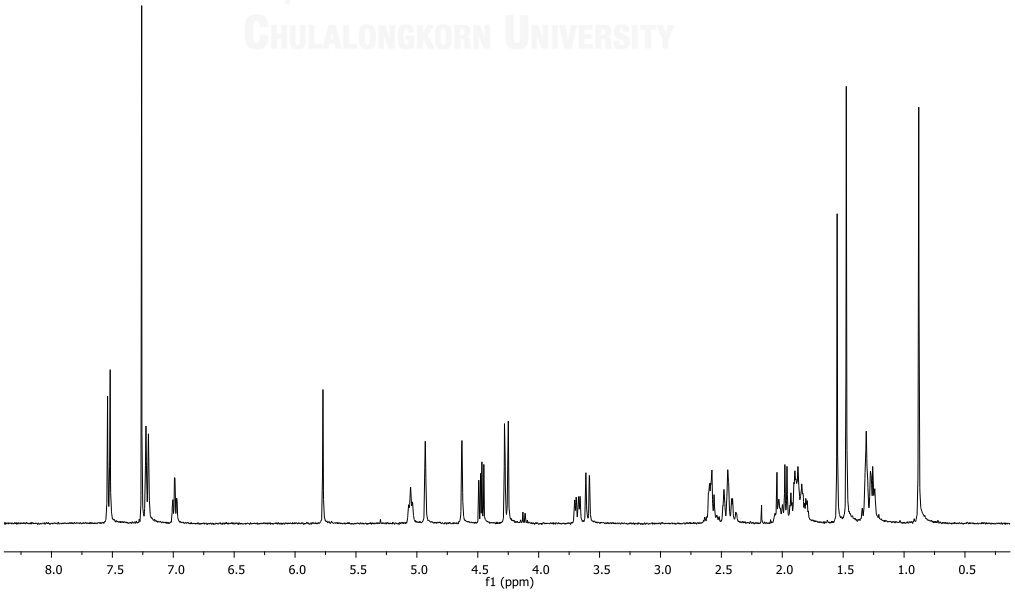

Figure A.127 ^{1}H NMR (400 MHz, $CDCl_3$) spectrum of compound **168**

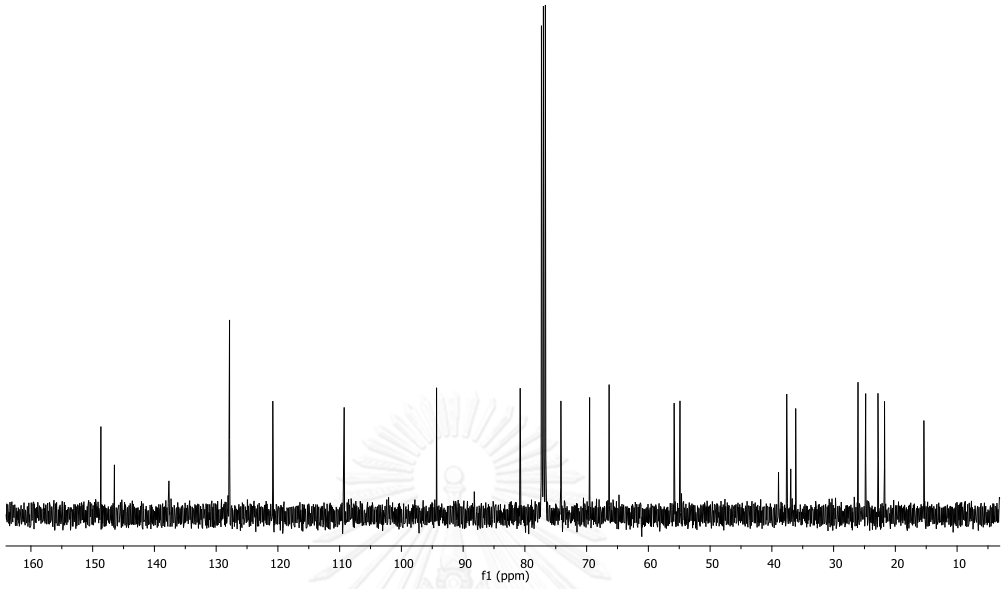

Figure A.128 ^{13}C NMR (100 MHz, $CDCl_3$) spectrum of compound **168**

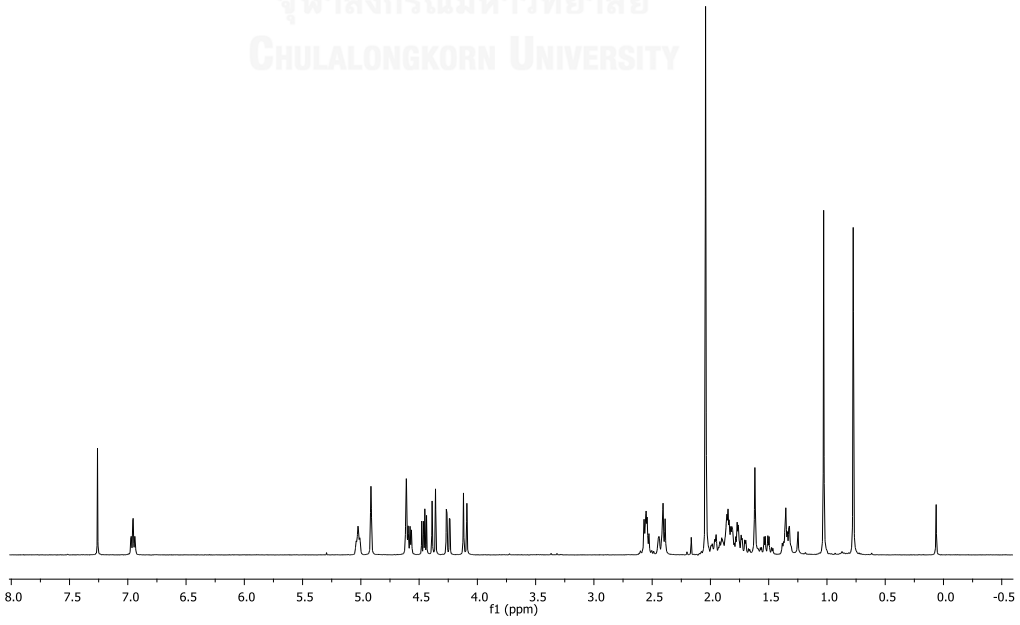

Figure A.129 ^{1}H NMR (400 MHz, $CDCl_3$) spectrum of compound **169**

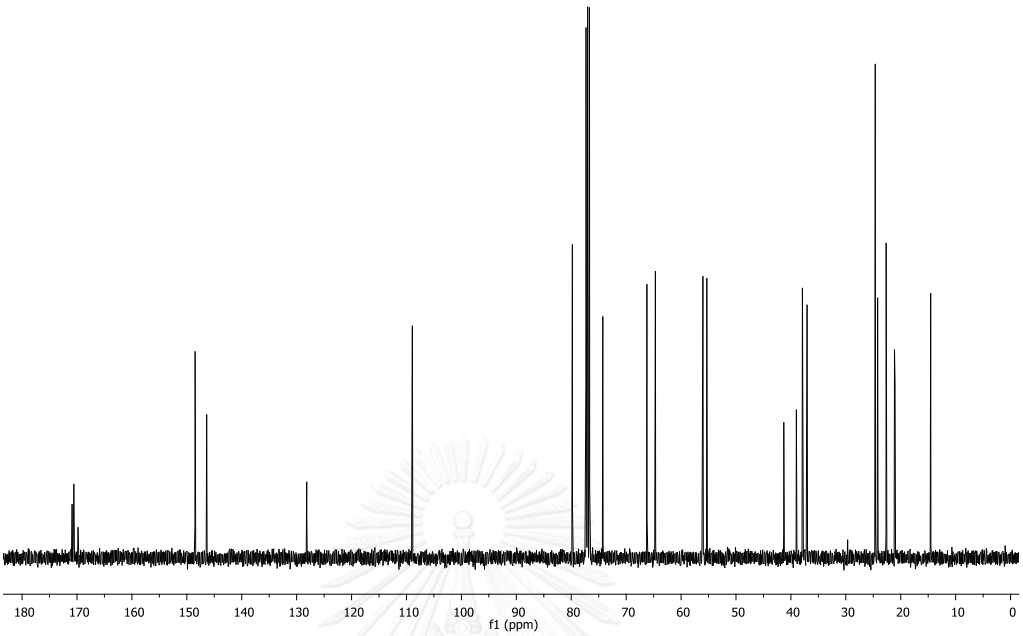

Figure A.130 ^{13}C NMR (100 MHz, $CDCl_3$) spectrum of compound **169**

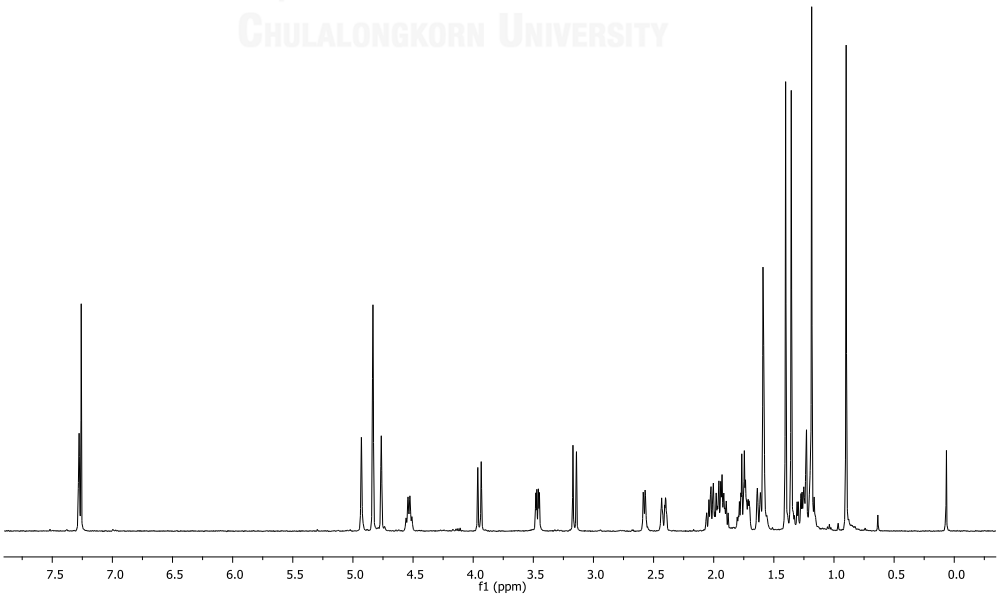

Figure A.131 ^{1}H NMR (400 MHz, $CDCl_3$) spectrum of compound **170**

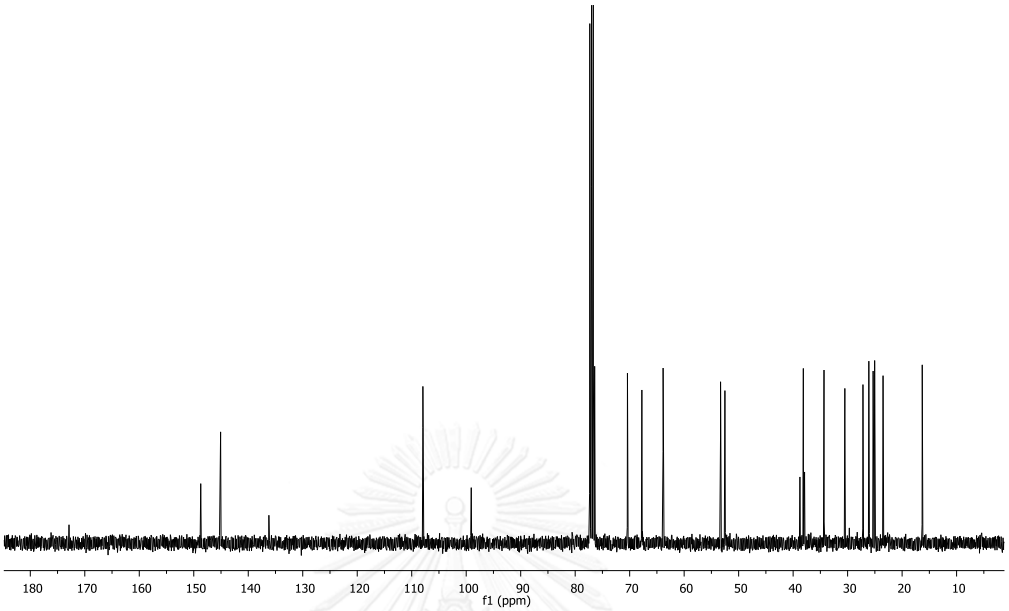

Figure A.132 ^{13}C NMR (100 MHz, $CDCl_3$) spectrum of compound **170**

VITA

Mr. Chanin Sarigaputi was born on January 5, 1986 in Bangkok, Thailand.

He graduated with Bachelor's Degree of Science in Biology from Faculty of Science, Kasetsart University, in 2007 and graduated with the degree of Master of Science at Program in Biotechnology, Faculty of Science, Chulalongkorn University, in 2009. During the time he was studied in the Doctoral Degree in Biotechnology program, Faculty of Science, Chulalongkorn University. He received Thailand Research Fund and Chulalongkorn University through the Royal Golden Jubilee Ph.D. Program (PHD/0009/2553) and The 90th Anniversary of Chulalongkorn University Fund (Ratchadaphiseksomphot Endowment Fund) for supporting his research project.

His present address is 310/887 Soi Songprapa 14, Songprapa Rd. Seekan, Donmuang, Bangkok, Thailand, 10210, Tel: +669-4995-9115.

Publications:

1. Sarigaputi, C., Teerawatananond, T., Pengpreecha, S., Muangsin, N., Pudhom, K., 2010. Xyloccensin E, Acta Crystallographica Section E: Structure Reports Online 66: 1348-1349.

2. Sarigaputi, C., Nuanyai, T., Teerawatananond, T., Pengpreecha, S., Muangsin, N., Pudhom, K., 2010. Xylorumphiins A-D, mexicanolide limonoids from the seed kernels of Xylocarpus rumphii, Journal of Natural Products 73: 1456-1459.

3. Sarigaputi, C., Sommit, D., Teerawatananond, T., Pudhom, K., 2014. Weakly Anti-inflammatory Limonoids from the Seeds of Xylocarpus rumphii, Journal of Natural Products 77:2037-2043.